



SAKARYA ÜNİVERSİTESİ

FEN BİLİMLERİ ENSTİTÜSÜ DERGİSİ

Sakarya University Journal of Science (SAUJS)



SAKARYA
ÜNİVERSİTESİ

e-issn: 2147-835X

Volume: 28

Issue: 4

Agust 2024

VOLUME: 28 ISSUE: 4
E-ISSN 2147-835X

Agust 2024
<https://dergipark.org.tr/tr/pub/saufenbilder>

SAKARYA UNIVERSITY JOURNAL OF SCIENCE



SAKARYA
ÜNİVERSİTESİ

The Owner on Behalf of Sakarya University

Prof. Dr. Hamza Al
Sakarya University, Sakarya-Türkiye

Publishing Manager

Hüseyin Özkan Toplan
Department of Metallurgical and Materials Engineering
Sakarya University, Sakarya-Türkiye
toplano@sakarya.edu.tr

Editor in Chief

Ömer Tamer
Department of Physics
Sakarya University, Sakarya-Türkiye
omertamer@sakarya.edu.tr

Associate Editors

İhsan Hakan Selvi
Department of Information Systems Engineering
Sakarya University, Sakarya-Türkiye
ihselvi@sakarya.edu.tr

Editorial Board

Asude Ateş
Department of Environmental Sciences and
Engineering
Sakarya University
Sakarya - Türkiye
aates@sakarya.edu.tr

Bahadır Respect
Department of Nuclear Physics
Ankara University
Ankara - Türkiye
bsaygi@ankara.edu.tr

Berrin Denizhan
Department of Industrial Engineering
Sakarya University
Sakarya - Türkiye
denizhan@sakarya.edu.tr

Hüseyin Aksoy
Department of Biology
Sakarya University
Sakarya - Türkiye
haksoy@sakarya.edu.tr

Mehmet Uysal
Department of Metallurgical and
Materials Engineering
Sakarya University
Sakarya - Türkiye
mehmetu@sakarya.edu.tr

Muhammed Fatih Adak
Department of Computer Science and Engineering
Sakarya University
Sakarya - Türkiye
fatihadak@sakarya.edu.tr

Muhammet Hilmi Nişancı
Department of Electrical and Electronics Engineering
Sakarya University
Sakarya - Türkiye
nisanci@sakarya.edu.tr

Mustafa Gülfen
Department Analytical Chemistry
Sakarya University
Sakarya - Türkiye
mgulfen@sakarya.edu.tr

Osman Sönmez
Department of Civil Engineering
Sakarya University
Sakarya - Türkiye
osonmez@sakarya.edu.tr

Serap Coşansu
Department of Food Engineering
Sakarya University
Sakarya - Türkiye
scosansu@sakarya.edu.tr

Tahsin Turgay
Department of Architecture
Sakarya University
Sakarya - Türkiye
turgay@sakarya.edu.tr

Ufuk Durmaz
Department of Mechanical Engineering
Sakarya University
Sakarya - Türkiye
udurmaz@sakarya.edu.tr

Section Editor (Civil Engineering)

Elif Ağcakoca
Department of Civil Engineering
Sakarya University
Sakarya - Türkiye
elifd@sakarya.edu.tr

Faruk Fırat Çalım
Department of Civil Engineering
Adana Alparslan Türkeş
Science and Technology University
Adana - Türkiye
ffcalim@atu.edu.tr

Issa Al-Harthy
Department of Civil and Architectural Engineering
Sultan Qaboos University
Oman
aissa@squ.edu.om

Jamal Khatib
Department of Civil Engineering
University of Wolverhampton
United Kingdom
jmkhatib@wlv.ac.uk

Khalifa Al-Jabri
Department of Civil and Architectural Engineering
Sultan Qaboos University
Oman
aljabri@squ.edu.om

Hakan Alp
Department of Geophysical Engineering
İstanbul University-Cerrahpaşa
İstanbul - Türkiye
hakanalp@iuc.edu.tr

Tuba Tatar
Department of Civil Engineering
Sakarya University
Sakarya - Türkiye
ttatar@sakarya.edu.tr

Gökhan Dok
Department of Civil Engineering
Sakarya University of Applied Sciences
Sakarya - Türkiye
gokhandok@subu.edu.tr

Section Editor (Chemistry)

Can Serkan Keskin
Department of Chemistry
Sakarya University
Sakarya - Türkiye
ckeskin@sakarya.edu.tr

Gražyna Simha Martynková
Department of Chemistry Education Vsb-Technical
University of Ostrava
Czech Republic
grazyna.simha@vsb.cz

Murat Tuna
Department of Chemistry
Sakarya University
Sakarya - Türkiye
tuna@sakarya.edu.tr

Aligholi Niaie
Department Chemical Engineering
University of Tabriz
Iran
aniaei@tabrizu.ac.ir

Nahit Gencer
Department of Biochemistry
Balıkesir University
Sakarya - Türkiye
ngencer@balikesir.edu.tr

Section Editor (Biology)

Cansu Akbulut
Department of Biology
Sakarya University
Sakarya - Türkiye
cansua@sakarya.edu.tr

Luis Materon
Department of Biology
University of Texas Rio Grande Valley
USA
luis.materon@utrgv.edu

Nazan Deniz Yön Ertuğ
Department of Biology
Sakarya University
Sakarya - Türkiye
nkoc@sakarya.edu.tr

Nihan Akıncı Kenanoğlu
Department of Biology
Çanakkale Onsekiz Mart University
Çanakkale - Türkiye
nakinci@comu.edu.tr

Oğuz Kurt
Department of Biology
Manisa Celal Bayar University
Manisa - Türkiye
oguz.kurt@cbu.edu.tr

Sezgi Somuncu
Department of Biology
Sakarya University
Sakarya - Türkiye
sezgisomuncu@sakarya.edu.tr

Sezen Toksoy Köseođlu
Department of Biology
Sakarya University
Sakarya - Türkiye
sezentoksoy@sakarya.edu.tr

Section Editor (Mathematics)

Murat Güzeltepe
Department of Mathematics
Sakarya University
Sakarya - Türkiye
mguzeltepe@sakarya.edu.tr

Murat Sarduvan
Department of Mathematics
Sakarya University
Sakarya - Türkiye
msarduvan@sakarya.edu.tr

Ali Demir
Department of Mathematics
Kocaeli University
Kocaeli - Türkiye
ademir@kocaeli.edu.tr

Luan Hoang
Department of Mathematics
Texas Tech University
USA
luan.hoang@ttu.edu

Selma Özçađ
Department of Mathematics
Hacettepe University
Ankara - Türkiye
sozcag@hacettepe.edu.tr

Necati Olgun
Department of Mathematics
Gaziantep University
Gaziantep - Türkiye
olgun@gantep.edu.tr

Section Editor (Computer Science and Engineering)

Fahrettin Horasan
Computer Science and Engineering
Kırıkkale University
Kırıkkale - Türkiye
fhorasan@kku.edu.tr

Kevser Ovaz Akpınar
Computer Science and Engineering
Rochester Dubai Institute of Technology
Dubai
kxocad1@rit.edu

Muhammed Maruf Öztürk
Computer Science and Engineering
Süleyman Demirel University
Isparta - Türkiye
muhammedozturk@sdu.edu.tr

Mustafa Akpınar
Computer Science and Engineering
High Tech Collages
United Arab Emirates
mustafakpınar@gmail.com

Section Editor (Physics)

Ceren Tayran
Department Physics
Gazi University
Ankara - Türkiye
c.tayran@gazi.edu.tr

Grzegorz Jaworski
Department Physics
University of Warsaw
Poland
grzegorz.jaworski@pwr.edu.pl

Section Editor (Industrial Engineering)

Feyza Gürbüz
Department Industrial Engineering
Erciyes University
Kayseri - Türkiye
feyza@erciyes.edu.tr

Caner Erden
Department Industrial Engineering
Sakarya University of Applied Sciences
Sakarya - Türkiye
cerden@subu.edu.tr

Hatice Esen
Department Industrial Engineering
Kocaeli University
Kocaeli - Türkiye
hatice.eris@kocaeli.edu.tr

Mehmet Emin Aydın
Department Industrial Engineering
University of The West of England Bristol
England
mehmet.aydin@uwe.ac.uk,

Barış Yüce
Department Industrial Engineering
University of Exeter
United Kingdom
b.yuce@exeter.ac.uk

Benjamin Durakovic
Department Industrial Engineering
International University of Sarajevo
Bosnia and Herzegovina
bdurakovic@ius.edu.ba

Section Editor (Mechanical Engineering)

Elif Eker Kahveci
Department of Mechanical Engineering
Sakarya University
Sakarya - Türkiye
eeker@sakarya.edu.tr

Erman Aslan
Department of Mechanical Engineering
Kocaeli University
Kocaeli - Türkiye
erman.aslan@kocaeli.edu.tr

Mohammad Sukri Bin Mustapa
Department of Mechanical Engineering
University Tun Hussein Onn Malaysia
Malaysia
sukri@uthm.edu.my

Raja Mazuir Bin Raja Ahsan Shah
Department of Mechanical Engineering
Coventry University
United Kingdom
ac9217@coventry.ac.uk

Seong Jin Park
Department of Mechanical Engineering
Pohang University of Science and Technology
Korea
sjpark87@postech.ac.kr

Abderrahmane Benbrik
Department of Mechanical Engineering
M'hamed Bougara University
Egypt
abderrahmane.benbrik@univ-boumerdes.dz

Ali Cemal Benim
Department of Mechanical Engineering
Düsseldorf University of Applied Sciences
Germany
alicemal@prof-benim.com

Herman Nied
Department of Mechanical Engineering
Lehigh University
USA
hfn2@lehigh.edu

Shi-Chune Yao
Department of Mechanical Engineering
Carnegie Mellon University
USA
sy0d@andrew.cmu.edu

Tauseef Aized
Department of Mechanical Engineering
Uet Lahore
Pakistan
tauseef.aized@uet.edu.pk

Section Editor (Environmental Sciences and Engineering)

Ece Ümmü Deveci
Department of Environmental Sciences and
Engineering
Niğde Omer Halisdemir University
Niğde - TÜRKİYE
eudeveci@ohu.edu.tr

Senay Çetin Doğruparmak
Department of Environmental Engineering
Kocaeli University
Kocaeli - Türkiye
senayc@kocaeli.edu.tr

Section Editor (Food Science)

Aslı Uçar
Department of Food Sciences
Ankara University
Ankara - Türkiye
aucar@ankara.edu.tr

Edgar Perez Esteve
Department of Food Sciences
Polytechnic University of Valencia
Spain
edpees@upv.es

Syed Abbas
Department of Cereal Technology, Food Microbiology
Curtin University
Australia
s.abbas@curtin.edu.au

Section Editor

(Electrical and Electronics Engineering)

Abdullah Oğuz Kızılcay
Department of Electrical and Electronics Engineering
Zonguldak Bülent Ecevit University
Zonguldak - Türkiye
oguzkizilcay@yyu.edu.tr

İbrahim Bahadır Başıyigit
Department of Electrical and Electronics Engineering
Isparta University of Applied Sciences
Isparta - Türkiye
bahadirbasyigit@isparta.edu.tr

Francesco De Paulis
Department of Electrical and Electronics Engineering
L'Aquila University
Italy
francesco.depaulis@univaq.it

Mesut Baran
Department of Electrical and Electronics Engineering
North Carolina State University
USA
baran@ncsu.edu

Ozan Erdinç
Department of Electrical and Electronics Engineering
Yıldız Technical University
İstanbul - Türkiye
oerdinc@yildiz.edu.tr

Rıfki Terzioğlu
Department of Electrical and Electronics Engineering
Bolu Abant İzzet Baysal University
Bolu - Türkiye
rifkiterzioğlu@ibu.edu.tr

Section Editor (Architecture)

İsmail Hakkı Demir
Department of Architecture
Sakarya University
Sarkaya - Türkiye
idemir@sakarya.edu.tr

Section Editor (Materials Science)

Miraç Alaf
Department Metallurgical and Materials Engineering
Bilecik Şeyh Edebali University
Bilecik - Türkiye
mirac.alaf@bilecik.edu.tr

Kamaruzzaman Sopian
Department Metallurgical and Materials Engineering
Universiti Kebangsaan
Malaysia
ksopian@ukm.edu.my

English Language Editor

Seçkin Arı
Department of Computer Engineering
Sakarya University, Sakarya-Türkiye
ari@sakarya.edu.tr

Editorial Assistant

Evrım Yüksel
Department of Environmental Engineering
Institute of Sciences, Sakarya University
Sakarya-Türkiye
eyuksel@sakarya.edu.tr

Statistical Editor

Önder Gökmen Yıldız
Department of Mathematics
Bilecik Şeyh Edebali University, Bilecik-Türkiye
ogokmen.yildiz@bilecik.edu.tr

Managing Editor

Hüseyin Yasin Uzunok
Department of Physics
Sakarya University, Sakarya-Türkiye
hyuzunok@sakarya.edu.tr

Technical Editor

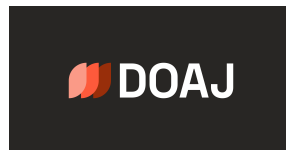
Hatice Vural
Department of Electrical and Electronics Engineering
Amasya University, Amasya-Türkiye
hatice.vural@amasya.edu.tr

Layout Editor

Mehmet Emin Çolak
Scientific Journals Coordinatorship
Sakarya University
Sakarya-Türkiye
mehmetcolak@sakarya.edu.tr

Yakup Beriş
Scientific Journals Coordinatorship
Sakarya University
Sakarya-Türkiye
yakupberis@sakarya.edu.tr

Indexing



Contents

Research Article

- 1 A Novel Correlation Measurement Method for Multi-Attribute Decision-Making Problems Based on Double Hierarchy Hesitant Fuzzy Linguistic Evaluation and Player Assignment Application in Football
Veysel Çoban 685-696
- 2 Investigation of the Effect of Ulexite Additive on the Mechanical Strength and Thermal Conductivity of Cement Mortar
Ahmet Filazi, Muharrem Pul, Zühtü Onur Pehlivanlı, İbrahim Uzun 697-707
- 3 Exploring the Link between Job Satisfaction and Productivity in Architectural Offices
Yiğit Can Yardımcı, Yasemin Erbil 708-718
- 4 The Effect of Grape Pomace Fiber Addition on Quality Parameters of Yogurt
Hatice Sıçramaz, Ahmet Ayar 719-725
- 5 Smart Agriculture Applications and Data Analysis with Industry 4.0
Yasin Ömercikoğlu, Abdullah Sevin 726-734
- 6 Content of Fatty Acids in Callus Cultures of Endemic *Ajuga vestita* BOISS.
Pınar Orcan, Mehmet Yusuf Orcan 735-741
- 7 Investigation of Caffeine Degradation by Anodic Oxidation Using Boron-Doped Diamond Electrode
Gökçe Didar Değermenci 742-755
- 8 Enhancing Industrial Robot Arms Data Security with a Hybrid Encryption Approach
Mustafa Emre Erbil, Merdan Özkahraman, Hilmi Cenk Bayrakçı 756-773
- 9 Analyzing TorrentLocker Ransomware Attacks: A Real Case Study
İlker Kara 774-781
- 10 Determination of Potential Distribution Areas of *Quercus cerris* (Turkish oak) in Anatolia According to Climate Change Scenarios
Cercis İkiel 782-793
- 11 Forensic comparison of Soil Samples in Omerli Dam by FTIR and ICP-OES
Soner Kızıl, İkra Sedef Boler, Sevil Atasoy 794-803
- 12 Investigation of Permeability of Thiocolchicoside Through Transdermal Drug Delivery System Using Franz Diffusion Cell
Hale Karagüzel, Sezen Sivrikaya Özak, Aslıhan Dalmaz 804-815
- 13 Improving Automatic Migraine Classification Performance with Naive Bayes
Arzum Karataş 816-823
- 14 Evaluating the Impact of Building Materials on Indoor Air Quality: A Critical Analysis
Tuğçe Pekdoğan 824-843
- 15 Impact of Iron Clamps and Dowels on the Vulnerability of Ancient Masonry Walls
Funda Gençer 844-854
- 16 Validating the Credibility of Photovoltaic Systems Simulation Tools with a Case Study
Barış Alaçam, Hatice Vural, Metin Orbay 855-865

17	Elemental Impurity Analysis in Five Different Types of Coffee: Assessment of Carcinogenic and Non-carcinogenic Risks <i>Fadime Canbolat</i>	866-875
18	A Novel Compact GNSS Antenna with Plasma Frequency Selective Surface <i>Olca Yigit, Fadıl Kuyucuođlu, Yavuz Öztürk</i>	876-883
19	Characterization of Micro-seismic Activity in Northern Cyprus Using Complexity and Corner Frequency Methods <i>Evrım Yavuz</i>	884-898
Review		
20	Fog Harvesting: An Effective Solution to The Water Scarcity Problem <i>Kadriye Oktor, Makoi Gai Riak Dhuol, Merve Ercan Kalkan</i>	899-911



A Novel Correlation Measurement Method for Multi-Attribute Decision-Making Problems Based on Double Hierarchy Hesitant Fuzzy Linguistic Evaluation and Player Assignment Application in Football

Veysel Çoban 

Bilecik Seyh Edebali University, Faculty of Engineering, Department of Industrial Engineering, Bilecik, Türkiye, veysel.coban@bilecik.edu.tr

ARTICLE INFO

ABSTRACT

Keywords:

Double hierarchy hesitant fuzzy linguistic term set
Multi-Attribute decision making
Correlation coefficient
Footballsport



Article History:

Received: 30.12.2022

Accepted: 14.06.2024

Online Available: 01.08.2024

Linguistic expressions are widely used to reflect the decision maker's evaluations more easily and clearly in the decision-making problems, The Double Hierarchy Hesitant Fuzzy Linguistic Term Set (DHHFLTS), an extension of linguistic expressions, helps the decision maker to reflect their hesitant evaluations in complex decision making problems using two different sets of linguistic terms. Correlation measurements are used as an important tool in making decisions by making comparative evaluations in complex decision making problems based on common criteria. In this study, a new method is proposed to improve the existing correlation measurement method using DHHFLTSs. The proposed method aims to increase the reflective power of hesitant thoughts in the evaluation process by including fuzzy linguistic expressions in the calculation process. In order to prove the validity of the proposed method, the original problem of choosing the most suitable player for the positions in football sport is considered as a Multi-Attribute Decision Making (MADM) problem. Correlation values and assignment results obtained from the proposed method are compared with the current method values. Consistency of results and values between methods reveals the validity of the proposed method.

1. Introduction

The increase in factors in decision-making problems causes complexity in the evaluation and calculation processes of the problem. Evaluation of alternatives with their increasing features and factors leads to the emergence of Multi-Attribute Decision Making (MADM) problems [1]. Linguistic information is applied to meet the quantitative expressions that are insufficient in making evaluations in MADM problems. The fuzzy linguistic approaches proposed by Zadeh [2] for expressing and measuring linguistic information differ according to the characteristics of decision-making methods.

The Double Hierarchy Linguistic Term Set (DHLTS) is an important extension of fuzzy linguistic approaches and consists of two sets of

linguistic terms that support each other [3]. In order to reflect the hesitations of decision makers in the DHLTS evaluation, the Double Hierarchy Hesitant Fuzzy Linguistic Term Set (DHHFLTS) is developed as an extension of DHLTS [4]. Similarity and distance measurements developed based on Double Hierarchy Unstable Fuzzy Linguistic Elements (DHHFLE) provide new methods and applications for DHHFLTSs [5]. DHHFLTs find an important application area especially in decision making problems and provide new approaches to classical methods [4, 6–9].

Correlation coefficient measurement, which is an important measurement tool in reflecting the strength of the linear relationship between two quantitative variables [10, 11], is used as an important solution method in decision making problems based on DHHFLE and DHHFLTS [3,

12]. The determination of correlation values based on fuzzy information is carried out on the basis of statistics and information energy calculation [11, 13]. While statistical-based correlation calculation defines the relationship between variables in the $[-1,1]$ range, the correlation value calculated with less data based on information energy is defined in the $[0,1]$ range.

The first correlation calculation studies for fuzzy membership functions [14] are extended for fuzzy, heuristic fuzzy and hesitant fuzzy sets [13, 15]. The extension of the application area enables the development of correlation coefficient calculations for hesitant fuzzy sets and double hierarchy hesitant fuzzy sets [16, 17]. The use of linguistic information, which is evaluated in terms of information entropy, in correlation measure constitutes an important field of study [18]. In this context, correlation calculations based on information energy are used in hesitant fuzzy sets [19], hesitant fuzzy linguistic terms [20] and dual hesitant fuzzy sets [15].

Identifying and directing talents in sports is an important step in achieving athletic success. Achieving success in team sports depends on positioning the player in the game position that best suits their characteristics and abilities [21]. Achieving success in football depends on determining the relationship between the characteristics of the field positions and the skills of the players [22]. Assigning the most suitable player to positions under these multiple attributes emerges as a multi-attribute decision-making problem. Evaluation of players and positions and assignment of players according to field positions are decided by qualitative evaluations based on the knowledge and experience of the coaches.

DHHFLTS is an appropriate evaluation method in defining the characteristics and expectations of players and positions in player selection problems based on linguistic evaluation. Correlation coefficient measurements based on DHHFLTS are identified as an important decision-making tool in reflecting the fit between player and position based on assessments with DHHFLTS. Fuzzy linguistic expressions are directly converted to classical values by

calculating the degree of membership in the current correlation measurement application based on DHHFLTSs. This method prevents adequately reflecting the hesitancies of the linguistic assessments in the correlation calculations. Elimination of this drawback in the current method constitutes the main motivation of the study.

This study proposes a new correlation coefficient measurement model that integrates linguistic assessments into calculations with primary and secondary definition values of DHHFLTSs. The validity and applicability of the model is observed by considering the player selection problem in football, which is a novel MADM problem for DHHFLTSs evaluations. The case study aims to measure the correlation coefficient between the skills of the players and needs of the positions that are defined by DHHFLTS and to assign the most suitable player to the field positions. The proposed method and application case study constitute the original features of the study.

The organization of the study is as follows: Section 2 mentions the basic definitions of DHLTS and DHHFLTS and explains their arithmetic operations. In Section 3, DHHFLTS-based covariance, variance and correlation coefficient measurement models are discussed. Section 4 describes the original model proposed for the development of the current model based on DHHFLTS. Section 5 deals with the player selection problem to prove the validity of the proposed method and the results are compared with the current methods. The conclusion section, Section 6, makes an overall assessment based on the study results and makes recommendations for future studies.

2. Preliminaries

Linguistic terms, which are an important evaluation tool in complex decision making problems, are extended with fuzzy linguistic terms so that the decision maker's evaluations can be expressed more easily and clearly [23]. This section discusses extensions of linguistic term sets that incorporate decision-makers' assessments in detail and hesitancies.

2.1. Double hierarchy linguistic term sets

DHLTS consists of two hierarchical structures as the primary hierarchy being the primary linguistic term set (LTS) and the secondary hierarchy describing the primary linguistic term set [4]. DHLTS was developed to provide a detailed description of linguistic considerations expressed using the Hesitant Fuzzy Linguistic Term Set (HFLT) [3], [23]. $S = \{s_t \mid t = -\tau, \dots, -1, 0, 1, \dots, \tau\}$ first hierarchy LTS and $O^t = \{o_k^t \mid k = -\zeta, \dots, -1, 0, 1, \dots, \zeta\}$ is the second hierarchy LTS of s_t , the mathematical definition of DHLTS is as follows:

$$S_O = s_{t(o_k)} \mid t = -\tau, \dots, -1, 0, 1, \dots, \tau; k = -\zeta, \dots, -1, 0, 1, \dots, \zeta \tag{1}$$

in the equation $s_{t(o_k)}$ is defined as DHLT, and o_k defines different degrees of the linguistic term s_t . Figure 1 shows the semantic distribution of DHLTS for $\tau = 3$ and $\zeta = 3$. The second hierarchy LTS of the first hierarchy linguistic term s_1 is defined as $O^1 = \{o_k^1 \mid k = -3, -2, -1, 0, 1, 2, 3\}$ [24].

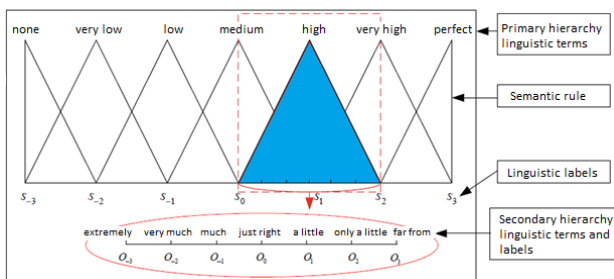


Figure 1. Definition of a linguistic term in LTS in the primary hierarchy with the secondary hierarchy LTS [24]

According to the t value of the first hierarchy LTS, the order and expressions of the secondary hierarchy LTS change. For example, if $t \geq 0$ in Figure 1, the second hierarchy LTS is in ascending order ($O^{\geq 0} = \{o_{-3} = \text{far from}, o_{-2} = \text{only a little}, o_{-1} = \text{a little}, o_0 = \text{just right}, o_1 = \text{much}, o_2 = \text{very much}, o_3 = \text{extremely}\}$), while if $t \leq 0$ the LTS of the second hierarchy decreases ($O^{\leq 0} = \{o_{-3} = \text{extremely}, o_{-2} = \text{very much}, o_{-1} = \text{much}, o_0 = \text{just right}, o_1 = \text{a little}, o_2 = \text{only a little}, o_3 = \text{far from}\}$). Also, when $t = \tau$, the second hierarchy is $O = \{o_k \mid k = -\zeta, \dots, -1, 0\}$ of LTS, while $t = -\tau$, the second hierarchy is considered the $O = \{o_k \mid k = 0, 1, \dots, \zeta\}$ part of LTS [5, 8].

2.2. Double hierarchy hesitant fuzzy linguistic term sets

DHHFLTS, which emerged as an extension of DHLTS, takes into account the hesitations of experts in the evaluation process in the decision-making process [4]. The mathematical expression of DHHFLTS defined in X , with S_O being DHLTS, is as follows:

$$H_{S_O} = \{ \langle x_i, h_{S_O}(x_i) \rangle \mid x_i \in X \} \tag{2}$$

in the equation Double Hierarchy Hesitant Fuzzy Linguistic Element (DHHFLE) $h_{S_O}(x_i) = \{ s_{\phi_l(o_{\varphi_l})}(x_i) \mid s_{\phi_l(o_{\varphi_l})} \in S_O; l = 1, \dots, L; \phi_l = -\tau, \dots, 0, \dots, \tau; \varphi_l = -\zeta, \dots, 0, \dots, \zeta \}$ denotes the possible degree of linguistic variable from x_i to S_O . L denotes the number of DHLTs in $h_{S_O}(x_i)$. The envelopment method of DHHFLEs provides a more comfortable understanding of DHHFLTS [24]. Functions that perform the conversion of continuous DHLTSs defined as $\bar{S}_O = \{ s_{\phi_l(o_{\varphi_l})}(x_i) \mid \phi_l \in [-\tau, \tau], \varphi_l \in [-\zeta, \zeta] \}$ to real numbers (f) and returning ϕ_l and φ_l of the DHLT equivalent to γ_l membership degree (f^{-1}) are defined as follows [24]:

$$f: [-\tau, \tau] \times [-\zeta, \zeta] \rightarrow [0, 1], f(\phi_l, \varphi_l) = \frac{\varphi_l + (\tau + \phi_l)\zeta}{2\tau\zeta} = \gamma_l \tag{3}$$

$$f^{-1}: [0, 1] \rightarrow [-\tau, \tau] \times [-\zeta, \zeta], f^{-1}(\gamma_l) \tag{4}$$

The calculations of the transformation function, $f^{-1}(\gamma_l)$ according to the values of the membership degree (γ_l) are as follows [12, 24]:

- if $\gamma_l = 1$ then $f^{-1}(\gamma_l) = s_{\tau(o_0)}$
- if $1 \leq 2\tau\gamma_l - \tau < \tau$ then $f^{-1}(\gamma_l) = S_{[2\tau\gamma_l - \tau]}(o_{\zeta(2\tau\gamma_l - \tau - [2\tau\gamma_l - \tau])})$
- if $-1 \leq 2\tau\gamma_l - \tau \leq 1$ then $f^{-1}(\gamma_l) = s_{0(o_{\zeta(2\tau\gamma_l)})}$
- if $-\tau \leq 2\tau\gamma_l - \tau \leq -1$ then $f^{-1}(\gamma_l) = S_{[2\tau\gamma_l - \tau] + 1}(o_{\zeta(2\tau\gamma_l - \tau - [2\tau\gamma_l - \tau] - 1)})$
- if $\gamma_l = -1$ then $f^{-1}(\gamma_l) = s_{-\tau(o_0)}$

HFEs and Hesitant Fuzzy Sets (HFS) consist of membership degrees defined for DHHFLEs. The transformations between DHHFLE (h_{S_0}) and HFE (h_γ) are calculated with the functions F and F^{-1} , respectively [6, 24]:

$$F(h_{S_0}) = F\left(\left\{s_{\phi_l(\varphi_l)} \mid s_{\phi_l(\varphi_l)} \in S_0; l = 1, \dots, L; \phi_l \in [-\tau, \tau]; \varphi_l \in [-\zeta, \zeta]\right\}\right) = \{\gamma_l \mid \gamma_l = f(\phi_l, \varphi_l)\} = h_\gamma \quad (5)$$

$$F^{-1}(h_\gamma) = F^{-1}(\{\gamma_l \mid \gamma_l \in [0,1]; l = 1, \dots, L\}) = \left\{s_{\phi_l(\varphi_l)} \mid \phi_l(\varphi_l) = f^{-1}(\gamma_l)\right\} = h_{S_0} \quad (6)$$

3. Correlation Calculation for DHHFLTSS

The correlation coefficient is an important evaluation tool that defines the size and direction of the relationship between two variables [11]. Extended correlation coefficient calculations with fuzzy methods help to make the most appropriate matches in complex decision making problems [25]. This section discusses the correlation calculation method based on DHHFLTSS defined by hesitant fuzzy linguistic evaluations.

Correlation coefficient calculations are made based on the means of DHHFLE and the mean and variances of DHHFLTSS by considering the degree of hesitancy, which is an important indicator in the evaluation process [26]. DHHFLTSS $S_0 = \{s_{t_{(o_k)}} \mid t = -\tau, \dots, 0, \dots, \tau; k = -\zeta, \dots, 0, \dots, \zeta\}$ defined for DHHFLE, h_{S_0} and the mean, \bar{h}_{S_0} and the hesitancy degree, $\eta(h_{S_0})$ are calculated as [24, 26]:

$$\bar{h}_{S_0} = f^{-1}\left(\frac{1}{L} \sum_{l=1}^L f(\phi_l, \varphi_l)\right) \quad (7)$$

$$\eta(h_{S_0}) = \frac{1}{\sqrt{\frac{1}{L} \sum_{l=1}^L \left(f(\phi_l, \varphi_l) - \frac{1}{L} \sum_{l=1}^L f(\phi_l, \varphi_l)\right)^2}} \quad (8)$$

Example 1: The average and hesitancy degrees of $h_{S_0}^1 = \{s_{0_{(o_{-1})}}, s_{1_{(o_0)}}, s_{2_{(o_{-2})}}\}$ and $h_{S_0}^2 = \{s_{-2_{(o_2)}}, s_{-1_{(o_1)}}, s_{0_{(o_{-3})}}\}$ DHHFLEs, including DHHFLTSS $S_0 = \{s_{t_{(o_k)}} \mid t \in [-3,3]; k \in [-3,3]\}$, are calculated as follows:

$$\bar{h}_{S_0}^1 = f^{-1}(1/3 (4/9+2/3+13/18)) = s_{0_{(2)}}$$

$$\bar{h}_{S_0}^2 = f^{-1}(1/3 (5/18+7/18+1/3)) = s_{-1_{(0)}}$$

$$\eta(h_{S_0}^1) = \frac{1}{\sqrt{\frac{1}{L_1} \sum_{l=1}^{L_1} \left(f(\phi_l^1, \varphi_l^1) - \frac{1}{L_1} \sum_{l=1}^{L_1} f(\phi_l^1, \varphi_l^1)\right)^2}} = 0.120$$

$$\eta(h_{S_0}^2) = \frac{1}{\sqrt{\frac{1}{L_2} \sum_{l=1}^{L_2} \left(f(\phi_l^2, \varphi_l^2) - \frac{1}{L_2} \sum_{l=1}^{L_2} f(\phi_l^2, \varphi_l^2)\right)^2}} = 0.045$$

The means and hesitancy degrees of DHHFLEs, $h_{S_0}^1$ and $h_{S_0}^2$ are calculated as $s_{0_{(2)}}$ and $s_{-1_{(0)}}$ and 0.120 and 0.045, respectively. Considering the Euclidean distance between DHHFLEs, the correlation coefficient between two DHHFLTSS ($H_{S_0}^1, H_{S_0}^2$) is calculated as [24, 27]:

$$\rho(H_{S_0}^1, H_{S_0}^2) = \frac{c(H_{S_0}^1, H_{S_0}^2)}{\sqrt{\text{var}(H_{S_0}^1)} \sqrt{\text{var}(H_{S_0}^2)}} = \frac{\sum_{i=1}^n \left[\frac{1}{L_1^i} \sum_{l=1}^{L_1^i} f(\phi_{l_1}^i, \varphi_{l_1}^i) - \bar{H}_{S_0}^1 \right] \left[\frac{1}{L_2^i} \sum_{l=1}^{L_2^i} f(\phi_{l_2}^i, \varphi_{l_2}^i) - \bar{H}_{S_0}^2 \right]}{\sqrt{\left(\sum_{i=1}^n \left(\frac{1}{L_1^i} \sum_{l=1}^{L_1^i} f(\phi_{l_1}^i, \varphi_{l_1}^i) - \bar{H}_{S_0}^1 \right)^2 \right) \left(\sum_{i=1}^n \left(\frac{1}{L_2^i} \sum_{l=1}^{L_2^i} f(\phi_{l_2}^i, \varphi_{l_2}^i) - \bar{H}_{S_0}^2 \right)^2 \right)}} \quad (9)$$

in the equation, the denominator defines the square root of the product of the variances of the hesitant sets, and the variance of $\bar{H}_{S_0}^1$ DHHFLTSS is calculated as [4, 24]:

$$\text{Var}(H_{S_0}) = \frac{1}{n} \left(\sum_{i=1}^n \left(\frac{1}{L_1^i} \sum_{l=1}^{L_1^i} f(\phi_{l_1}^i, \varphi_{l_1}^i) - \bar{H}_{S_0} \right)^2 \right) \quad (10)$$

in the equation, \bar{H}_{S_0} defines the mean of DHHFLTSS and is calculated as [24]:

$$\bar{H}_{S_0} = F^{-1}\left(\frac{1}{n} \sum_{i=1}^n \left(\frac{1}{L^i} \sum_{l=1}^{L^i} f(\phi_l^i, \varphi_l^i) \right)\right) \quad (11)$$

The correlation value between the DHHFLTSS ($H_{S_0}^1, H_{S_0}^2$) is expected to meet the basic Pearson

correlation coefficient conditions. The expected conditions are as follows [12]:

- $\rho(H_{S_0}^1, H_{S_0}^2) = \rho(H_{S_0}^2, H_{S_0}^1)$
- $\rho(H_{S_0}^1, H_{S_0}^1) = 1$
- $-1 \leq \rho(H_{S_0}^1, H_{S_0}^2) \leq 1$

Example 2: In calculating the correlation coefficient between $H_{S_0}^1$ and $H_{S_0}^2$ DHHFLTS defined in $S_0 = \{s_{t(o_k)} \mid t \in [-3, 3]; k \in [-3, 3]\}$ DHLTS, firstly, the membership degrees of each DHHFLTS elements are calculated using Equation 3.

$$H_{S_0}^1 = \left\{ \begin{array}{l} \{s_{0(o_{-2})}, s_{1(o_0)}, s_{2(o_{-1})}\}, \\ \{s_{1(o_1)}, s_2\}, \{s_{1(o_{-3})}, s_{2(o_2)}, s_{3(o_{-2})}\} \end{array} \right\}$$

$$H_{S_0}^2 = \left\{ \begin{array}{l} \{s_{-1(o_0)}\}, \{s_{-2(o_3)}, s_{-1(o_{-2})}, s_{0(o_2)}\}, \\ \{s_{1(o_0)}, s_{2(o_{-3})}, s_{3(o_{-1})}\} \end{array} \right\}$$

$$f_{11}^1 = 7/18, f_{12}^1 = 2/3, f_{13}^1 = 13/18, \bar{f}_1^1 = (1/3 (7/8 + 2/3 + 13/18)) = 16/27$$

$$f_{21}^1 = 13/18, f_{22}^1 = 5/6, \bar{f}_2^1 = (1/2 (13/18 + 5/6)) = 7/9$$

$$f_{31}^1 = 1/2, f_{32}^1 = 17/18, f_{33}^1 = 8/9, \bar{f}_3^1 = (1/3 (1/2 + 17/18 + 8/9)) = 7/9$$

$$\bar{H}_{S_0}^1 = (1/3 (16/27 + 7/9 + 7/9)) = 58/81$$

$$f_{11}^2 = 1/3, f_{12}^2 = 1/2, f_{13}^2 = 1/2, \bar{f}_1^2 = (1/3 (1/3 + 1/2 + 1/2)) = 4/9$$

$$f_{21}^2 = 1/3 = \bar{f}_2^2$$

$$f_{31}^2 = 2/3, f_{32}^2 = 2/3, \bar{f}_3^2 = (1/2 (2/3 + 2/3)) = 2/3$$

$$\bar{H}_{S_0}^2 = (1/3 (4/9 + 1/3 + 2/3)) = 13/27$$

The covariance between DHHFLTSs is calculated as [12, 24]:

$$C(H_{S_0}^1, H_{S_0}^2) = \frac{1}{n} \left(\sum_{i=1}^n \left[\frac{1}{L_1^i} \sum_{l_1}^{L_1^i} f(\phi_{l_1}^i, \phi_{l_1}^i) - \bar{H}_{S_0}^1 \right] \left[\frac{1}{L_2^i} \sum_{l_2}^{L_2^i} f(\phi_{l_2}^i, \phi_{l_2}^i) - \bar{H}_{S_0}^2 \right] \right) \quad (12)$$

The covariance value between $H_{S_0}^1, H_{S_0}^2$ is calculated according to Equation 12 as follows:

$$C(H_{S_0}^1, H_{S_0}^2) = 1/3((16/27-58/81)(4/9-13/27) + (7/9-58/81)(1/3-13/27)+(7/9-58/81)(2/3-13/27)) = 0.0023$$

The variation values of the DHHFLTSs are obtained as (Eq. 10).

$$Var(H_{S_0}^1) = \sqrt{(1/3 ((16/27-58/81)^2+(7/9-58/81)^2+(7/9-58/81)^2))} = 0.0076$$

$$Var(H_{S_0}^2) = \sqrt{(1/3 ((4/9-13/27)^2+(1/3-13/27)^2+(2/3-13/27)^2))} = 0.0192$$

The correlation coefficient value between DHHFLTSs ($H_{S_0}^1, H_{S_0}^2$) is calculated according to Equation 9 as follows:

$$\rho(H_{S_0}^1, H_{S_0}^2) = 0.0023 / \sqrt{(0.0076 * 0.192)} = 0.1890$$

The correlation result shows weak positive correlation between $H_{S_0}^1$ and $H_{S_0}^2$ DHHFLTS.

When attributes are defined with different weights in Multi-Attribute Decision Problems (MADM), the correlation coefficient between DHHFLTSs is found by including attribute weights in the calculations [24]. The weight of each element in the DHHFLTS defined in $S_0 = \{s_{t(o_k)} \mid t \in [-\tau, \tau], k \in [-\phi, \phi]\}$ is $w_i \in [0, 1]$ and the weights of the elements are defined as $w = \{w_1, w_2, \dots, w_n\}^T$ and $\sum_{i=1}^n w_i = 1$. The correlation coefficient between DHHFLTSs ($H_{S_{0_1}}, H_{S_{0_2}}$) based on the weighted hesitancy degree is calculated as follows [12, 24]:

$$\rho_w(H_{S_0}^1, H_{S_0}^2) = \frac{c_w(H_{S_0}^1, H_{S_0}^2)}{\sqrt{\text{Var}_w(H_{S_0}^1)}\sqrt{\text{Var}_w(H_{S_0}^2)}} = \frac{\sum_{i=1}^n \left[\frac{w_i}{L^1} \sum_{l=1}^{L^1} f(\phi_{l1}^i, \varphi_{l1}^i) - \bar{H}_{S_0}^{1w} \right] \left[\frac{w_i}{L^2} \sum_{l=1}^{L^2} f(\phi_{l2}^i, \varphi_{l2}^i) - \bar{H}_{S_0}^{2w} \right]}{\sqrt{\left(\sum_{i=1}^n \left(\frac{w_i}{L^1} \sum_{l=1}^{L^1} f(\phi_{l1}^i, \varphi_{l1}^i) - \bar{H}_{S_0}^{1w} \right)^2 \right)} \sqrt{\left(\sum_{i=1}^n \left(\frac{w_i}{L^2} \sum_{l=1}^{L^2} f(\phi_{l2}^i, \varphi_{l2}^i) - \bar{H}_{S_0}^{2w} \right)^2 \right)}} \quad (13)$$

in the equation, the weighted mean ($\bar{H}_{S_0}^w$) and weighted variance ($\text{Var}_w(H_{S_0})$) for DHHFLTSS ($H_{S_0}^1, H_{S_0}^2$) are defined, respectively, as follows [24]:

$$\bar{H}_{S_0}^w = F^{-1} \left(\frac{1}{n} \sum_{i=1}^n \left(\frac{w_i}{L^i} \sum_{l=1}^{L^i} f(\phi_{li}^i, \varphi_{li}^i) \right) \right) \quad (14)$$

$$\text{Var}_w(H_{S_0}) = \sqrt{\frac{1}{n} \left(\sum_{i=1}^n \left(\frac{w_i}{L^i} \sum_{l=1}^{L^i} f(\phi_{li}^i, \varphi_{li}^i) - \bar{H}_{S_0}^w \right)^2 \right)} \quad (15)$$

If weights are not defined for DHHFLEs, the elements are assumed to be equally weighted and the weighted correlation coefficient (p_w) calculation is reduced to the normal correlation calculation (p). The conditions provided by the weighted correlation coefficient (p_w) are as follows [12]:

- $\rho_w(H_{S_0}^1, H_{S_0}^2) = \rho_w(H_{S_0}^2, H_{S_0}^1)$
- $\rho_w(H_{S_0}^1, H_{S_0}^1) = 1$
- $-1 \leq \rho_w(H_{S_0}^1, H_{S_0}^2) \leq 1$

Example 3: If the weight values of the x_i attributes of $H_{S_0}^1$ and $H_{S_0}^2$ DHHFLTSS in Example 2 are defined as $w = (0.2, 0.5, 0.3)^T$, the weighted mean values $\bar{H}_{S_0}^{1w} = 0.247$ and $\bar{H}_{S_0}^{2w} = 0.152$, variation values $\text{Var}_w(H_{S_0}^1) = 0.123$ and $\text{Var}_w(H_{S_0}^2) = 0.0022$, covariation value $C_w(H_{S_0}^1, H_{S_0}^2) = 0.0032$ and the correlation coefficient value is calculated as $\rho_w(H_{S_0}^1, H_{S_0}^2) = 0.616$. According to the results of

Example 2, the direction of the relationship does not change, but its size increases.

4. New Correlation Coefficient Measurement Proposal for DHHFLTSS

The proposed method aims to continue the correlation coefficient calculation process on real linguistic terms rather than the direct use of membership degrees of DHHFLTSSs. The method performs aggregation operations on primary and secondary linguistic terms of linguistic term sets and obtains new DHHFLEs. Covariance, variance and correlation coefficient calculations are made by calculating the membership degrees of the obtained DHHFLEs.

So is DHLTS and the aggregation operations of primary and secondary hierarchical degrees of DHHFLEs, $h_{S_0}(x_i) = \{s_{\phi_{l(o\varphi_l)}(x_i)} \mid s_{\phi_{l(o\varphi_l)}} \in S_0; l=1, \dots, L; \phi_l = -\tau, \dots, 0, \dots, \tau; \varphi_l = -\zeta, \dots, 0, \dots, \zeta\}$ of DHHFLTSS defined in X and the combined DHHFLTSS definitions are applied as follows:

$$\phi' = \frac{1}{L} \sum_{l=1}^L \phi_l \text{ and } \varphi' = \frac{1}{L} \sum_{l=1}^L \varphi_l \quad (16)$$

$$h_{S_0} = \cup_{s_{\phi_{l(o\varphi_l)}} \in h_{S_0}} \left\{ s_{\phi'_{(o\varphi')}} \mid \phi' \leq \tau; \varphi' \leq \zeta \right\} \quad (17)$$

in the equation, L represents the number of DHLTS in $h_{S_0}(x_i)$. The covariance ($C(\dot{H}_{S_0}^1, \dot{H}_{S_0}^2)$), variance ($\text{Var}(\dot{H}_{S_0})$) and correlation coefficient ($\rho'(\dot{H}_{S_0}^1, \dot{H}_{S_0}^2)$) among the combined DHHFLEs obtained from DHHFLTSS ($\dot{H}_{S_0}^1, \dot{H}_{S_0}^2$) are calculated as follows:

$$C(\dot{H}_{S_0}^1, \dot{H}_{S_0}^2) = \frac{1}{n} \left(\sum_{i=1}^n \left[f \left((\phi_{11}^i, \varphi_{11}^i) - \bar{H}_{S_0}^1 \right) \right] \left[f \left((\phi_{21}^i, \varphi_{21}^i) - \bar{H}_{S_0}^2 \right) \right] \right) \quad (18)$$

$$\text{Var}(\dot{H}_{S_0}) = \sqrt{\frac{1}{n} \left(\sum_{i=1}^n \left(f \left((\phi_{11}^i, \varphi_{11}^i) - \bar{H}_{S_0} \right) \right)^2 \right)} \quad (19)$$

$$\rho'(\dot{H}_{S_0}^1, \dot{H}_{S_0}^2) = \frac{C(\dot{H}_{S_0}^1, \dot{H}_{S_0}^2)}{\sqrt{\text{Var}(\dot{H}_{S_0}^1, \dot{H}_{S_0}^2)}}$$

$$= \frac{\sum_{i=1}^n [f((\phi_{1,1}^i, \phi_{1,1}^i) - \bar{H}_{S_0})][f((\phi_{2,2}^i, \phi_{2,2}^i) - \bar{H}_{S_0}^2)]}{\sqrt{\left(\sum_{i=1}^n \left(f((\phi_{1,1}^i, \phi_{1,1}^i) - \bar{H}_{S_0})\right)^2\right) \left(\sum_{i=1}^n \left(f((\phi_{2,2}^i, \phi_{2,2}^i) - \bar{H}_{S_0}^2)\right)^2\right)}} \quad (20)$$

in the equation, the mean of DHHFLTS, \bar{H}_{S_0} , is defined as:

$$\bar{H}_{S_0} = \left(\frac{1}{n} \sum_{i=1}^n \phi^i, \frac{1}{n} \sum_{i=1}^n \phi^i\right) \quad (21)$$

The proposed method meets the basic Pearson correlation coefficient conditions, and the conditions for DHHFLTSs ($\dot{H}_{S_0}^1, \dot{H}_{S_0}^2$) are expressed as:

- $\rho'(\dot{H}_{S_0}^1, \dot{H}_{S_0}^2) = \rho'(\dot{H}_{S_0}^2, \dot{H}_{S_0}^1)$
- $\rho'(\dot{H}_{S_0}^1, \dot{H}_{S_0}^1) = 1$
- $-1 \leq \rho'(\dot{H}_{S_0}^1, \dot{H}_{S_0}^2) \leq 1$

If the attributes are weighted, the weighted correlation coefficient calculation method for DHHFLTSs ($H_{S_{01}}, H_{S_{02}}$) is recommended as follows:

$$\rho'_w(\dot{H}_{S_0}^1, \dot{H}_{S_0}^2) = \frac{c_w(\dot{H}_{S_0}^1, \dot{H}_{S_0}^2)}{\sqrt{\text{var}_w(\dot{H}_{S_0}^1, \dot{H}_{S_0}^2)}} = \frac{\sum_{i=1}^n [w_i f((\phi_{1,1}^i, \phi_{1,1}^i) - \bar{H}_{S_0}^1)][w_i f((\phi_{2,2}^i, \phi_{2,2}^i) - \bar{H}_{S_0}^2)]}{\sqrt{\sum_{i=1}^n (w_i f((\phi_{1,1}^i, \phi_{1,1}^i) - \bar{H}_{S_0}^1))^2 \sum_{i=1}^n (w_i f((\phi_{2,2}^i, \phi_{2,2}^i) - \bar{H}_{S_0}^2))^2}} \quad (22)$$

The basic correlation coefficient conditions provided by the proposed weighted method (p'_w) are as follows:

- $\rho'_w(H_{S_0}^1, H_{S_0}^2) = \rho'_w(H_{S_0}^2, H_{S_0}^1)$
- $\rho'_w(H_{S_0}^1, H_{S_0}^1) = 1$
- $-1 \leq \rho'_w(H_{S_0}^1, H_{S_0}^2) \leq 1$

The proposed method is applied in the case study and its application steps are explained in the Section 5. The validity of the method is proved by comparing with the current method.

5. Case Study: Assignment of Players to The Positions in Football

Identifying the right player in the right position, which ensures success in team games, cannot be done with mathematical calculations [22]. The assignment of the player to the position takes place with the expertise gained from the experience and observations of the coaches [28]. This case study aims to identify and assign the most suitable players for goal, defender, midfielder and forward football positions according to their physical, technical and mental characteristics [22, 29]. The skills required for the positions and the level of players to have these skills are defined by the expert coach with DHHFLTs. The most suitable player for the position is selected based on the highest level of correlation with the position requirements. The proposed correlation coefficient method based on the DHHFLTS is used to define the fit between positions and players. The positive and highest correlation coefficient value ($\in [-1,1]$) defines the player most suitable for the position.

The basic skills used in determining the relationship between the position and the football players are defined in the main titles as physical, mental and technical. Characteristics of basic skills are as follows [22, 29, 30]:

- Physical: speed, agility, jumping, acceleration, height, strength
- Mental: ability to read the game, leadership, creativity, calmness, courage, belief in decision
- Technical: finishing, passing, shooting, heading, tackle, dribbling.

The basic skills expected for the positions are as follows [22, 29, 30]:

- Goal: height, reflex, high jump, flexibility, balance, playmaking
- Defender: strong physics, effectiveness in airballs, speed, move timing, passing ability
- Midfield: ability to read the game, passing ability, ball control, possession of the ball, calmness
- Forward: shooting, power, passing ability, speed, ball efficiency, ball control, reading the game.

Table 1. Double hierarchy linguistic expressions of expected properties for positions

	Physical	Mental	Technical
Goal	only a little good	far from very good	between a little medium and a little very good
Defender	between only a little very good and a little perfect	just right good	between good and far from perfect
Midfielder	only a little good	between a little very good and far from perfect	just right very good
Forward	between very much good and only a little perfect	between extremely medium and very much very good	a little very good

The case study aims to assign four player (A_1 , Burak; A_2 , Mehmet; A_3 , Servet; A_4 , Umut) candidates to four game positions (R_1 , Goal; R_2 , Defense; R_3 , Midfielder; R_4 , Forward) based on three general characteristics (P_1 , Physical; P_2 , Mental; P_3 , Technical). The primary (S) and secondary (O) hierarchical LTSs of DHHFLTS, $H_{S_O} = \{ \langle x_i, h_{(S_O)}(x_i) \rangle \mid x_i \in X \}$ defined in X used in DHHFLEs, $h_{S_O}(x_i) = \{ s_{\phi_{l(o, \phi_l)}}(x_i) \mid s_{\phi_{l(o, \phi_l)}} \in S_O; l = 1, \dots, L; \phi_l = -\tau, \dots, 0, \dots, \tau; \phi_l = -\zeta, \dots, 0, \dots, \zeta \}$ to define the position and characteristics of the players are as follows.

$S = \{ s_{-3} = \text{none}, s_{-2} = \text{very bad}, s_{-1} = \text{bad}, s_0 = \text{medium}, s_1 = \text{good}, s_2 = \text{very good}, s_3 = \text{perfect} \}$

$O^- = \{ o_{-3} = \text{extremely}, o_{-2} = \text{very much}, o_{-1} = \text{much}, o_0 = \text{just right}, o_1 = \text{a little}, o_2 = \text{only a little}, o_3 = \text{far from}; \phi_l \leq 0 \}$

$O^+ = \{ o_{-3} = \text{far from}, o_{-2} = \text{only a little}, o_{-1} = \text{a little}, o_0 = \text{just right}, o_1 = \text{much}, o_2 = \text{very much}, o_3 = \text{extremely}; \phi_l \geq 0 \}$

Table 2. Double hierarchy linguistic expressions of player skills

	Physical	Mental	Technical
Burak	between far from medium and only a little medium	between a little medium and a little good	just right good
Mehmet	much very good	between very much medium and extremely very good	between just right good and far from perfect
Servet	between only a little medium and good	only a little perfect	between medium and extremely good
Umut	extremely very good	between extremely medium and a little very good	between good and perfect

Table 3. Definition position properties with DHHFLTS and transformations to HFLTEs

	Physical	Mental	Technical	Physical	Mental	Technical
Goal	$\{s_{1(o_{-2})}\}$	$\{s_{2(o_{-3})}\}$	$\{s_{0(o_{-1})}, s_{1}, s_{2(o_{-1})}\}$	$\{s_{1(o_{-2})}\}$	$\{s_{2(o_{-3})}\}$	$\{s_{1(o_{-1})}\}$
Defender	$\{s_{2(o_{-2})}, s_{3(o_{-1})}\}$	$\{s_{1(o_0)}\}$	$\{s_{1(o_0)}, s_{2}, s_{3(o_{-3})}\}$	$\{s_{2,5(o_{-1,5})}\}$	$\{s_{1(o_0)}\}$	$\{s_{2(o_{-3})}\}$
Midfielder	$\{s_{1(o_{-2})}\}$	$\{s_{2(o_{-1})}, s_{3(o_{-3})}\}$	$\{s_{2(o_0)}\}$	$\{s_{1(o_{-2})}\}$	$\{s_{2,5(o_{-2})}\}$	$\{s_{2(o_0)}\}$
Forward	$\{s_{1(o_2)}, s_{2}, s_{3(o_{-2})}\}$	$\{s_{0(o_3)}, s_{1}, s_{2(o_2)}\}$	$\{s_{2(o_{-1})}\}$	$\{s_{2(o_0)}\}$	$\{s_{1(o_{2,5})}\}$	$\{s_{2(o_{-1})}\}$

Table 4. Definition player skills with DHHFLTS and transformations to HFLTEs

	Physical	Mental	Technical	Physical	Mental	Technical
Burak	$\{s_{0(o_{-3})}, s_{0(o_{-2})}\}$	$\{s_{0(o_{-1})}, s_{1(o_{-1})}\}$	$\{s_{1(o_0)}\}$	$\{s_{0(o_{-2,5})}\}$	$\{s_{0,5(o_{-1})}\}$	$\{s_{1(o_0)}\}$
Mehmet	$\{s_{2(o_1)}\}$	$\{s_{0(o_2)}, s_{1}, s_{2(o_3)}\}$	$\{s_{1(o_0)}, s_{2}, s_{3(o_{-3})}\}$	$\{s_{2(o_1)}\}$	$\{s_{1(o_{2,5})}\}$	$\{s_{2(o_{-1,5})}\}$
Servet	$\{s_{0(o_{-2})}, s_{1(o_0)}\}$	$\{s_{3(o_{-2})}\}$	$\{s_{0(o_0)}, s_{1(o_3)}\}$	$\{s_{0,5(o_{-2})}\}$	$\{s_{3(o_{-2})}\}$	$\{s_{0,5(o_3)}\}$
Umut	$\{s_{2(o_3)}\}$	$\{s_{0(o_3)}, s_{1}, s_{2(o_{-1})}\}$	$\{s_{1(o_0)}, s_{2}, s_{3(o_0)}\}$	$\{s_{2(o_3)}\}$	$\{s_{1(o_1)}\}$	$\{s_{2(o_0)}\}$

The application steps of the proposed correlation coefficient measurement method based on DHHFLTS are as follows:

Step 1. The skill characteristics expected for the positions and the characteristics of the players are defined in Table 1 and Table 2, respectively, using hesitant linguistic expressions.

Step 2. The linguistic domains defined in Table 1 and Table 2 are transformed to the DHHFLTSs in Table 3 and Table 4, respectively.

Step 3. The DHHFLTSs defined in Table 3 and Table 4 are aggregated using Equation 16, and mean HFLTEs are calculated for each position and player using Equation 21 (Table 3, Table 4).

Step 4. The membership degrees of the difference of the HFLTEs from the average HFLTEs are calculated using Equation 3. Variance values are calculated over the difference between positions and players from the average HFLTE using Equation 19 (Table 5, Table 6).

Step 5. Correlation coefficient values reflecting the relationship between positions and players are defined using Equation 20 (Table 7).

Table 5. Membership degrees and variance values of positions

	Physical	Mental	Technical	Variance
Goal	0.556	0.667	0.611	0.0021
Defender	0.833	0.667	0.667	0.0062
Midfielder	0.556	0.806	0.833	0.0156
Forward	0.833	0.806	0.778	0.0005

Table 6. Membership degrees and variance values of players

	Physical	Mental	Technical	Variance
Burak	0.361	0.528	0.667	0.0156
Mehmet	0.889	0.806	0.750	0.0033
Servet	0.472	0.889	0.750	0.0300
Umut	1.000	0.722	0.833	0.0130

According to the results of Table 7 and Figure 2, which reflect the relations between positions and

players, Servet is assigned to goal, Umut to defender, Burak to midfielder and Mehmet to forward. Umut is determined as the most unsuitable player for the goal position. Although Mehmet and Umut have equal similarity values for the defender, the most suitable person for the forward is determined as Mehmet and Umut is assigned to the defender position.

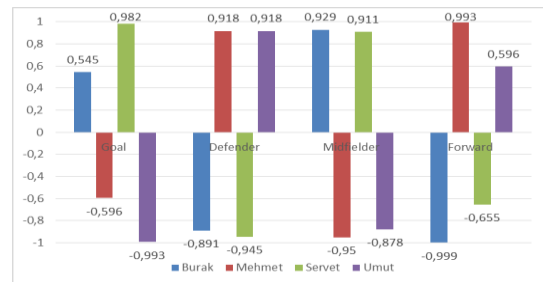


Figure 1. The Relationship between positions and players

While Burak is chosen as the most suitable person in the midfield, Mehmet is seen as the most unsuitable player for the midfield position. While Mehmet is assigned with the highest correlation value for the forward position, the most inappropriate player is determined as Burak.

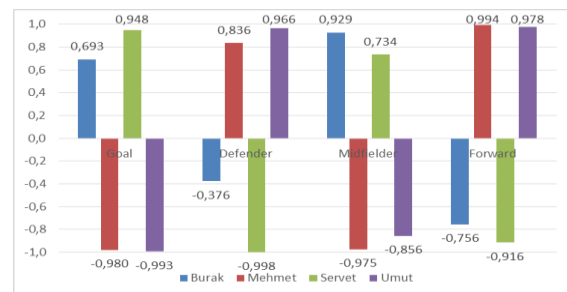


Figure 3. Position player relationship according to current method

The consistency and validity of the proposed method are revealed by comparing the proposed method with the current method (Figure 3). While Servet (0.948) is the most suitable player for the goal position, Umut (-0.993) and Mehmet (-0.980) are the most unsuitable players. Burak is the most suitable player for midfielder (0.929) with

Table 7. Correlation coefficient matrix reflecting position and player relationship

	Goal	Defender	Midfielder	Forward	Position
Burak	0.545	-0.891	0.929	-0.999	Midfielder
Mehmet	-0.596	0.918	-0.950	0.993	Forward
Servet	0.982	-0.945	0.911	-0.655	Goal
Umut	-0.993	0.918	-0.878	0.596	Defender

While it is necessary to choose between Mehmet and Umut between the forward and the defender, Mehmet is chosen with the highest correlation value (0.994) with the forward position and Umut (0.966) is appointed as the most suitable player for the defender.

Comparative evaluations show that the new method, which proposes to continue with the fuzzy calculation method, is consistent with the current method. By continuing the process with fuzzy calculations, the efficiency of hesitancy evaluations in calculations is increased and the power of reflecting the evaluations of the experts to the result increases.

6. Conclusion

Linguistic terms are an important tool in reflecting the evaluations of experts more easily in complex decision making problems. This study deals with the correlation coefficient-based decision making method using DHHFLT_Ss, which are an important tool in reflecting complex linguistic assessments. In the current method, the direct correlation coefficient calculation over the membership degrees of fuzzy evaluations based on DHFLT_S is seen as an important shortcoming.

The proposed method continues the calculation process of the correlation degree with hesitant linguistic evaluations, and hesitancy evaluations are included in the calculations. The proposed method deals with the original decision making problem as assigning the most suitable player to the positions in football. The existing and proposed new method are compared based on this decision-making problem and the consistency of the proposed method is revealed with the results.

Future studies may include incorporating HFLT_S with different aggregation methods in correlation calculations based on DHHFLT_S. Thus, hesitant expressions are transferred to evaluation processes more comprehensively. In addition, the proposed method can be applied to different and comprehensive decision making problems.

Article Information Form

Funding

The author(s) has no received any financial support for the research, authorship or publication of this study.

The Declaration of Conflict of Interest/ Common Interest

No conflict of interest or common interest has been declared by the authors.

The Declaration of Ethics Committee Approval

This study does not require ethics committee permission or any special permission.

The Declaration of Research and Publication Ethics

The authors of the paper declare that they comply with the scientific, ethical and quotation rules of SAUJS in all processes of the paper and that they do not make any falsification on the data collected. In addition, they declare that Sakarya University Journal of Science and its editorial board have no responsibility for any ethical violations that may be encountered, and that this study has not been evaluated in any academic publication environment other than Sakarya University Journal of Science.

Copyright Statement

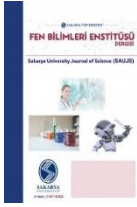
Authors own the copyright of their work published in the journal and their work is published under the CC BY-NC 4.0 license.

References

- [1] A. S. Yalcin, H. S. Kilic, "Green supplier selection via an integrated multi-attribute decision making approach", Sakarya University Journal of Science, vol. 23, no 6, pp. 1066-1079, 2019.
- [2] L. A. Zadeh, R. A. Aliev, Fuzzy logic theory and applications: part I and part II. World Scientific Publishing, 2018.
- [3] X. Gou, H. Liao, Z. Xu, F. Herrera, "Double hierarchy hesitant fuzzy linguistic term set and MULTIMOORA method: A case of study to evaluate the

- implementation status of haze controlling measures”, *Information Fusion*, vol. 38, pp. 22-34, 2017.
- [4] X. Gou, H. Liao, Z. Xu, F. Herrera, “Double hierarchy hesitant fuzzy linguistic term set and MULTIMOORA method: A case of study to evaluate the implementation status of haze controlling measures”, *Information Fusion*, vol. 38, pp. 22-34, 2017.
- [5] X. Gou, Z. Xu, H. Liao, F. Herrera, “Multiple criteria decision making based on distance and similarity measures under double hierarchy hesitant fuzzy linguistic environment”, *Computers & Industrial Engineering*, vol. 126, pp. 516-530, 2018.
- [6] X. Gou, Z. Xu, H. Liao, F. Herrera, “Multiple criteria decision making based on distance and similarity measures under double hierarchy hesitant fuzzy linguistic environment”, *Computers & Industrial Engineering*, vol. 126, pp. 516-530, 2018.
- [7] Z. Liu, X. Zhao, L. Li, X. Wang, D. Wang, “A novel multi-attribute decision making method based on the double hierarchy hesitant fuzzy linguistic generalized power aggregation operator”, *Information*, vol. 10, no 11, p. 339, 2019.
- [8] X. Gou, Z. Xu, “Managing noncooperative behaviors in large-scale group decision-making with linguistic preference orderings: The application in Internet venture capital”, *Information Fusion*, vol. 69, pp. 142-155, 2021.
- [9] X. Wang, X. Gou, Z. Xu, “Appessment of traffic congestion with ORESTE method under double hierarchy hesitant fuzzy linguistic environment”, *Applied Soft Computing*, vol. 86, p. 105864, 2020.
- [10] E. Gumus, “A Case Study on the Relationship between Water Quality Parameters: Bursa”, *Sakarya University Journal of Science*, vol. 26, no 5, pp. 867-878, 2022.
- [11] A. G. Asuero, A. Sayago, A. González, “The correlation coefficient: An overview”, *Critical reviews in analytical chemistry*, vol. 36, no 1, pp. 41-59, 2006.
- [12] R. Zhang, X. Gou, Z. Xu, “A multi-attribute decision-making framework for Chinese medicine medical diagnosis with correlation measures under double hierarchy hesitant fuzzy linguistic environment”, *Computers & Industrial Engineering*, vol. 156, p. 107243, 2021.
- [13] B. Chaudhuri, A. Bhattacharya, “On correlation between two fuzzy sets”, *Fuzzy Sets and Nostems*, vol. 118, no 3, pp. 447-456, 2001.
- [14] VOL. Murthy, S. Pal, D. D. Majumder, “Correlation between two fuzzy membership functions”, *Fuzzy sets and nostems*, vol. 17, no 1, pp. 23-38, 1985.
- [15] H. Garg, K. Kumar, “A novel correlation coefficient of intuitionistic fuzzysets based on the connection number of set pair analysis and its application”, *Scientia Iranica*, vol. 25, no 4, pp. 2373-2388, 2018.
- [16] Z. Ren, Z. Xu, H. Wang, “Dual hesitant fuzzy VIKOR method for multi-criteria group decision making based on fuzzy measure and new comparison method”, *Information Sciences*, vol. 388, pp. 1-16, 2017.
- [17] J. Montserrat-Adell, Z. Xu, X. Gou, N. Agell, “Free double hierarchy hesitant fuzzy linguistic term sets: An application on ranking alternatives in GDM”, *Information Fusion*, vol. 47, pp. 45-59, 2019.
- [18] T. Gerstenkorn, J. Mańko, “Correlation of intuitionistic fuzzy sets”, *Fuzzy sets and nostems*, vol. 44, no 1, pp. 39-43, 1991.
- [19] A. Singh, “Modified expreption to evaluate the correlation coefficient of dual hesitant fuzzy sets and its application to multi-attribute decision making”, *Fuzzy Nostems-Theory and Applications*, 2020.

- [20] R. Zhang, Z. Li, H. Liao, “Multiple-attribute decision-making method based on the correlation coefficient between dual hesitant fuzzy linguistic term sets”, *Knowledge-Based Systems*, vol. 159, pp. 186-192, 2018.
- [21] J. Lago-Ballesteros, VOL. Lago-Peñas, “Performance in team sports: Identifying the keys to success in soccer”, *Journal of Human kinetics*, vol. 25, no 1, pp. 85-91, 2010.
- [22] N. Razali, A. Mustapha, F. A. Yatim, R. Ab Aziz, “Predicting player position for talent identification in association football”, *IOP Conference Series: Materials Science and Engineering*, 2017, vol. 226, no 1, s. 012087.
- [23] Z. Ayağ, F. Samanlıoğlu, “A hesitant fuzzy linguistic terms set-based AHP-TOPSIS approach to evaluate ERP software packages”, *International Journal of Intelligent Computing and Cybernetics*, 2020.
- [24] X. Gou, Z. Xu, “Double hierarchy linguistic term set and its extensions”, *Double Hierarchy Linguistic Term Set and Its Extensions*, Springer, 2021, pp. 1-21.
- [25] M. Bhatia, H.D. Arora, N. Anjali “Some New Correlation Coefficient Measures Based on Fermatean Fuzzy Sets using Decision Making Approach in Pattern Analysis and Supplier Selection”, *International Journal of Mathematical*, 8 (2), 2023.
- [26] D. Li, W. Zeng, J. Li, “New distance and similarity measures on hesitant fuzzy sets and their applications in multiple criteria decision making”, *Engineering Applications of Artificial Intelligence*, vol. 40, pp. 11-16, 2015.
- [27] X. Gou, Z. Xu, W. Zhou, “Interval consistency repairing method for double hierarchy hesitant fuzzy linguistic preference relation and application in the diagnosis of lung cancer”, *Economic Research-Ekonomika Istraživanja*, vol. 34, no 1, pp. 1-20, 2021.
- [28] S. Buyrukoğlu, S. Savaş, “Stacked-Based Ensemble Machine Learning Model for Positioning Footballer”, *Arabian Journal for Science and Engineering*, pp. 1-13, 2022.
- [29] D. Barron, G. Ball, M. Robins, VOL. Sunderland, “Identifying playing talent in professional football using artificial neural networks”, *Journal of Sports Sciences*, vol. 38, no 11-12, pp. 1211-1220, 2020.
- [30] VOL. T. Woods, J. P. Veale, N. Collier, S. Robertson, “The use of player physical and technical skill match activity profiles to predict position in the Australian Football League draft”, *Journal of sports sciences*, vol. 35, no 4, pp. 325-330, 2017.



Investigation of the Effect of Ulexite Additive on the Mechanical Strength and Thermal Conductivity of Cement Mortar

Ahmet Filazi¹ , Muharrem Pul^{2*} , Zühtü Onur Pehlivanlı³ , İbrahim Uzun³ 

¹ Kırıkkale University, Kırıkkale Vocational School, Department of Construction, Kırıkkale, Türkiye, ahmetfilazi@kku.edu.tr

² Kırıkkale University, Kırıkkale Vocational School, Department of Electricity and Energy, Kırıkkale, Türkiye, mpul@kku.edu.tr

³ Kırıkkale University, Faculty of Engineering and Natural Sciences, Department of Mechanical Engineering, Kırıkkale, Türkiye, pehlivanli@kku.edu.tr, uzun@kku.edu.tr

*Corresponding Author

ARTICLE INFO

ABSTRACT

Keywords:

Ulexite
Pozzolanic activity
Compressive strength
Flexural strength
Thermal conductivity



Article History:

Received: 03.01.2023

Accepted: 28.05.2024

Online Available: 01.08.2024

In this study, the effect of ulexite substitution in cement mortar and its physical and mechanical properties on cement mortar properties were investigated. First of all, the pozzolanic activity of the ulexite material was determined. Then, cement mortars with ulexite additives at different rates (0.5%, 1%, 2%, 4%); Specific gravity, specific surface, setting start and end times, consistency and expansion tests, as well as 7 and 28 days flexural and compressive strength of the mortar samples were determined and compared with the control sample. As a result of the study, with the increase of the ulexite substitution ratio, the set start and set expiration times were extended, and all of the ulexite-substituted cement mortars provided the lowest mechanical strength required in related standard. It was observed that the cement mortars with 0.5%, 1%, 2% ulexite substituted cement mortars exceeded the reference sample and the best replacement rate was in the mortars with 0.5% replacement. However, depending on the increase in the ulexite substitution ratio, a decrease in mechanical strength was detected among themselves. According to the results obtained from the thermal conductivity tests, the thermal conductivity values of the cement mortars decreased with the ulexite substitution. Depending on the ulexite substitution rate, the thermal conductivity value decreased by approximately 50%. The lowest thermal conductivity value was measured in the test sample with 4% ulexite substitute.

1. Introduction

Cement production is one of the important industrial activities in terms of its contribution to greenhouse gas emissions, and approximately 5% of global carbon emissions originate from cement production. Various studies are carried out for an alternative binder or cement substitute materials to reduce the greenhouse effect of cement production. As a result of the studies, it is understood that pozzolanic materials can be a good alternative as a substitute material [1]. In addition, it is predicted that the use of pozzolanic

materials will be effective in reducing the CO₂ emissions caused by the production of Portland cement. One of the characteristics of pozzolanic materials is that they are light and heat resistant. It is also known that pozzolanic materials increase the fire resistance of concretes. In recent years, the use of fly ash, blast furnace slag (BFS) and silica fume as mineral additives in mixtures to provide high temperature resistance has become widespread [2]. Naturally, the element boron does not exist freely in nature; it typically combines with oxygen and other elements to form salts, commonly referred

to as "borates." Over 250 boron-bearing minerals have been identified worldwide, with the most common ones being sodium, calcium, or magnesium salts. Boron is a rare element in nature (with an average content of 10 ppm in the Earth's crust); however, extraordinary concentrations can be found in specific regions. The formation of borate deposits can be attributed to different groups; and borates, in an academic context, refer to compounds containing boric oxide. The most significant ones commercially include borax, kernite, ulexite, and colemanite [3]. Notable results have been obtained in some studies on cement mortars produced with boron mineral substitution. It has been evaluated that the materials with new properties to be produced can be used in different areas of the industry.

In a study in the literature, colemanite and ulexite were used separately as fillers in the preparation of epoxy composites. The effects of filler amount, hardener type and plasticizer addition on the properties of new composites were investigated by instrumental analyzes and tests. Improvements in tensile properties were achieved up to 5% wt filler content in composites. Compared to pure epoxy, water absorption decreased significantly with increasing filler amount. Excellent corrosion resistance and strong adhesion properties were observed in all composites. The cold resistance of the composites was quite high. Given these inherent advantages, it is conceivable that composites could find successful applications across a range of industries including construction, coating, and flooring [4].

Another study, specifically investigated the impact of borogypsum and calcineborogypsum on the physical properties of ordinary Portland cement (OPC). The results showed that increasing the borogypsum level from 5% to 7% in Portland cement resulted in an increase in setting time and a decrease in strength expansion and compressive strength. It was found that the cement prepared with borogypsum (5%) had similar strength properties to those obtained with natural gypsum, and a mixture containing 5% hemihydrate borogypsum developed 25% higher compressive strength than the OPC control mixtures in 28 days. Thus, the exploration of

using calcined borogypsum in cement applications is expected to yield superior outcomes compared to unprocessed borogypsum. Additionally, the utilization of hemihydrate borogypsum as a retarder for Portland cement holds promise in contributing to the reduction of environmental pollution [5]. A different study conducted an investigation into light concrete production using boron waste at varying ratios (1, 3, 5, 7, and 9%) as a substitute material.

The aim of this study was to achieve a water-resistant and lighter material with enhanced physical and mechanical properties compared to lightweight concrete. The findings of this study indicated that the physical and mechanical properties of the material improved with increasing boron waste content, with the most favorable results observed at the 9% boron waste substitution level. This suggests that by recycling environmentally harmful boron wastes commonly used in construction, a contribution to sustainability can be made [6]. Furthermore, an experimentally and analytically focused study was conducted to assess the impact of incorporating commercial boron carbide (B_4C) powder, with an average particle diameter of 2.64 μm , on the hydration reaction of Portland cement, along with the resulting mechanical and radiation shielding properties of concrete.

The findings indicated that the presence of sassolite in the studied B_4C powder led to a delayed hydration reaction for the initial 24 hours, followed by significant improvements in concrete strength with increasing boron carbide content, attributed to the filler effect. Furthermore, the incorporation of boron carbide was found to measurably enhance the neutron shielding capabilities of concrete mixes [7]. The compressive strength is widely recognized as one of the most vital parameters influenced by the addition of boron to concrete mixtures. The impact of boron addition on concrete compressive strength and other physical properties has been investigated through various studies [8-12]. In line with these findings, numerous studies have explored the applicability of boron wastes in cement production. For instance, one study indicated that the inclusion of tincal ore wastes in cement at a 1% displacement

level led to an enhancement in the qualities of Portland cement (PC), despite causing a delay in setting time. This suggests that tincal ore waste could potentially serve as an additive, replacing cement up to 5% [13]. Another experimental study noted that the 90th-day strength of concrete samples incorporating 4% colemanite waste, 5-15% natural pozzolan, and 81-96% Portland clinker ground cements achieved 90% of the strength observed in control samples. Furthermore, it was observed that concretes produced with higher levels of pozzolan cements exhibited superior 28th-day strength compared to those with lower levels of pozzolan content [14].

A different study delved into the properties of concretes containing varying percentages (0%, 3%, 5%, 10%, and 15%) of boron chips, evaluating parameters such as setting time, volumetric expansion, unit weight, consistency, compressive strength, and splitting tensile strength. This study explored the potential of boron chips as a concrete admixture. The findings suggested that concrete samples containing 3-5% boron chips exhibited higher compressive strength than control samples, and that 5-10% boron chips could be effectively used as an additive. The study also identified that the inclusion of borogypsum led to reduced concrete consistency and delayed setting in C52 concrete, indicating its potential use as a set retarder [15]. In their research, Bothe and Brown [16] examined the formation of a hydration product called ettringite. They identified two different compounds formed with the influence of boron-containing compounds: high boron ettringite and low boron ettringite.

The high boron ettringite is associated with the formula $C_3A \cdot 2Ca(B[OH]_4)_2 \cdot Ca(OH)_2 \cdot 30H_2O$, whereas the low boron ettringite has the formula O and $C_3A \cdot Ca(B[OH]_4)_2 \cdot 2Ca(OH)_2 \cdot 36H_2O$.

This study demonstrates that boron-containing compounds can affect the chemical composition of hydration products. While research related to ulexite in construction materials and the building sector is limited, specific studies indicate that ulexite can be utilized within cement [17, 18]. Collectively, the aforementioned studies underscore the beneficial impact of boron

additives on various properties of cement mortars. The present experimental study seeks to contribute to this body of knowledge by preparing test samples incorporating ground ulexite at different weight ratios into CEM I 42.5 R Portland cement, with a focus on investigating their mechanical and thermal properties. The study encompasses compression and flexural tests, along with measurements of thermal conductivity for the resulting samples. This research aims to provide further insights into the potential of boron-containing composites in enhancing the performance of cement-based materials.

2. General Methods

The ulexite boron mineral provided by Eti Maden General Directorate, exhibits a high boron content (%37 B_2O_3) compared to other boron minerals, and is notably rich in calcium (CaO) as its dominant component with a calcium content of 19%, data sourced from Eti Maden Operations General Directorate. The study's ulexite mineral and the technical attributes of the CEM I 42.5 R Portland cement used in mixture preparation are detailed in Table 1.

Table 1. Technical properties of CEM I 42.5 R cement and ULEXITE

Elements (%)	CEM I 42.5 R	ULEXITE
SiO ₂	21.01	4
Al ₂ O ₃	5.39	0.25
Fe ₂ O ₃	3.23	0.04
CaO	62.11	19
MgO	1.97	2.5
Na ₂ O+ K ₂ O	0.121	3.5
SO ₃	3.10	-
B ₂ O ₃	-	37
Physical Properties		
Specific Weight (g/cm ³)	3.17	2.52
Blaine Fineness (cm ² /g)	3351	3850
Ignition Loss (%)	2.36	32.46

Experimental studies were carried out in two main parts as mechanical experiments and thermal conductivity measurement experiments. First, the "Puzolanic Activity" of ulexite, which was determined in terms of its compressive strength with water and slaked lime Ca(OH)₂,

was determined. For this purpose, sieve analysis, specific surface area produced in accordance with TS EN 196-6 [19] standard and produced according to TS EN 196-1 [20] standard, taking into account the mixture amounts of slaked lime, standard sand, ulexite and water specified in the TS 25 [21] standard and density tests and compressive strength test in accordance with TS EN 196-1 standard.

After determining the pozzolanic activity of ulexite, cement mixtures were prepared by substituting ground ulexite at 0.5%, 1%, 2%, 4% by weight into CEM I 42.5R cement. The specific gravity, specific surface, setting times, consistency and volume expansion tests of the mixtures are based on the test methods in TS EN 196-1, TS EN 196-2 [22] and TS EN 196-3 [23] standards. It was done in a laboratory environment where it was $60 \pm 5\%$. The material mixture design for the compressive strength test is given in Table 2.

Table 2. Material mix design

Material	Cement (g)	Ulexite (g)	Sand (g)	Water (g)
U-0 (Reference)	450	0.00	1350	225
U-0.5	447.75	2.25	1350	225
U-1	445.50	4.50	1350	225
U-2	441.00	9.00	1350	225
U-4	432.00	18.00	1350	225

Flexural and compressive strength test specimens of ulexite substituted cement mortars were prepared in accordance with TS EN 196-1. $40 \times 40 \times 160$ mm samples, which were kept in normal water for 7 days and 28 days for flexural strength, were removed from the curing pool and subjected to a flexural test with a flexural press at a loading speed of (50 ± 10) N/s. Compressive strength was determined from $40 \times 40 \times 40$ mm samples. The compressive strength device was adjusted at a suitable capacity for the test and a loading speed of (2400 ± 200) N/s in accordance with TS 196-1. Photographs taken during the compression and flexural tests are given in Figure 1.

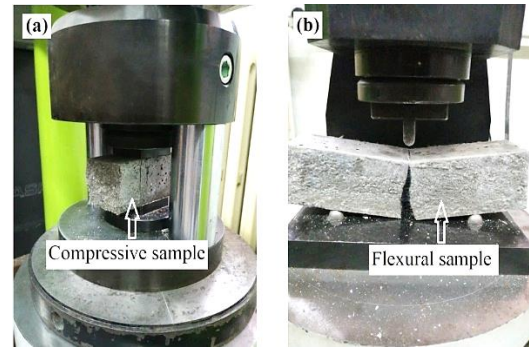


Figure 1. Compression test (a), Flexural test (b)

For the thermal conductivity tests in the second stage, test samples in the form of plates of $15 \times 150 \times 150$ mm were prepared in the mixing ratios given in Table 2 and subjected to the same curing process. The images of the prepared samples are given in Figure 2.

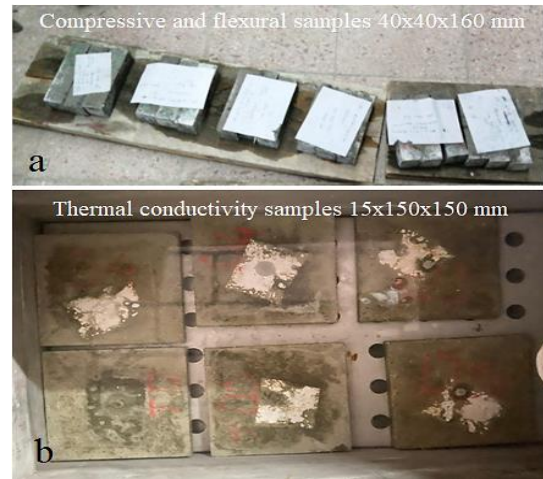


Figure 2. Compression and flexural test specimens (a), Thermal conductivity test specimens (b)

Thermal conductivity tests were carried out in Kırıkkale University Scientific and Technical Research Application and Research Center Machinery and Materials Laboratory, which is within the scope of accreditation according to TS EN 12667 [24] standard. The samples were first kept in an oven at 105°C until the change in mass (m , kg) reached a constant weight. Drying was continued until the mass change $[\Delta m = (m_1 - m_2)/m_2]$ reached constant weight ($\Delta m < 0.005$). After drying, they were kept under laboratory conditions ($23 \pm 1^\circ\text{C}$ and $(50 \pm 10)\%$ RH) for one day and then tested. Laser Comp. for thermal conductivity tests. Company's Fox-314 device was used. Measurement ranges and other test parameters in the thermal conductivity measurement of the device (Thermal conductivity range $0.01 - 0.2$ W/m.K, Accuracy

~1%, Repeatability ~0.2%, Reproducibility ~0.5%, Maximum temperature of hot plate 75 °C, Minimum temperature of cold plate -20°C, Temperature control stability $\pm 0.03^\circ\text{C}$, Thickness measurement accuracy ± 0.025 mm, Cooling - water flow $\sim 18^\circ\text{C}$ rate 57-75 liters per hour). As can be seen in Figure 3, the thermal conductivity measurement in the device is made with the principle of one-dimensional heat transfer based on the Fourier Heat Conduction Law. In the device, the heat flux (q'' , W/m^2) is determined by keeping a temperature difference (ΔT) of the sample with a thickness (L , m) in a way that one surface is hot and the other surface is cold. The thermal conductivity ($\lambda = q'' \cdot L / \Delta T$, $\text{W}/\text{m}\cdot\text{K}$) value was calculated by using the entered temperature difference, measured heat flux and thickness. In addition, in such

measurements, the results may be affected as the sample thicknesses are too high ($L > 20$ mm) will increase the edge heat losses. For this reason, the sample thickness was determined as 18 mm.

3. Results and Discussion

3.1. Evaluation of mechanical properties

As a result of the experiments, it was observed that the setting times of the mixtures prepared with different ulexite additive ratios were also different. In Table 3, setting times and some physical properties of the test samples without ulexite additive and with 0.5% - 1.0% - 2% - 4% ulexite additive by weight are given. the graph created according to the obtained values is given in Figure 3.

Table 3. Setting time and physical properties of cement with and without additives

	U-0	U-0.5	U-1	U-2	U-4
Density (g/cm^3)	3.09	3.08	3.07	3.08	3.06
Specific Surface (cm^2/gr)	3955	3982	3945	3944	3930
Setting Time (Initial) (min)	185	215	2095	365	565
Setting Time Final (min)	205	235	315	390	565
Water Required for Standard Consistency (%)	26.6	26.6	26.8	27.1	28.0
Volume Expansion (mm)	7	7	6	7	7

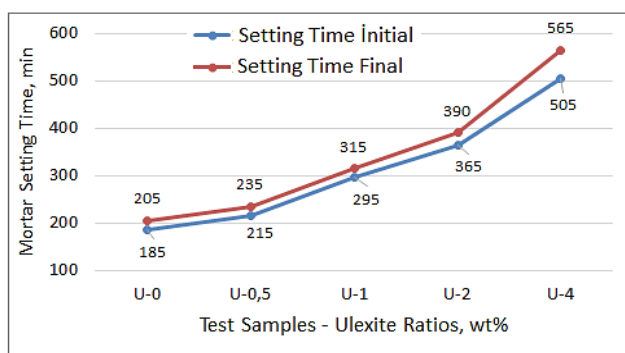


Figure 3. Setting time of cement with and without ulexite additives

Looking at the graph in Figure 3, it is understood that the setting time is prolonged due to the increase in the rate of ulexite substituted into the cement. Looking at Table 3, it is seen that the time between the beginning and the end of the setting was equal to 20 minutes in the samples numbered U-0, U-0.5, U-1, U-2 and U-4, but increased to 60 minutes in the sample numbered U-4. It is understood that ulexite, which is substituted up to 2% in cement, does not make a difference between the beginning and the end of

the setting, but it also significantly increases the time between the beginning and the end of the setting with the increase in the rate of ulexite to 4%. With the increase of the ulexite content in the cement, both the total setting time and the time between the beginning and the end of the setting increased. In a study in the literature, it is stated that boric acid substituted into cement increases the setting initiation and setting end times by 2-4 times [25].

Likewise, in another study, it is reported that colemanite substituted into cement both delays the setting time and reduces the mechanical properties of concrete [26]. Improvements and additional properties of boron compounds to concrete and cementitious composites are closely related to the boron trioxide (B_2O_3) concentration of the boron compound used. However, as the B_2O_3 concentration increases, it is a well-known and intensively researched phenomenon that cement hydration slows down or even stops, and accordingly, the setting time is prolonged. In a study in the literature, borates were very briefly

referred to as cement hydration retarding compounds, possibly resulting from a precipitation mechanism [27]. In this study, inorganic material was ground and a paste was formed that hardened by hydration reactions compared to water. This cement paste preserved its strength and stability thanks to the stable hydrated phases formed after hydration. This definition fully complies with the cement definition in TS EN 197-1. The physical analyzes of the test samples prepared with a lime-ulexite mixture in the pozzolanic activity test, the 7-day compressive strength value and the values that must be met in the standard are given in Table 4.

Table 4. Physical analysis of ulexite and compressive strength test result

Features		TS 25
Density (g/cm ³)	2.52	-
Specific Surface (cm ² /g)	3850	4000 ± 25%
Residue on 90µm Sieve (%)	0.2	≤ 8%
Compressive Strength (MPa) 7 Days	4.3	≥ 4
Compressive Strength (MPa) 28 Days	4.6	-

The graphs created according to the values obtained from the compression and flexural tests performed to determine the mechanical properties of the prepared ulexite cement mortar samples are given in Figure 4 and Figure 5.

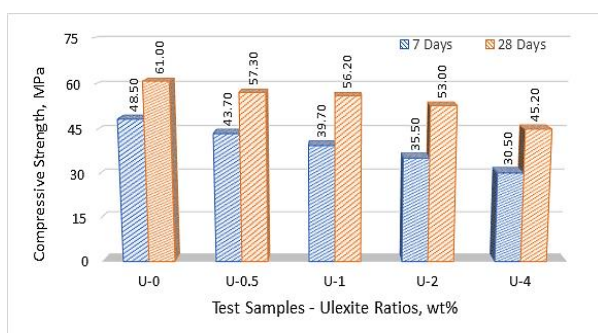


Figure 4. Compressive strength of mortar samples after 7 and 28 days of waiting period

When Figure 4 is examined, it is seen that the compressive strengths decrease as the ulexite substitution ratio increases. Another important point is that higher compressive strength was obtained in the samples in 28 days of waiting time compared to 7 days of waiting time. The highest compressive strength was determined as

61.0 MPa in the control sample, which was kept for 28 days. Among the ulexite added samples, the highest compressive strength was measured as 57.3 MPa in the U-0.5 coded sample with 0.5% substitution, which was also kept for 28 days. The graph created according to the flexural strength test results of ulexite substituted cement mortars in accordance with TS EN 196-1 is given in Figure 5.

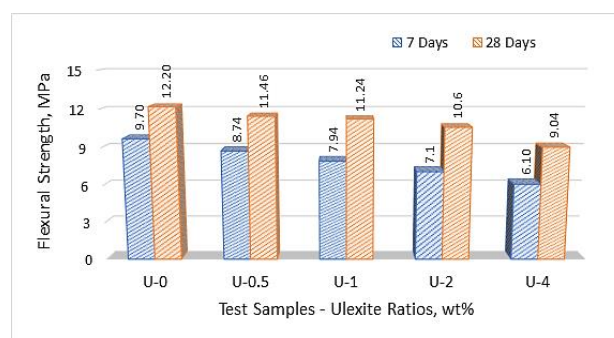


Figure 5. Flexural strength of mortar samples after 7 and 28 days of waiting period

Looking at Figure 5, it is understood that the flexural strength of the samples decreases as the ulexite substitution ratio increases. The flexural strength values of the samples that waited for 28 days were higher than the samples that waited for 7 days. These general results are in agreement with the compression test results. In these two test methods in which the mechanical properties were examined, it was observed that the ulexite substitution had a negative effect on the mechanical strength of the cement mortars. The highest flexural strength value among the ulexite added samples was obtained as 12.20 MPa from the U-0.5 coded sample, which was waited for 28 days and replaced with 0.5% ulexite.

The study conducted by I. Ustabaş (2011) demonstrates that the addition of ulexite has negative effects on fundamental mechanical properties such as flexural strength and compressive strength [28]. Piotrowski et al. (2019) [17] revealed that a significant amount of ulexite content in cement almost completely hindered hydration; simultaneously, samples containing 3% ulexite exhibited successful long-term performance. Studies reporting similar results for concretes with different boron compounds are available in the literature [1, 27, 29-31]. In a study in the literature, it is stated that

colemanite and barite added samples have lower compressive strength values than 7 days reference samples. This was explained by the delay in the hydration process caused by the pozzolanic mineral additives [32, 33]. During the hydration reaction, calcium oxide (CaO) reacts with water (H₂O) to form calcium hydroxide (Ca[OH]₂). During this reaction, the pore water quickly turns into an alkaline solution. While the concentration of calcium (Ca²⁺) cations and hydroxyl (OH⁻) anions increase in the pore water that turns into alkaline solution, B[OH]₃ dissolves rapidly. B[OH]₃ ions and OH⁻ anions in the mixture react to form B[OH]₄⁻ compound.

Afterwards, Ca⁺ cations react with B[OH]₄⁻. The resulting calcium di borate (CBH₆) compound precipitates and covers a portion of the cement particle surface on all or part of it. The hydration reaction of cement particles, whose surface is completely or partially covered with an impermeable layer of CBH₆, either stops completely or is rather delayed. This causes the particles to agglomerate (cut-coagulate) and pseudo-setting occurs. A decrease in Ca²⁺ occurs due to the formation of CH and CBH₆ in the pore solution. However, when alkalis (Na₂O, K₂O etc.) are released as a result of cement hydration, sodium (Na⁺), potassium (K⁺) cations are formed in the pore solution and OH⁻ anions increase in parallel. Depending on the increase of OH⁻ anions, the pH value of the pore water increases again, and after a while, CBH₆ can dissolve again to form the Ca²⁺ cation. As the CBH₆ crystal layers covering the cement particle surface dissolve, the hydration reaction will accelerate and the above-mentioned chemical cycle will be renewed. If there is pore water in the environment to maintain hydration, these reversible reactions will continue until cement hydration is complete. As the soluble B₂O₃ concentration in the medium increases, the initial CaO solubility also increases. However, after a while, the concentration of Ca²⁺ cations and OH⁻ anions decreases in the pore solution to form CBH₆ compound. As a result, the CBH₆ compound quickly covers the surface of the cement particles and hydration stops. Depending on the increasing B₂O₃ concentration, the solubility of the CBH₆ compound is also delayed. This phenomenon weakens bond formation

between binder grains. Therefore, while the hardening time after the hydration reaction is prolonged depending on the B₂O₃ concentration, the strength of the cement matrix decreases [33]. In some studies investigating the properties of the cement produced by using the wastes from colemanite and tincal production together with fly ash, natural pozzolan and bottom ash in cement, it has been found that the setting time is delayed with the use of additives in cement, bentonite increases strength at early ages, natural pozzolana has the same positive effect, and high It was determined that the use of tincal and colemanite (over 5%) resulted in decreases in compressive strength [8, 13]

As a result, it was evaluated that ulexite was effective on the performance of cement mortars. With this study, it was understood that ulexite substitute would be beneficial for concrete and cement and could be used as a mineral additive.

3.2. Evaluation of thermal conductivities

Thermal conductivity measurements were made on test samples that were kept for 28 days. The graph created with the values obtained as a result of the thermal conductivity measurements of the ulexite substituted and unsubstituted samples is given in Figure 6.

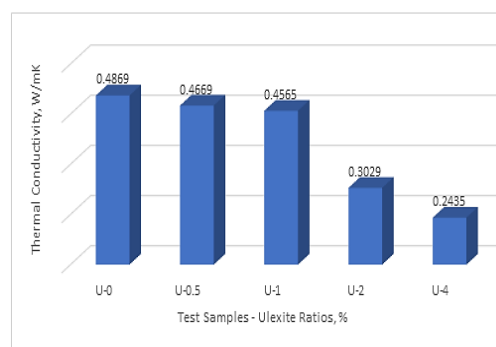


Figure 6. Graph of thermal conductivity values of mortar samples with 7 and 28 days waiting time

The thermal conductivity coefficients of the test samples without ulexite additive and with 0.5% - 1.0% - 2% - 4% ulexite by weight were 0.4869 W/m.K 0.4669 W/m.K, 0.4565 W/m.K, 0.3029 W/m.K and 0.2435 W/m.K respectively and the lowest thermal conductivity was found in cement mortar with 4% ulexite. This situation affects the strength values of the material as expected. When

the thermal conductivity values of the additives in mixed materials are low, the effective thermal conductivity values of the material must also decrease. Here, since the density of ulexite is lower than the mortar material, its thermal conductivity is also partially low. For this reason, it has been observed that the ulexite additive decreased the thermal conductivity positively, but negatively affected and reduced the strength values of the material. When the thermal conductivity values of the additives in composite materials are low, the effective thermal conductivity values of the material must also decrease. It is very important that the material has a homogeneous structure in order to obtain the values in the thermal conductivity measurements with the least error.

The homogeneous distribution of the pores in the material is one of the parameters that affect the thermal measurement results. When the values obtained from the thermal conductivity measurements of ulexite added cement mortars are evaluated among themselves, it is thought that the pores inside the structure increase with the increase in the ulexite additive ratio. Because, although there was a double difference between the 0.5% ulexite added sample and the 1% ulexite added sample, the difference between the thermal conductivity values was 2%. However, with the increase of the ulexite substitution ratio from 1% to 2%, the difference between the thermal conductivities became 50%.

With the increase in the ulexite ratio from 2% to 4%, this difference emerged as 24%. It can be seen from these results that the amount of porosity in cement mortars increased with ulexite substitution. However, there is no direct correlation between these porosity rates and ulexite substitution rates, and the pores in the structure are not homogeneously distributed. The thermal conductivity values decrease with the effect of the air in the building. Therefore, it is considered that whether it is distributed as homogeneously as the amount of pores in the cement mortar plays an important role in determining the thermal conductivity values.

4. Conclusion

Pozzolanic Activity, Compressive Strength, Flexural Strength, Thermal Conductivity of ulexite-substituted cement mortars according to the research results of its properties;

- As stated in the TS 25 Standard, it can be said that ulexite has pozzolanic activity, since the 7-day minimum compressive strength value meets 4 MPa. The fact that it contains C-S-H gels with high binding properties provides an increase in strength and increases the resistance of concrete against external effects by decreasing the paste void ratio. Therefore, in accordance with TS 25 limit values, it is similar to some pozzolanic materials used in the cement industry.

- With the increase of ulexite substitution in the cement mortar, decreases in specific gravity and specific surface areas were observed.

- With ulexite substitution, the rate of substitution increased as the set start and set end times increased. It is slightly longer than the setting time and volume expansion limits of cements with additives given in TS EN 197-1. It shows us that it will be very ideal for cements used in mass concrete. Therefore, it can be said that ulexite will have a setting retarding effect. This situation is closely related to the B_2O_3 (boroxide) concentration in ulexite. As the B_2O_3 concentration decreases, the curing delay and strength decrease will also improve in direct proportion.

- As the ulexite substitution rates increased, the compressive strength of ulexite added cement mortars decreased. It was concluded that this situation weakens the bond formation between the binder grains. Therefore, it is thought that while the hardening time after the hydration reaction is prolonged depending on the B_2O_3 concentration, the strength of the cement matrix decreases.

Although it is the control sample with the highest compressive strength, it has been observed that ulexite added cement mortars have values close to the control sample.

It has been observed that the substitution of ulexite in cement reduces the thermal conductivity coefficient of the mortars. It was found as 0.2435 W/m.K in the mortar. When the thermal conductivity values of the additives in composite materials are low, the effective thermal conductivity values of the material must also decrease.

It has been determined that the thermal conductivity values increase accordingly with the increase in the ulexite substitution ratio. The lowest thermal conductivity value was obtained in 4% ulexite substituted mortars. In addition, as a result of this study, it was evaluated that ulexite substituted cement mortars could be used in thermal barrier development studies.

In addition, considering the CO₂ emission and energy consumption, it will be possible to contribute to sustainability by minimizing the negative impact on the environment during cement production and by recycling boron wastes that harm the environment.

Understanding the importance of ulexite in the field of construction materials should be seen as a step forward. Attention should be drawn to the positive effects of ulexite on the strength, thermal properties, and environmental sustainability of cement mortar. The interaction of ulexite with different dosages and various cement compositions should be examined more thoroughly. Furthermore, further research is needed to explore the economic and environmental impacts of ulexite's industrial-scale usage. Therefore, future studies should be expanded to better understand the role of ulexite in the construction materials industry and fully assess its potential.

These results show that ulexite can be developed with more use in experimental researches and different usage areas for ulexite may emerge.

Article Information Form

Funding

The author (s) has no received any financial support for the research, authorship or publication of this study.

Authors' Contribution

The authors contributed equally to the study.

The Declaration of Conflict of Interest/ Common Interest

No conflict of interest or common interest has been declared by the authors.

The Declaration of Ethics Committee Approval

This study does not require ethics committee permission or any special permission.

The Declaration of Research and Publication Ethics

The authors of the paper declare that they comply with the scientific, ethical and quotation rules of SAUJS in all processes of the paper and that they do not make any falsification on the data collected. In addition, they declare that Sakarya University Journal of Science and its editorial board have no responsibility for any ethical violations that may be encountered, and that this study has not been evaluated in any academic publication environment other than Sakarya University Journal of Science.

Copyright Statement

Authors own the copyright of their work published in the journal and their work is published under the CC BY-NC 4.0 license.

References

- [1] T. Mutuk, B. Mesci, "Analysis of mechanical properties of cement containing boron waste and rice husk ash using full factorial design," *Journal of Cleaner Production*, vol. 69, pp. 128–132, Apr. 2014.
- [2] B. Dündar, E. Çınar, "Farklı Mineral Katkılı Hafif Harçların Mekanik ve Fiziksel Özelliklerine Yüksek Sıcaklığın Etkisi," *Türk Doğa ve Fen Dergisi*, vol. 9, no. 2, pp. 42–49, 2020.
- [3] C. Helvacı, "Borate deposits: An overview and future forecast with regard to mineral deposits," *Journal of Boron*, vol. 2, no. 2, pp. 59–70, 2017.

- [4] G. Guzel, O. Sivrikaya, H. Deveci, "The use of colemanite and ulexite as novel fillers in epoxy composites: Influences on thermal and physico-mechanical properties," *Composites Part B: Engineering*, vol. 100, pp. 1–9, Sep. 2016.
- [5] I. Y. Elbeyli, E. M. Derun, J. Gülen, S. Pişkin, "Thermal analysis of borogypsum and its effects on the physical properties of Portland cement," *Cement and Concrete Research*, vol. 33, no. 11, pp. 1729–1735, Nov. 2003.
- [6] A. Aldakshe, H. Çağlar, A. Çağlar, Ç. Avan, "The investigation of use as aggregate in lightweight concrete production of boron wastes," *Civil Engineering Journal.*, vol. 6, no. 7, pp. 1328–1335, 2020.
- [7] S. E. Chidiac, M. G. El-Samrah, M. A. Reda, M. A. E. Abdel-Rahman, "Mechanical and radiation shielding properties of concrete containing commercial boron carbide powder," *Construction and Building Materials*, vol. 313, no. June, p. 125466, 2021.
- [8] Ç. Targan, A. Olgun, Y. Erdoğan, V. Sevinç, "Effects of supplementary cementing materials on the properties of cement and concrete," *Cement and Concrete Research*, vol. 32, no. 10, pp. 1551–1558, Oct. 2002.
- [9] Y. Erdoğan, M. S. Zeybek, A. Demirbas, "Cement Mixes Containing Colemanite from Concentrator Wastes," *Cement and Concrete Research*, vol. 28, no. 4, pp. 605–609, Apr. 1998.
- [10] B. Çomak, A. Bideci, Ö. Salli Bideci, "Effects of hemp fibers on characteristics of cement based mortar," *Construction and Building Materials*, vol. 169, pp. 794–799, Apr. 2018.
- [11] R. Boncukcuoğlu, O. İçelli, S. Erzeneoğlu, M. Muhtar Kocakerim, "Comparison of radioactive transmission and mechanical properties of Portland cement and a modified cement with trommel sieve waste," *Cement and Concrete Research*, vol. 35, no. 6, pp. 1082–1087, Jun. 2005.
- [12] A. Filazi, M. Pul, "Effect of Borax Pentahydrate Substitution on Sound proofing and Mechanical Properties of Cement Mortar," *Uluslararası Muhendislik. Araştırma ve Geliştirme Dergisi*, vol. 14, no. 2, pp. 604–610, Jul. 2022.
- [13] I. Kula, A. Olgun, V. Sevinc, Y. Erdogan, "An investigation on the use of tincal ore waste, fly ash, and coal bottom ash as Portland cement replacement materials," *Cement and Concrete Research*, vol. 32, no. 2, pp. 227–232, Feb. 2002.
- [14] Ş. Targan, A. Olgun, Y. Erdoğan, V. Sevinç, "Influence of natural pozzolan, colemanite ore waste, bottom ash, and fly ash on the properties of Portland cement," *Cement and Concrete Research*, vol. 33, no. 8, pp. 1175–1182, Aug. 2003.
- [15] U. K. Sevim, M. Öztürk, M. B. Bankir, U. Aydın, "Utilization of Colemanite waste in Concrete Design," *International Journal of Advanced Engineering Research and Science*, vol. 4, no. 12, pp. 172–175, 2017.
- [16] J. V. Bothe, P. W. Brown, "Phase formation in the system CaO–Al₂O₃–B₂O₃–H₂O at 23±1°C," *Journal of Hazardous Materials*, vol. 63, no. 2–3, pp. 199–210, Dec. 1998.
- [17] T. Piotrowski, J. Glinicka, M. A. Glinicki, P. Prochoń, "Influence of gadolinium oxide and ulexite on cement hydration and technical properties of mortars for neutron radiation shielding purposes," *Construction and Building Materials*, vol. 195, pp. 583–589, Jan. 2019.
- [18] Standard, B. (2003). *British Standard Methods of testing cement*.
- [19] TS EN 196-6. (2010). *Methods of testing cement–part 6: determination of fineness*.

- [20] Turkish Standard Institute-TSE. (2002). TS EN 196-1: methods of testing cement: part 1: determination of strength.
- [21] TSE, T. (2011). Natural pozzolan (Trass) for use in cement and concrete-Definitions, requirements and conformity criteria. Turkish Standard Institute. Ankara, Turkey.
- [22] TSE, (2002). TS EN 196-2: Methods of testing cement. Part 2: Chemical analysis of cement.
- [23] EN, T. (2017). 196-3. Methods of testing cement-Part, 3.
- [24] EN, T. (2003). 12667 Turkish Standards Institute. Thermal performance of building materials and products.
- [25] H. E. Pehlivanoğlu, M. Davraz, Ş. Kılınçarslan, "The effect of boron compound to setting time of cement and controllability," *International Journal of Technologic Sciences*, vol. 5, no. 3, pp. 39-48, 2013.
- [26] O. Gencil, W. Brostow, C. Ozel, M. Filiz, "An investigation on the concrete properties containing colemanite," *International Journal of Physical Sciences*, vol. 5, no. 3, pp. 216–225, 2010.
- [27] N. Yaltay, C. E. Ekinçi, "Investigation Of Compression Strength Of Lightweight Concrete, Subjected To Elevated Temperature, Produced With Pumice Aggregate And Colemanite Addition By Non-Destructive Method," *Süleyman Demirel University International Journal of Technologic Sciences*, vol. 5 no. 2, pp. 30-41, 2013.
- [28] Ustabaş, İ., "Investigation of the Usability of Colemanite and Ulexite in Cement", Ready-Mixed Concrete Congress, Istanbul, 2011.
- [29] H. F. W Taylor, "Cement chemistry," 2nd ed., Thomas Telford publishing, London, 1997.
- [30] E. Erdogmus, "Combined effect of waste colemanite and silica fume on properties of cement mortar," *Science and Engineering of Composite Materials*, vol. 21, no. 3, pp. 369–375, 2014.
- [31] İ. Yakar Elbeyli, "Utilization of Industrial Borax Wastes (BW) for Portland Cement Production," *The Turkish Journal of Engineering & Environmental Sciences*, vol. 28, pp. 281-287, 2004.
- [32] O. Aksoğan, H. Binici, E. Ortlek, "Durability of concrete made by partial replacement of fine aggregate by colemanite and barite and cement by ashes of corn stalk, wheat straw and sunflower stalk ashes," *Construction and Building Materials*, vol.106, pp.253-263, 2016.
- [33] M. Davraz, "The effect of boron compound on the properties of cementitious composites," *Science and Engineering of Composite Materials*, vol.17, no. 1, pp. 1-17, 2010.



Exploring the Link between Job Satisfaction and Productivity among Architects in Architectural Offices

Yiğit Can Yardımcı^{1*}, Yasemin Erbil¹

¹ Bursa Uludağ University, Faculty of Architecture, Department of Architecture, Bursa, Türkiye, yardimci@uludag.edu.tr, yaseminerbil@uludag.edu.tr

*Corresponding Author

ARTICLE INFO

ABSTRACT

Keywords:

Architects
Architectural offices
Job satisfaction
Productivity



Article History:

Received: 12.02.2024
Accepted: 13.05.2024
Online Available: 01.08.2024

Job satisfaction is an important factor that directly affects an employee's productivity. The relationship between job satisfaction and productivity is a critical factor in many professions, including architecture. Therefore, it is important that they are satisfied with their jobs in terms of productivity. The aim of this study is to examine demographic features, job satisfactions and productivity levels of architects working in architectural offices in Bursa and to determine whether there is a relationship with each other. In this study, a questionnaire was used as a data collection method. A survey was conducted with 203 architects working in Bursa. The survey consists of 3 parts. In the first part demographic features, in the second part job satisfactions and in the third part, there are questions about productivity. According to the findings, the correlation coefficient value between the productivity of job satisfactions in the working environment is between 0 and 0.50, revealing the importance of job satisfaction and productivity for the companies and the employees. As a result of the research, it was concluded from the correlation analysis that the parameters of architects' job satisfactions were effective on productivity. It has been observed that the productivity of the employees who are satisfied with their job, organization of the working environment has also increased. In terms of architects, it is thought that this study will contribute to the scientific field in terms of the absence of a study examining the three issues together and reflecting the perspectives of architects on their profession. In the context of architectural offices, studies examining job satisfactions or productivity are very limited.

1. Introduction

Architects have many different fields of work. These areas are; public institutions, architectural offices, design offices, construction sites, supply and production companies for the building sector and building inspection companies, etc. [1]. Architects spend most of the day in the office. For this reason, it is important for them to be satisfied with their job in terms of being productive and efficient in their work.

Job satisfaction is the happiness that an employee gets from his job [2]. There are two main factors that can affect the job satisfaction of employees. These factors are; organizational and individual

factors. Individual factors; personality factor, ability and mental factor, gender, education, marital status, age, status and seniority. Organizational factors are; wages, features of the job, working conditions, co-workers, promotion and advancement opportunities and management style [3]. Determining the factors affecting the job satisfaction of the architects working in the office and making the necessary improvements will increase the internal and external satisfaction levels of the architects. Increasing satisfaction levels of employees will increase input/output results in the organization.

There are numerous studies on architects' professional responsibilities, their future in the

profession, working conditions, and job satisfaction. For example, Sang, Ison, and Dainty (2009) explored the job satisfaction of UK architects, revealing that 20 to 40 percent of respondents were dissatisfied with their pay, promotion prospects, and opportunities to use their abilities [4]. They also noted significant work-life balance difficulties among architects. Burr and Jones (2010) discussed the evolving role of the architect, indicating that successful future architects might need to reclaim lost responsibilities and promote higher collaboration levels [5].

Faber (2010) highlighted architects as service providers, emphasizing their crucial role in agile development projects and the importance of participating in coding activities to sustain the architecture's effectiveness throughout a project's lifetime [6]. Rickaby (1979) speculated on the future practice of architecture, suggesting that interdisciplinary practices and design cooperatives could respond appropriately to current and future problems [7]. Kuruçay and Karadağ (2022) investigated the future of architects', indicating a shift in skill requirements and suggesting a reevaluation of architectural education to ensure architects can compete in the future [8]. Salama and Courtney (2013) examined the spatial qualities of the workplace on architects' job satisfaction in Belfast, Northern Ireland, finding relatively high satisfaction levels but identifying significant factors such as control over thermal conditions and acoustics [9].

These studies collectively underscore the complexity of the architectural profession, where job satisfaction intertwines with professional responsibilities, evolving roles, and changing work environments. Future research might delve deeper into how emerging technologies, changing societal expectations, and evolving workplace models impact architects' roles and satisfaction levels.

1.1. Job satisfaction

Before 1933, 32 studies on job satisfaction were examined by Robert Hoppock, the concept of job satisfaction became the focus of attention in the literature. According to Hoppock, job satisfaction is a combination of physiological,

environmental and psychological conditions that cause a person to say that he is truly satisfied with his job [10]. Employee's job satisfaction is related to how employees feel, although it is influenced by many external factors. According to Davis and Nestrom, job satisfaction represents the combination of positive and negative feelings of workers towards their jobs. A worker brings with him experiences, needs and desires that determine his expectations at work. Job satisfaction represents matching expectations with actual rewards [11]. Vroom focuses on the employee's role in the workplace. According to Vroom, job satisfaction is defined as the emotional orientations of employees related to their work roles [12].

Many researchers have conducted research on the factors affecting job satisfaction and have reached various findings. McDonald and Gunderson emphasized that wage and years of service are very important for job satisfaction [13]. According to Sydney and Duane Schultz, while individuals are satisfied with some aspects of the work environment, they may be dissatisfied with others. Individuals may not be satisfied with their jobs in all circumstances and may not like every aspect of their job. In general, it is the effects of health status, social life, emotional situations, age and family life [14].

According to Porteous, job satisfaction factors consist of 2 groups. These; individual factors and work-related factors [15]. Individual factors are those that arise due to individual-specific differences. The change created by the individual characteristics in the wishes, expectations and needs of the person causes the job satisfaction to differ. Job satisfaction of an individual varies according to his individual characteristics. These factors are; gender, age, education, personality, intelligence, ability, status and seniority. Organizational factors are the factors provided and created by the organization in order to provide job satisfaction and meet the expectations of the employees. These factors are; wage, job characteristics, working conditions, working group, promotion and advancement opportunities and management style.

1.2. Productivity

According to Prokopenko, productivity is defined as the active use of inputs in the production of different services and goods. Therefore, it explains aiming to save money due to active use of resources and goods [16]. According to OECD (Organisation for Economic Co-operation and Development), productivity is the number of products produced as a result of production divided by one of the products. According to ILO (International Labour Organization), the ratio of suitable products to factors such as capital, labor, land and entrepreneurs is defined as productivity [17].

The main purpose of a business management; raising the income ratio of capital and increasing net incomes. The most important factor in the success of an organization that adapts to market

conditions in a timely manner; it is the reduction of the input volume required for the unit output [18]. The second importance of productivity measurement for the organization is the benefits it provides to the organization's management. The basic functioning signs of the organization can only be revealed in a healthy way with productivity measurements. The third importance of productivity measurement for businesses is that it is a more reliable criterion than profitability. Another importance of productivity measurements for businesses is that they allow comparison between businesses [19].

Factors affecting productivity are examined in two groups as internal factors and external factors. Since it is not under the control of the enterprise, it is more difficult to control external factors than internal factors [16]. Table 1 shows the factors that affecting productivity [20].

Table 1. Factors Affecting Productivity

Internal factors			External factors		
Solid factors	Flexible factors	Structural resources	Natural resources	State and infrastructure	and
Factory and equipment	Organization and systems	Economic	Manpower	Institutional mechanisms	
Product	Human	Population and social structure	Land	Policy	
Technology	Working methods		Energy	Infrastructure	
Material and energy	Forms of administration		Raw materials	Public enterprises	

2. General Methods

The sample of the research consists of architects working in architectural offices in Bursa. In this study, a questionnaire was used as a data collection method.

The survey was mostly applied online due to the conditions of the thesis and the survey form was created via Google Forms. In this direction, a total of 203 architects, 117 women and 86 men, working in architectural offices in Bursa were reached [21].

The survey consists of 3 parts. In the first part, there are questions about demographics. In the second part, a 20-question short version of the Minnesota Job Satisfaction Questionnaire was used to measure the job satisfaction of the architects in the office. The Minnesota

Satisfaction Questionnaire is measured at three levels: internal, external, and general satisfaction. 12 questions in the questionnaire are about internal satisfaction, 8 questions are about external satisfaction, and all of the questions are used for general satisfaction [22].

The reason for choosing the Minnesota Job Satisfaction Survey to measure job satisfaction values is that it is reliable, validated and internationally widespread. In the last part of the questionnaire, there are questions about the levels of productivity. A total of 19 questions were determined under 3 sub-headings (economic, psycho-social and organizational managerial factors). A 5-point Likert-type scale was used as the questionnaire scale. The evaluation criteria and score ranges of the answers given to the questionnaire are shown in Table 2.

Table 2. The evaluation criteria and score ranges of the answers

Likert Scale	Options	Ranges	Evaluation Criteria
5	Absolutely agree	4.20-5.00	very high level
4	I agree	3.40-4.19	high level
3	Undecided	2.60-3.39	medium level
2	I do not agree	1.80-2.59	low level
1	I strongly disagree	1.00-1.79	very low level

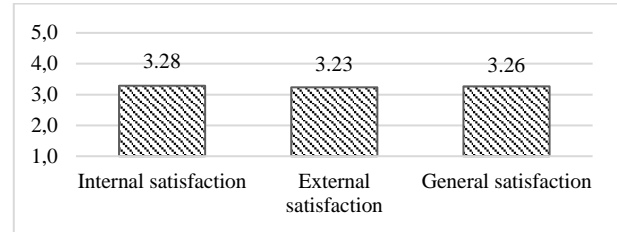
SPSS 23.0 software program was used in the analysis of the data obtained from the sample through the questionnaire. While investigating the effects of various factors on the sample, analysis methods such as descriptive statistics, Cronbach Alpha reliability coefficient, Spearman Correlation analysis and Mann Whitney U test were used. Non-parametric analysis methods were preferred because the data were not normally distributed.

3. Results and Discussion

When the demographic features of the participants is examined, the participants consist of 117 women (57.6%) and 86 men (42.4%) participants. It was seen that the architects in the 22-30 age group were in the majority with a rate of 61.57%. Users in the 30-40 age group follow the majority with 32.51%. When their marital status was examined, it was seen that 70% were single and 30% were married. When their educational status is examined, 84.70% of participants have bachelor's degree and 15.60% of participants have postgraduate degrees. Values are shown in Table 3.

3.1. Findings on job satisfaction of architects

As a result of the evaluations; general satisfaction value was found to be 3.26 out of 5, internal satisfaction value was 3.28 and external satisfaction value was 3.23. These values were determined as "neutral" according to the score ranges. Based on the data, architects have moderate job satisfaction. The average distribution of job satisfaction levels is shown in Figure 1.

**Figure 1.** The average distribution of job satisfaction levels.**Table 3.** Participants' demographic features

Gender	N	%
Women	117	57.6%
Men	86	42.4%
Age	N	%
22-25	62	30.54%
25-30	63	31.03%
30-34	50	24.63%
35-40	16	7.88%
40-45	9	4.43%
45-50	3	1.48%
Marital status	N	%
Single	142	70.0%
Married	61	30.0%
Education level	N	%
Bachelors degree	172	84.70%
Postgraduate	31	15.30%
Professional experience	N	%
2-5 year	109	54.0%
5-10 year	58	28.70%
10-15 year	19	9.40%
15-20 year	14	6.90%
20-30 year	2	1.00%
Working Time in the Company	N	%
1-5 year	168	82.76%
5-10 year	29	14.29%
10-15 year	2	0.99%
20-30 year	4	1.97%

The frequency and percentage distributions of the internal satisfaction values are shown in Table 4.

Table 4. The frequency and percentage distributions of the internal satisfaction

Parameter	Measures						Total
	1	2	3	4	5		
Task performed	Freq.	2	12	13	171	5	203
	%	1	5.9	6.4	84.2	2.5	100%
Independence	Freq.	3	34	100	57	9	203
	%	1.5	16.7	49.3	28.1	4.4	100%
Variety	Freq.	2	87	30	75	9	203
	%	1	42.9	14.8	36.9	4.4	100%
Social status	Freq.	3	70	45	77	8	203
	%	1.5	34.5	22.2	37.9	3.9	100%
Moral values	Freq.	1	33	56	103	10	203
	%	0.5	16.3	27.6	50.7	4.9	100%
Security	Freq.	8	87	56	47	5	203
	%	3.9	42.9	27.6	23.2	2.5	100%
Social services	Freq.	1	48	54	90	10	203
	%	0.5	23.6	26.6	44.3	4.9	100%
Authority	Freq.	4	61	54	76	8	203
	%	2	30	26.6	37.4	4	100%
Benefiting from talents	Freq.	2	29	50	110	12	203
	%	1	14.3	24.6	54.2	5.9	100%
Responsibility	Freq.	4	51	50	90	8	203
	%	2.1	25.1	24.6	44.3	3.9	100%
Creativity	Freq.	4	39	32	118	10	203
	%	2	19.2	15.8	58.1	4.9	100%
Achievement	Freq.	2	26	43	122	10	203
	%	1	12.8	21.2	60.1	4.9	100%

1= Strongly dissatisfied, 2=Dissatisfied 3= Undecided 4= Satisfied 5= Totally satisfied

When the internal satisfaction sub-factors of the architects working in the office are examined, some values were found to be higher than the average of internal satisfaction. These values are task performed, achievement, benefiting from talents, creativity and moral values. According to the range of scores, these values are equivalent to “agree”. Some values of the sub-factors were found to be lower than the average internal satisfaction value. These values are responsibility, independence, authority and variety.

These values were determined as “neutral” according to the score ranges. Security values were determined as “disagree” according to the score ranges. The average distribution of internal satisfaction values is shown in Figure 2.



Figure 2. The average distribution of internal satisfaction values

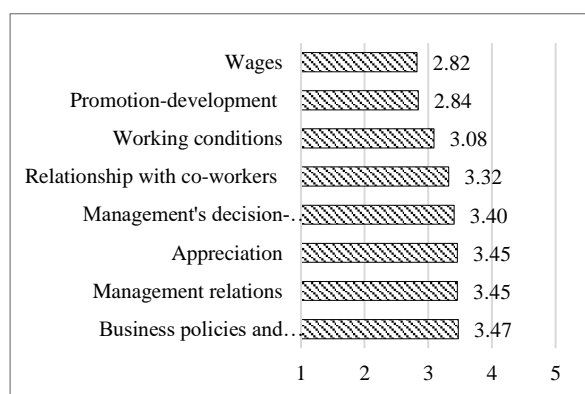
Frequency and percentage distributions of external satisfaction values are shown in Table 5.

Table 5. Frequency and percentage distributions of external satisfaction values

Parameter		Measures					Total
		1	2	3	4	5	
Management relations	Freq.	2	25	61	108	7	203
	%	1	12.3	30	53.2	3.4	100%
Management's decision making ability	Freq.	2	39	48	103	11	203
	%	1	19.2	23.6	50.7	5.4	100%
Business policies and practices	Freq.	1	36	41	116	9	203
	%	0,5	17.7	20.2	57.1	4.4	100%
Wage	Freq.	7	90	45	54	7	203
	%	3.4	44.3	22.2	26.6	3.4	100%
Promotion and development)	Freq.	4	81	68	43	7	203
	%	2	39.9	33.5	21.2	3.4	100%
Working conditions	Freq.	6	57	60	73	7	203
	%	3	28.1	29.6	36	3.4	100%
Relationships with coworker	Freq.	4	47	42	100	10	203
	%	2	23.2	20.7	49.3	4.9	100%
Appreciation at work	Freq.	2	37	39	116	9	203
	%	1	18.2	19.2	57.1	4.4	100%

When the external satisfaction sub-factors of the architects working in the office were examined, it was seen that some values were high. These values are; business policies and practices, management relations, appreciation, and management's decision-making ability. These values were determined as “agree” according to the score ranges. It was observed that some values of the sub-factors were lower than the average external satisfaction value. These values are working conditions and the relationship with co-workers. These values were determined as “neutral” according to the score ranges.

Wages and promotion-development values were determined as “disagree” according to the score ranges. Average distributions of external satisfaction values are shown in Figure 3.

**Figure 3.** The average distribution of external satisfaction values

3.1.1. Distribution of job satisfaction values by demographic features

Spearman correlation analysis was applied to examine whether there is a statistically significant relationship between job satisfaction and demographic variables. Based on Spearman's correlation analysis, when the correlation coefficient (r) is <0.20 , there is a very weak relationship or no relationship, a weak relationship when $r= 0.20-0.39$, and medium level when $r= 0.40-0.59$ relationship means a high level relationship when $r= 0.60-0.79$, and a very high level relationship when $r= 0.80-1.00$ (Şen, 2016).

A statistically significant and weak relationship was found between job satisfaction factors and demographic variables such as age, professional experience, organization's type, working time, average working hours, working's way and working order, since the values were 0-0.39. The strongest statistical correlation with general satisfaction and internal satisfaction level was the average working hours and the weakest statistical correlation was the working's way. The strongest statistical correlation with external satisfaction level was found to be age, while the weakest statistically correlation was found to be working's way. The correlation analysis between job satisfaction and demographic characteristics is shown in Table 6.

Table 6. The correlation analysis between job satisfaction and demographic features.

Parameter	Age	Working hours	Professional experience	Way of working	Working Time(year)
General satisfaction	0.199	0.269	0.143	-0.202	0.158
External satisfaction	0.224	0.146	0.174	-0.159	0.201
Wages	-	0.216	0.226	-	-
University policies and practices	0.175	-	-	-	-
Business policies and practices	-	0.229	-	-0.181	-
Relationship with co-workers	-	0.173	-	-	-
Working conditions	-	-	-	-0.155	0.267
Internal satisfaction	0.173	0.319	-	-0.2	-
Task performed	0.151	-	0.151	-	-
Achievement	-	0.234	-	-	-
Creativity	-	0.313	-	-0.255	0.138
Independence	-	0.192	-	-	-
Moral Values	-	0.21	-	-0.156	-
Responsibility	-	0.211	-	-	-
Social service	-	0.27	-	-	-
Benefiting from talents	-	0.274	-	-0.16	-
Variety	-	0.177	-	-	-
Achievement	-	-	-	-0.152	-

(0.00) - (0.20)= Very weak relationship, (0.21) - (0.40)= Weak relationship, (0.41) - (0.59)= Medium relationship, (0.60) - (0.79)= High relationship, (0.80) - (1.00)= Very high relationship

3.2. Findings on productivity of architects

When the findings of the study are examined, it is seen that the architects working in the office are satisfied with productivity. The overall productivity value was found to be 3,43 out of 5. This value was determined as “agree”. The economic and organizational-managerial factor values that make up the overall productivity value are 3.57 and 3.47 out of 5. These values are equivalent to the statement “agree”. Psycho-social factors were determined as “neutral”. The average distribution of productivity levels is shown in Figure 4.

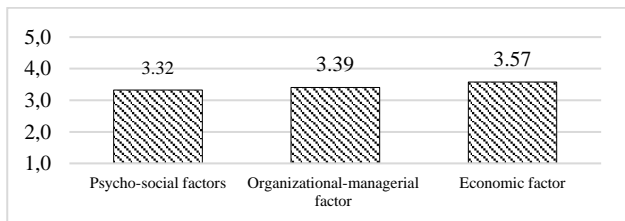


Figure 4. The average distribution of productivity

Frequency and percentage distributions of productivity levels are examined in Table 7.

When the productivity sub-factors of the architects working in the office are examined; some values were found to be higher than the average values. These values are; wages,

management sensitivity, equipment and tools, working hours, satisfaction with work, fair wages, responsibility, management-employee relationship and status were determined as “agree.

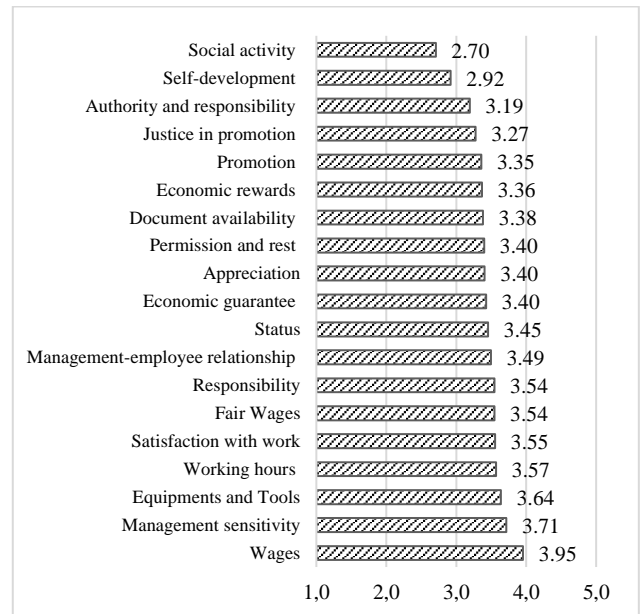


Figure 5. The average distribution of productivity sub-factors

When the productivity sub-factors of the architects working in the office are examined, some values were found to be lower than the average values. Among these values; social

activity, self-development, authority and responsibility, fair promotions, promotion, economic rewards and document availability values were determined as “neutral”. Permission

and rest, appreciation and economic guarantee were determined as “agree”. Average values of productivity are shown in Figure 5.

Table 7. Frequency and percentage distributions of productivity

Parameter	Measures							Total
		1	2	3	4	5	Missing	
Wage	Freq.	2	4	11	169	16	1	203
	%	1	2	5.4	83.3	7.9	0.5	100%
Fair wage	Freq.	2	12	80	90	18	1	203
	%	1	5.9	39.4	44.3	8.9	0.5	100%
Economic rewards	Freq.	1	51	37	99	14	1	203
	%	0.5	25.1	18.2	48.8	6.9	0.5	100%
Economic guarantee	Freq.	2	35	51	103	11	1	203
	%	1	17.2	25.1	50.7	5.4	0.5	100%
Status	Freq.	1	33	53	103	12	1	203
	%	0,5	16.3	26.1	50.7	5.9	0.5	100%
Appreciation	Freq.	2	32	59	100	9	1	203
	%	1	15.8	29.1	49.3	4.4	0.5	100%
Relationships with management	Freq.	1	32	51	102	16	1	203
	%	0,5	15.8	25.1	50.2	7.9	0.5	100%
Satisfaction with work	Freq.	1	33	36	117	15	1	203
	%	0.5	16.3	17.7	57.6	7.4	0.5	100%
Social activity	Freq.	2	108	49	33	10	1	203
	%	1	53.2	24.1	16.3	4.9	0.5	100%
Authority	Freq.	1	56	56	79	9	1	203
	%	0.5	27.6	27.6	38.9	4.4	0.5	100%
Document availability	Freq.	1	41	49	100	10	2	203
	%	0.5	20.2	24.1	49.3	4.9	1	100%
Responsibility	Freq.	1	27	50	109	15	1	203
	%	0.5	13.3	24.6	53.7	7.4	0.5	100%
Promotion	Freq.	3	42	46	102	9	1	203
	%	1.5	20.7	22.7	50.2	4.4	0.5	100%
Fair promotion	Freq.	2	41	68	81	10	1	203
	%	1	20.2	33.5	39.9	4.9	0.5	100%
Self development	Freq.	2	88	45	58	9	1	203
	%	1	43.3	22.2	28.6	4.4	0.5	100%
Working Hours	Freq.	2	31	34	120	15	1	203
	%	1	15.3	16.7	59.1	7.4	0.5	100%
Permission status	Freq.	2	43	43	99	14	2	203
	%	1	21.2	21.2	48.8	6.8	1	100%
Equipments and tools	Freq.	1	20	47	117	17	1	203
	%	0.5	9.9	23.2	57.6	8.4	0.5	100%
Management sensivity	Freq.	0	19	34	133	15	2	203
	%	0	9.4	16.7	65.5	7.4	1	100%

A statistically significant and weak relationship was found between productivity levels and sub-factors and demographic variables such as professional experience, type of organization, working time (year), average working hours, working's way and working order, since the values were 0-0.39. The strongest statistical correlation with economic factors was found to

be average working hours and the weakest statistical correlation was found to be working way. The strongest statistical correlation with organizational-managerial factors was found to be average working hours while the weakest statistical correlation was found to be working time in the organization. The correlation analysis between productivity and demographic features in Table 8 is shown.

Table 8. The correlation analysis between productivity and demographic features

Parameter	Av. working hours	Way of working	Type of Organization	Working order	Working Time
Economic Factors	0.233	-0.161	0.144	0.167	
Economic Rewards	0.263	-0.208	0.163	0.213	
Promotion Justices	-	-	0.216	-	-
Document availability	-	-	-	-	-
Appreciation	-	-	-0.139	-	-
Equipment and Tools	0.197	-0.181		0.182	-0.16
Management-employee relationship	0.184	-		-	-
Responsibility	-	-	-		-0.209
Self-development	-		-		-0.2
Social activity		0.18			
Working Time				0.179	

(0.00) - (0.20)= Very weak relationship, (0.21) - (0.40)= Weak relationship, (0.41) - (0.59)= Medium relationship, (0.60) - (0.79)= High relationship, (0.80) - (1.00)= Very high relationship

3.3. Correlation between job satisfaction and productivity

The internal satisfaction level has moderate correlation with economic, psycho-social and organizational-managerial factors. External satisfaction level with economic, psycho-social and organizational-managerial are weakly correlated. General satisfaction level has moderate correlation with economic, psycho-social and organizational-managerial factors. The correlation analysis between job satisfaction and productivity in Table 9 is shown.

4. Conclusion

In this study, we discussed the various individual and organizational factors that influence architects' job satisfaction and productivity. The findings of this research open up new perspectives and pose further questions for future exploration. It has been determined that architects' job satisfaction is influenced by specific individual and organizational factors. However, it is expected that organizational structures and personal desires will evolve over time. Consequently, the variables affecting architects' job satisfaction may also undergo changes.

The advent of the pandemic has popularized the concept of remote working, and technological advancements have introduced new opportunities, fundamentally altering the working conditions for architects, both in the office and in the field. The impact of these changes on architects' job satisfaction and

productivity, considering the evolution of location, time, and working environments, will be an important subject for future studies.

Table 9. The correlation analysis between job satisfaction and productivity levels

Parameter	Internal Job Satisfaction	External Job Satisfaction	General Job Satisfaction
Economic factor	0.443	0.395	0.462
Fair Wages	0.337	0.322	0.322
Economic rewards	0.389	0.358	0.411
Economic guarantee	0.338	0.323	0.363
Psycho-social factors	0.472	0.391	0.459
Status	0.38	0.316	0.358
Appreciation	0.365	0.265	0.34
Management-employee relationship	0.335	0.285	0.339
Responsibility	0.403	0.247	0.356
Satisfaction with work	0.334	0.299	0.343
Working hours	0.406	0.24	0.363
Organizational-managerial factor	0.542	0.365	0.50
Authority	0.354	0.189	0.362
Document availability	0.326	0.222	0.305
Promotion	0.27	0.189	0.251
Fair promotion	0.305	-	0.229
Management sensitivity	0.421	0.233	0.385
Permission and rest	0.203	0.185	0.204
Equipments and Tools	0.414	0.299	0.396

(0.00) - (0.20)= Very weak relationship, (0.21) - (0.40)= Weak relationship, (0.41) - (0.59)= Medium relationship, (0.60) - (0.79)= High relationship, (0.80) - (1.00)= Very high relationship

Moreover, the integration of emerging technologies such as virtual reality, AI-driven design tools, and sustainable building technologies presents both challenges and opportunities for architects. These technologies

can enhance creativity, efficiency, and the ability to work on more complex projects. However, they also require architects to continuously learn and adapt, which can influence job satisfaction levels. Understanding how these technological shifts affect architects' work-life balance, career progression, and overall job satisfaction will provide valuable insights into adapting organizational practices and individual strategies for a rapidly evolving profession.

Article Information Form

Funding

The authors has no received any financial support for the research, authorship or publication of this study.

Authors' Contribution

The authors contributed equally to the study.

The Declaration of Conflict of Interest/ Common Interest

No conflict of interest or common interest has been declared by the authors.

The Declaration of Ethics Committee Approval

This study requires ethics committee permission or any special permission.

The Declaration of Research and Publication Ethics

The authors of the paper declare that they comply with the scientific, ethical and quotation rules of SAUJS in all processes of the paper and that they do not make any falsification on the data collected. In addition, they declare that Sakarya University Journal of Science and its editorial board have no responsibility for any ethical violations that may be encountered, and that this study has not been evaluated in any academic publication environment other than Sakarya University Journal of Science.

Copyright Statement

Authors own the copyright of their work published in the journal and their work is published under the CC BY-NC 4.0 license.

References

- [1] H. Begeç, Mimarlık bilgisi: mühendislik-mimarlık öğrencileri için, First Edition. Yalın Yayıncılık, 2012.
- [2] J. R. Hackman, G. R. Oldham, "Development of the job diagnostic survey," *Journal of Applied Psychology*, vol. 60, no. 2, pp. 159–170, 1975.
- [3] M. Porteous, *Occupational psychology*, First Edition. Prentice Hall, 1997.
- [4] K. Sang, S. Ison, A. Dainty, "The job satisfaction of UK architects and relationships with work-life balance and turnover intentions" *Engineering, Construction and Architectural Management*, Vol. 16 No. 3, pp. 288-300, 2009.
- [5] K. Burr, C. B Jones, "The role of the architect: changes of the past, practices of the present, and indications of the future" *International Journal of Construction Education and Research*, Vol.6 No.2, pp. 122-138, 2010.
- [6] R. Faber, "Architects as Service Providers", *IEEE Software*, Vol. 27 No.2, pp. 33-40, 2010.
- [7] P. Rickaby, "Speculations on the future practice of architecture", *Design Studies*, Vol. 1 No. 2, pp. 118-123, 1979.
- [8] E. Kuruçay, İ. Karadağ, "Computational Approaches in 21st Century Architectural Design: Defining Digital Representation Methods", *DUBİTED*, Vol. 10, No. 3, pp. 1201–1217, 2022.
- [9] A. M. Salama, L. Courtney, "The impact of the spatial qualities of the workplace on architects' job satisfaction" *International Journal of Architectural Research: Archnet-IJAR*, Vol. 7 No. 1, pp. 52-64, 2013.

- [10] R. Hoppock, Job Satisfaction, Harper and Brothers, 1935. [Online]. Available: <https://onlinelibrary.wiley.com/doi/epdf/10.1002/j.2164-5892.1938.tb00348.x>
- [11] K. Davis, J.W. Nestrom, Human behavior at work: organizational behavior, Seventh Edition. McGraw Hill, 1989.
- [12] V.H. Vroom, Work and motivation. Ninetieth edition. John Wiley and Sons, 1964.
- [13] B. W. McDonald, E. K. Gunderson, "Correlates of job satisfaction in naval environments," Journal of Applied Psychology, vol. 59 no. 3, pp. 371-373, 1974.
- [14] D. Schultz, S. E. Schultz, Psychology and industry today: an introduction to industrial and organizational psychology, Macmillan Publishing Co., 1986.
- [15] B. Horman, "Türk inşaat sektöründe örgütsel bağlılık ve iş tatmini" M.S thesis, Istanbul Technical University, Türkiye, 2010.
- [16] J. Prokopenko, Verimlilik yönetimi uygulamalı elkitabı, Seventh Edition. Milli Prodüktivite Merkezi Yayınları, 2001.
- [17] K. Köroğlu, Verimlilik yönetimine Japon yaklaşımı ve Kazukiyo Kurosawa modeli, First Edition. MPM Yayınları, 1993.
- [18] Ü. Doğan, Verimlilik analizleri ve verimlilik-ergonomi ilişkileri, First Edition. Ticaret Borsası Yayınları, 1987.
- [19] H. İleri, "Verimlilik, verimlilik ile ilgili kavramlar ve işletmeler açısından verimliliğin önemi," Selçuk Üniversitesi Sosyal Bilimler MYO Dergisi, vol.1, no.2, pp. 9-24, 1999.
- [20] Z. Sabuncuoğlu, T. Tokol, İşletme, First Edition. Alfa Aktuel Basım Yayınları, 2005.
- [21] Y. C. Yardımcı, "Mimarların iş tatmini ve çalışma ortamındaki konfor koşulları ile verimlilik ilişkisinin incelenmesi," M.S. thesis, Bursa Uludağ University, Türkiye, 2021.
- [22] D. J. Weiss, R. V. Davis, G. W. England, L.H. Lofquist, Manual for the Minnesota satisfaction questionnaire, The University of Minnesota Press, 1967. [Online]. Available: https://vpr.psych.umn.edu/sites/vpr.umn.edu/files/files/monograph_xxii_-_manual_for_the_mn_satisfaction_questionnaire.pdf

The Effect of Grape Pomace Fiber Addition on Quality Parameters of Yogurt

Hatice Sıçramaz^{1*} , Ahmet Ayar¹ 

¹ Sakarya University, Faculty of Engineering, Department of Food Engineering, Sakarya, Türkiye, haticesicramaz@sakarya.edu.tr, aayar@sakarya.edu.tr

*Corresponding Author

ARTICLE INFO

ABSTRACT

Keywords:

Food waste
Sustainability
Grape pomace
Dietary fiber
Yogurt



Article History:

Received: 21.02.2024

Accepted: 05.07.2024

Online Available: 01.08.2024

Reducing food and industrial waste is essential to match the novel objectives of sustainable living. In this context, grape pomace, a fiber-rich by-product of wine production, was used as a fiber supplement in yogurt after enriching its fiber content through preprocessing. Within the aim of this study, 0.5% and 1% grape pomace fiber were incorporated into yogurt, and the effect on physicochemical, microbial, and sensory quality was investigated. Throughout the 14-day storage period, no significant changes were observed in pH, acidity, and water holding capacity. The total mesophilic aerobic bacteria count ranged between 2-3 log.cfu/g, and the addition of fiber did not result in any undesirable alterations in these counts. Similarly, the fiber did not affect the counts of specific yogurt bacteria, which was 8-9 log.cfu/g. Moreover, sensory evaluations consistently resulted in scores above “5” for all products, with acidity rated level as moderate as expected for yogurt. There were no adverse effects on sensory quality concerning color, flavor, texture, acidity, and overall acceptability. In conclusion, fiber-enriched yogurt from wine waste is feasible without compromising product quality. This study is expected to contribute to the progress of current sustainable living goals.

1. Introduction

In the food industry, large amounts of food waste, referred to as by-products, are generated as a result of processing. Many of these wastes are either not utilized, leading to significant environmental pollution, or they are used as low-value by-products such as animal feed, fertilizer, etc., using simple technologies. . The effective utilization of waste generated during food processing is important for sustainability with reference to the Sustainable Development Goals (SDGs) set by the United Nations. The evaluations are not only for preventing environmental pollution but also for introducing the by-products to new generation healthy products. Many food industry wastes contain essential nutrients, dietary fibers, and other functional ingredients [1].

Dietary fiber is a crucial food ingredient to maintain digestive health, regulate cholesterol levels, and control blood sugar. Vegetables, fruits, legumes, and grains are sources of dietary fiber. For a healthy life, a total of 25-30 g of fiber is recommended daily. However, with the increasing consumption of fast food in modern diets, the intake of fiber-rich foods has declined, probably to 15 g daily intake, leading to various health issues [2]. Therefore, it is essential to incorporate dietary fibers into our diets through various food sources to promote overall health and well-being.

Yogurt is consumed worldwide and is particularly popular in countries like Turkey, Greece, Bulgaria, Lebanon, and India [3]. It is valued for its various health benefits, including being a rich source of protein, calcium, vitamins, and probiotics. Regular consumption of yogurt is associated with improved digestion and gut

health due to its probiotic content. Additionally, it is rich in calcium, protein, B vitamins, and other essential nutrients, offering benefits ranging from bone health to muscle development. Its high protein content can increase satiety and aid in weight management. Being fiber-rich, yogurt supports digestive health and regulates bowel movements [4].

In recent years, the significance of dietary fibers in by-product-fruit pomaces has been recognized, so, researchers gained an increasing interest towards valorization of this by-product. , A study on cranberry pomace in yogurt production was reported to enhance the dietary fiber and antioxidant contents of yogurt, affecting rheological characteristics differently depending on addition before or after fermentation and maintaining the viable lactic acid bacteria count [5].

In another research, the use of 1% and 3% wheat bran adversely affected the flavor of yogurt and caused water release while increasing the total mineral content [6]. A study investigated the impact of enriching yogurt with various dietary fibers (inulin, pea, oat, and wheat) on its rheological, physicochemical, and sensory properties, significant effects on viscosity, syneresis, and sensory acceptance, indicating the potential for incorporating fibers into yogurt to enhance its nutritional profile and create functional food products with diverse health benefits [7].

In accordance with the sustainability and healthier food production goals, this study aimed to investigate the potential utilization of grape pomace in yogurt. In this context, the effect of grape pomace on the physicochemical, textural, sensory, and microbiological properties of yogurt was investigated during a 14-day storage period.

2. Materials and Methods

2.1. Preparation of grape pomace fiber

The pomace was obtained from grape must lees from a wine plant in Tekirdag. The pomace was boiled for 25 min in a 1% citric acid solution with a 1:1 (w:v) ratio and then filtered. Consequently, it was concentrated to 24°B using 600 ppm sulfur

dioxide. Pectin was precipitated with pure alcohol, dried under vacuum at 40°C, and ground to obtain the grape pomace fiber. The total dietary fiber content of the grape pomace fiber obtained was determined to be 66.5±1.1%.

2.2. Preparation of yogurt samples

First, set-type yogurt production was carried out using raw milk. The chemical composition of yogurt was analyzed using Milkana Express Plus milk analyzer (Mayasan Biotech, Turkey) as 13.6% total solids, 3.6% protein, 4.0% fat, and 4.8% lactose. Milk was pasteurized at 90°C for 10 min. Then, the milk was rapidly cooled to 43°C and inoculated at a ratio of 1:10000 (w:v) with YC-X16 yogurt culture (CHR Hansen, Denmark) containing strains of *Lactobacillus delbrueckii subsp. bulgaricus* (*L. bulgaricus*) and *Streptococcus thermophilus* (*S. thermophilus*). The mixture was incubated at 43°C until a pH of 4.6. The obtained set-yogurt was divided into batches for the addition of other powdered ingredients.

The amount of fiber added to the yogurt was determined through preliminary sensory tests. During trials, it was determined that grape pomace fiber negatively affected the yogurt's sensory properties, so the freeze-dried cherry powder was added to the products at a rate of 2% to mask the off-flavor. In summary, the composition of the resulting fiber-enriched yogurts consisted of 10% sugar, 2% cherry powder, and either 0.5% or 1% grape pomace fiber, depending on the product type. Plain yogurt without powdered additives was referred to as the "control" and coded as "C" in the study. Products containing 0.5% and 1% fiber were labeled "05GF" and "1GF," respectively. All productions were carried out in duplicate.

2.3. Physicochemical analyses

The total solids (TS), titratable acidity in terms of lactic acid (LA), protein, fat, and ash contents were carried out according to AOAC [8] standards. The pH of yogurt was measured at 25°C with a Mettler Toledo Seven Compact S220 pH meter (Switzerland). The water holding capacity (WHC) was determined according to the method described by Silva and O'Mahony [9]

with slight modifications: Yogurt samples (5 g) were centrifuged at 5000 rpm for 15 min at 4°C, and the serum phase was weighed. The WHC was calculated as the percentage of total yogurt weight.

2.4. Microbiological analyses

The total mesophilic aerobic bacteria (TMAB) counts were determined by counting the colonies obtained by the spreading on Plate Count Agar and incubation at 25°C for 2 days. The total count of yeasts and molds were enumerated on oxytetracycline glucose yeast extract (OGYE) agar at 25°C for 5-7 days of incubation. For the enumeration of yogurt bacteria, the pour-plate method was applied using de Man, Rogosa, and Sharpe (MRS) agar and M17 agar for inoculations. The incubation parameters were 37°C and 43°C, respectively, for 3 days [10].

2.5. Determination of sensory quality

Sensory tests were carried out with the approval of Sakarya University Ethical Committee on 10 pretrained panel members aged 18-50, both males and females, from Sakarya University. Color, texture, flavor, acidity, and overall acceptability were evaluated using a 9-point Hedonic rating scale, where 9 = like extremely and 1 = dislike extremely [11].

2.6. Statistical analysis

The compositional analyses were conducted in the 1st week of storage. The remaining measurements were performed in triplicate on storage days 1, 7, and 14. The collected data were evaluated using one-way analysis of variance (ANOVA) followed by Tukey's multiple range test in Minitab software (ver.16, USA). Statistical significance was determined at a *P*-value of less than 0.05.

3. Results and Discussion

3.1. The physicochemical properties of yogurt samples

The compositional properties of yogurt samples are given in Table 1.

Table 1. The compositional properties of yogurts

	TS %	Protein %	Fat %	Ash %
C	20.8 ±0.3 C	3.57 ±0.1 A	3.72 ±0.1 B	0.71 ±0.0 C
05GF	23.9 ±0.1 B	3.09 ±0.1 B	3.96 ±0.0 A	0.84 ±0.0 B
1GF	24.8 ±0.0 A	3.05 ±0.1 B	4.02 ±0.0 A	0.87 ±0.0 A

The capital letters in the same column indicate the difference between the samples (*P*<0.05)

The increased fiber content significantly affected the TS content yogurt. In plain yogurt (C), TS was measured as 20.8%, while in 1GF as 24.8%. In contrast, the protein content in yogurt significantly decreased with the addition of fiber, whereas the fat content increased. Similar to the TS, the ash content revealed a significant increase proportional to the increased fiber content. The pH, acidity, and WHC measurements of yogurts are given in Table 2.

Table 2. The physicochemical properties of yogurts

Day	pH		
	C	05GF	1GF
1	4.18 ±0.03 Aa	4.08 ±0.07 Aa	4.05 ±0.13 Aa
7	4.11 ±0.06 Aa	3.99 ±0.15 Aa	3.96 ±0.11 Aa
14	4.04 ±0.08 Aa	3.98 ±0.13 Aa	3.96 ±0.12 Aa
	LA %		
	C	05GF	1GF
1	0.952 ±0.02 Aa	0.959 ±0.03 Aa	0.945 ±0.04 Aa
7	0.963 ±0.01 Aa	1.030 ±0.01 Aa	0.987 ±0.03 Aa
14	0.985 ±0.02 Aa	1.071 ±0.01 Aa	1.069 ±0.06 Aa
	WHC %		
	C	05GF	1GF
1	55.4 ±0.2 Cb	64.9 ±0.0 Aa	62.8 ±0.8 Ba
7	60.7 ±0.2 Aa	65.3 ±2.8 Aa	64.9 ±0.5 Aa
14	60.1 ±1.1 Aa	63.6 ±1.7 Aa	62.0 ±1.1 Aa

The differences between samples within the same row is indicated by uppercase letters, and the differences between storage days within the same column is indicated by lowercase letters. (*P*<0.05).

The pH values ranged from 3.96 to 4.18, showing no significant variations between samples and no changes during the 14-d-storage period. Similarly, the acidity levels varied between 0.945% and 1.071% but were not affected by product differences or storage duration. The water holding capacity (WHC) was initially lowest in the control sample on the first day of storage, likely because the hydrogen bonds in the yogurt had not fully formed yet. Subsequently, on days 7 and 14, WHC remained consistent at 60.1% to 65.3%, regardless of storage duration or product type.

A study on yogurt enrichment with 1% pea fiber revealed, consistent with our findings that the titratable acidity was not affected by the addition of fiber [12]. In a study on fiber-enriched yogurt production, similar to our results, the pH and water-binding properties of the products remained unchanged during the 21-day storage period [13]. In another study, it was observed that adding rice bran as a fiber supplement to yogurt before fermentation resulted in better texture stabilization effects. At the same time, when added after fermentation, it was determined that it could lead to a destabilization [14].

3.2. Microbiological properties of yogurt samples

The total bacterial count in yogurts is significant as it directly reflects the product's quality, safety, and shelf life. The TMAB counts of yogurt samples are given in Figure 1. During the storage period, the TMAB counts in all samples remained below the microbial risk factor of 5 log cfu/g recommended by FAO and WHO [15]. In addition, the sample differences and the storage process did not affect these counts ($P>0.05$).

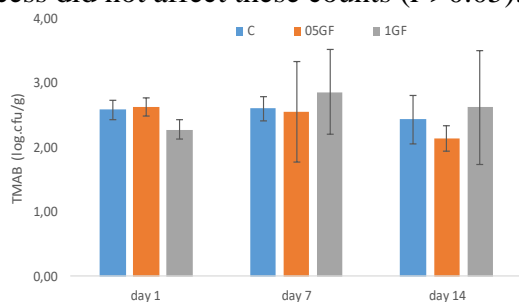


Figure 1. The TMAB counts of yogurt samples during 14-d-storage

In all samples, the total counts of yeasts and molds remained below detectable limits during the storage period.

The counts of *S. thermophilus* and *L. bulgaricus* were as illustrated in Figure 2. The counts of *S. thermophilus* ranged from 8.50 - 8.91 log cfu/g, while the counts of *L. bulgaricus* varied between 7.10 and 7.84 log cfu/g. These results are consistent with the "yogurt" values specified in the regulation [16]. In addition, no differences were observed in strain counts across products and storage durations ($P>0.05$).

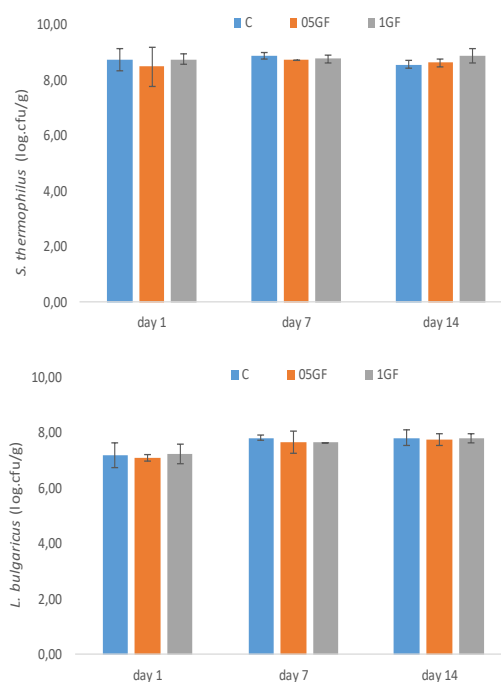


Figure 2. The specific yogurt bacteria counts of yogurt samples during 14-d-storage

Since pomace fiber can also act as a prebiotic supplement, the viability of specific lactic starter cultures could be enhanced through yogurt enrichment with fiber. For instance, in a study involving yogurt supplemented with maltodextrin and konjac fibers, lactic bacteria were reported to be supported by fiber addition [17].

3.3. Sensory properties of yogurt samples

Sensory evaluation ensures the quality and consistency of flavors, ultimately enhancing consumer satisfaction and product acceptance. The sensory properties of the products were evaluated in terms of color, texture, flavor, acidity, and overall acceptability, and the results are presented in Figure 3. To observe the differences between the obtained results, a principle component analysis (PCA) was applied, as illustrated in Figure 4.

The principle component-1 (PC1) explained 88.2 % of the results, while PC2 accounted for 6.6 %. Considering the positive and negative regions of PC1 and PC2, all results formed four distinct regions. Regarding color scores, samples C, 05GF, and 1GF were diverse and diverted into different regions, as the fiber content gave color differences. When examined in terms of texture,

the control product (C) was positioned in the positive region of PC1, while the two products with added fiber showed similar results and were positioned in the negative region. In terms of acidity, all products were positioned in the negative region of PC1, while they differentiated in PC2: 05GF and 1GF products showed similar acidity results, whereas the control product (C) diverged from the fiber-added products.

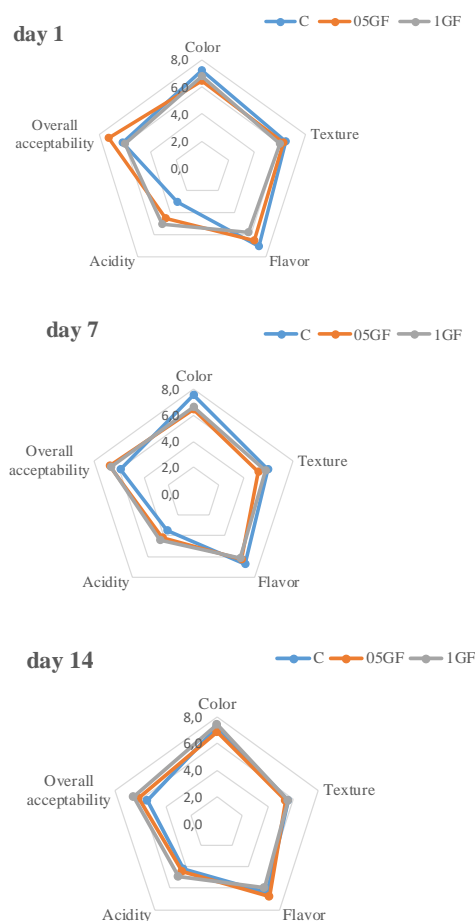


Figure 3. The sensory properties of yogurt samples on storage days 1, 7, and 14

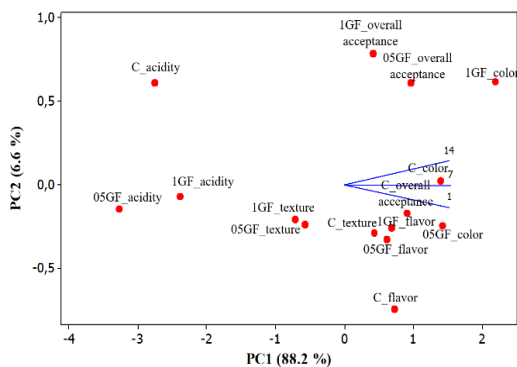


Figure 4. The principle component analysis on sensory properties of yogurt samples

When evaluated with Figure 3, it can be concluded that the addition of fiber increases acidity perception. Regarding flavor, according to PC1, all products were positioned in the same region, however according to PC2, the fiber-added products separated from the control product. When statistically evaluated, it was determined that the difference in flavor was statistically insignificant ($P>0.05$). Regarding overall acceptability, fiber-added products received higher scores than the control according to Figures 3 and 4.

The addition of fiber can have varying effects on the sensory quality of yogurts, both enhancing and decreasing it. For instance, in a study, apple fiber was found unacceptable in yogurt, whereas bamboo and wheat fiber revealed acceptable sensory results [18]. In another study, it was noted that with a dietary fiber content of 4.5%, the overall acceptability decreased, while it was suggested that date fiber at a 3% level could be utilized to enhance the nutritional value of yogurt [19].

4. Conclusion

This study examined the potential use of grape pomace, a by-product of wine production, as a food component by enriching its fiber content through preprocessing. The investigation revealed that the addition of grape pomace fiber at levels of 0.5% and 1% to yogurt formulation did not negatively affect the physical and chemical properties of yogurt.

In conclusion, it was determined that the addition of grape pomace fiber to yogurt is available without any adverse effect on the product quality. It is believed that this study will have a contribution to sustainability by promoting healthy lifestyles, reducing production wastes, preserving the environment, and supporting the circular economy.

Article Information Form

Funding

The authors has received a financial support from Tubitak for the research of this study with a project number 111O195.

Authors' Contribution

The authors contributed equally to the study. All authors have read and agreed to the published version of the manuscript.

The Declaration of Conflict of Interest/ Common Interest

No conflict of interest or common interest has been declared by the authors.

The Declaration of Ethics Committee Approval

The sensory test was carried out with the approval of the Sakarya University Ethics Committee.

The Declaration of Research and Publication Ethics

The authors of the paper declare that they comply with the scientific, ethical and quotation rules of SAUJS in all processes of the paper and that they do not make any falsification on the data collected. In addition, they declare that Sakarya University Journal of Science and its editorial board have no responsibility for any ethical violations that may be encountered, and that this study has not been evaluated in any academic publication environment other than Sakarya University Journal of Science.

Copyright Statement

Authors own the copyright of their work published in the journal and their work is published under the CC BY-NC 4.0 license.

References

- [1] R. Ravindran, A. K. Jaiswal, "Exploitation of food industry waste for high-value products", *Trends in Biotechnology*, vol. 34, pp. 58–69, 2016.
- [2] University of California San Francisco, "Increasing fiber intake", Health (Irvine, California). <https://www.ucsfhealth.org/education/increasing-fiber-intake> (Access date: 12.02.2024), 2024.
- [3] R. C. Chandan, A. Kilara, "Manufacturing Yogurt and Fermented Milks", Wiley, 2013.
- [4] A. Murette, E. Picard-Deland, M. A. Fernandez, "Yogurt: Roles in Nutrition and Impacts on Health", 1st ed., CRC Press, 2020.
- [5] L. Varnaitė, M. Keršienė, A. Šipailienė, R. Kazernavičiūtė, P. R. Venskutonis, D. Leskauskaitė, "Fiber-rich cranberry pomace as food ingredient with functional activity for yogurt production", *Foods*, vol. 11, p. 758, 2022.
- [6] S. Yalçinkaya, A. Ayar, A. Elgün, "Production of high nutritional value yogurt with wheat germ and phytase addition", *Selcuk Journal of Agriculture and Food Science*, vol. 17, pp. 57–63, 2003.
- [7] A. Dabija, G. G. Codină, A.-M. Gâțlan, L. Rusu, "Quality assessment of yogurt enriched with different types of fibers", *CyTA - Journal of Food*, vol. 16, pp. 859–867, 2018.
- [8] AOAC, "Official Methods of Analysis of AOAC International", 17th ed., MD, USA, 2000.
- [9] J. V. C. Silva, J. A. O'Mahony, "Microparticulated whey protein addition modulates rheological and microstructural properties of high-protein acid milk gels", *International Dairy Journal*, vol. 78, pp. 145–151, 2018.
- [10] E. Y. Bridson, "The Oxoid manual", 8th ed., Oxoid, Basingstoke, England, 1998.
- [11] H. Stone, J. L. Sidel, "Measurement", in: *Sensory Evaluations Practice*, Elsevier, pp. 69–97, 2004.
- [12] C. Damian, A. Olteanu, "Influence of dietary fiber from pea on some quality characteristics of yoghurts", *Journal Agroalimnet Process Technology*, vol. 20, pp. 156–160, 2014.
- [13] M. D. Staffolo, N. Bertola, M. Martino, y A. Bevilacqua, "Influence of dietary fiber addition on sensory and rheological properties of yogurt", *International Dairy Journal*, vol. 14, pp. 263–268, 2004.

- [14] T. Wu, C. Deng, S. Luo, C. Liu, X. Hu, "Effect of rice bran on properties of yogurt: Comparison between addition of bran before fermentation and after fermentation", *Food Hydrocolloids*, vol. 135, 108122, 2023.
- [15] FAO, WHO, "Microbiological risk assessment guidance for food". <https://www.fao.org/3/cb5006en/cb5006en.pdf>. (Access date: 02.02.2024). 2021.
- [16] TGK, Fermente Sütler Tebliği. <https://www.resmigazete.gov.tr/eskiler/2022/11/20221130-5.htm>. 2022.
- [17] E. Tahra Ammar, M. Abo-Srea, E. El-Raghy, "Effect of certain dietary fibers on the properties of functional yoghurt", *Journal of Food and Dairy Science*, vol. 4, pp. 611–619, 2013.
- [18] A. K. Seçkin, E. Balandura, "Effect of using some dietary fibers on color, texture and sensory properties of strained yogurt", *Gıda*, vol. 37, pp. 63–69, 2012.
- [19] I. B. Hashim, A. H. Khalil, H. S. Afifi, "Quality characteristics and consumer acceptance of yogurt fortified with date fiber", *Journal of Dairy Science*, vol. 92, pp. 5403–5407, 2009.

Smart Agriculture Applications and Data Analysis with Industry 4.0

M.A. Yasin Ömercikoğlu^{1*}, Abdullah Sevin¹

¹ Sakarya University, Faculty of Science, Department of Computer Engineering, Sakarya, Türkiye, ali.omecirkoglu@ogr.sakarya.edu.tr, asevin@sakarya.edu.tr

*Corresponding Author

ARTICLE INFO

ABSTRACT

Keywords:
Industry 4.0
Smart agriculture
IoT
Big data
Image processing

The world's food demand is predicted to exceed its food supply significantly in the coming periods. Many physical factors, such as climate change in access to water, change the production amount and food prices. Efficient resource utilization can be achieved by developing smart agricultural applications using the IoT and image processing techniques. For this purpose, in the proposed study, a smart agriculture application was developed using IoT technology with image processing. In the proposed image processing algorithm, the crops' images were processed, weight estimates were made, and their numbers were taken. The data we collect instantly can be uploaded to the cloud, and the data collected on the cloud side can be analyzed over the mobile application. Thanks to data analysis with the mobile application we have developed, we can see the current status of the crops and make instant decisions, and it also plays a role in determining market prices. With all these studies, it has been seen that agriculture can be digitalized with the technologies we use, and thus, productivity in agriculture can increase significantly.

Article History:

Received: 06.01.2023

Accepted: 24.06.2024

Online Available: 01.08.2024

1. Introduction

Agriculture is the centuries-old culture of humanity and the technique of raising plants and animals, which is necessary for the basic need of humankind to feed and sustain its life. It comes first among the physical demands of people. It is essential for the continuation of life. According to a study by the United Nations in 2015, the world population is expected to be 9.7 billion in 2050 and 11.2 billion in 2100. The increase in the population of humanity requires further improvement of agricultural activities due to factors that negatively affect agriculture, such as environmental factors such as climate change, global warming, and drought. Information technologies are needed to ensure that the food supply can be sufficient in the future. Agriculture has developed continuously from the past to the present, and the processes in this development have been called versioning in the industry [1].

Industry 4.0, the Internet of Things (IoT), big data, cloud systems, sensors, etc., is the new version of the production system created by using technologies in communication. Large countries such as Germany, China, Japan, and America are investing to switch to this technology. Many countries have established research units for this purpose. In our country, research in this field continues.

One of the primary purposes of Industry 4.0 is to prevent waste by making maximum use of technology. For this reason, it aims to increase efficiency by establishing automation systems and following all production stages with correct planning and timely intervention. As with Industry 4.0, the development of agriculture has not stopped and has passed through specific steps. These stages have existed since the existence of humanity. Various factors, such as the development of technology and the increase in the human population, have influenced the

development of the stages. These phases continue as follows;

Agriculture 1.0 – A farming method using only human and animal power. We can say that it is the most primitive form of agriculture used for centuries.

Agriculture 2.0 – Using pesticides and synthetic fertilizers and pesticides is the beginning of mechanization in agriculture.

Agriculture 3.0 – Use of GPS and computer software for data processing in agriculture.

Agriculture 4.0 – We can also call it smart agriculture. Using unmanned aerial vehicles and image processing techniques.

It aims to develop a smart agriculture system and strategy with the integrated operation of technologies such as the developing IoT, cloud computing, image processing, sensors, and big data. Also, it aims to integrate the industry in a way that provides maximum benefit from informatics, increases production efficiency, prevents wastage, and thus prevents various global crises.

It is possible to prevent the food crisis by integrating the same technologies into all agriculture processes. In particular, price fluctuations, which are frequently experienced today, affect the market negatively. It can be used to stabilize the food market due to the integration of information technologies and agriculture. Thus, our resources will be used as needed.

We can express the aim of the study as using Industry 4.0 technologies in agriculture to ensure planned production as needed. It is among our goals to minimize the effects of the food crisis that will occur in agriculture due to climate change, global warming, drought, and other problems affecting productivity in agriculture by making maximum use of technology.

The literature on smart agriculture has also developed in parallel with technology. The Israeli-based CROPX application has developed a solution that enables agricultural enterprises to consume fewer chemicals, energy, and water by collecting data from sensors and software and

mapping the terrain from the satellite, guiding the user by giving advice. Isaac Bentwich, the founder of the CROPX company, stated that the farmers who installed this system achieved 25 percent savings in water and energy [2, 3].

Another technology company, Phytech, uses sensor and cloud technologies in agriculture. It allows monitoring and planning based on the data directly received from the system with the help of sensors. It counts every drop of water the crop receives and records it as data. The rapidly developing drone technology has been used to automate and accelerate image processing procedures for smart agriculture [4, 5].

There are also applications such as Dronedeploy, one of the new drone-based internet services. These applications can generate datasets from their acquired images and quickly interpret the results. Even near real-time response is expected soon [5, 6].

England, Israel, and the Netherlands have become leading countries in the world with their investments and practices in smart agriculture. The UK established its first field crops analysis facility in 2015. The facility operates 24 hours a day and has a scanner that can scan an area of 1800 square meters with sensors and cameras on it. Thanks to the scanner, plant health and development can be followed.

According to the smart agriculture market research conducted by Huawei in 2017, the market value of the world smart agriculture market, which was 13.7 billion dollars in 2015, is expected to increase to 26.8 billion dollars in 2020. According to these data, the market will double in value within five years [7].

2. Smart Agricultural Technologies

In smart agriculture, several technologies can be used for each process. Before the production process, production planning can be done using technologies such as big data analytics and data warehouses. The fields to be produced can be addressed by the images taken from the satellite and the processing of these images. The production can be planned with the analysis by keeping the information on which crop can be

grown in which fields. An extensive database open to any large farmer or producer can be developed with crop cards containing the characteristics of the crops to be produced. Since crops are physical objects, IoT can be used to retrieve data.

2.1. Internet of Things (IoT)

The IoT enables physical objects to transfer data to the network with the help of sensors, sensors, RFID, devices, and software. This concept allows automation systems to be created by digitizing data from physical objects. Since it is based on constantly receiving data from things, it needs Big Data and Cloud technologies so that the received data can be processed, made meaningful, and stored. There is no specific architecture in the literature, but many examples of architecture can be found. The architecture of the IoT system is shown in Figure 1.

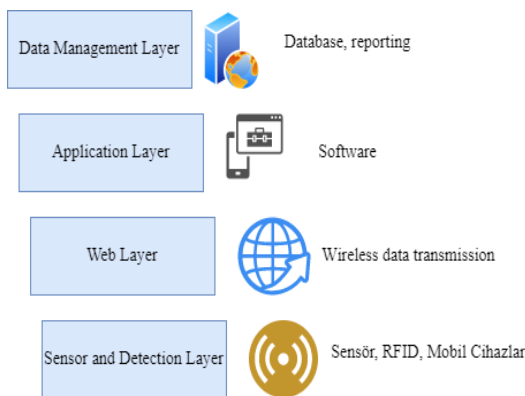


Figure 1. IoT architecture

Data collected from objects is sent to the cloud server. The size of the data is increasing due to the diversity of objects and the constant incoming data. Big Data technology is used to analyze and report this data. Big Data technologies enable us to draw meaningful assumptions from data. Many applications, such as smart cities and environments, have been developed, and more application areas are available. IoT technologies build the system's basis for developing smart farming applications. Environmental variables such as ambient temperature, humidity, and mineral content in the soil can be collected and processed through sensors and software, thus optimizing environmental factors such as humidity and temperature. Digitization and storing agricultural data are crucial to

establishing a smart agriculture system. Instant data provides immediate response to environmental factors. If the moisture in the soil drops, the optimum moisture balance can be achieved by using drip irrigation technology. An example of a Crop Irrigation system with IoT is given in Figure 2.

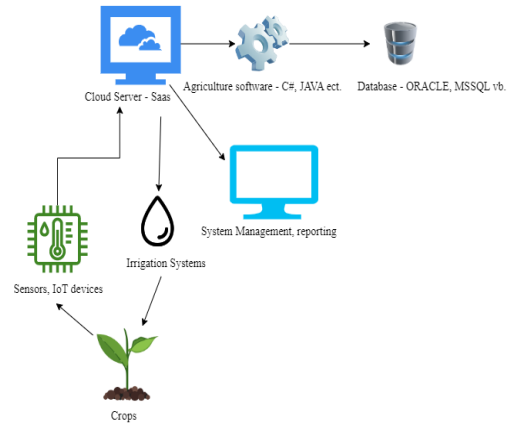


Figure 2. Crop irrigation system with IoT

2.2. Image processing

Image processing is analyzing the image data in the digital environment within the framework of algorithms determined according to the purpose of use in the digital environment. For example, the fields in the digitally transferred image data taken from the air by Unmanned Aerial Vehicles (UAVs) or drones can be shown by an algorithm that recognizes the uncultivated areas by color, painting them with red or the desired color. Even the percentile of the uncultivated areas from the image can be extracted with the algorithm.

This image-processing technology is also used in agriculture. In his article, Nan Xu [8] showed that image processing technology is mainly used in agriculture in the following five directions. These are monitoring crop growth, diagnosing diseases and pests, diagnosing diseases and pests, monitoring maturity, and recognizing crop color. In addition, the study obtained results that positively affect the agricultural development of image-processing technology.

Images from the field are transferred to the cloud system for image processing technology using camera drones and UAVs. By analyzing the image data processed with specific algorithms, the actions that need to be taken in the digital environment can be shown to the user, and their

automation can be provided. An image processing system in agriculture is given in Figure 3.

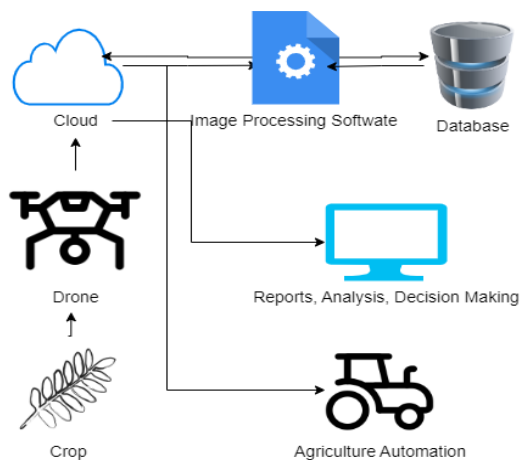


Figure 3. Image processing in agriculture

2.3. Big data

Data emerged with the concept of computer technologies and consisted of digits (0,1) combined. Raw data doesn't mean anything by itself. It becomes information if it is processed. Today, with the increase in data collecting and smart devices, the amount of data collected is increasing exponentially. Data sets that are incrementally obtained in this way are called big data. Big data has three elements: volume, velocity, and diversity. Volume (V) is the size of the data; velocity is the rate at which data is acted upon. Since the data obtained with the IoT is real-time, the speed of writing to the memory is also important. Variety refers to the type of data. Data such as video and audio are expressed as unstructured data types, while data held in relational databases are expressed as structured.

The data collected in agriculture and the fields managed with smart agriculture applications will increase over the years. Big data technologies will be needed to analyze and make sense of these data. Since IoT technologies in smart agriculture are mandatory, technologies such as data mining and data science, which cannot be considered independently of big data technologies, should work in an integrated manner. In addition, due to the increasing data over the years, an agricultural memory will be formed. Agricultural activities in the following years will be planned more easily, and market stability will be ensured. Farmers across the

country are often confused when deciding on the type of crop to plant. If the analysis of the data collected from a single center is provided, necessary guidance will be provided.

3. Smart Farming Application with Image Processing

Images were taken by taking photos in our application. A black background is used to make the image easy to process. It is possible to take and process images outside the black background, but it is desired to be affected by noise in the least way. This application can take and process images instantly with a drone camera. However, efforts have been made to make the application work primarily in its basic form. The overall flow chart and layers of the Smart Agriculture Image Processing Application are shown in Figure 4.

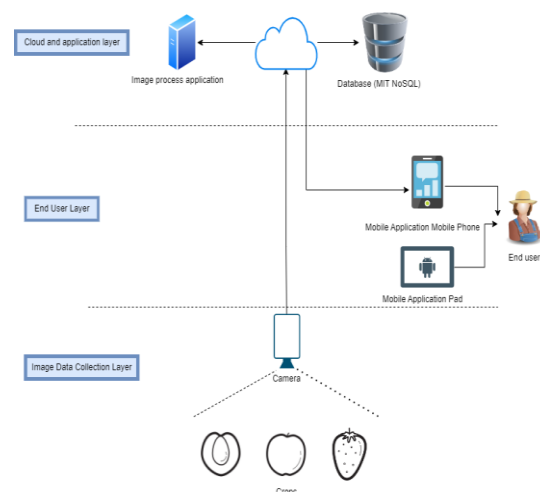


Figure 4. Smart agriculture image processing application

3.1. Image processing

Then, the file path of the image we will process into the project is taken. The image is scaled for easier processing. At this stage, a matrix equal to the picture's dimensions is created, and the value of each pixel of the picture is assigned to this matrix. Since our picture is colored, a third dimension comes with RGB. The scaled version of the image we want to process is seen in Figure 5. As seen in the picture, there is 1 TL and one lemon.

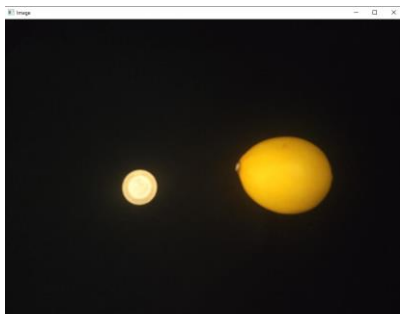


Figure 5. Scaled image to be processed

In the next step of the algorithm, we make our image black and white for easy processing. The cvtColor function of OpenCV is used to create a black-white image. As in Figure 6, the image has become black and white.



Figure 6. Black and white state of the image

In the image, the three dimensions that came from RGB are dispersed. In the next step of the algorithm, the threshold function from OpenCV is used. This function converts the image to a binary image. In this way, the borders are now easier to draw. The format of the image in this step of the algorithm is given in Figure 7.



Figure 7. Binary format of the image

With the histogram function of the matplotlib library, histogram graphics of the picture in black and white and binary format, as in Figure 8, are produced. When the graphs are examined, the threshold function used will facilitate the calculation of contours, which is the next step of the algorithm.

When the histogram graphs are examined, it is observed that the black and white picture can take more than one value between 0 and 50, while the histogram graph of the binary image can only take 0 and 255 values. In the image on the double base, the borders have become well-defined, and the picture has now been prepared to be passed to the contour drawing stage.

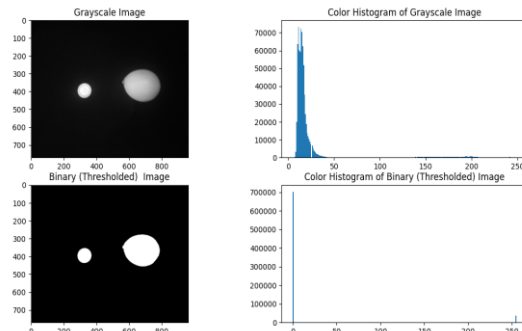


Figure 8. Color histogram charts of image gray and binary formats

The next step of the algorithm is drawing contours by going over the image on the binary base. The drawContours function, which is in the OpenCV library's functions, is used for contour drawing. When this function is used, the objects in the picture are detected one by one. Then, the objects are sorted from the smallest to the largest. Since there are two objects in our painting, two objects are detected only for contour drawing.

The number of objects detected here shows that the algorithm has worked correctly up to this stage. Figure 9 shows the contour drawing where the borders of the coin and lemon are drawn. With the contour drawing, the borders of the objects are now determined, and we can now calculate how many pixels there are within the borders.

In the next stage of the algorithm, the pixel numbers in the area within the contours of the codes are calculated as the values taken from the screen output in Table 1 from the console screen of the application.



Figure 9. Drawing the contours of the objects detected in the image

Table 1. Pixel counts calculated in the app

Image	Pixel Counts Calculated
1 TL	5520
Lemon	30470

According to the pixel numbers obtained from the function, the areas of each pixel actually calculated in square centimeters are shown in Table 2. Knowing the area of the coin helped when calculating the actual area of the pixel. By dividing the coin’s area by the number of pixels, the actual area of 1 pixel was calculated as in the screen output written next to the 1-pixel parameter. The actual area of the lemon in the picture was estimated by establishing the proportion.

Table 2. Actual area conversion of pixel counts calculated in the application

	Actual area (cm ²)
1-Pixel	0.00097295821
Lemon	29.6460368612

In part, up to this algorithm stage, we calculated the crop area in the photo, whose weight we wanted to calculate in square centimeters. After this stage, weight estimation will be made depending on the crop type. A unique calculation method for the crop will be used so that our algorithm will work correctly. As seen in Table 3, as a result of the quantitative measurements, the parameters of the randomly selected crops were as in the table.

Table 3. Density calculations of crops

Crop	Mass (gram)	Volume cm ³	Density Mass (gram/cm ³)
LEMON1	85.4	90	0.9488
LEMON2	121.2	125	0.9696
MANDARIN1	48.1	55	0.8745
MANDARIN 2	77.7	90	0.8633

The selected crops’ images are processed using our application’s algorithm in the next step. As a result, the values shown in Table 4 were obtained. The averages of the area/mass values we obtained from our image processing calculated from these values were taken. The estimated weight of the crop is calculated using the values we get from here.

Table 4. Values of crops obtained from image processing

Crop	Calculated with image processing (cm ²)	Calculated Area / Mass
LEMON1	29.64	0.3470
LEMON2	38.12	0.3145
MANDARIN1	21.83	0.4538
MANDARIN2	33.04	0.4252

The averages of the collected data were calculated in Table 4.5. We will use these averages when calculating the mass from the image we are processing. As can be seen, the area/mass value used for each type of crop is different, and the average values should be calculated using the necessary physical measurements.

In the next step of our algorithm, the system weight estimation software was calculated as 89,6200 grams with the Area / Mass parameter specific to our crop.

Table 5. Density calculations of crops

Crop	Average Calculated Area / Mass
LEMON	0.3307
MANDARIN1	0.4395

The same algorithm was tested with the same crop type and with a different crop type. The results and error rates table is shown in Table 6.

Our algorithm worked and obtained weight estimates with a nominal error rate. The total error rates are shown in Table 7. Our algorithm made predictions for all measurements with an average error of 4.13%.

Table 6. Comparison of the actual mass of crops and their calculated mass by image processing

Crop	Mass (gram)	Calculated with image processing (gram)	Error Rate
LEMON1	85.4	89.62	4.94%
LEMON2	121.2	115.25	5%
MANDARIN1	48.1	49.68	3.28%
MANDARIN2	77.7	75.17	3.3%

Table 7. Total error rate table

Parameter	Value
Total mass (gram)	332.4
Mass Calculated by Image Processing (gram)	329.72
Average Error Rate	4.13%

3.2. IoT application

The proposed IoT architecture starts with the acquisition of data with the help of a camera. The collected data is first processed in our running application in the cloud and transferred wirelessly to our Firebase Cloud Platform. Our Mobile application, which we developed on the MIT platform, also allows data analysis by pulling data from the Firebase Cloud Platform. The whole system works in integration with each other. The architecture of our IoT application is shown in Figure 10.

3.3. Data analysis

Data analysis was performed by using Python’s Pandas library. Methods in the Pandas library were used to analyze the data collected from the environment.



Figure 10. IoT system architecture

The size of our data will grow a lot later in the implementation. Pandas library has been preferred in our application because of its efficient speed performance in extensive data analysis. Due to the application, the number and estimated weight data can be collected while the crops are in the field. Due to these data, we can perform predictions for the future. The collected

data can be compared with previous years and used in production planning.

Example screenshots of bar, column, and line graphics used in our mobile application by performing data analysis are given in Figure 11 and Figure 12, respectively.



Figure 11. Line chart data analysis

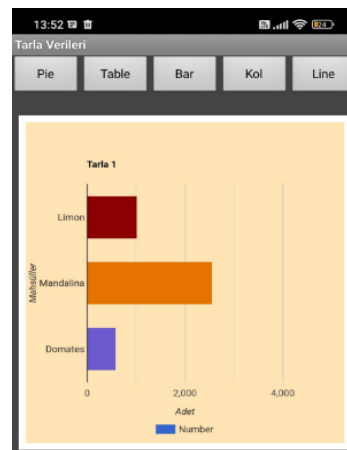


Figure 12. Bar chart data analysis

4. Discussion and Conclusion

As a result of the research, it is seen that due to factors such as increasing population rate, drought, and climate change, humanity needs to use agricultural resources correctly to survive. It is seen that the way to manage these resources correctly is through the digitalization of agriculture by integrating agriculture with the Internet of Things, image processing, and big data technologies.

Governments are investing in this issue, which has also been studied worldwide. Although Türkiye’s climate and soils are suitable for agriculture, it is still at risk of a serious food crisis. Countries such as the Netherlands, England, and Israel have made applications that

increase productivity in agriculture with their technological studies. It is necessary to increase the applications of similar models in our country.

In our application, the OpenCV image processing library is used in Python. Visual Studio Code was used on the code side as a development environment, and Colab was used as an online alternative. On the database side, the NoSQL database structure was used in the Firebase environment. Instantly, the images of the crops were processed with our algorithm, the data were kept in the database, and successful results were obtained with a low error rate by making weight estimations. In the study, it is seen that the use of technology in agriculture increases productivity.

In addition, the image processing project we have done also contributes to this. The positive results we have obtained from our work show that the project can produce even more successful results by maturing as the technologies develop. Based on these positive results, investments should also increase in agriculture, which is a very important area. In our country, whose soils and climate are highly suitable for agriculture, incentives should support efforts. Due to the importance of agriculture, as technological developments continue, the scope of the study has the infrastructure that can mature over time.

Article Information Form

Funding

The authors have not received any financial support for the research, authorship, or publication of this study.

Authors' Contribution

The authors contributed equally to the study.

The Declaration of Conflict of Interest/ Common Interest

No conflict of interest or common interest has been declared by the authors.

The Declaration of Ethics Committee Approval

This study does not require ethics committee permission or any special permission.

The Declaration of Research and Publication Ethics

The authors of the paper declare that they comply with the scientific, ethical, and quotation rules of SAUJS in all processes of the paper and that they do not make any falsification of the data collected. In addition, they declare that Sakarya University Journal of Science and its editorial board have no responsibility for any ethical violations that may be encountered and that this study has not been evaluated in any academic publication environment other than Sakarya University Journal of Science.

Copyright Statement

Authors own the copyright of their work published in the journal and their work is published under the CC BY-NC 4.0 license.

References

- [1] E. Kılavuz, & İ. Erdem, "Agriculture 4.0 applications in the world and transformation of Turkish agriculture," *Social Sciences*, 14(4), pp. 133-157, 2019
- [2] The CropX Company (2022) [Online]. Available: <https://cropx.com/cropx-system/>
- [3] CropX: Advanced Farm Management System (2022) [Online]. Available: <https://agtecher.com/tr/urun/cropx-farm/>
- [4] The Phytech Company (2022) [Online]. Available: <https://www.phytech.com/>
- [5] R. Näsi, T. Hakala, N. Viljanen, E. Honkavaara, P. Peltonen-Sainio, (2017). "How farmer can utilize drone mapping?" [Online]. Available: https://www.fig.net/resources/proceedings/fig_proceedings/fig2017/papers/ts05f/TS05F_naesi_honkavaara_et_al_9004.pdf
- [6] Dronedeploy application (2022) [Online]. Available: <https://www.dronedeploy.com>
- [7] F. Saygılı, A. A., Kaya, E. T. Çalışkan, Ö. E. Kozal, İzmir Ticaret Borsası. Tükeltmat A.Ş. TÜRK TARIMININ GLOBAL

ENTEGRASYONU VE TARIM 4.0,
2019.

- [8] N. Xu, (2021, April). “Image processing technology in agriculture”. In Journal of Physics: Conference Series (Vol. 1881, No. 3, p. 032097). IOP Publishing.

Content of Fatty Acids in Callus Cultures of Endemic *Ajuga vestita* BOISS.

Pınar Orcan^{1*} , Mehmet Yusuf Orcan² ¹Batman University, Technical Science Vocational School, Department of Food Process, Batman, Türkiye, pınar.karakus@batman.edu.tr²Batman University, Central Laboratory Application and Research Center, Batman, Türkiye, mehmetyusuf.orcan@batman.edu.tr

*Corresponding Author

ARTICLE INFO

ABSTRACT

Keywords:

Ajuga vestita BOISS

Callus culture

Endemic

Fatty acid

In vitro

Article History:

Received: 20.09.2023

Accepted: 07.07.2024

Online Available: 01.08.2024

Ajuga L., a member of the Lamiaceae family, is one of the most popular species due to its medicinal, decorative, and pharmacological properties. One of them is *Ajuga vestita* BOISS. which is endangered and placed in the "Endangered (EN)" category. In the present study, using *in vitro* tissue culture techniques, *Ajuga vestita* BOISS. seeds were germinated in hormone-free 1/4 MS medium, and callus were regenerated from leaf explants of germinated seeds in 1/1 MS medium containing BAP (benzylaminopurine) and Kin (kinetin). It was aimed at comparatively examining the fatty acid content of *Ajuga vestita* BOISS. callus. When the fatty acid content of the callus obtained from the control (hormone-free), BAP, and Kin media were examined, major saturated fatty acid amounts were palmitic acid in all three extracts (59.137%, 38.836%, and 24.295%) for control, BAP, and Kin respectively. The major unsaturated fatty acid amounts were octadecanoic acid (21.097%, 32.283%) for control and BAP, respectively, and linoleic acid (21.209%) for Kin considering that high amounts of unsaturated fatty acids make the plants more reliable in terms of health, the higher amount of unsaturated fatty acid content determined in the Kin extract in our study compared to the control will shed light on future studies in this sense that can be done with tissue culture techniques.

1. Introduction

Rare or locally endemic species are sensitive to changes in environmental conditions because they have less genetic diversity than common species. When their environmental conditions change, they are more in danger of extinction. According to the IUCN 2001 criteria, approximately 600 of our endemic species are in the "Very Endangered CR" category, and 700 of them are in the "Endangered EN" category [1, 2]. For this reason, studies on conservation and reproduction methods gain more importance. It is at this point that *in vitro* plant culture has emerged for the conservation and mass clonal propagation of rare plants.

The *ajuga* genus belonging to the Lamiaceae family contains more than 300 annual or perennial species, and the demand for them has increased sharply due to their medicinal, decorative, and pharmacological properties. These wide-ranging plants are in danger of rapid extinction due to over-collection for ornamental and medicinal purposes, as well as habitat destruction and deforestation. *Ajuga boninsimae*, *Ajuga bracteosa*, *Ajuga ciliate*, *Ajuga genevensis*, *Ajuga incisa*, *Ajuga makinoi*, *Ajuga multiflora*, *Ajuga pyramidalis*, *Ajuga shikotanensis*, *Ajuga reptans* and *Ajuga vestita* are categorized as endangered and protected plants. One of these species is *Ajuga vestita* BOISS. which is medically important, endemic, and in the "EN-Endangered" category.

Phytochemical studies have revealed that *Ajuga* species contain many bioactive compounds, such as anthocyanidin-glycosides, essential oils, iridoid glycosides, flavonoids, phytoecdysteroids, sterols, and terpenoids. The studies conducted with other *Ajuga* species have observed that these species have phenolic compounds, the components of their essential oils are determined, and they have many pharmacological activities such as antioxidant, cytotoxic, and antimicrobial activity [3-7].

In recent years, there has been an increasing interest in the production of components with pharmacological effects (secondary metabolites, fatty acid components, etc.) by tissue culture methods. These components can also be obtained by conventional methods, but these methods have disadvantages, especially for rare endemic plants. *In vitro* culture methods provide different alternatives to overcome the problems encountered in obtaining these metabolites naturally. With these studies, it is aimed at obtaining a large number of plants to be produced and then to producing them on an industrial scale and at a low cost for some applications [8].

In this study, it was aimed at comparatively determining the fatty acid content (control, BAP, Kin) in callus regenerated from leaf explants of seedlings obtained from *in vitro* shoots of *Ajuga vestita* BOISS. The fact that there is no study in the literature in which the fatty acid compositions of this plant were presented comparatively before increases the importance of this study. These data will shed light on any possible future study with this and similar endemic plants.

2. Material and Method

2.1. Plant material and cultivation

Ajuga vestita BOISS. seeds, which were used as starting material in the study, were collected from the Savur district of Mardin and identified by Prof. A. Selçuk ERTEKIN (*Ajuga vestita*-HM00000282) [9].

Mature seeds of *Ajuga vestita* were washed and then pre-sterilized by soaking them in 70% alcohol for 30 seconds. The seeds were soaked in a 5% NaOCl solution for 15 minutes and

sterilized. They were then rinsed in sterile distilled water five times for five minutes each to remove NaOCl. The seeds were cultured in ¼ MS medium supplemented with 30 g/L sucrose with a pH adjusted to 5.8 to support germination and growth [10]. Sterile seeds, along with cracked testa, were cultured and left to germinate in the growth chamber (25±2 °C temperature, 16 hours of light, 8 hours of dark light period; 3000-5000 lux).

After a two-week culture period, the shoot tips of the germinated seeds were cultured in medium supplemented with Kin for propagation, and *in vitro* shoots were obtained for use as starting material in callus formation studies. Following 4-weeks development period, leaf explants from *in vitro* shoots were used in callus formation studies with different concentrations of BAP and Kin (0.125-4.0 mg/L). Callus samples grown in 1/1 MS medium containing BAP and Kin, as well as those without hormones (control), were dried in a cool and dry environment for use in fatty acid content studies.

2.2. Determination of fatty acid methyl esters (FAME)

Each explant, which was powdered, then extracted for 4 hours by the Soxhlet continuous extraction method using hexane. The extracted product was evaporated in reflux, and the obtained extract was completed with 10 mL of hexane. 1 mL of 2 N methanolic KOH solution was added to the hexane extract and shaken vigorously. The sample was kept in the dark for 1-2 hours until the phase separation took place and the upper phase became clear, then the supernatant was taken into vials and the fatty acid methyl ester analysis was performed with a gas chromatography flame ionization detector (GC-FID).

Analysis was performed on the Shimadzu GC-2030 instrument combined with the AOC-20 i Plus auto injector. The Restek RT-2560 column (0.20 µm film thickness, 0.25 mm inner diameter, 100 m length, cat# no, 13198) was used. The column temperature program began 100 °C hold for 4 minutes, followed by an increase at a rate of 3 °C/min until reaching a final temperature of 240 °C, where it was held for

20 minutes. The sample injection volume was set at 1.0 μ l in a split mode ratio of 1:20, and helium (flow rate of 1 ml/min) was used as the carrier gas. The hydrogen flow rate of 32.0 ml/min and the air flow rate of 200.0 ml/min. The injection and detector temperatures were both set at 250 °C. The total time of the analysis was 70 minutes. The "Food Industry FAME Mix Standard, Restek (cat# no, 35077, 37 components)" was used as a standard. FAME's are identified according to the retention times of this standard.

3. Results and Discussion

Ajuga vestita BOISS. mature seeds were subjected to sterilization by first soaking them in 70% ethanol for 30 seconds, followed by immersion in 5% NaOCI for 15 minutes. The seeds were then rinsed with sterile distilled water to remove any residual NaOCI, completing the sterilization process. After sterilization, the seeds were placed in a hormone-free 1/4 MS medium and allowed to grow in a plant growth chamber.

Following a development period of 3 weeks, leaf explants from the germinated seedlings were used for callus initiation studies. These leaf explants were cultured in a 1/1 MS medium supplemented with hormone-free (control), BAP and Kin. The fatty acid contents of the callus extracts obtained from leaf explants cultured in the medium containing BAP, and Kin were compared with those of the control plants and presented in Table 1.

The researchers conducted a study on the fatty acid contents of four plants from the Lamiaceae family, including *Salvia verticillata*, using the GC/MS method [7]. They identified tricosanoic acid and lignoceric acid as the major saturated fatty acids, while nervonic acid, eicosadienoic acid, and docosadienoic acid were identified as the major unsaturated ones in each plant. The researchers emphasized the positive impact of high unsaturated fatty acid content on plant health and suggested that their findings would inform future studies involving these plants. In our study, while the total saturated fatty acid ratios were 63.661%, 45.373%, and 53.342%, the total unsaturated fatty acid ratios were 36.339%, 54.626%, and 46.659% for control, BAP, and Kin, respectively.

In another study, researchers conducted a comparison of the carotenoid, fatty acid, and tocopherol content of leaves from *A. multiflora* plants that were either transferred to soil or obtained from shoots cultured *in vitro* [11]. They found that the highest levels of carotenoids, fatty acids, and tocopherols were obtained from the leaves of shoots cultured in MS medium. This study, which compared these characteristics between plants from natural environments and those from *in vitro* cultures, underscores the significance of studies conducted using tissue culture techniques. It suggests that extracts from *in vitro* cultures yield superior results compared to those obtained from plants grown in natural environments. This finding highlights the potential advantages and importance of utilizing tissue culture techniques in plant research.

The leaves of *Ajuga iva* were analyzed for fatty acids, essential oils, and phenolic compounds in a study cited as [12]. The analysis revealed that linolenic and linoleic acids were the primary components of the fatty acid profile. Additionally, another study [13] conducted a comparative examination of neutral lipids, including their fatty acid composition, in callus cultures and leaves of *Ajuga genevensis* and *Ajuga chia* plants. The study highlighted the significant influence of species, the origin of the callus, and the age of the culture (number of subcultures) on both the composition and content of lipids and fatty acids. Among unsaturated fatty acids, linoleic acid has been reported as a predominant component in callus tissues, whereas palmitic acid is dominant in saturated fatty acids. Palmitic acid is a fatty acid that can be converted into stearic acid and oleic acid in all organisms [14].

The researchers concluded that the high palmitic acid content in all samples studied can be attributed to this situation. In the present study, palmitic acid was found to be the predominant component among saturated fatty acids in all treatments. Additionally, a similar study investigating the fatty acid compositions of *Ajuga reptans* L. plants yielded results consistent with our findings. According to the results of this study, palmitic acid exhibited the highest proportion among saturated fatty acids, while

linolenic and linoleic acids showed the highest proportions among unsaturated fatty acids [15].

Table 1. Fatty acid contents of callus extracts of *A. vestita* BOISS. (%m/m)

Fatty Acids	Extracts		
	Control	BAP	KIN
4:0 Butyric acid	ND	ND	1.324
6:0 Caproic acid	1.840	3.915	6.898
10:0 Decanoic acid	ND	ND	3.604
11:0 Undecanoic acid	ND	ND	2.827
12:0 Dodecanoic acid	0.884	1.159	0.864
14:0 Myristic acid	1.800	1.463	1.576
14:1 (<i>cis</i> -9) Myristoleic acid	ND	ND	0.909
15:1 (<i>cis</i> -10) Pentadecanoic acid	ND	ND	1.092
16:0 Palmitic acid	59.137	38.836	24.295
17:1 (<i>cis</i> -10) Heptadecanoic acid	8.284	7.524	0.985
18:0 Stearic acid	ND	ND	6.631
18:1 (<i>trans</i> -9) Octadecanoic acid	21.097	32.283	13.498
18:1 (<i>cis</i> -9) Oleic acid	ND	ND	0.508
18:2 (<i>cis</i> -9,12) Linoleic acid	2.578	12.033	21.209
18:3 (<i>cis</i> -9,12,15) Linolenic acid	ND	2.087	5.873
20:0 Arachidic acid	ND	ND	2.328
22:0 Behenic acid	ND	ND	1.026
22:1 (<i>cis</i> -13) Erucic acid	ND	ND	2.585
22:6 (<i>cis</i> -4,7,10,13,16,19) Docosahexaenoic acid (DHA)	1.281	0.143	ND
23:0 Tricosanoic acid	ND	ND	0.438
24:0 Lignoceric acid	ND	ND	1.531
24:1 (<i>cis</i> -15) Nervonic acid	3.099	0.556	ND
Saturated fatty acids	63.661	45.373	53.342
Monounsaturated fatty acids	32.48	40.363	19.577
Polyunsaturated fatty acids	3.859	14.263	27.082
Total	100.000	99.999	100.001

BAP: benzylaminopurine, KIN: kinetin, ND: not detected

In our study, arachidic acid was detected only in the Kin extract, albeit in low amounts, while linolenic acid was present in extracts other than the control. It is known that linoleic acid is converted to jasmonic acid, which plays a significant role in plant metabolism, particularly in defense mechanisms, through 12-oxophytodienoic acid [16-19]. The level of linoleic acid was found to be the lowest in the control group and the highest in the medium supplemented with Kin in the present study. The major fatty acids were determined by reviewing literature studies that investigated the fatty acid composition of the plants. Plant

contents may vary due to numerous factors, including the geographical location where the plant was collected, the time of collection, the

specific plant part used, the solvent utilized for extract preparation, and the conditions of analysis. This situation renders it impossible to obtain exactly the same results as the studies previously recorded in the literature. A study comparing the amount and composition of neutral lipids and their fatty acids in the leaves and callus cultures of *Ajuga genevensis* and *Ajuga chia* plants in their natural environment found that lipid and fatty acid content varied

depending on factors such as species, the origin of the callus, and the number of subcultures. [12]. Topdemir et al. applied different hormone concentrations and combinations (BAP and NAA) to the cotyledon explants of kiwi plants (*Actinidia deliciosa*). They observed a decrease in the ratios of palmitoleic, stearic, and linoleic acids in groups with different hormone combinations, while an increase in the ratio of linolenic acid was detected [20].

Aly et al. investigated the effect of 2,4-D and benzyladenine on the stimulation of fatty acid synthesis *in vitro*. They found a decrease in saturated fatty acids, such as palmitic and stearic acid levels, in groups where plant growth regulators were added compared to the control group [21]. In the current study, hormone application led to a decrease in palmitoleic acid content and an increase in linoleic acid and stearic acid levels compared to the control group. The differences in the results of these studies may be attributed to the use of different plant species as materials and the variation in the hormones applied.

4. Conclusion

Unsaturated fatty acids, due to the double bonds they contain, exhibit higher reactivity compared to saturated fatty acids. This reactivity increases proportionally with the number of double bonds in the fatty acid chain. Unsaturated fatty acids play constructive and reparative roles in the biochemical and physiological activities of the body, as well as in maintaining healthy tissue development and balanced organ function [22]. They are known to play a crucial role in preventing various diseases such as cardiovascular diseases, depression, migraines, rheumatism, diabetes, high cholesterol, hypertension, allergies, and cancer [23].

Therefore, the high content of unsaturated fatty acids found in the callus extracts of *Ajuga vestita* BOISS., particularly those containing BAP and Kin obtained from leaf explants under *in vitro* conditions, holds significant importance for the aforementioned reasons.

The fact that a limited study comparing the fatty acid compositions of this plant has been found in

the literature further emphasizes the importance of this study. The data obtained from this study will provide valuable insights for future research involving these plants. It will serve as a reference for any potential studies conducted with this plant in the future.

Article Information Form

Funding

The authors has no received any financial support for the research, authorship or publication of this study.

Authors' Contribution

The authors contributed equally to the study.

The Declaration of Conflict of Interest/Common Interest

No conflict of interest or common interest has been declared by authors.

The Declaration of Ethics Committee Approval

This study doesn't require ethics committee permission or any special permission.

The Declaration of Research and Publication Ethics

The authors of the paper declare that in the writing process of this study, international scientific, ethical and citation rules were followed, and no falsification was made on the collected data. Sakarya University Institute of Science Journal and editorial board bear no responsibility for all ethical violations that may be encountered. All responsibility belongs to the corresponding author and this study has not been evaluated in any academic publications other than Sakarya University Journal of Science.

Copyright Statement

Authors own the copyright of their work published in the journal and their work is published under the CC BY-NC 4.0 license.

References

- [1] R. B. Primack, "Essentials of conservation biology," Environment, 5th. Sunderland, Massachusetts: Sinauer Associates, 2006, pp. 564.

- [2] Tehlike Altında Bitki Türleri Listesi. (2018, July. 31). *Ajuga vestita* [Online]. <http://www.tehditaltindabitkiler.org.tr/v2/index.php?sayfa=detay&id=NzQyNA>.
- [3] Z.H. Israili, B. Lyoussi, "Ethnopharmacology of the plants of genus *ajuga*", Pakistan Journal of Pharmaceutical Sciences, vol. 22, no. 4, pp. 425-462, 2009.
- [4] N. Haşimi, "*Ajuga vestita* ve *Ajuga xylorrhiza* bitkilerinin petrol eteri, aseton ve metanol ekstraktlarının bazı biyolojik aktivitelerinin belirlenmesi", Doktora Tezi, Biyoloji Bölümü, Dicle Üniversitesi, Diyarbakır, Türkiye, 2012.
- [5] E. Sönmez, Y. B. Köse, "Morpho-anatomical investigations on *Ajuga postii* Briq and *Ajuga relictia*", Biological Diversity and Conservation, vol. 10, no. 1, pp. 39-48, 2016.
- [6] B. Ş. Aydınarığ, "Endemik *Ajuga vestita* BOISS. bitkisinin farklı eksplantlarından itibaren kallus oluşturma potansiyeli ve oluşan kallusun biyolojik aktivitesinin araştırılması", Yüksek Lisans Tezi, Biyoloji Bölümü, Batman Üniversitesi, Batman, Türkiye, 2019.
- [7] P. Taştan, D. Bırım, T. Fafal, G. Armagan, B. Kıvçak, "Bazı Lamiaceae bitkilerinin yağ asidi bileşiminin belirlenmesi," Kahramanmaraş Sütçü İmam Üniversitesi Tarım ve Doğa Dergisi, vol. 25, no. 6, pp. 1199-1204, 2022.
- [8] A. Güven, İ. Gürsul, "Bitki doku kültürlerinde sekonder metabolit sentezi," Gıda, vol. 39, no. 5, pp. 299-306, 2014.
- [9] A.S. Ertekin. Mezopotamya Herbaryumu. (2013, June. 19). Mezaopotamya Herbaryumu [Online]. <https://www.mezopotamyaherbaryumu.com/katalog/hm00000282>
- [10] T. Murashige, F. Skoog, "A revised medium for rapid growth and bio-assays with tobacco tissue cultures," Plant Physiology, vol. 15, no. 3, pp. 473-497, 1962.
- [11] I. Sivanesan, R. K. Saini, R. Noorzai, A. J. Zamany, D. H. Kim, "*In vitro* propagation, carotenoid, fatty acid, and tocopherol content of *Ajuga multiflora* bunge," in 3. Biotechnology, Berlin Germany, 2016, p. 91.
- [12] H. Ammar, I. Touihri, A. E. Kholif, Y. M'Rabet, R. Jaouadi, M. Chahine, M. E. de Haro Marti, E. Vargas-Bello-Pérez, K. Hosni, "Chemical composition, antioxidant, and antimicrobial activities of leaves of *Ajuga iva*," Molecules, vol. 27, no.20, 2022.
- [13] N. Z. Sahakyan, M. T. Petrosyan, Y. G. Popov, V. V. Volodin, N.V. Matistov, I. V. Gruzdev, T. I. Shirshova, "Content of neutral lipids and fatty acids in callus cultures and leaves of intact plants of *Ajuga genevensis* and *Ajuga chia*," Biotechnology & Biotechnological Equipment, vol. 24, no. 1, pp. 87-90, 2010.
- [14] De. W. Stetten, R. Schoeneimer, "The conversion of palmitic acid into stearic and palmitoleic acids in rats," Journal of Biological Chemistry, vol. 133, pp. 329-345, 1940.
- [15] A. Grytsyk, S. Maliuvanchuk, "Fatty acid composition of common bugle herb (*Ajuga reptans* L.)," Pharmaceutical Science, vol. 4, no. 20, pp. 21-26, 2019.
- [16] R. Johnson, J. Narvaez, G. An, C. Ryan, "Expression of proteinase inhibitors I and II in transgenic tobacco plants: Effects on natural defense against *Manduca sexta* larvae," Proceedings of the National Academy of Sciences, vol. 86, pp. 9871-9875, 1989.
- [17] R. A. Creelman, J. E. Mullet, "Biosynthesis and action of jasmonates in plants," Annual Review of Plant Physiology and Plant Molecular Biology, vol. 48, pp. 355-381, 1997.

- [18] F. Sefidkon, M. S. Khajavi, "Chemical composition of the essential oils of two salvia species from Iran: *Salvia verticillata* L. and *Salvia santolinifolia* BOISS," Flavour and Fragrance Journal, vol. 14, no. 2, pp. 77-78, 1999.
- [19] Z. Rajabi, M. Ebrahimi, M. Farajpour, M. Mirza, H. Ramshini, "Compositions and yield variation of essential oils among and within nine salvia species from various areas of Iran," Industrial Crops and Products, vol. 61, pp. 233-239, 2014.
- [20] A. Topdemir, T. Okutan, G. Kırmızııkaya, Ö. Yılmaz, "Naftalin asetik asit, 6-benzilaminopürin ve indol-3-bütirik asit kombinasyonlarının *Actinidia deliciosa* kallus gelişimi üzerine biyokimyasal bir araştırma," Kahramanmaraş Sütçü İmam Üniversitesi Tarım ve Doğa Dergisi, vol. 27, no. 2, pp. 249-260, 2024.
- [21] M. A. M. Aly, E. A. Amer, W. A. Al-Zayadneh, A. E. N. Eldin, "Growth regulators influence the fatty acid profiles of *in vitro* induced jojoba somatic embryos," Plant Cell, Tissue And Organ Culture, vol. 93, pp. 107-114, 2008.
- [22] U. Gogus, C. Smith, "n-3 Omega fatty acids: a review of current knowledge," International Journal of Food Science & Technology, vol. 45, no. 3, pp. 417-436, 2010.
- [23] P. Wassell, G. Bonwick, C. J. Smith, E. Almiron-Roig, N. V. G. Young, "Towards a multidisciplinary approach to structuring in reduced saturated fat-based systems – a review," International Journal of Food Science & Technology, vol. 45, no. 4, pp. 642-655, 2010.

Investigation of Caffeine Degradation by Anodic Oxidation Using Boron-Doped Diamond Electrode

Gökçe Didar Değermenci Kastamonu University, Faculty of Architecture and Engineering, Department of Environmental Engineering, Kastamonu, Türkiye, gdegermenci@kastamonu.edu.tr

ARTICLE INFO

ABSTRACT

Keywords:

Anodic oxidation
Caffeine removal
Boron-Doped diamond

Article History:

Received: 14.12.2023
Accepted: 04.06.2024
Online Available: 01.08.2024

In this study, the purification of caffeine by electrochemical oxidation, one of the advanced oxidation processes, was systematically investigated. A boron-doped diamond electrode was used as the anode, which has a high potential for the production of large amounts of hydroxyl radicals. The effects of applied current density, initial pH, supporting electrolyte concentration, cathode type, anode-cathode distance, and initial caffeine concentration were evaluated. The results showed that the electrochemical degradation rates of caffeine follow pseudo-first-order kinetics, with rate constants ranging from 0.0154 to 0.0496 min⁻¹ depending on the operating parameters. The applied current density and the electrolysis time proved to be the most important parameters influencing both caffeine degradation and energy consumption. However, varying the initial caffeine concentration and the concentration of the supporting electrolyte also influenced the caffeine degradation rates. Changing the anode-cathode distance and the type of cathode has no effect on the rate of caffeine degradation, but it does have an effect on energy consumption. A current density of 20 mA cm⁻², a supporting electrolyte concentration of 50 mM K₂SO₄, an anode-cathode distance of 2 mm, a cathode type of stainless steel, and an initial solution pH of 3 were found to be optimal values for the degradation of a solution containing 25 mg L⁻¹ caffeine in 45 minutes using a boron-doped diamond anode. Finally, it was found that the pH value of the solution tended to increase during electrolysis.

1. Introduction

The pollution of surface waters such as rivers and lakes with organic pollutants is a growing concern today. Protecting surface waters from potential contamination is of great importance as they are the main source of drinking water in many countries around the world. Pharmaceuticals and personal care products, endocrine-disrupting compounds, and pesticides are the primary pollutants of concern [1-3]. Pharmaceuticals and personal care products have become a primary concern for scientists and regulators as they have been shown to negatively impact freshwater fish and invertebrates and contribute to the development of antibiotic-resistant bacteria [4-6].

Caffeine is one of the most widely consumed food ingredients in the world and has been used for thousands of years. Caffeine is a methylxanthine alkaloid found in varying amounts in the beans, leaves, and fruits of more than 60 plants, including coffee beans, tea leaves, kola nuts, and cocoa beans [7, 8]. It is found in coffee, tea, chocolate, and some soft drinks, as well as in medicines and dietary supplements [9]. Coffee in particular, with 2.25 billion cups consumed every day, is the world's most traded beverage after oil [10].

Caffeine is also an important compound used in the pharmaceutical industry. Therefore, large amounts of caffeine are needed for the

production of various beverages, foods, and medicines. In line with increasing consumption, caffeine is continuously discharged into water bodies worldwide. Caffeine was detected at 8.5-50 $\mu\text{g L}^{-1}$ in effluent from hospital wastewater treatment plants in Spain [11], 2.9-83 $\mu\text{g L}^{-1}$ in wastewater in the Czech Republic [12], 0.23-20.7 $\mu\text{g L}^{-1}$ in wastewater in Saudi Arabia [13], 5.64-6.20 $\mu\text{g L}^{-1}$ in wastewater in Pakistan [14], 27.8-642 $\mu\text{g L}^{-1}$ in wastewater in China [15], and 20.8-159 $\mu\text{g L}^{-1}$ in wastewater and 62.6 to 129.3 $\mu\text{g L}^{-1}$ in hospital wastewater in Türkiye [16].

After the discharge of caffeine into the aquatic environment, it is extremely stable due to its high solubility in water and a half-life reported to be 100-240 days [16, 17]. Conventional wastewater treatment processes cannot completely remove caffeine, which leads to its presence in surface waters, groundwater, oceans, and other water bodies and thus has a negative impact on ecosystems and the environment [18, 19]. Caffeine can also have negative effects, such as neurological damage and reproductive effects, and can even affect the survival of aquatic organisms [20]. Therefore, wastewater containing caffeine must be treated before discharge into the receiving environment to avoid environmental problems caused by the excessive use of caffeine and the low removal efficiency of conventional wastewater treatment.

Conventional wastewater treatment systems for domestic and industrial wastewater are insufficient to remove some persistent organic pollutants. Other treatment systems are required to remove these persistent pollutants [21]. Advanced oxidation processes (AOPs) are used to remove various persistent organic pollutants in wastewater. AOPs such as sonophotocatalysis [22], UV/chlorine [23], ozonation [24], and UV/H₂O₂ [25] have been applied for caffeine removal. In recent years, new AOPs based on electrochemical technology, so-called electrochemical advanced oxidation processes (EAOPs), have been developed for the treatment of various wastewater containing refractory pollutants [26-28]. EAOPs are based on the direct or indirect oxidation of organic materials using an insoluble anode material (Ti, Ti/Pt, Ti/RuO₂, Ti/IrO₂, graphite, boron-doped diamond) [29-31]. BDD electrodes have

technologically important properties such as an inert surface with low adsorption properties, remarkable stability against corrosion even in strong acids, and extremely high overpotentials for oxygen evolution. Due to these properties, BDD electrodes are known to have a high potential for producing large amounts of hydroxyl radicals, which are strong oxidising agents capable of mineralizing any class of organic pollutants, making it an effective application for water purification [3, 32].

In this study, the degradation of caffeine was investigated in a batch reactor operated in galvanostatic mode using a BDD anode. The effects of different current densities, initial solution pH, supporting electrolyte concentration, cathode type, inter-electrode distance, and initial caffeine concentration on caffeine degradation were investigated. Based on the experimental data obtained, the degradation kinetics were analyzed using the pseudo-first-order rate equation, and the energy consumption was also evaluated.

2. Materials and Methods

2.1. Chemicals

Caffeine (C₈H₁₀N₄O₂, >98.5%), sulfuric acid (H₂SO₄, 95-98%), sodium hydroxide (NaOH, >99%), and potassium sulfate (K₂SO₄, >99%) were purchased from Merck. All solutions were prepared with distilled water at room temperature.

2.2. Analytical procedures

A standard caffeine stock solution was prepared and diluted with distilled water to obtain known caffeine concentrations of 2, 5, 10, 20, 30, 40, and 50 mg L^{-1} . The absorbance values of these caffeine concentrations were measured in a UV-Vis spectrophotometer (DR 6000, HachLange) at a specific wavelength of 273 nm, and the calibration curve was plotted. The absorbance was found to be linearly related to the caffeine concentration, and the coefficient of determination for the experimental data was $R^2=0.9997$. The degradation efficiency and energy consumption were calculated using Equation 1 and Equation 2, respectively:

$$\text{Removal, (\%)} = (1 - C_t / C_0) \times 100 \quad (1)$$

$$E_c, (\text{kWh m}^{-3}) = V \times I \times t / V_s \quad (2)$$

where C_0 is the initial caffeine concentration (mg L^{-1}), C_t is the caffeine concentration at time t (mg L^{-1}), V is mean cell voltage (V), I is electrolysis current (A), t is electrolysis duration (h), and V_s is solution volume (L).

2.3. Experimental setup

The electrolysis experiments were carried out in an undivided cylindrical electrochemical cell (Figure 1) made of glass with a diameter of 7.5 cm and a capacity of 400 mL of aqueous solution. A single boron-doped diamond electrode (BDD) with an area of 50 cm^2 (5 cm x 10 cm) was used as the anode. The BDD electrode with a $12 \mu\text{m}$ thick diamond layer on niobium was purchased from DiaCCon GmbH (Germany). Stainless steel (SS), graphite, and BDD electrodes with an area of 50 cm^2 (5 cm x 10 cm) were used as cathodes. The anode and cathode electrodes were immersed 7 cm deep in the solution. Therefore, 35 cm^2 was used as the anode area.

The temperature of the solution was kept constant at 25°C using a temperature-controlled cooling/heating circulator (LABO, C200-H13). Potassium sulfate (K_2SO_4) was added to the reactor as a supporting electrolyte to improve the conductivity of the solution. The caffeine-containing solution was stirred continuously at 600 rpm using a magnetic stirrer (IKA, RCT basic) to improve mass transfer. The electrolysis experiments were performed with a constant current power supply (GW Instek, PSW 80-40.5). This device also displayed the cell voltage during the entire process. Experiments were performed at the natural pH of the caffeine solution, 5.8, unless otherwise stated. Without adding a buffer solution, the pH of the solution was adjusted to the desired value only once at the beginning of the experiment with 1 M H_2SO_4 or 1 M NaOH and was not changed during the experimental run. At each sampling time, the change in the pH value of the solution was monitored using the portable WTW MultiLine® Multi 3620 IDS meter (Xylem Analytics, Germany).

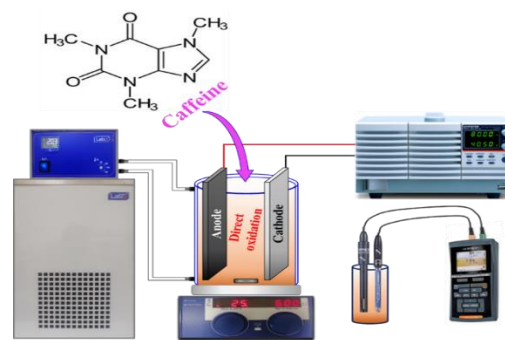


Figure 1. Diagram of the experimental setup

2.4. Kinetic analysis

The removal of organic compounds by the electrooxidation process follows pseudo-first-order kinetics [27, 33, 34]. The reaction rate constant (k_I) can, to a certain extent, indicate the rate of the overall reaction. Therefore, the nonlinear form of the pseudo-first-order kinetic model shown in Equation 3 is used in this study to understand the degradation kinetics of caffeine under different reaction conditions:

$$dC/dt = -k_I t \quad (3)$$

where k_I is the rate constant (min^{-1}) for the pseudo-first-order kinetic model, t is the reaction time, and C_0 and C_t are the caffeine concentrations (mg L^{-1}) in the initial sample and in the sample at any time, respectively. The Microsoft Excel solver add-in tool was used to estimate the parameters of the kinetic model.

3. Results and Discussion

The effects of applied current density ($5\text{-}20 \text{ mA cm}^{-2}$), supporting electrolyte concentration ($10\text{-}50 \text{ mM}$), initial solution pH ($3\text{-}10$), initial caffeine concentration ($25\text{-}75 \text{ mg L}^{-1}$), cathode type (SS, graphite, BDD), and anode-cathode distance ($2\text{-}14 \text{ mm}$) on caffeine degradation in the electrooxidation system were systematically analyzed.

3.1. Effect of applied current density

The applied current density is the most important parameter affecting both the degradation kinetics and the treatment costs, as it influences the amount of oxidizing species produced [35]. The effect of the applied current density on caffeine degradation is shown in Figure 2. The

experimental conditions were an initial pH of 5.8, a supporting electrolyte concentration of 50 mM, an initial caffeine concentration of 25 mg L⁻¹, an anode-cathode distance of 2 mm, and cathode type of SS. Figure 2(a) shows that caffeine removal varies at different current densities. At the end of the electrolysis time (120 min), caffeine removal was 75.2%, 92.7%, and 96.3% at current densities of 5, 10, and 20 mA cm⁻², respectively.

After 60 minutes of electrolysis, the efficiency of caffeine degradation was 59.1%, 75.0%, and 96.0% at current densities of 5, 10, and 20 mA cm⁻², respectively. Increasing the applied current density increases the rate and amount of hydroxyl radical production on the BDD surface according to Equation 4 [28, 35], and thus increases the efficiency of caffeine degradation. As the current density increases, the caffeine degradation time decreases. Li et al. reported the electrochemical degradation of ciprofloxacin with a BDD anode and found that ciprofloxacin was completely degraded in about 10 minutes at a current density of 40 mA cm⁻² [36]. The pseudo-first-order reaction rate constant calculated by the non-linear method is 0.0154, 0.0238, and 0.0438 min⁻¹ for current densities of 5, 10, and 20 mA cm⁻², respectively. These results indicate that the rate of caffeine degradation depends significantly on the current density. The pseudo-first-order rate constant showed a linear correlation with the increase in applied current density ($k_1 = 0.0019 \times J + 0.0051$; $R^2 = 0.9988$). Similar results were obtained in the ibuprofen removal study [37].

The effect of applied current density on energy consumption in electrolysis experiments conducted at different current densities was calculated using Equation 2 and shown in Figure 2(b). As the current density of the system increases, the energy consumption increases along with the voltage increase. The energy consumption for current densities of 5, 10, and 20 mA cm⁻² is calculated as 3.80, 8.44, and 18.75 kWh m⁻³, respectively. With increasing current density, the amount of oxidizing species produced according to Equation 4 increases [35], which can lead to chemical changes on the electrode surface and reduce the lifetime of the electrode [38]. Although a high current density

increases caffeine removal, it can lead to a decrease in current efficiency above a certain value [31, 39]. The decrease in current efficiency can be attributed to the degradation of caffeine by BDD([•]OH) and the formation of less degradable by-products and parasitic reactions of BDD([•]OH). The most important of these parasitic reactions is the oxidation of BDD([•]OH) to O₂ at the anode, according to Equation 5. However, it can also occur by dimerization of BDD([•]OH) to H₂O₂ according to Equation 6 and formation of hydroperoxyl radicals, which have a low oxidation capacity of BDD([•]OH) and H₂O₂ according to Equation 7. Increasing the speed of these reactions means that less oxidizing BDD([•]OH) is formed, and thus the degradation of organic pollutants is reduced [31, 40–42]. For these reasons, higher current densities were not investigated.

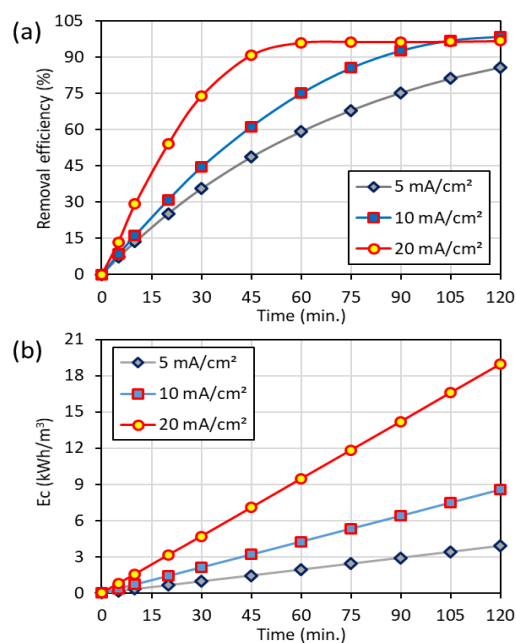
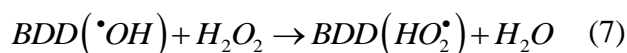
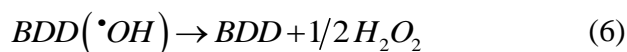
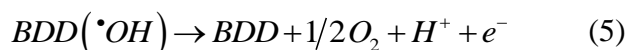
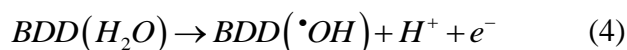


Figure 2. Variation of caffeine degradation efficiency (a) and energy consumption (b) over time with applied current density



3.2. Effect of supporting electrolyte concentration

Supporting electrolytes (SEs) are one of the important parameters that influence the electrochemical degradation process [43]. Increasing the SE concentration plays an important role in increasing the conductivity of the solution and accelerating electron transfer [44]. In this study, K_2SO_4 was used as SE, and the effect of different SE concentrations (10, 25, and 50 mM K_2SO_4) on caffeine degradation was investigated (Figure 3). The experimental conditions were an initial pH of 5.8, a current density of 20 mA cm^{-2} , an initial caffeine concentration of 25 mg L^{-1} , an anode-cathode distance of 2 mm, and cathode type SS. SE has a major influence on the degradation of caffeine in the BDD-SS system. Figure 3(a) shows that the efficiency of caffeine degradation varies with the different SE concentrations.

The efficiency of caffeine degradation at 60 min of electrolysis time is 67.7%, 87.7%, and 96.0% at 10, 25, and 50 mM SE concentrations, respectively. After 120 minutes of electrolysis, caffeine removal was 93.4 %, 98.7 %, and 96.7 % for 10, 25, and 50 mM SE concentrations, respectively. These results show that the caffeine removal rate depends on the SE concentration and that the caffeine removal time decreases with increasing SE concentration. The pseudo-first-order reaction rate constants are 0.0196, 0.0308, and 0.0438 min^{-1} for supporting electrolyte concentrations of 10, 25, and 50 mM, respectively. The pseudo-first-order reaction rate constant showed a linear correlation with the concentration of the supporting electrolyte ($k_f = 0.0006 \times [K_2SO_4]_0 + 0.0145$; $R^2 = 9901$).

The required voltage decreases as the SE concentration increases. By increasing the SE concentration to 10, 25, and 50 mM, the average voltage decreased to 6.0, 5.5, and 5.4 V, respectively. The energy consumption was calculated as 21.11, 19.17, and 18.75 kWh m^{-3} with increasing SE concentration (Figure 3(b)). Therefore, considering the electrical energy consumption, a higher SE concentration would be more suitable for the operation of the system. However, if the salt concentration (i.e., the SE concentration) exceeds a certain threshold value,

a salt film may form on the electrode surface, which reduces the number of active sites on the electrode or causes a change in the chemistry of the active sites, leading to a reduction in the pollutant degradation rate [45, 46].

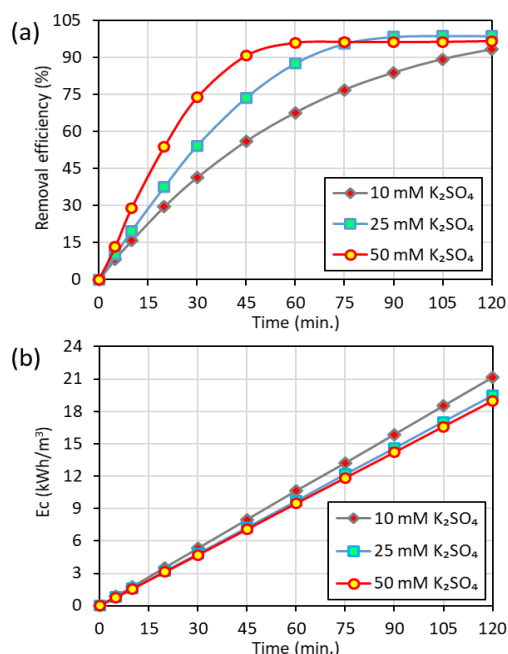


Figure 3. Variation of caffeine degradation efficiency (a) and energy consumption (b) over time with SE concentration

3.3. Effect of anode-cathode distance

Various studies on the electrooxidation process have reported that the distance between the anode and cathode influences the rate of decomposition and the electrical energy consumption [47-49]. The effects of different anode-cathode distances (2, 8, and 14 mm) on caffeine degradation were investigated; the results are shown in Figure 4. In the experiments, the initial pH was 5.8, the current density was 20 mA cm^{-2} , the supporting electrolyte concentration was 50 mM, the initial caffeine concentration was 25 mg L^{-1} , and the cathode type was SS. After 120 minutes of electrolysis, the degradation efficiencies are almost the same regardless of the distance between the anode and cathode (Figure 4(a)).

Examination of the pseudo-first-order reaction rate constants shows that the degradation of caffeine is faster with smaller anode-cathode distances. The caffeine degradation rates for 2, 8, and 14 mm distances are 0.0438 , 0.0403 , and 0.0392 min^{-1} , respectively. In studies where coking wastewater, sulfamethoxazole, and

perfluorooctanoic acid were removed, it was reported that electrolysis proceeds at higher reaction rates under shorter distances between the anode and cathode [47, 49, 50]. By increasing the anode-cathode distance to 2, 8, and 14 mm, the average voltage increased to 5.4, 5.7, and 6.6 V, respectively. Since the electrolysis system was operated at a constant current, the energy consumption increased with the increase in voltage. By increasing the anode-cathode distance to 2, 8, and 14 mm, the energy consumption was calculated to be 18.75, 19.94, and 22.99 kWh m⁻³, respectively (Figure 4(b)). Therefore, considering the electrical energy consumption, a shorter distance would be more suitable for the operation of the system.

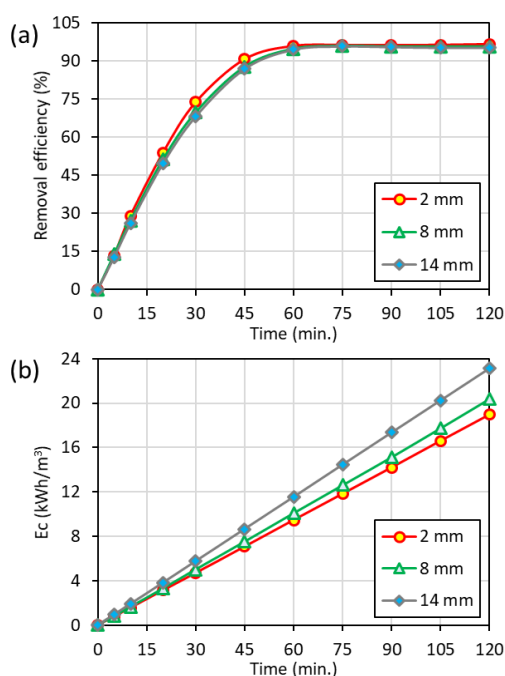


Figure 4. Variation of caffeine degradation efficiency (a) and energy consumption (b) over time with anode-cathode distance

3.4. Effect of initial caffeine concentration

To determine the effects of the initial concentration of caffeine, several experiments were performed with initial concentrations of 25, 50, and 75 mg L⁻¹ using 50 mM K₂SO₄ solutions as the supporting electrolyte (Figure 5). Further experimental parameters were an initial pH value of 5.8, a current density of 20 mA cm⁻², an anode-cathode distance of 2 mm, and a cathode SS. At an electrolysis time of 60 minutes, the efficiency of caffeine degradation was 96.0%, 86.2%, and 77.8% for initial caffeine concentrations of 25,

50, and 75 mg L⁻¹, respectively. After 105 minutes of electrolysis time, the change in initial caffeine concentration had no significant effect on caffeine degradation. As the caffeine concentration was increased from 25 to 75 mg L⁻¹, the absolute caffeine removal amounts increased from about 24 mg L⁻¹ to 58 mg L⁻¹ at the end of the 60 minutes electrolysis time. The total amount of caffeine removed by electrolysis was higher with increasing initial caffeine concentration. One possible reason for this was that increasing the initial caffeine concentration increased the concentration gradient and mass transfer through the diffusion layer, which in turn increased degradation at the electrode [51, 52].

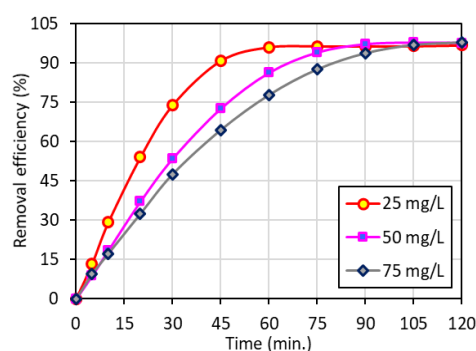


Figure 5. Variation of caffeine degradation efficiency over time with initial caffeine concentration

The rate of caffeine degradation decreased with increasing initial caffeine concentration. The pseudo-first-order reaction rate constants were 0.0438, 0.0297, and 0.0251 min⁻¹ for initial caffeine concentrations of 25, 50, and 75 mg L⁻¹, respectively. The results were similar to the electrochemical oxidation of ciprofloxacin and the decolorization of reactive orange 122 by the UV/H₂O₂ process [52, 53]. The decrease in the reaction rate constant at higher caffeine concentrations can be attributed to the formation of a larger amount of by-products that can compete with the caffeine itself. The energy consumption was calculated to be 18.75, 17.79, and 17.59 kWh m⁻³ for initial caffeine concentrations of 25, 50, and 75 mg L⁻¹, respectively. It can be concluded that the energy consumption was not significantly affected by changing the initial caffeine concentration.

3.5. Effect of different cathodes

Figure 6 shows the effects of cathode type on caffeine degradation during the electrolysis of caffeine. The experiments were performed with stainless steel (SS), graphite, and boron-doped diamond (BDD) cathodes and a BDD anode. The experiments were carried out at the natural pH of the solution (5.8). The initial caffeine concentration was 25 mg L^{-1} , the current density was 20 mA cm^{-2} , the anode-cathode distance was 2 mm and the concentration of the supporting electrolyte was $50 \text{ mM K}_2\text{SO}_4$.

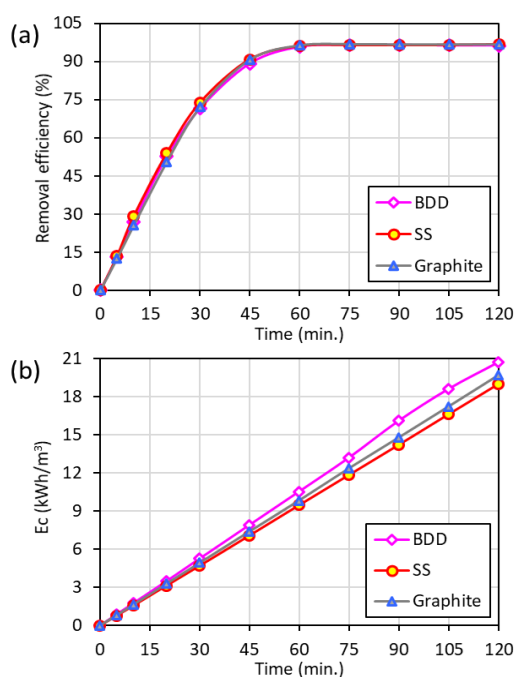


Figure 6. Variation of caffeine degradation efficiency (a) and energy consumption (b) over time with different cathodes

The results showed that the type of cathode used had no significant effect on the degradation efficiency of caffeine as a function of electrolysis time (Figure 6(a)). However, in a study conducted on the removal of tetracycline, it was reported that the use of carbon felt as a cathode was more efficient than stainless steel [54]. The pseudo-first-order reaction rate constants calculated with the non-linear method are 0.0438 , 0.0422 , and 0.420 min^{-1} for SS, graphite, and BDD, respectively. The estimated removal rate is slightly higher when SS is used as a cathode.

When analyzing the energy consumption, 18.75 , 19.66 , and 21.09 kWh m^{-3} were calculated for

SS, graphite, and BDD, respectively (Figure 6(b)). From this, it can be seen that the cathode type affects the energy consumption, and SS is the cathode type with the lowest energy consumption. It should also be noted that SS as a cathode is less expensive than graphite and BDD [55, 56]. Therefore, SS was chosen as the cathode material.

3.6. Effect of initial solution pH

The results of the experiments to investigate the influence of initial solution pH on caffeine degradation are shown in Figure 7. Without the addition of buffer solution, the pH value of the solution was adjusted to the desired value only once at the beginning of the experiment with $1 \text{ M H}_2\text{SO}_4$ or 1 M NaOH and was not changed during the experiment. In the experiments, the applied current density was 20 mA cm^{-2} , the initial caffeine concentration was 25 mg L^{-1} , the anode-cathode distance was 2 mm, the cathode type was SS, and the supporting electrolyte concentration was 50 mM . At an electrolysis time of 45 minutes, the efficiency of caffeine degradation was 98.5% , 90.8% , and 92.2% at an initial pH of 3, 5.8, and 10, respectively.

At an electrolysis time of 120 minutes, the change in initial pH had no significant effect on the degradation of caffeine. This shows that a wide range of initial pH values can be applied in the degradation of caffeine at the BDD anode (Figure 7(a)). The rate constants of the pseudo-first-order reaction calculated by the non-linear method were 0.0496 , 0.0438 , and 0.0483 min^{-1} for initial pH 3, 5.8, and 10, respectively. The degradation of caffeine was faster at an initial pH of 3 than at a higher initial pH. The difference in the degradation rate of organic matter at different pH values is often attributed to the higher redox potential of hydroxyl radicals under acidic conditions compared to alkaline conditions [57]. Similar results were obtained in the electrochemical oxidation of 2,4-dichlorophenoxyacetic acid and sulfamerazine [58, 59]. The energy consumption was calculated to be 18.25 , 18.75 , and 18.17 kWh m^{-3} for an initial pH of 3, 5.8, and 10, respectively. It can be concluded that changing the initial pH of the solution has no effect on energy consumption.

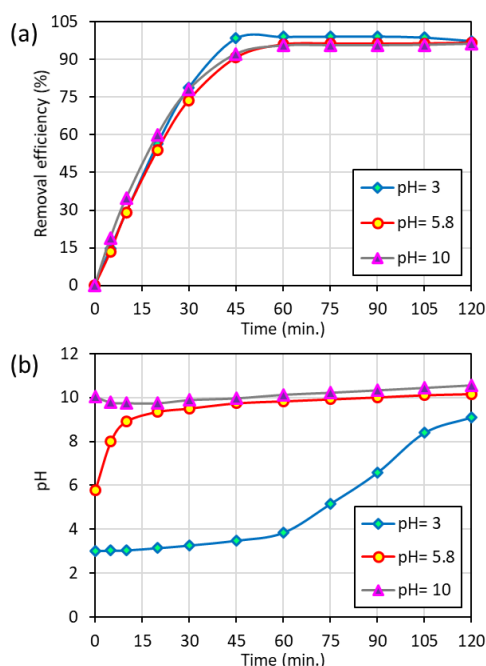
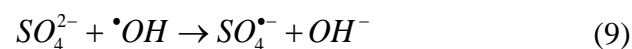
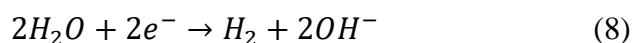


Figure 7. Variation of caffeine degradation efficiency (a) and solution pH (b) over time with initial pH value

The change in pH of the solution with time during electrolysis is shown in Figure 7(b). In the experiment conducted at an initial solution pH of 3, an increase in pH with electrolysis time was observed. After 60 minutes of electrolysis, the pH value of the solution reached 3.8. The pH value of the solution then increased rapidly and reached 9.1 after 120 minutes. With an initial pH value of the solution of 5.8, the pH value of the solution increased to 9.4 after 20 minutes of electrolysis. Thereafter, the pH of the solution slowly increased and reached 10.2 at the end of 120 minutes. With an initial solution pH of 10, the solution pH value first decreased to 9.8 and then increased to 10.6. Therefore, it can be said that the pH value tends to increase during the electrochemical degradation of caffeine using a BDD anode and an SS cathode.

The oxidation reaction at the anode decreases the pH of the solution, while the reduction reaction at the cathode causes an increase in the pH of the solution (Equations 4 and 5) [46]. The oxidation reaction of the water on the cathodic surface (Equation 8) and the resulting release of hydroxyl ions, which are formed during this process, into the aqueous environment can lead to an increase in the pH value with the electrolysis time [57, 60, 61]. In addition, the increase in the pH of the solution may also be related to the scavenging of

the hydroxyl radical in the presence of sulfate, according to Equation 9 [62].



4. Conclusion

This study demonstrates the efficient degradation of caffeine by anodic oxidation using a BDD electrode. From a kinetic point of view, it was found that the degradation of caffeine follows the pseudo-first-order kinetics, while the reaction rate constant increases with increasing current density and concentration of the supporting electrolyte and decreases with increasing initial caffeine concentration. It was found that the influence of the anode-cathode distance, the cathode type, and the initial pH of the solution on the reaction rate constant was not very significant. When analyzing the energy consumption, the applied current density and the electrolysis time were found to be the most effective parameters.

It was found that the supporting electrolyte concentration, the anode-cathode distance, and the cathode type have a minor influence on energy consumption. A current density of 20 mA cm⁻², a supporting electrolyte concentration of 50 mM K₂SO₄, an anode-cathode distance of 2 mm, a cathode type of SS, and an initial solution pH of 3 were found to be the optimum values for degrading a solution containing 25 mg L⁻¹ caffeine in 45 minutes using a BDD anode. It was found that the pH of the solution tended to increase during electrolysis.

Article Information Form

Funding

The author has not received any financial support for the research, authorship or publication of this study.

The Declaration of Conflict of Interest/ Common Interest

No potential conflict of interest was declared by the author.

The Declaration of Ethics Committee Approval

This study does not require ethics committee approval or any special permission.

The Declaration of Research and Publication Ethics

The author of the paper declare that she complies with the scientific, ethical and quotation rules of SAUJS in all processes of the paper and that she does not make any falsification on the data collected. In addition, she declares that Sakarya University Journal of Science and its editorial board have no responsibility for any ethical violations that may be encountered and that this study has not been evaluated in any academic publication environment other than Sakarya University Journal of Science.

Copyright Statement

Authors own the copyright of their work published in the journal and their work is published under the CC BY-NC 4.0 license.

References

- [1] M. Ghosh, K. Manoli, X. Shen, J. Wang, A. K. Ray, "Solar photocatalytic degradation of caffeine with titanium dioxide and zinc oxide nanoparticles," *Journal of Photochemistry and Photobiology A: Chemistry*, vol. 377, pp. 1-7, May 2019.
- [2] L. Cizmas, V. K. Sharma, C. M. Gray, T. J. McDonald, "Pharmaceuticals and personal care products in waters: occurrence, toxicity, and risk," *Environmental Chemistry Letters*, vol. 13, no. 4, pp. 381-394, Aug. 2015.
- [3] S. W. da Silva, E. M. O. Navarro, M. A. S. Rodrigues, A. M. Bernardes, V. Pérez-Herranz, "Using p-Si/BDD anode for the electrochemical oxidation of norfloxacin," *Journal of Electroanalytical Chemistry*, vol. 832, pp. 112-120, Jan. 2019.
- [4] T. S. Oliveira, M. Murphy, N. Mendola, V. Wong, D. Carlson, L. Waring, "Characterization of Pharmaceuticals and Personal Care products in hospital effluent and waste water influent/effluent by direct-injection LC-MS-MS," *Science of the Total Environment*, vol. 518-519, pp. 459-478, Jun. 2015.
- [5] A. Pal, K. Y. H. Gin, A. Y. C. Lin, M. Reinhard, "Impacts of emerging organic contaminants on freshwater resources: Review of recent occurrences, sources, fate and effects," *Science of the Total Environment*, vol. 408, no. 24, pp. 6062-6069, Nov. 2010.
- [6] L. Guardabassi, A. Petersen, J. E. Olsen, A. Dalsgaard, "Antibiotic resistance in *Acinetobacter* spp. isolated from sewers receiving waste effluent from a hospital and a pharmaceutical plant," *Applied and Environmental Microbiology*, vol. 64, no. 9, pp. 3499-3502, Sep. 1998.
- [7] A. Rajkamal, H. Kim, "Theoretical verification on adsorptive removal of caffeine by carbon and nitrogen-based surfaces: Role of charge transfer, π electron occupancy, and temperature," *Chemosphere*, vol. 339, p. 139667, Oct. 2023.
- [8] M. A. Heckman, J. Weil, E. G. de Mejia, "Caffeine (1, 3, 7-trimethylxanthine) in foods: A comprehensive review on consumption, functionality, safety, and regulatory matters," *Journal of Food Science*, vol. 75, no. 3, pp. 77-87, Apr. 2010.
- [9] T. H. Pham, N. M. Viet, P. T. T. Hoai, N. H. Tung, H. M. Tran, M. G. Mapari, T. Kim, "Synthesis of solar-driven Cu-doped graphitic carbon nitride photocatalyst for enhanced removal of caffeine in wastewater," *Environmental Research*, vol. 233, p. 116483, Sep. 2023.
- [10] S. Mayson, I. D. Williams, "Applying a circular economy approach to valorize spent coffee grounds," *Resources Conservation and Recycling*, vol. 172, p. 105659, Sep. 2021.
- [11] M. Fernández, M. Fernández, A. Laca, A. Laca, M. Díaz, "Seasonal occurrence and

- removal of pharmaceutical products in municipal wastewaters,” *Journal of Environmental Chemical Engineering*, vol. 2, no. 1, pp. 495-502, Mar. 2014.
- [12] J. Vymazal, T. D. Březinová, M. Koželuh, L. Kule, “Occurrence and removal of pharmaceuticals in four full-scale constructed wetlands in the Czech Republic-the first year of monitoring,” *Ecological Engineering*, vol. 98, pp. 354-364, Jan. 2017.
- [13] Y. Picó, R. Alvarez-Ruiz, A. H. Alfarhan, M. A. El-Sheikh, H. O. Alshahrani, D. Barceló, “Pharmaceuticals, pesticides, personal care products and microplastics contamination assessment of Al-Hassa irrigation network (Saudi Arabia) and its shallow lakes,” *Science of The Total Environment*, vol. 701, p. 135021, Jan. 2020.
- [14] M. Ashfaq, Y. Li, M. S. U. Rehman, M. Zubair, G. Mustafa, M. F. Nazar, C. P. Yu, Q. Sun, “Occurrence, spatial variation and risk assessment of pharmaceuticals and personal care products in urban wastewater, canal surface water, and their sediments: A case study of Lahore, Pakistan,” *Science of the Total Environment*, vol. 688, pp. 653-663, Oct. 2019.
- [15] L. Bo, L. Feng, J. Fu, X. Li, P. Li, Y. Zhang, “The fate of typical pharmaceuticals in wastewater treatment plants of Xi’an city in China,” *Journal of Environmental Chemical Engineering*, vol. 3, no. 3, pp. 2203-2211, Sep. 2015.
- [16] Z. Ayman, M. Işık, “Pharmaceutically active compounds in water, Aksaray, Turkey,” *Clean-Soil Air Water*, vol. 43, no. 10, pp. 1381-1388, Oct. 2015.
- [17] O. Hillebrand, K. Nödler, T. Licha, M. Sauter, T. Geyer, “Caffeine as an indicator for the quantification of untreated wastewater in karst systems,” *Water Research*, vol. 46, no. 2, pp. 395-402, Feb. 2012.
- [18] F. Comeau, C. Surette, G. L. Brun, R. Losier, “The occurrence of acidic drugs and caffeine in sewage effluents and receiving waters from three coastal watersheds in Atlantic Canada,” *Science of the Total Environment*, vol. 396, no. 2-3, pp. 132-146, Jun. 2008.
- [19] H. B. Quesada, T. P. de Araújo, L. F. Cusioli, M. A. S. D. de Barros, R. G. Gomes, R. Bergamasco, “Caffeine removal by chitosan/activated carbon composite beads: Adsorption in tap water and synthetic hospital wastewater,” *Chemical Engineering Research and Design*, vol. 184, pp. 1-12, Aug. 2022.
- [20] J. Tejedor, R. Álvarez-Briceño, V. H. Guerrero, C. A. Villamar-Ayala, “Removal of caffeine using agro-industrial residues in fixed-bed columns: Improving the adsorption capacity and efficiency by selecting adequate physical and operational parameters,” *Journal of Water Process Engineering*, vol. 53, p. 103778, Jul. 2023.
- [21] K. K. Beltrame, A. L. Cazetta, P. S. C. de Souza, L. Spessato, T. L. Silva, V. C. Almeida, “Adsorption of caffeine on mesoporous activated carbon fibers prepared from pineapple plant leaves,” *Ecotoxicology and Environmental Safety*, vol. 147, pp. 64-71, Jan. 2018.
- [22] A. Moghaddasfar, M. Darbandi, Z. A. Li, “Mesoporous cobalt oxide nanoparticles synthesized by a sonochemical method in the presence of a deep eutectic solvent for oxidative sonophotocatalytic decomposition of caffeine,” *Journal of Water Process Engineering*, vol. 54, p. 104056, Aug. 2023.
- [23] S. Cheng, X. Zhang, X. Yang, C. Shang, W. Song, J. Fang, Y. Pan, “The Multiple Role of Bromide Ion in PPCPs Degradation under UV/Chlorine Treatment,” *Environmental Science and Technology*, vol. 52, no. 4, pp. 1806-1816, Feb. 2018.




- [24] F. S. Souza, L. A. Féris, "Degradation of caffeine by advanced oxidative processes: O_3 and O_3/UV ," *Ozone: Science and Engineering*, vol. 37, no. 4, pp. 379-384, Jan. 2015.
- [25] K. Guo, Z. Wu, S. Yan, B. Yao, W. Song, Z. Hua, X. Zhang, X. Kong, X. Li, J. Fong, "Comparison of the UV/chlorine and UV/ H_2O_2 processes in the degradation of PPCPs in simulated drinking water and wastewater: Kinetics, radical mechanism and energy requirements," *Water Research*, vol. 147, pp. 184-194, Dec. 2018.
- [26] N. Tran, P. Drogui, L. Nguyen, S. K. Brar, "Optimization of sono-electrochemical oxidation of ibuprofen in wastewater," *Journal of Environmental Chemical Engineering*, vol. 3, no. 4, pp. 2637-2646, Dec. 2015.
- [27] R. J. A. Felisardo, E. Brillas, E. Bezerra Cavalcanti, S. Garcia-Segura, "Revealing degradation of organic constituents of urine during the electrochemical oxidation of ciprofloxacin via boron-doped diamond anode," *Separation and Purification Technology*, vol. 331, p. 125655, Mar. 2024.
- [28] H. Hai, X. Xing, S. Li, S. Xia, J. Xia, "Electrochemical oxidation of sulfamethoxazole in BDD anode system: Degradation kinetics, mechanisms and toxicity evaluation," *Science of The Total Environment*, vol. 738, p. 139909, Oct. 2020.
- [29] G. D. Değermenci, "Removal of reactive azo dye using platinum-coated titanium electrodes with the electro-oxidation process," *Desalination and Water Treatment*, vol. 218, pp. 436-443, Apr. 2021.
- [30] B. A. Fil, S. Günaslan, "Treatment of Slaughterhouse Wastewaters with $Ti/IrO_2/RuO_2$ Anode and Investigation of Energy Consumption," *Arabian Journal for Science and Engineering*, vol. 48, no. 1, pp. 457-466, Jan. 2023.
- [31] E. Brillas, A. Thiam, S. Garcia-Segura, "Incineration of acidic aqueous solutions of dopamine by electrochemical advanced oxidation processes with Pt and BDD anodes," *Journal of Electroanalytical Chemistry*, vol. 775, pp. 189-197, Aug. 2016.
- [32] A. Kapałka, G. Fóti, C. Comninellis, "The importance of electrode material in environmental electrochemistry. Formation and reactivity of free hydroxyl radicals on boron-doped diamond electrodes," *Electrochimica Acta*, vol. 54, no. 7, pp. 2018-2023, Feb. 2009.
- [33] B. Boye, E. Brillas, B. Marselli, P. A. Michaud, C. Comninellis, M. M. Dieng, "Electrochemical decontamination of waters by advanced oxidation processes (AOPS): Case of the mineralization of 2,4,5-T on BDD electrode," *Bulletin of the Chemical Society of Ethiopia*, vol. 18, no. 2, pp. 205-214, Dec. 2004.
- [34] J. E. L. Santos, D. R. da Silva, C. A. Martínez-Huitle, E. V. dos Santos, M. A. Quiroz, "Cathodic hydrogen production by simultaneous oxidation of methyl red and 2,4-dichlorophenoxyacetate aqueous solutions using Pb/PbO_2 , Ti/Sb -doped SnO_2 and Si/BDD anodes. Part 1: Electrochemical oxidation," *RSC Advances*, vol. 10, no. 62, pp. 37695-37706, Oct. 2020.
- [35] B. Marselli, J. Garcia-Gomez, P.-A. Michaud, M. A. Rodrigo, C. Comninellis, "Electrogeneration of Hydroxyl Radicals on Boron-Doped Diamond Electrodes," *Journal of The Electrochemical Society*, vol. 150, no. 3, pp. 79-83, Feb. 2003.
- [36] G. Li, S. Zhou, Z. Shi, X. Meng, L. Li, B. Liu, "Electrochemical degradation of ciprofloxacin on BDD anode using a differential column batch reactor: mechanisms, kinetics and pathways," *Environmental Science and Pollution*

- Research, vol. 26, no. 17, pp. 17740-17750, Jun. 2019.
- [37] S. Cho, C. Kim, I. Hwang, "Electrochemical degradation of ibuprofen using an activated-carbon-based continuous-flow three-dimensional electrode reactor (3DER)," *Chemosphere*, vol. 259, p. 127382, Nov. 2020.
- [38] E. GilPavas, P. Arbeláez-Castaño, J. Medina, D. A. Acosta, "Combined electrocoagulation and electro-oxidation of industrial textile wastewater treatment in a continuous multi-stage reactor," *Water Science and Technology*, vol. 76, no. 9, pp. 2515-2525, Nov. 2017.
- [39] N. Flores, I. Sirés, R. M. Rodríguez, F. Centellas, P. L. Cabot, J. A. Garrido, E. Brillas "Removal of 4-hydroxyphenylacetic acid from aqueous medium by electrochemical oxidation with a BDD anode: Mineralization, kinetics and oxidation products," *Journal of Electroanalytical Chemistry*, vol. 793, pp. 58-65, May 2017.
- [40] E. B. Cavalcanti, S. Garcia-Segura, F. Centellas, E. Brillas, "Electrochemical incineration of omeprazole in neutral aqueous medium using a platinum or boron-doped diamond anode: Degradation kinetics and oxidation products," *Water Research*, vol. 47, no. 5, pp. 1803-1815, Apr. 2013.
- [41] M. Panizza, G. Cerisola, "Application of diamond electrodes to electrochemical processes," *Electrochimica Acta*, vol. 51, no. 2, pp. 191-199, Oct. 2005.
- [42] I. Sirés, E. Brillas, M. A. Oturan, M. A. Rodrigo, M. Panizza, "Electrochemical advanced oxidation processes: Today and tomorrow. A review," *Environmental Science and Pollution Research*, vol. 21, no. 14, pp. 8336-8367, Apr. 2014.
- [43] S. Kul, R. Boncukcuoğlu, F. Ekmekyapar Torun, Z. Reçber, O. Sözüdoğru, E. Aladağ, "Investigation of the Treatment of Olive Mill Wastewater by Electrooxidation," *Water Air Soil and Pollution*, vol. 233, no. 10, p. 421, Oct. 2022.
- [44] A. Dargahi, D. Nematollahi, G. Asgari, R. Shokoohi, A. Ansari, M. R. Samarghandi, "Electrodegradation of 2,4-dichlorophenoxyacetic acid herbicide from aqueous solution using three-dimensional electrode reactor with G/ β -PbO₂ anode: Taguchi optimization and degradation mechanism determination," *RSC Advances*, vol. 8, no. 69, pp. 39256-39268, Nov. 2018.
- [45] M. R. Samarghandi, A. Dargahi, A. Shabanloo, H. Z. Nasab, Y. Vaziri, A. Ansari, "Electrochemical degradation of methylene blue dye using a graphite doped PbO₂ anode: Optimization of operational parameters, degradation pathway and improving the biodegradability of textile wastewater," *Arabian Journal of Chemistry*, vol. 13, no. 8, pp. 6847-6864, Aug. 2020.
- [46] I. Ali, A. B. de Souza, S. D. Laet, K. V. Eyck, R. Dewil, "Anodic oxidation of sulfamethoxazole paired to cathodic hydrogen peroxide production," *Chemosphere*, vol. 319, p. 137984, Apr. 2023.
- [47] H. Lin, J. Niu, S. Ding, L. Zhang, "Electrochemical degradation of perfluorooctanoic acid (PFOA) by Ti/SnO₂-Sb, Ti/SnO₂-Sb/PbO₂ and Ti/SnO₂-Sb/MnO₂ anodes," *Water Research*, vol. 46, no. 7, pp. 2281-2289, May 2012.
- [48] J. G. Kim, H. B. Kim, S. Lee, E. E. Kwon, K. Baek, "Mechanistic investigation into flow-through electrochemical oxidation of sulfanilamide for groundwater using a graphite anode," *Chemosphere*, vol. 307, p. 136106, Nov. 2022.
- [49] H. Lin, J. Niu, J. Xu, Y. Li, Y. Pan, "Electrochemical mineralization of sulfamethoxazole by Ti/SnO₂-Sb/Ce-

- PbO₂ anode: Kinetics, reaction pathways, and energy cost evolution,” *Electrochimica Acta*, vol. 97, pp. 167-174, May 2013.
- [50] D. Zhi, J. Zhang, J. Wang, L. Luo, Y. Zhou, Y. Zhou, “Electrochemical treatments of coking wastewater and coal gasification wastewater with Ti/Ti₄O₇ and Ti/RuO₂–IrO₂ anodes,” *Journal of Environmental Management*, vol. 265, p. 110571, Jul. 2020.
- [51] T. S. Chen, Y. M. Kuo, J. L. Chen, K. L. Huang, “Anodic degradation of ofloxacin on a boron-doped diamond electrode,” *International Journal of Electrochemical Science*, vol. 8, no. 6, pp. 7625-7633, Jun. 2013.
- [52] Y. Wang, C. Shen, M. Zhang, B. T. Zhang, Y. G. Yu, “The electrochemical degradation of ciprofloxacin using a SnO₂-Sb/Ti anode: Influencing factors, reaction pathways and energy demand,” *Chemical Engineering Journal*, vol. 296, pp. 79-89, Jul. 2016.
- [53] K. Çobanoğlu, N. Değermenci, “Comparison of reactive azo dye removal with UV/H₂O₂, UV/S₂O₈²⁻ and UV/HSO₅⁻ processes in aqueous solutions,” *Environmental Monitoring and Assessment*, vol. 194, no. 4, p. 302, Apr. 2022.
- [54] N. Oturan, J. Wu, H. Zhang, V. K. Sharma, M. A. Oturan, “Electrocatalytic destruction of the antibiotic tetracycline in aqueous medium by electrochemical advanced oxidation processes: Effect of electrode materials,” *Applied Catalysis B: Environmental*, vol. 140-141, pp. 92-97, Aug. 2013.
- [55] M. R. Samarghandi, D. Nemattollahi, G. Asgari, R. Shokoohi, A. Ansari, A. Dargahi, “Electrochemical process for 2,4-D herbicide removal from aqueous solutions using stainless steel 316 and graphite Anodes: optimization using response surface methodology,” *Separation Science and Technology*, vol. 54, no. 4, pp. 478-493, Mar. 2019.
- [56] T. Muddemann, R. Neuber, D. Haupt, T. Graßl, M. Issa, F. Bienen, M. Enstrup, J. Möller, T. Matthée, M. Sievers, U. Kunz, “Improving the treatment efficiency and lowering the operating costs of electrochemical advanced oxidation processes,” *Processes*, vol. 9, no. 9, p. 1482, Sep. 2021.
- [57] A. Pieczyńska, T. Ossowski, R. Bogdanowicz, E. Siedlecka, “Electrochemical degradation of textile dyes in a flow reactor: effect of operating conditions and dyes chemical structure,” *International Journal of Environmental Science and Technology*, vol. 16, no. 2, pp. 929-942, Feb. 2019.
- [58] A. Fabiańska, A. Biak-Bielińska, P. Stepnowski, S. Stolte, E. M. Siedlecka, “Electrochemical degradation of sulfonamides at BDD electrode: Kinetics, reaction pathway and eco-toxicity evaluation,” *Journal of Hazardous Materials*, vol. 280, pp. 579-587, Sep. 2014.
- [59] J. Cai, M. Zhou, Y. Pan, X. Lu, “Degradation of 2,4-dichlorophenoxyacetic acid by anodic oxidation and electro-Fenton using BDD anode: Influencing factors and mechanism,” *Separation and Purification Technology*, vol. 230, p. 115867, Jan. 2020.
- [60] S. Vasilie, F. Manea, A. Baciuc, A. Pop, “Dual use of boron-doped diamond electrode in antibiotics-containing water treatment and process control,” *Process Safety and Environmental Protection*, vol. 117, pp. 446-453, Jul. 2018.
- [61] P. V. Nidheesh, A. Kumar, D. Syam Babu, J. Scaria, M. Suresh Kumar, “Treatment of mixed industrial wastewater by electrocoagulation and indirect electrochemical oxidation,” *Chemosphere*, vol. 251, p. 126437, Jul. 2020.

- [62] F. C. Moreira, R. A. R. Boaventura, E. Brillas, V. J. P. Vilar, “Electrochemical advanced oxidation processes: A review on their application to synthetic and real wastewaters,” *Applied Catalysis B: Environmental*, vol. 202, pp. 217-261, Mar. 2017.

Enhancing Industrial Robot Arms Data Security with a Hybrid Encryption Approach

Mustafa Emre Erbil¹ , Merdan Özkahraman^{1*} , Hilmi Cenk Bayrakçı¹ 

¹ Isparta University of Applied Sciences, Faculty of Technology, Department of Mechatronics Engineering, Isparta, Türkiye, mail@mustafaemreerbil.com, merdanozkahraman@isparta.edu.tr, cenkbayrakci@isparta.edu.tr

*Corresponding Author

ARTICLE INFO

ABSTRACT

Keywords:

Industrial robot arms
Hybrid encryption
Cryptography
Data security



Article History:

Received: 21.02.2024

Accepted: 14.06.2024

Online Available: 01.08.2024

In the context of the widespread application of robotics technology across numerous industrial sectors, the security of data communication in industrial robot arms emerges as a paramount concern. These robotic arms are instrumental in enhancing productivity and safety in a variety of fields, including but not limited to transportation, agriculture, construction, and mining, by automating tasks and reducing human exposure to hazardous conditions. This paper proposes a novel hybrid encryption strategy to fortify the data security of these industrial robot arms, particularly focusing on preventing data breaches during both wired and wireless communications. The suggested encryption framework combines the strengths of Elliptic Curve Cryptography (ECC) for its efficient asymmetric encryption capabilities, ChaCha20 for its rapid and low-energy symmetric encryption, and Poly1305 for ensuring data integrity through its message authentication code (MAC) algorithm. By leveraging these technologies, the paper outlines the development and application of a secure communication protocol, implemented using Python, that guarantees the confidentiality and integrity of data shared among robot arms and between these arms and their control systems. Additionally, the research conducts a comparative analysis between the ECC-based method and the RSA encryption standard, highlighting the efficiency and effectiveness of the proposed hybrid approach through various tests on different data types and sizes. The findings illustrate a marked improvement in safeguarding against potential data leaks, thereby significantly contributing to the enhancement of industrial robot arms' data security. This study not only addresses the pressing need for robust data protection mechanisms in the face of evolving cyber threats but also sets a benchmark for future research in the field of industrial robotics security.

1. Introduction

Under the leadership of technological innovation, the role of robots, especially industrial robot arms, in modern society has been steadily increasing, particularly in areas such as manufacturing and assembly. One of the key reasons for the preference of robots is their ability to move quickly and precisely [1]. Industrial robot arms are designed to automate processes, save labor costs, reduce risky working conditions, and provide support in situations where human labor is inadequate. These robot arms find widespread applications, ranging from

factory automation to surgical operations, from the agricultural sector to military applications, and they have been highly successful in increasing the efficiency of business processes while reducing costs. However, the wireless or wired communication capabilities of industrial robot arms pose serious challenges in terms of data security. Security vulnerabilities in communication can potentially lead to unauthorized access to sensitive industrial data, necessitating significant measures to be taken to ensure the communication security of industrial robot arms.

The data security of industrial robot arms has become critical with the increasing automation and system complexity. However, most previous studies have focused on the security of automation systems [2] and robot operating systems [3], leaving a gap in the area of data security for robot arms. With the aim of addressing this gap, the objective of this study is to propose a hybrid encryption method based on ECC (Elliptic Curve Cryptography), ChaCha20, and Poly1305 to ensure data security during the communication of industrial robot arms.

This hybrid method combines symmetric encryption with a message authentication code algorithm and combines this combination with asymmetric encryption to provide an optimal solution in terms of both security and communication speed. ECC is known for its strong security features while offering advantages in terms of processor intensity and computation time. On the other hand, symmetric encryption methods provide fast communication but may face challenges such as key management. In this study, the ChaCha20-Poly1305 combination created with the security advantages of ECC and its fast, data-integrity-ensuring communication capacity will be used to securely encrypt communication between industrial robot arms and control systems.

Furthermore, a comparison will be made between ECC and the RSA (Rivest-Shamir-Adleman) asymmetric encryption method, elucidating the advantages of ECC. The ECC-ChaCha20-Poly1305 hybrid encryption method developed using the cryptography, Crypto.Cipher, and Crypto.Random libraries within the Python programming language aims to prevent potential data leaks during communication and to protect the confidentiality and integrity of transmitted data. The results obtained through this methodology will represent a significant step in ensuring data security for industrial robot arms.

Industrial robot arms have become an indispensable part of modern production processes. These robot arms, complex devices created by the combination of mechanical and control systems, can automate various tasks and enhance the efficiency of the production process. They can replace human labor in complex,

repetitive, or hazardous tasks [4]. Equipped with advanced control systems and precision sensors, industrial robot arms can be programmed to learn, execute, and optimize the movements and processes required to complete specific tasks [5]. Used in various industrial sectors such as automotive, electronics, food and beverage, pharmaceuticals, these robot arms complete operations quickly and consistently, increasing overall production efficiency. Additionally, the use of robot arms in hazardous or challenging work conditions enhances workplace safety, reducing work accidents and injuries [6].

The application areas of industrial robot arms are extensive and diverse. Tasks such as material handling, assembly, welding, paint spraying, packaging, and quality control can be automated with the assistance of robot arms. The use of this technology accelerates the workflow, increases efficiency and safety, reduces production costs, and enhances product quality [7]. Robot arms enable businesses to produce faster and more effectively while safeguarding worker health. Robot arms equipped with various sensors and artificial intelligence technology can perceive their surroundings and move independently, adapt to various applications, and successfully complete complex tasks [8].

With advancing technology, the capabilities of industrial robot arms are increasing, making it easier to complete more complex and precise operations with their assistance. This facilitates the automation of the production process and reduces labor costs. The use of robot arms enhances production process flexibility, enabling businesses to respond more quickly and effectively to market demands [9]. Furthermore, robot arms efficiently complete tasks, leading to energy savings and waste reduction, contributing to environmental sustainability [10].

2. State of the Art

Encryption is a method employed for ensuring the secure protection of information and data security. This method transforms information into a format that can only be accessed or understood by authorized individuals. This transformation process is carried out using one or more private keys, resulting in the conversion of

plain text, which is the understandable form of information, into unreadable encrypted text [11]. Encryption technology holds vital importance, particularly in the realms of information security and data privacy. Encryption methods are generally categorized into two main categories: asymmetric encryption and symmetric encryption. Both of these methods play a critical role in safeguarding data.

Wireless and wired communication refer to communication conducted over networks that are commonly used today, encompassing mobile devices, sensor networks, Internet of Things (IoT) devices, and broadband connections, among others. Both of these communication types face a range of security challenges. Wireless communication, in particular, becomes more vulnerable to attacks due to the transmission of data in a physically unprotected environment, emphasizing the significance of data security and privacy [12].

Encryption methods are widely employed in both communication systems to ensure data security. Encryption protects data against unauthorized access by transforming it from a comprehensible state into an encrypted form. Encryption methods used in wireless and wired communication systems are designed to meet security requirements and ensure data integrity, confidentiality, and identity authentication. Hybrid encryption is a security strategy commonly preferred in both systems. In this method, asymmetric encryption, symmetric encryption, and message authentication code algorithms, such as ECC, ChaCha20, and Poly1305, are used together to combine the advantages of each algorithm, resulting in a stronger security solution [13].

Asymmetric encryption (ECC) is used for operations like key exchange and identity verification, symmetric encryption (ChaCha20) is used for data encryption and decryption, and the message authentication code algorithm (Poly1305) is used to enhance symmetric encryption [14]. In this way, the hybrid encryption approach provides a secure key exchange while offering a fast and efficient solution for data encryption. Additionally, this method examines and elucidates the differences

between ECC and RSA asymmetric encryption methods, which have been frequently compared in recent times, to explain why ECC encryption method is the preferred choice.

The use of hybrid encryption in both wireless and wired communication systems offers significant advantages in terms of data security. Asymmetric encryption algorithms reduce the risk of unauthorized access during data transfer by providing a secure key exchange. Simultaneously, symmetric encryption algorithms offer rapid data encryption and decryption, facilitating high-performance data transmission. Therefore, the hybrid encryption approach strikes a balance between security and performance in wireless and wired communication systems [15].

2.1. Asymmetric encryption

Asymmetric encryption, also known as public-key cryptography, is a method that enables secure data transfer using two keys. These two keys form a pair, one being public and the other private. The public key is shared openly with everyone, while the private key is known only to the recipient of the message. Data is encrypted using the public key and can only be decrypted using the matching private key. This ensures secure data transmission but is computationally more expensive. Asymmetric encryption is widely used today in many security protocols and applications, particularly due to its ability to provide secure data transmission [16]. Asymmetric encryption relies on the complex structure of mathematics, and its security is based on the difficulty of solving specific mathematical problems. It is a combination of mathematical concepts that form the foundation of encryption, allowing its use in various applications [17].

Asymmetric encryption is based on the following mathematical principles:

- **One-way Functions;** These are mathematical functions that can be easily calculated in one direction but are difficult to reverse. For example, multiplying two large prime numbers is easy, but factoring the product back into its prime factors is challenging.

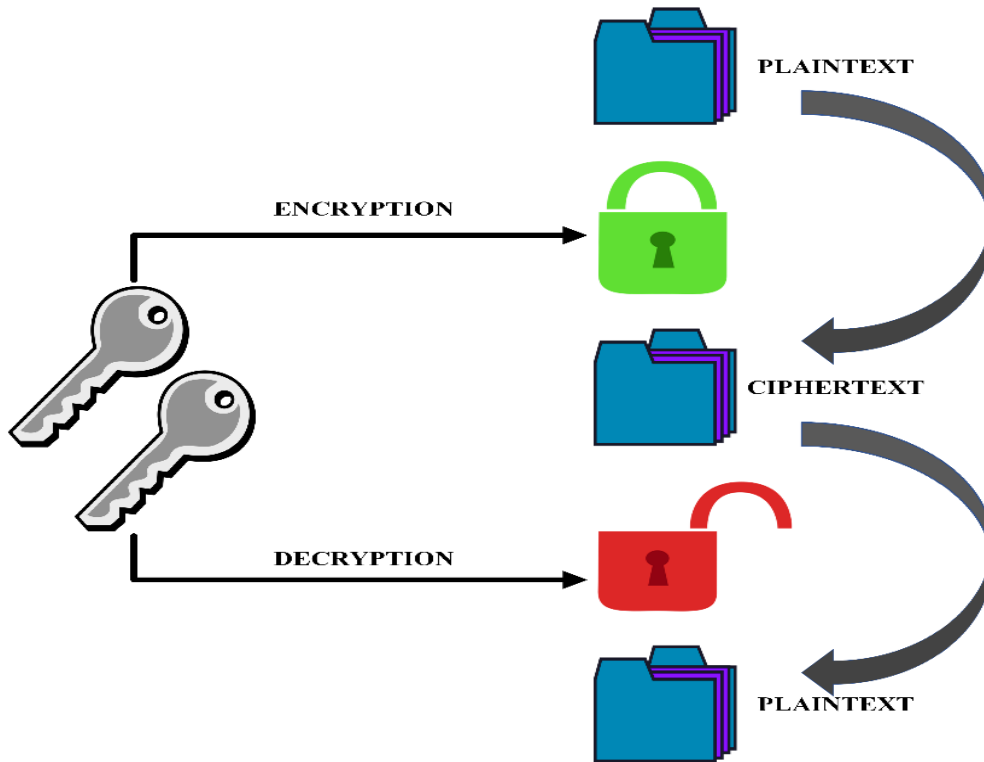


Figure 1. Asymmetric encryption scheme.

- Modular Arithmetic; This involves processing numbers within a limited system defined by a modulus value. Modular arithmetic is commonly used in encryption operations because some operations are difficult to reverse.
- Distributed Systems; Asymmetric encryption allows both keys to operate independently. The public key is accessible to everyone, while the private key is known only to authorized users.

These principles enable the application of asymmetric encryption in areas such as data security, digital signatures, and secure electronic transactions [18]. Figure 1 illustrates the asymmetric encryption scheme.

2.1.1. RSA (Rivest-Shamir-Adleman)

RSA, an asymmetric encryption algorithm proposed by Ron Rivest, Adi Shamir, and Leonard Adleman in 1977, employs two keys: a private key and a public key. The public key is used for data encryption, while the private key is utilized for data decryption. RSA finds common application in digital signatures and key exchange protocols [19]. RSA encryption is grounded in the principle of one-way functions in

asymmetric cryptography. Its security hinges on the complexity of factoring large prime numbers. The RSA encryption and decryption process consists of key generation, encryption, and decryption steps [20]. In the key generation phase, two large prime numbers (p) and (q) are initially selected as a fundamental security measure. This selection is at the core of the algorithm's security. The product of these prime numbers (n) defines the modulus employed in encryption and decryption operations, as expressed in Equation 1.

$$n = p \times q \tag{1}$$

Euler's totient function is calculated, as depicted in Equation 2, and is an integral part of security based on the difficulty of factoring prime numbers.

$$\varphi(n) = (p-1) \times (q-1) \tag{2}$$

The public key (e) is typically chosen as a small, commonly used prime number such as 65537, and is employed for encryption. The private key (d), calculated as specified in Equation 3, ensures the secure decryption of data.

$$e \times d \equiv 1 \pmod{\varphi(n)} \tag{3}$$

The encryption process involves encrypting the message (M) using the public key (e, n), expressed in Equation 4. This process ensures data protection and security against unauthorized access.

$$C = M^e \pmod{n} \quad (4)$$

The decryption process, on the other hand, decrypts the encrypted message (C) using the private key (d, n), as indicated in Equation 5. This enables only authorized recipients to access the original content of the message.

$$M = C^d \pmod{n} \quad (5)$$

These processes of RSA establish a robust security foundation based on the complexity of factoring large numbers, making it one of the fundamental security tools in the digital world.

2.1.2. ECC (Elliptic Curve Cryptography)

Elliptic Curve Cryptography (ECC) is an advanced asymmetric encryption technology commonly employed in digital signature generation and encrypted data exchange. This method operates using two keys: a private key, known only to the individual, and a public key, openly shared with everyone.

While the public key is influential in data encryption, the corresponding private key is solely used during the decryption process. ECC's robustness relies on the mathematical operations involving elliptic curves, which are considered one-way functions. This characteristic allows for superior security with shorter key lengths. ECC's essence lies in the ease of performing these mathematical operations while making it considerably challenging to calculate their inverses, especially scalar multiplication on elliptic curves.

Thanks to these features, ECC ensures secure key distribution and data integrity, rendering it a popular choice in wireless communication and smart device technologies. ECC's unique advantages include its energy efficiency and the ability to provide high-level security and performance even in devices with limited computational capacity. The mathematical

complexity of operations defined on elliptic curves produces flexible secure solutions that meet modern encryption requirements [21]. The ECC encryption and decryption process consists of key generation, encryption, and decryption steps [22]. In the key generation phase, an elliptic curve and a starting point (G) are initially selected. Then, a random number (k) is chosen as the private key. Finally, the public key is calculated as the product of (k) and (G), as shown in Equation 6.

$$P = k \times G \quad (6)$$

During the encryption phase, the message (M) is encrypted using the recipient's public key (P) and a randomly chosen number (r). An interim point is calculated as demonstrated in Equation 7.

$$R = r \times G \quad (7)$$

Another point is determined using the recipient's public key, as depicted in Equation 8.

$$S = r \times P \quad (8)$$

The message (M) is encrypted as a function of point (S). In the decryption phase, the encrypted message (C) is decrypted using the private key (k). A multiplication of the private key (k) and the point (R) received from the sender is computed, as illustrated in Equation 9.

$$T = k \times R \quad (9)$$

The multiplication given in Equation 9 is equivalent to the point (S) created during encryption. Message (M) is then decoded using (T). Both systems are founded on mathematical complexities: factoring large prime numbers in RSA and finding the inverse of scalar multiplication on elliptic curves in ECC. These attributes make both systems powerful tools in modern cryptography.

From a security and efficiency perspective, ECC is particularly suitable for devices with constrained energy consumption and computational capacity. Hence, ECC is a preferred method in blockchain technologies, smart contracts, and numerous advanced cryptographic applications.

2.2. Symmetric encryption

Symmetric encryption, also known as symmetric cryptography, is a encryption method where both encryption and decryption processes are performed using the same key. This method requires less computational power compared to asymmetric cryptography, making it faster. However, the weakness of symmetric encryption lies in the necessity of securely sharing the key between two parties. If the key falls into the hands of malicious individuals, the encrypted data can be easily decrypted. Symmetric encryption is particularly advantageous when there is a need to encrypt a large amount of data quickly [23]. Figure 2 illustrates the Symmetric Encryption Scheme.

the security of the entire encryption system.

- **Processing Speed and Efficiency:** Symmetric encryption offers a fast and efficient solution for encryption and decryption processes due to the use of the same key for both operations. This feature makes it ideal for scenarios that require the processing of large volumes of data.
- **Operation on Data Blocks:** These systems typically divide data into fixed-size blocks and encrypt each block separately. This block-based approach ensures the organized and secure processing of data [24].

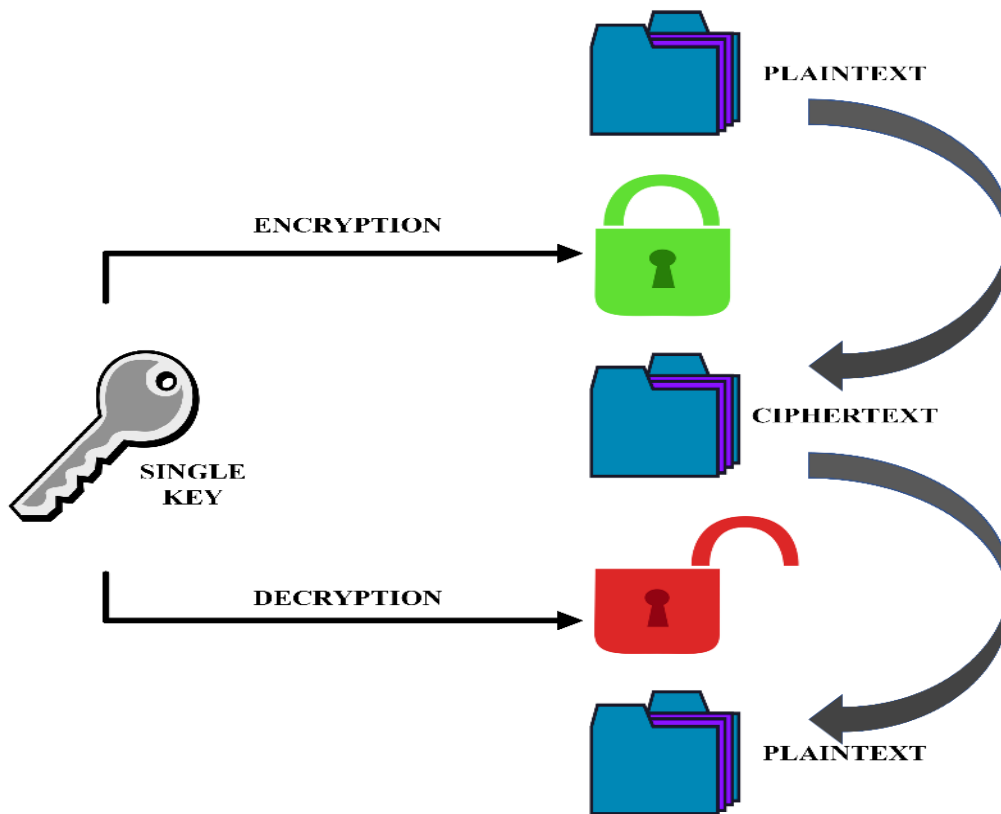


Figure 2. Symmetric encryption scheme

The fundamental principles of symmetric encryption are as follows:

- **Key Protection:** The security of encryption relies on the careful protection of the key by both the sender and the recipient. The compromise of the key under any circumstances can jeopardize

Thanks to these fundamental principles, symmetric encryption has become an effective tool in various fields, especially in internet security and network encryption. This method offers speed and efficiency while also requiring the secure management of keys, making it a domain that demands technical expertise.

In the field of data protection, symmetric encryption plays a fundamental role,

encompassing a variety of algorithms. Each algorithm offers unique characteristics and benefits, making them suitable for different requirements. For instance, the Advanced Encryption Standard (AES) is renowned for its wide acceptance as a security standard and its robust protection features.

Most symmetric encryption methods have emerged as alternatives to AES. Blowfish is ideal for small-scale projects due to its ease of adaptation. Twofish is considered a strong competitor to AES due to its flexibility in key management. RC6, with its unique structure, is also a strong contender against AES. Serpent, like Twofish and RC6, is another rival to AES, known for its high security performance. Camellia, as a Japan-based encryption standard, offers high security and speed. Salsa20 is known for its speed and efficiency, while ChaCha20, as an improved version of Salsa20, provides superior security and speed features [25-27]. The comparison of encryption methods in terms of performance and security has been thoroughly investigated in a study by Indla et al. [28]. Table 1 provides a Comparison of Symmetric Encryption Methods. The table presented in the study compares various algorithms based on key length, block size, processing speed, and security levels. By examining only the test results of symmetric encryption methods, the table clearly shows the advantages and disadvantages of these methods relative to each other.

These comparisons form an important guide in the selection of symmetric encryption methods. Selecting the appropriate encryption method according to different application requirements and security needs is of critical importance.

This table provides a comprehensive comparison of various symmetric encryption methods, highlighting key aspects such as security level, performance speed, key length options, block size, implementation complexity, and availability status. The table serves as an invaluable resource for understanding the differences and suitability of each encryption method for specific applications. It distinctly outlines how each algorithm, from widely used ones like AES to more niche options like Blowfish and Twofish, varies in terms of efficiency, security robustness, and practical deployment considerations, thereby aiding in the informed selection of encryption techniques for diverse security needs.

ChaCha20 is an advanced symmetric key encryption algorithm that encrypts data using a series of cyclic operations. Designed by Daniel J. Bernstein, this algorithm offers both high speed and security [29]. One of the key advantages of ChaCha20 is its strong security while being able to operate efficiently even on low-cost hardware. These features make it an ideal solution for systems that prioritize security and have limited processing power, such as industrial robotic arms.

Table 1. Comparison of Symmetric Encryption Methods [28]

Algorithm	Security	Performance	Key Length	Block Size	Implementation Complexity	Availability
AES	High	Fast	128, 192, or 256 bits	128 bits	Low	Widely Available
Blowfish	Medium	Fast	32 to 448 bits	64 bits	Low	Widely Available
Twofish	High	Fast	128 to 256 bits	128 bits	Moderate	Limited
RC6	High	Fast	128, 192, or 256 bits	128 bits	Moderate	Limited
Serpent	High	Moderate	128 to 256 bits	128 bits	High	Limited
Camellia	High	Fast	128, 192, or 256 bits	128 bits	Moderate	Limited
Salsa20	High	Fast	128 or 256 bits	64 or 128 bits	Low	Limited
ChaCha20	High	Fast	256 bits	64 or 128 bits	Low	Limited

Additionally, it seamlessly integrates with MAC algorithms. Therefore, it was chosen as the symmetric encryption algorithm for the project.

ChaCha20 relies on complex cyclic operations and sequence generation. The fundamental steps of this algorithm include key and nonce initialization, creating an initial state matrix, the cyclic operation process, and encryption and decryption. The steps of ChaCha20 can be outlined as follows:

- Key: A 256-bit key (K) is used.
- Nonce and Block Counter: A 64-bit nonce and a block counter are used for security.
- ChaCha20 operates on a 512-bit state matrix.
- The initial state consists of a "magic constant" (σ), the key (K), block counter, and nonce.
- The state matrix is processed for a specified number of rounds.
- Each round involves addition, XOR operations, and bit shifting; Addition is performed *mod* 2^{32} , XOR operation involves bitwise XOR of two words, and bit shifting plays a crucial role in data encryption.
- Encryption is achieved by adding and XORing the processed state matrix with the original state matrix.
- Decryption is performed in the reverse manner of encryption.

These mathematical characteristics and its relationship with MAC algorithms make ChaCha20 a secure and efficient encryption option. Additionally, its low hardware requirements and high parallelizability allow for effective implementation across various platforms [30].

Message Authentication Code (MAC) algorithms play a critical role in ensuring data integrity and authentication. These algorithms are used to verify that a message has reached its destination without being altered or subject to unauthorized interference. The primary function of MAC algorithms is to produce a fixed-size output using a message and a secret key. This output serves as a digest of the message and is

used to verify the integrity of the message. The security of MAC algorithms relies on the secrecy of the secret key and the cryptographic strength of the algorithm [31, 32]. The characteristics of MAC algorithms are as follows:

- Integrity and Identity Verification: MAC algorithms guarantee both the integrity of the message and the authenticity of its source. This helps detect possible alterations or unauthorized interventions during data transmission.
- Secret Key Usage: MAC algorithms produce a digest of the message using a secret key, allowing both the sender and receiver to verify it.
- Collision Resistance: An effective MAC algorithm makes it difficult to find two different messages that produce the same MAC value. This feature enhances the algorithm's reliability.
- Application Variety: MAC algorithms are used across a wide range of applications, from financial transactions to network security.

Popular MAC algorithms include HMAC, CMAC, and Poly1305. These algorithms can serve various requirements and security levels. These fundamental characteristics of MAC algorithms play a crucial role in data security and authentication processes, making their usage an essential part of preserving data integrity and ensuring secure communication in the digital world.

Poly1305 is a MAC (Message Authentication Code) algorithm designed to ensure the integrity and authenticity of messages in secure communications. Developed by Daniel J. Bernstein, this algorithm sets high standards for both speed and security [33]. Poly1305 is particularly used in encrypted data transmission and works in conjunction with encryption algorithms such as ChaCha20 to secure data integrity [34, 35]. The fundamentals of Poly1305 are as follows:

- Key Generation and Usage: Poly1305 uses a 256-bit key, consisting of two parts: a 128-bit key and a 128-bit nonce. The key is used in the calculation of the

MAC value, while the nonce must be unique for each message.

- **MAC Value Computation:** Poly1305 computes the MAC value for a given message. This process is repeated for each block of the message, and the results are combined. Polynomial multiplication is performed on each block using arithmetic $\text{mod } (2^{130}-5)$. This forms the basis of Poly1305's security.
- **Verification Process:** The recipient calculates the MAC value for the received message using the same key and nonce. If the calculated MAC value matches the transmitted MAC value, the integrity and authenticity of the message are verified.

Poly1305 is a strong MAC algorithm in terms of security. Proper use of the key and nonce provides a high level of security. Poly1305 is designed to operate quickly on modern processors, making it particularly suitable for real-time applications. It finds a wide range of applications for preserving data integrity, especially in encrypted communications and network security. These features make Poly1305 a popular choice in modern cryptography applications. The mathematical foundations and practicality of the algorithm provide an effective and reliable data authentication solution.

2.3. Hybrid encryption

Hybrid encryption combines asymmetric and symmetric encryption techniques to create a robust security protocol. This method blends the advantages of symmetric and asymmetric encryption methods to provide a comprehensive security solution.

The ChaCha20-Poly1305 Combination is a merger of two powerful cryptographic algorithms designed by Daniel J. Bernstein. This combination is used as a vital element of data security in hybrid encryption systems. While ChaCha20 is an efficient symmetric encryption algorithm, Poly1305 serves as a reliable Message Authentication Code (MAC) algorithm. The combination of these two algorithms offers an effective solution for both encryption and data integrity security [36-38]. The fundamentals of

the ChaCha20-Poly1305 Combination are as follows:

- **Enhanced Security and Performance:** ChaCha20 offers high standards of speed and security, especially functioning effectively on low-cost hardware. Poly1305 ensures message integrity and authenticity by using a unique nonce for each message.
- **Advantages of the Combination:** This combination brings together ChaCha20's fast encryption capabilities and Poly1305's robust data verification mechanisms. Both encryption and MAC operations are performed using the same key set, simplifying the process and enhancing security.
- **Application Areas:** ChaCha20-Poly1305 is often preferred in applications requiring encrypted communication, network security, and data integrity. It provides high-level security and performance, particularly in devices with limited energy consumption and processing capacity.

ChaCha20 encrypts data, while Poly1305 calculates the MAC value over the encrypted data. ChaCha20 relies on XOR operations and bit shifts, whereas Poly1305 provides security through arithmetic $\text{mod } (2^{130}-5)$. This hybrid system stands out in the field of modern cryptography, particularly as a product of Bernstein's work. The efficiency of ChaCha20-Poly1305 offers a powerful and flexible solution that meets complex encryption requirements.

ChaCha20-Poly1305-ECC Encryption Method is an advanced hybrid encryption technique that combines three powerful technologies of modern cryptography. This combination integrates the ChaCha20 and Poly1305 algorithms developed by Daniel J. Bernstein with Elliptic Curve Cryptography (ECC) [39-42]. This triple combination offers an excellent balance in data security: the fast and efficient encryption of ChaCha20, the robust message authentication of Poly1305, and the superior security and efficiency features of ECC. ECC, especially with short key lengths, provides high-security levels. Mathematical operations on elliptic curves

enhance encryption security. While ChaCha20 effectively encrypts data, Poly1305 is used to ensure the integrity and authenticity of this encrypted data. ChaCha20 stands out with low hardware requirements and high parallelizability. ECC is advantageous, particularly in fields like blockchain technologies and smart contracts. This hybrid system combines the strengths of each algorithm to provide a comprehensive security solution, offering an integrated approach in data encryption, authentication, and key management processes. The Encryption and Decryption Processes of ChaCha20-Poly1305-ECC Combination are as follows:

- ECC is used to establish a secure key exchange. During encryption and decryption operations, elliptic curve-based mathematical operations are used to securely create a shared common key between parties. This common key then serves as the basis for symmetric encryption.
- ChaCha20 is a symmetric encryption algorithm. The common key generated with ECC is used by the ChaCha20 algorithm for encrypting or decrypting data. ChaCha20 is designed to efficiently and securely encrypt data.
- Poly1305 is a Message Authentication Code (MAC) algorithm used in conjunction with ChaCha20 to verify the integrity and authenticity of encrypted data. Poly1305 produces a tag appended to the encrypted data, allowing for the verification of whether the data has been manipulated during decryption.

3. Material and Method

This study focuses on the comparison of asymmetric encryption methods as applications, because asymmetric encryption, which uses two different keys (a public and a private one), enhances security and data integrity in the transmission of sensitive data. Unlike symmetric encryption methods, asymmetric encryption has a structure that does not require the same key to be present at both ends of the communication [43]. Therefore, examining the advantages of asymmetric encryption for systems containing

sensitive data, such as industrial robotic arms, is the main purpose of this study.

To compare asymmetric encryption methods, the RSA encryption method has been chosen. The proposed hybrid encryption algorithm has been compared with the same encryption method's algorithm that uses RSA instead of ECC. The reason for choosing RSA as the asymmetric encryption method to be compared is that RSA is a long-established, reliable asymmetric encryption method in the field of cryptography [44]. The RSA Algorithm is known for its security comparable to the ECC encryption method. Additionally, RSA stands out with its key generation process based on complex mathematical calculations and the use of large numbers. In contrast, ECC offers high security with shorter key sizes, making it more efficient in terms of energy and processing power. This comparison is critical in evaluating the performance of the proposed hybrid encryption method [45].

The use of .bin files in the comparison of the proposed hybrid encryption algorithm and the algorithm with RSA instead of ECC is due to the fact that such files typically contain large, unstructured data. This allows for testing the effectiveness of encryption algorithms on large and unstructured data sets.

The sizes of 100 MB, 500 MB, and 1 GB represent a broad range of data sizes and are important in assessing how encryption algorithms perform across various data magnitudes. These sizes are used to compare the processing times and efficiencies of the algorithms on large and small data sets. This choice is a standardization approach to understand the overall performance and scalability of the algorithms. Particularly, large file sizes (like 1 GB) more clearly reveal the processing times and efficiencies of the algorithms on large data sets, an important factor in understanding how the algorithms perform in real-world scenarios.

Testing the proposed hybrid encryption algorithm on different file types (MP4, PDF, TXT) with varying sizes such as 50, 100, and 200 MB allows for a detailed examination of how

encryption methods perform relative to changing data sizes. The use of 50 MB is due to it being one of the standard sizes frequently used in encryption algorithm performance tests. For example, a study has compared the encryption and decryption times of symmetric encryption algorithms for files of 3 MB and 50 MB [46]. The reason for using 100 to 200 MB is to evaluate the scalability of the algorithms and their performance under larger data loads, while not deviating too far from the 50 MB size.

3.1. ChaCha20-Poly1305-ECC algorithm

In this hybrid encryption algorithm developed using the Python language, the following libraries, modules, and packages have been used:

- "cryptography.hazmat.primitives.asymmetric.ec"
- "cryptography.hazmat.primitives.serialization"
- "cryptography.hazmat.primitives.kdf.hkdf"
- "Crypto.Cipher.ChaCha20_Poly1305"
- "Crypto.Random"

A private key is generated using ECC (Elliptic Curve Cryptography) in this hybrid encryption algorithm. This process, which is a form of asymmetric encryption, results in both a private key and a public key. The generated private key is exported in PEM format and saved to a file. This key possesses the authority to decrypt data and should be securely stored. During the testing phase, the data at the specified path is read, representing the original data to be encrypted. A shared key for the ChaCha20-Poly1305 symmetric encryption algorithm is derived from the common key generated using ECC with ECDH (Elliptic Curve Diffie-Hellman) and HKDF (HMAC-based Key Derivation Function). A ChaCha20-Poly1305 encryption object is created, and the data is encrypted using the `encrypt_and_digest` method. This process results in encrypted data and a tag (MAC). The encrypted data, nonce, and tag are written to a file named "encrypted_data.bin." This file is used to store and securely transmit the encrypted data.

Decryption is performed in the reverse order of the encryption process. Firstly, the private key is

read from the file. The encrypted data is read from the file, and the encryption applied by ChaCha20-Poly1305 is deciphered using the key. If the deciphered data matches the generated tag, the integrity of the data is verified, and the decrypted data is presented to the user. This process ensures the secure transfer of data and restricts access to authorized individuals. The hybrid encryption method combines various encryption techniques to safeguard the security and privacy of data. The flowchart for this method is provided in Figure 3.



Figure 3. ChaCha20-Poly1305-ECC Encryption-Decryption Flowchart

3.2. ChaCha20-Poly1305-RSA algorithm

In this hybrid encryption algorithm developed using the Python language, the PyCryptodome library is utilized, including the following modules:

- "Crypto.PublicKey.RSA"
- "Crypto.Cipher.PKCS1_OAEP"
- "Crypto.Cipher.ChaCha20_Poly1305"
- "Crypto.Random"

To begin, a 2048-bit RSA key pair is generated. This is achieved using the RSA algorithm, which is an asymmetric encryption method, resulting in both a private key and a public key. The generated private key is exported in PEM format and saved to a file. This key possesses the authority to decrypt data and must be securely stored. To read the data to be tested, a file at the specified path is accessed. This data represents the original data to be encrypted. A key and nonce are generated for the ChaCha20-Poly1305 symmetric encryption algorithm. These key and nonce values are used for encrypting the data. Subsequently, a ChaCha20-Poly1305 encryption object is created, and the data is encrypted. This process results in encrypted data and a tag (MAC). An RSA encryption object is then created, and the ChaCha20 key is encrypted with it. This step ensures that only the owner of the private key can decrypt the data. The encrypted ChaCha20 key, nonce, encrypted data, and tag are written to a file. This file is used for storing the encrypted data and securely transmitting it. Decryption is performed in the reverse order of the encryption process. Firstly, the private key is read from the file and loaded using RSA. The encrypted data is then read from the file, and the key is decrypted using RSA. Subsequently, this decrypted key is used to decrypt the data with ChaCha20-Poly1305. If the decrypted data matches the generated tag, the data's integrity is verified, and the decrypted data is presented to the user. This process ensures the secure transfer of data and restricts access to authorized individuals. The hybrid encryption method combines various encryption techniques to safeguard the security and privacy of data.

4. Results

Robotic systems have the capability to communicate with various data sources such as sensor readings, command instructions, visual media, and mapping data. When performing actions utilizing these capabilities, the algorithm's execution speed plays a crucial role. Data that originates from a source may experience delays if it is encrypted and then decrypted before reaching its destination, instead of directly reaching the target. Therefore, the ChaCha20 symmetric encryption method has been employed for this purpose. In conjunction

with ChaCha20, Poly1305 is used to ensure data integrity.

Asymmetric encryption algorithms tend to operate slightly slower than symmetric encryption algorithms. Hence, when choosing among asymmetric encryption methods, regardless of the degree of difference, it is essential to select the algorithm that operates more efficiently. In this test, the combination of ChaCha20-Poly1305 is compared with ECC, which is recommended for use, and RSA, one of the most commonly used asymmetric encryption methods. The test involves encrypting and then decrypting data in .bin format with sizes of approximately 100 MB, 500 MB, and 1 GB, using the ChaCha20-Poly1305 combination with RSA and ECC methods. The timing test was conducted using the "time" library built-in Python. The test results for the ChaCha20-Poly1305-ECC and ChaCha20-Poly1305-RSA algorithms are presented in Table 2.

Table 2. The test results for the ChaCha20-Poly1305-ECC and ChaCha20-Poly1305-RSA algorithms

Algorithm	Processing Time for 100 MB (s)	Processing Time for 500 MB (s)	Processing Time for 1 GB (s)
ChaCha20-Poly1305-ECC	0.89412	3.36814	6.49236
ChaCha20-Poly1305-RSA	1.63905	4.09316	8.13015

According to the results presented in Table 2, it is observed that the ChaCha20-Poly1305-ECC algorithm encrypts and decrypts data faster than the ChaCha20-Poly1305-RSA algorithm. In summary, it has been observed that the ECC asymmetric encryption method operates faster than the RSA asymmetric encryption method.

It is well-known that robotic systems have numerous functions such as communicating with sensor data, command instructions, camera feeds, and mapping data. While performing these functions, communication with different types of data is quite common. For example, data obtained from a camera is of a different type compared to data acquired from a distance sensor. Is the encryption and decryption speed, as well as memory usage, the same for data of

different types but the same size, when using the ChaCha20-Poly1305-ECC algorithm? To answer this question, files with sizes approximately 50 MB, 100 MB, and 200 MB, in PDF, MP4, and TXT formats, were tested using the ChaCha20-Poly1305-ECC algorithm. Data of the same size but different types were compared in terms of memory usage and processing time. The built-in "time" library of Python was used for measuring the algorithm's processing time, while the "memory_profiler" library was utilized for memory usage. The obtained results are presented in Table 3.

Table 3. Performance Metrics by File Type and Data Size

Data Size (MB)	File Type	Memory Usage (MB)	Processing Time (Seconds)
50 MB	PDF	4.03125	0.62131
	MP4	4.109375	0.60822
	TXT	4.03515625	0.5942
100 MB	PDF	3.98046875	1.17811
	MP4	4.0234375	0.97805
	TXT	4.0078125	1.02113
200 MB	PDF	3.90625	1.50388
	MP4	3.953125	1.5814
	TXT	4.00390625	1.57084

Table 3 provides a detailed analysis of performance metrics across various file types and data sizes. This analysis primarily focuses on two key parameters: memory usage (in MB) and processing time (in seconds). These parameters have been examined for three different file types (PDF, MP4, TXT) and different data sizes (50 MB, 100 MB, 200MB.).

From an initial observation, it appears that the memory usage remains relatively stable across different file types and sizes, indicating a consistent memory footprint regardless of file type or data size. However, there are slight variations in memory usage, which could be attributed to the inherent differences in the data structure and compression algorithms used by each file type. Processing time, another critical metric, shows a variation that correlates with the data size and file type. It suggests that as the data size increases, the processing time also increases, which is expected. The processing time is a crucial factor in scenarios where time efficiency is a priority, such as real-time data processing or

large-scale data analysis. This table provides valuable insights, particularly for applications where memory efficiency and processing speed are crucial. It allows one to anticipate the system resources required and processing time for handling different file types and sizes, which is vital for optimizing performance in data-intensive applications. Analyzing such data helps in making informed decisions about resource allocation, system design, and choice of file types based on the specific requirements of an application. These results are depicted in the graph found in Figure 4.

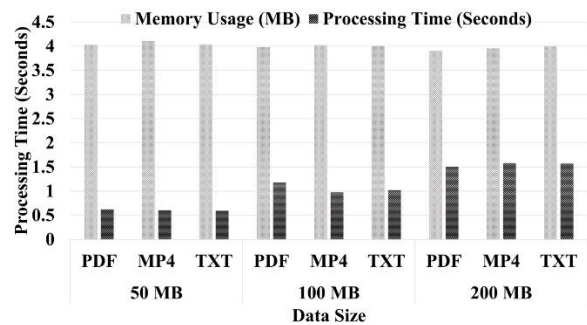


Figure 4. Comparative Analysis of Memory Usage and Processing Time Across Different File Types and Data Sizes

The graph presents a dual-axis bar chart comparing memory usage (in megabytes) and processing time (in seconds) for three different file types—PDF, MP4, and TXT—across three data sizes: 50 MB, 100 MB, and 200 MB. The left vertical axis corresponds to the processing time, while the right vertical axis presumably represents memory usage, although the right axis is not labeled in the image provided. Observations indicate that for all three file types, as the data size increases, the processing time escalates as well. This trend is consistent with computational theory, where larger data volumes typically require longer processing durations.

However, memory usage does not exhibit a proportional increase with data size; instead, it remains relatively constant or varies slightly. This could suggest an efficient memory management system where the memory footprint does not significantly increase with larger data sizes. The PDF and MP4 files display similar behaviors in terms of processing time, with only minor differences, which might be attributed to the complexity of data contained within each file

type. TXT files, by contrast, have a markedly lower processing time across all data sizes, reflecting their simpler structure and the less intensive processing required. In conclusion, the data conveyed in the graph supports the premise that while processing time is susceptible to changes in data volume, memory usage does not necessarily correlate directly with data size. This implies an optimized use of memory resources, which is particularly advantageous for systems with limited memory capacity. Additionally, the distinct difference in processing times between the file types underscores the importance of considering file structure and complexity when designing and optimizing data processing systems.

5. Conclusion

To improve the clarity and fluency of the paper, attention has been paid to clarify the distinction between encryption technologies and applications of industrial robot arms. By detailing the main features of encryption technologies and their integration into industrial applications, a comprehensive understanding of the transformation of theoretical concepts into practical applications is presented. This transition through sub-headings is intended to strengthen the overall coherence of the article and transform it into a more user-friendly and application-oriented resource.

The article uses material such as diagrams and example scenarios to clarify concepts and relate technical information to practical applications. The quality of images and tables has been improved and explanatory comments have been added so that readers can clearly see the topics. Care has been taken with grammar and punctuation, and consistency in technical terms has been ensured. Sentences have been shortened to improve clarity and a glossary of technical jargon has been included. Each term and concept is explained the first time it is used, and transitions between topics are made clear. These steps have improved the overall comprehensibility of the article. The detailed research systematically evaluated the effectiveness of a novel hybrid encryption method designed to enhance data security for industrial robot arms.

The method synergistically leverages the strengths of Elliptic Curve Cryptography (ECC) for asymmetric encryption capabilities, ChaCha20 for fast symmetric encryption, and Poly1305 for reliable message authentication to establish a robust security posture against data attacks during both wired and wireless communications. In this work, the importance of cybersecurity approaches, assets, and applications for protection is discussed [47, 48].

The encryption protocol developed for industrial robot arms is supported by detailed analysis and testing to offer robustness against potential security threats. Simulations and penetration tests validate the effectiveness of the protocol and its solutions to industry challenges. By highlighting the security advantages of the algorithm and its effectiveness in application scenarios, this study illuminates how to integrate encryption methods in industrial applications.

The study also analyzes how encryption methods scale on industrial robot arms by testing performance on data types such as .bin files, providing valuable results, especially with file sizes ranging from 100 MB to 1 GB. This information demonstrates the practical applicability of encryption methodologies by comparing between large and small datasets. Related works in the literature [49] highlight the performance and flexibility advantages of algorithms such as AES and BlowFish and provide a reference for determining the security potential of encryption methods. The selected algorithms fit the specific requirements of the project, with unique advantages such as ECC's high-security small keys, ChaCha20's balance of performance and security, and Poly1305's fast message authentication. These choices are based on an extensive analysis of the existing literature, including comparisons of these algorithms within and against each other, with critical factors such as data integrity and security. Empirical analysis shows that the ECC component significantly enhances the level of security, while ChaCha20 and Poly1305 contribute to high-speed data processing, providing not only secure communication channels but also minimal latency in data transfer operations. These findings underline the potential of the ECC-ChaCha20-

Poly1305 combination as a superior encryption strategy, especially for industrial applications where speed and security are crucial.

Furthermore, this paper evaluates the effects of encryption methods on performance metrics such as real-time processing time and memory utilization of industrial robotic arms and examines the effects of ECC on system performance compared to RSA [50].

This investigation contributes to the broader cryptographic community by providing a comparative analysis with existing methods, highlighting improved performance metrics in terms of both encryption speed and resource efficiency. In order to understand the place of the encryption method proposed in the paper in the current technological landscape, in addition to comparisons between common methods such as ECC and RSA, a wide range of symmetric encryption algorithms are also examined. In this context, a detailed analysis of the advantages and application scenarios of algorithms such as Advanced Encryption Standard (AES), Blowfish, Twofish, RC6, Serpent, Camellia, and many more is presented [51].

The insights gained from this research can serve as a cornerstone for future innovations in the field of encryption, especially in industrial automation and robotics, where data security is becoming increasingly critical. In summary, this research not only demonstrates that the hybrid method is a viable security solution, but also paves the way for its adoption in complex industrial ecosystems by providing a detailed academic and practical framework for implementation and evaluation.

Article Information Form

Funding

The author (s) has no received any financial support for the research, authorship or publication of this study.

Authors' Contribution

Conceptualization, M.Ö. and H.C.B.; methodology, H.C.B.; software, M.E.E.; validation, M.Ö., H.C.B. and M.E.E.; investigation, M.E.E.; data curation, M.Ö.;

writing—original draft preparation, M.E.E.; writing—review and editing, M.Ö. and H.C.B.; visualization, M.Ö. All authors have read and agreed to the published version of the manuscript.

The Declaration of Conflict of Interest/ Common Interest

No conflict of interest or common interest has been declared by the authors.

The Declaration of Ethics Committee Approval

This study does not require ethics committee permission or any special permission.

The Declaration of Research and Publication Ethics

The authors of the paper declare that they comply with the scientific, ethical and quotation rules of SAUJS in all processes of the paper and that they do not make any falsification on the data collected. In addition, they declare that Sakarya University Journal of Science and its editorial board have no responsibility for any ethical violations that may be encountered, and that this study has not been evaluated in any academic publication environment other than Sakarya University Journal of Science.

Copyright Statement

Authors own the copyright of their work published in the journal and their work is published under the CC BY-NC 4.0 license.

References

- [1] M. C. Cengiz, B. Kaftanoğlu, "Endüstriyel Bir Robot İçin İnsan Makina Arayüz Programının Geliştirilmesi," Makina Tasarım ve İmalat Dergisi, cilt. 6, no. 2, ss. 99-107, 2004.
- [2] M. E. Erbil, A. A. Süzen ve H. C. Bayrakçı, "Otonom mobil robotların güvenli veri iletimi için hibrit şifreleme yaklaşımı," UTBD, cilt 15, no. 2, s. 64-72, 2023.
- [3] B. Dieber, B. Breiling, S. Taurer, S. Kacianka, S. Rass ve P. Schartner, "Security for the Robot Operating System," Robotics and Autonomous Systems, cilt 98, s. 192-203, 2017.

- [4] M. P. Groover, "Automation, Production Systems, and Computer-Integrated Manufacturing", Prentice Hall, 2008.
- [5] J. J. Craig, "Introduction to Robotics: Mechanics and Control", Pearson/Prentice Hall, 2005.
- [6] G. J. Olling, R. E. Merritt, Eds., "The Factory Automation Handbook: History, Trends, and Forecasts", CRC Press, 1993.
- [7] J. N. Pires, J. R. Azinheira, Eds., "Progress in Robotics", Springer, 2008.
- [8] B. Siciliano, O. Khatib, Eds., "Springer Handbook of Robotics", Springer, 2008.
- [9] S. Kalpakjian, S. R. Schmid, "Manufacturing Engineering and Technology", Pearson Prentice Hall, 2006.
- [10] J. Elkington, "Cannibals with Forks: The Triple Bottom Line of 21st Century Business", Capstone, 1997.
- [11] A. J. Menezes, P. C. van Oorschot, S. A. Vanstone, "Handbook of Applied Cryptography", CRC Press, 1996.
- [12] W. Ding, L. Yan, R. H. Deng, "A survey on hybrid encryption schemes in vehicular ad-hoc networks," *IEEE Transactions on Intelligent Transportation Systems*, 18, no. 3, ss. 655-667, 2017.
- [13] B. Libert, M. Yung, "Efficient identity-based encryption without random oracles and its application to asymmetric searchable encryption," *Annual International Cryptology Conference*, ss. 600-619, Springer, Berlin, Heidelberg, 2009.
- [14] H. Wang, B. Qin, Q. Wu, J. Domingo-Ferrer, L. Zhang, "Privacy-preserving hybrid cloud with a homomorphic encryption," *IEEE Transactions on Cloud Computing*, 9, no. 3, ss. 1014-1026, 2019.
- [15] X. Wu, G. Revadigar, "A secure and efficient hybrid encryption scheme for securing RFID tag communications," *Journal of Network and Computer Applications*, cilt. 42, ss. 109-116, 2014.
- [16] A. S. Tanenbaum, M. Van Steen, "Distributed Systems: Principles and Paradigms", Prentice-Hall, 2002.
- [17] N. Koblitz, "A Course in Number Theory and Cryptography", 2. edition, Springer-Verlag, 1994.
- [18] A. J. Menezes, P. C. van Oorschot, S. A. Vanstone, "Handbook of Applied Cryptography", CRC Press, 1996.
- [19] R. Rivest, A. Shamir, L. Adleman, "A method for obtaining digital signatures and public-key cryptosystems," *Communications of the ACM*, 21, no. 2, ss. 120-126, 1977.
- [20] D. R. Stinson, "Cryptography: Theory and Practice", 3, CRC Press, 2005.
- [21] A. J. Menezes, P. C. Van Oorschot, S. A. Vanstone, "Handbook of Applied Cryptography", CRC Press, 2001.
- [22] D. R. Stinson, "Cryptography: Theory and Practice", 3, CRC Press, 2005.
- [23] W. Stallings, "Cryptography and Network Security: Principles and Practice", Pearson Education, 2016.
- [24] J. Katz, Y. Lindell, "Introduction to Modern Cryptography", 3, CRC Press, 2020.
- [25] B. Schneier, "Applied Cryptography: Protocols, Algorithms, and Source Code in C", John Wiley & Sons, 1996.
- [26] D. J. Bernstein, "ChaCha, a variant of Salsa20," 2008.
- [27] National Institute of Standards and Technology (NIST), "Advanced Encryption Standard (AES)," FIPS PUB 197, 2001.

- [28] S. Indla, A. Donald, A. T. Aditya, T. A. Srinivas, G. Thippanna, "Locking Down Big Data: A Comprehensive Survey of Data Encryption Methods," *International Journal of Advanced Research in Science, Communication and Technology*, 10, 48175, 2023.
- [29] D. J. Bernstein, "ChaCha, a variant of Salsa20," 2008.
- [30] D. J. Bernstein, "ChaCha, a variant of Salsa20," *Workshop Record of SASC*, sayı 4, 2008.
- [31] A. J. Menezes, P. C. Van Oorschot, S. A. Vanstone, "Handbook of Applied Cryptography", CRC Press, 1996.
- [32] M. Bellare, R. Canetti ve H. Krawczyk, "Keying Hash Functions for Message Authentication," *Advances in Cryptology, CRYPTO '96*.
- [33] D. J. Bernstein, "The Poly1305-AES message-authentication code," *Fast Software Encryption*, ss. 32-49, 2005.
- [34] D. J. Bernstein, "The Poly1305-AES message-authentication code," 2005.
- [35] National Institute of Standards and Technology (NIST), "Advanced Encryption Standard (AES)," *FIPS PUB 197*, 2001.
- [36] D. J. Bernstein, "The Poly1305-AES message-authentication code," 2005.
- [37] D. J. Bernstein, "ChaCha, a variant of Salsa20," 2008.
- [38] National Institute of Standards and Technology (NIST), "Advanced Encryption Standard (AES)," *FIPS PUB 197*, 2001.
- [39] D. J. Bernstein, "The Poly1305-AES message-authentication code," 2005.
- [40] D. J. Bernstein, "ChaCha, a variant of Salsa20," 2008.
- [41] A. J. Menezes, P. C. Van Oorschot, S. A. Vanstone, "Handbook of Applied Cryptography", CRC Press, 2001.
- [42] D. R. Stinson, "Cryptography: Theory and Practice", 3, CRC Press, 2005.
- [43] S. Padhiar, "A Comparative Study on Symmetric and Asymmetric Key Encryption Techniques," in 2021.
- [44] S. Asjad, "The RSA Algorithm," 2019.
- [45] M. Gobi, S. R. Sridevi, R. Rahini, "A Comparative Study on the Performance and the Security of RSA and ECC Algorithm," 2020.
- [46] A. Boicea, C.-O. Truică, F. Rădulescu, D.-C. Popeangă, I.-M. Radulescu ve C. Costea, "Cryptographic Algorithms Benchmarking: A Case Study," 2019.
- [47] M. Abutaha, B. Atawneh, L. Hammouri ve diğerleri, "Secure lightweight cryptosystem for IoT and pervasive computing," *Sci Rep*, cilt 12, no. 19649, 2022.
- [48] Ayman Alissa, Duarte Bacelar Begonha, Jim Boehm, Duarte Braga, Joana Candina, Hugo Espírito Santo, Wolf Richter ve Benjamim Vieira, "How to enhance the cybersecurity of operational technology environments," *McKinsey & Company*, 23 Mart 2023.
- [49] M. Alenezi, H. Alabdulrazzaq ve N. Mohammad, "Symmetric Encryption Algorithms: Review and Evaluation study," *International Journal of Communication Networks and Information Security*, cilt 12, s. 256, 2020.
- [50] Ayman Alissa, Duarte Bacelar Begonha, Jim Boehm, Duarte Braga, Joana Candina, Hugo Espírito Santo, Wolf Richter ve Benjamim Vieira, "How to enhance the cybersecurity of operational technology environments," *McKinsey & Company*, 23 Mart 2023.

- [51] P. Patil, P. Narayankar, D.G. Narayan ve M. S. Meena, "A Comprehensive Evaluation of Cryptographic Algorithms: DES, 3DES, AES, RSA and Blowfish," *Procedia Computer Science*, cilt 78, s. 617-624, 2016.

Analyzing TorrentLocker Ransomware Attacks: A Real Case Study

İlker Kara^{1,2} 

¹ Cankiri Karatekin University, Department of Faculty of Engineering, Electronics and Computer Engineering, Çankırı, Türkiye, karaikab@gmail.com

² Cankiri Karatekin University, Department of Medical Services and Techniques, Çankırı, Türkiye

ARTICLE INFO

ABSTRACT

Keywords:
Ransomware
TorrentLocker
Cybersecurity

Ransomware is malicious software that targets computers, mobile phones, tablets, and other digital devices. These types of software typically encrypt files on the target device, blocking access, and then demand a ransom. TorrentLocker attacks have become particularly popular in recent years, emerging as prominent threats in the realm of cybersecurity. TorrentLocker poses a serious threat to the digital data of users and organizations, exacerbating the financial and reputational damages stemming from cyberattacks. This study provides a framework to understand the target audience, attack strategies, and operations of TorrentLocker ransomware. Conducted through a real case analysis, this examination sheds light on the TorrentLocker attack strategy and elucidates the tracing and identification of the attacker post-attack. The aim of this study is to raise awareness among cybersecurity professionals, organizations, and individual users about TorrentLocker ransomware attacks, aiming to prevent such attacks and track down traces left by the attacker's post-incident. This detailed analysis of TorrentLocker ransomware attacks serves as a crucial resource to enhance protection against future ransomware attacks and contributes to the body of work in this field.



Article History:

Received: 25.02.2024

Accepted: 02.07.2024

Online Available: 01.08.2024

1. Introduction

In today's cybersecurity landscape, ransomware attacks have emerged as a growing threat [1]. With technological advancements and the increasing digitization of our world, cybercriminals' attack methods and techniques have become increasingly complex and sophisticated. Ransomware can inflict serious damage on the digital data of individual users and organizations, raising significant concerns in terms of cybersecurity [2]. The growing frequency and sophistication of these attacks demonstrate that this threat can have far-reaching consequences, not only affecting individuals but also impacting businesses, public institutions, and critical infrastructure. In this context, developing a deeper understanding of ransomware and establishing effective defense strategies are of critical importance in combating today's complex cyber threats. According to the

AV-Test Institute report, as of 2024, 950 million new malware were released [3]. The countries where these attacks have been most prevalent include Canada, Australia, and New Zealand, targeting users in these regions [4]. The victims have paid the attackers a ransom amounting to US\$585,401 in Bitcoins [4].

TorrentLocker stands out among ransomware and is a malicious software targeting computer users. This software infiltrates computer systems, encrypting files to block user access and then demands a ransom to decrypt the files unless paid. Ransomware attacks like TorrentLocker represent a milestone in the evolution of ransomware. Historically, ransomware attacks were documented with the emergence of the malicious software known as AIDS Trojan (PC Cyborg) in 1989 [5]. However, the widespread adoption and sophistication of modern ransomware began to be observed in the early

2000s. TorrentLocker, emerged in 2014, rapidly spreading as a prominent example of ransomware [6]. This period marked the significant rise of ransomware in the cybercrime arena and the development of various tactics. In this context, TorrentLocker and similar ransomware attacks serve as noteworthy examples of cybercriminals adopting complex and sophisticated attack strategies in cyberspace [7-11].

The infection of TorrentLocker ransomware is primarily facilitated through a variety of mechanisms including social engineering tactics, phishing emails, counterfeit software updates, and downloads. These malware programs deceive users with seemingly official, yet harmful links or attachments contained in messages or emails, leading to the malware infecting their devices when these links are clicked or attachments are opened. Moreover, the ransomware is capable of disseminating through the exploitation of security vulnerabilities and via the distribution of harmful files on widely used file-sharing platforms or cloud storage services.

Research on topics such as the origins of ransomware, propagation methods, encryption algorithms, and ransom payment systems contributes to understanding this threat and determining effective countermeasures. Therefore, the importance of research in this area is increasing. The findings of these studies can assist policymakers in cybersecurity, companies, and individuals in developing more effective protection strategies against such attacks.

This study focuses on a real case analysis and examination of TorrentLocker, one of the most significant examples in the field, to investigate the attack strategy and analysis methods of ransomware. Additionally, this case analysis provides an important contribution to understanding how ransomware operates in the real world and prepares against future attacks.

2. Related Work

Ransomware and particularly real-life case analyses have been a significant focal point in cybersecurity research. Numerous academic

studies have examined the prevalence, operation mechanisms, and impacts of ransomware. This section focuses on significant developments of ransomware throughout history.

In 2013, the emergence of Cryptolocker ransomware marked another significant development in the landscape of cyber threats. Characterized by its propagation through infected email attachments, Cryptolocker operated by encrypting victim files using the RSA encryption method. Victims were then coerced into paying ransom using digital currencies, notably Bitcoin, in exchange for the decryption key. Furthermore, attackers threatened to delete the private encryption key unless payment was made before a specified deadline.

While initial ransomware attacks predominantly targeted Windows operating systems, a notable shift occurred in 2015 when Fusob emerged, specifically targeting mobile devices, with attacks persisting until March 2016 [4]. Similar to its predecessors, Fusob employed intimidation tactics to coerce victims into paying ransom. Concurrently, TeslaCrypt Mukesh, active from 2015 to 2016, propagated through email and targeted specific system libraries such as ole32dir.dll, kernel32.dll, and apphelp.dll. Furthermore, it encrypted various file types including game files and special files (.doc, .pdf, .py, .ptx, .jpeg, etc.). However, in May 2016, the threat was neutralized with the release of the primary decryption key by the attackers [4].

In the subsequent year, 2021, the frequency of attacks surged to an alarming rate, averaging one attack every 11 seconds [12]. Beginning in 2012, the spread of Reveton ransomware marked a significant development in the realm of cyber threats. Distinguished from Xorist, Reveton employed intimidation tactics to coerce victims into paying ransoms. For instance, victims received threats indicating that their access had been logged in an illicit area, with law enforcement intervention imminent unless the ransom was paid. Furthermore, victims were compelled to comply with ransom demands by being informed that their IP addresses had been identified, accompanied by claims of capturing actual webcam footage. Payment of the ransom

was mandated through the use of MoneyPak cards.

In another study, ransomware continues to pose a significant threat by infiltrating victim systems through various means, typically encrypting files and demanding a ransom for decryption [13]. Despite the development of security measures such as firewalls, antivirus programs, and automated analysis tools to counter this threat, they have shown limited success in safeguarding valuable assets stored in both local and cloud storage resources. In response to this challenge, this study proposes an effective method for detecting and analyzing ransomware attacks, which is discussed in detail through a case study. Through the application of the proposed method, the study reveals insights into the characteristic behavior of the Onion ransomware, offering potential avenues for identifying attackers. Furthermore, this paper provides a comprehensive overview of the methods and techniques utilized in detecting and analyzing ransomware attacks, shedding light on the evolving landscape of this cybersecurity threat.

3. Materials and Methods

The TorrentLocker ransomware attacks typically occur through the dissemination of infected files via email. When users open these files, the ransomware infects their systems and begins encrypting files. Once the encryption process is complete, users lose access to their files, and a ransom demand is issued. In this section, we introduce a case example prepared for TorrentLocker ransomware attacks and the business computer and analysis tools used in the analysis.

3.1. Dataset

In case analysis studies, it is crucial that the selected sample is up-to-date and fully encompasses the problem at hand. To achieve this, collaboration was established with the information security department of companies operating in Turkey to utilize one of the latest examples for this purpose.

3.2. Preparation of analysis environment

All analyses were conducted on a Lenovo V530 Intel Core i7 7500U workstation. The

workstation was equipped with 128 GB of RAM and a 512 GB SSD. It operated on the Windows 10 Pro operating system.

The analyses were performed using "AccessData Forensic Toolkit v6.3.0.186 (Free version)" and "Wireshark 3.4.3 (Free version) 49.2". As the analyzed sample is a real cyber attack and forensic case, some information is presented with blur for confidentiality purposes.

3.3. Preparation of analysis environment

The examination of digital material was conducted using forensic practices within the framework of Digital Forensics, ensuring data integrity by writing protection (Write Blocker), and in compliance with international standards. Forensic copies were created using AccessData Forensic Toolkit program (Table 1).

Table 1. Image information of victim system

Description	Physical Disk, 967.373.186 Sectors 456,8 GB
Total Size	500.170.862.166 Bytes (456,8 GB)
Total Sectors	967.373.186
Acquisition MD5	953839c2a763adbce05a61f53f8ac988
Verification MD5	953839c2a763adbce05a61f53f8ac988
Acquisition SHA1	8acd345afecd3798763ca7dcb 166f5f78acd483c
Verification SHA1	8acd345afecd3798763ca7dcb 166f5f78acd483c

During the investigation, the internet history and suspicious activities on the target computer's last usage dates were examined. It was noted that the file named "TURKCELL_eFATURA.exe" was present during the recent activities, prompting a closer inspection of this suspicious file. The file "TURKCELL_eFATURA.exe" was initially queried on the website www.virustotal.com, which aggregates database information from 60 antivirus firms (Figure 1).

Upon thorough examination, it was determined that the suspicious file is a type of malicious software known as "TorrentLocker," a form of ransomware that encrypts users' personal files.

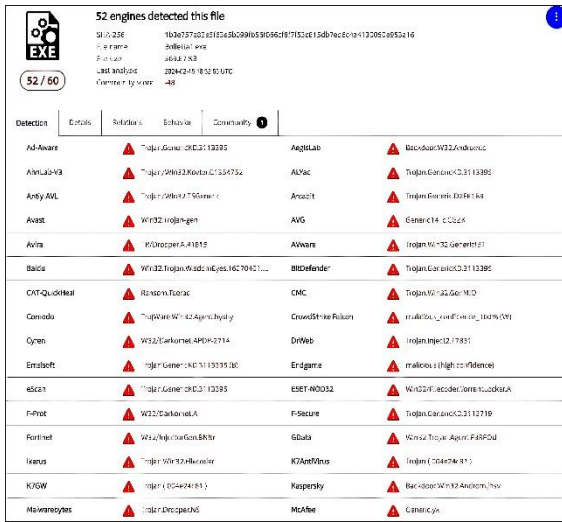


Figure 1. Screenshot of the query the www.virustotal.com website

Table 2. Image information of victim system

File Name	TURKCELL_eFATURA.exe
Change Date	15.02.2024 16:34:54 (2024-02-15 33:34:54 UTC)
File Size	378.749 bytes (369,9 KB)
Value of MD5	a1e75907b75ccf086882d7a01e0599e6
File Path	IMAGE.001/Partition 1/NONAME [NTFS]/[root]/RECYCLER/S-1-5-21-1417001333-261478967-682003330-1003/Dc234.zip»TURKCELL_eFATURA.exe

Upon detecting the encryption of personal files on the victim computer through the malicious software described in Table 2, an examination of file-directory and registry movements associated with this malicious software was conducted (Table 2).

As seen in Table 3, the "TURKCELL_eFATURA.exe" file initiates a process of creating itself under the Windows/temp folder. Subsequently, a file named "vssadmin.exe" is created in the system32 directory of the Windows system. This tactic is employed to prevent the detection and removal of the ransomware. Following this stage, when the "TURKCELL_eFATURA.exe" file is executed, it triggers a series of processes on your computer, including the encryption of files.

Table 3. Infiltration process of the "TURKCELL_eFATURA.exe" TorrentLocker file into the victim computer

Creates process:	C:\windows\temp\TURKCELL_eEATURA.exe {C:\windows\temp\TURKCELL_eEATURA.exe"}
Creates process:	C:\windows\SysWOW64\explorer.exe { "C:\Windows\system32\explorer.exe" }
Creates process:	C:\windows\SysWOW66\vssadmin.exe {vssadmin.exe Delete Shadows /All /Quiet}
Loads service:	ProtectedStorage [C:\windows\system32\lsass.exe]
Reads from process:	PID:1548 C:\windows\Temp\TURKCELL_eFATURA.exe
Writes to process:	PID:1548 C:\windows\Temp\TURKCELL_eFATURA.exe
Writes to process:	PID:1724 C:\windows\SysWOW64\explorer.exe
Terminates process:	C:\windows\Temp\TURKCELL_eFATURA.exe
Terminates process:	C:\windows\Temp\TURKCELL_eFATURA.exe

To examine this activity in more detail, Windows registry movements were investigated (Table 4).

Table 4. Windows registry movements of the "TURKCELL_eFATURA.exe" TorrentLocker file

Creates key:	HKLM\software\microsoft\windows\currentversion\run
Creates key:	HKLM \software\ microsoft \windows\currentversion\internet settings
Creates key:	HKLM \software\microsoft\internet explorer\phishingfilter
Creates key:	HKLM\ software\wor6432node\ microsoft \tracing
Deletes value:	HKCU\ software\microsoft\windows\currentversion\internet settings\proxyserver
Sets/Creates value:	HKLM\ microsoft\software\windows\currentversion\run\{ucerepat}
Sets/Creates value:	HKLM\ microsoft\internetexploler\ phishingfilter \{enebledv9}

After infiltrating the computer by TorrentLocker, such as the "TURKCELL_eFATURA.exe" file, various changes have been made in the Windows registry. These changes are typically made to enable the ransomware to operate more

effectively or to make it difficult for the user to use their computer. When examining Table 3, it is observed that the "TURKCELL_eFATURA.exe" file, a TorrentLocker file, has created startup entries in the Windows registry to automatically start at the computer's boot. This allows the "TURKCELL_eFATURA.exe" TorrentLocker ransomware to run automatically every time the system starts, making it difficult for the user to notice.

The "windows\currentversion\run" registry entry contains a list of programs that will automatically run at the startup of the Windows operating system. As a ransomware, TorrentLocker aims to use this registry entry to automatically start itself at computer boot. This registry entry typically contains a list of programs that will run when the user opens their computer in the current session. Therefore, by using this entry, ransomware can stealthily start itself at computer boot, making it difficult for the user to notice. This tactic enables the ransomware to continuously operate, performing tasks such as encrypting files and displaying the ransom note.

The creation of such a registry entry can enable the "TURKCELL_eFATURA.exe" TorrentLocker ransomware to operate more effectively. However, users can monitor such automatic startup entries and remove unnecessary or malicious entries.

Following the examination of file, directory, and registry movements, the network movements of the "TURKCELL_eFATURA.exe" TorrentLocker ransomware were investigated using Wireshark software. The obtained data allows for the analysis of network traffic. These network analyses provide an opportunity to thoroughly examine the interactions of TorrentLocker ransomware with computer systems. The examination of data recorded through Wireshark allows us to determine how the ransomware communicates with target systems, which network protocols it uses, and what types of data are being transferred.

These analyses have helped us develop a deeper understanding of the impact and propagation strategies of TorrentLocker ransomware.

Additionally, examining the network traffic data recorded through Wireshark allows for tracing the footprint of the attacker in case the ransomware communicates with the attacker (Figure 2).

16	10.74.11	171.25	TCP	49160-80	[SYN]	Seq=0 Win=8192 Len=0 MSS=1460 WS=256 SACK_PERM=1
17	171.25	10.74.11	TCP	80-49160	[SYN, ACK]	Seq=0 Ack=1 Win=65535 Len=0 MSS=1460 WS=64 SACK_PERM=1
18	10.74.11	171.25	TCP	49160-80	[ACK]	Seq=1 Ack=1 Win=65536 Len=0
19	10.74.11	171.25	TCP	49160-80	[PSH, ACK]	Seq=1 Ack=1 Win=65536 Len=100
20	171.25	10.74.11	TCP	80-49160	[PSH, ACK]	Seq=1 Ack=101 Win=65664 Len=7
21	171.25	10.74.11	TCP	80-49160	[FIN, ACK]	Seq=8 Ack=101 Win=65664 Len=0
22	10.74.11	171.25	TCP	49160-80	[ACK]	Seq=101 Ack=9 Win=65536 Len=0
23	10.74.11	171.25	TCP	49160-80	[FIN, ACK]	Seq=101 Ack=9 Win=65536 Len=0
24	171.25	10.74.11	TCP	80-49160	[ACK]	Seq=9 Ack=102 Win=65664 Len=0
25	10.74.11	194.109.206	TCP	49161-443	[SYN]	Seq=0 Win=8192 Len=0 MSS=1460 WS=256 SACK_PERM=1
26	194.109.206	10.74.11	TCP	443-49161	[SYN, ACK]	Seq=0 Ack=1 Win=29200 Len=0 MSS=1460 SACK_PERM=1 WS=128
27	10.74.11	194.109.206	TCP	49161-443	[ACK]	Seq=1 Ack=1 Win=65536 Len=0
28	10.74.11	194.109.206	TLSv1			Client Hello
29	194.109.206	10.74.11	TCP	443-49161	[ACK]	Seq=1 Ack=99 Win=29312 Len=0
30	194.109.206	10.74.11	TLSv1			Alert (Level: Fatal, Description: Handshake Failure)
31	194.109.206	10.74.11	TCP	443-49161	[FIN, ACK]	Seq=8 Ack=99 Win=29312 Len=0
32	10.74.11	194.109.206	TCP	49161-443	[ACK]	Seq=99 Ack=9 Win=65536 Len=0
33	10.74.11	194.109.206	TCP	49161-443	[FIN, ACK]	Seq=99 Ack=9 Win=65536 Len=0
34	194.109.206	10.74.11	TCP	443-49161	[ACK]	Seq=9 Ack=100 Win=29312 Len=0
35	10.74.11	194.109.206	TCP	49162-443	[SYN]	Seq=0 Win=8192 Len=0 MSS=1460 WS=256 SACK_PERM=1
36	194.109.206	10.74.11	TCP	443-49162	[SYN, ACK]	Seq=0 Ack=1 Win=29200 Len=0 MSS=1460 SACK_PERM=1 WS=128

Figure 2. Network movements recorded with Wireshark for the "TURKCELL_eFATURA.exe" file

Upon analyzing the network traffic of the "TURKCELL_eFATURA.exe" TorrentLocker ransomware, it was observed that it attempted to communicate with the IP addresses "171.25.XXX.X" and "194.109.XXX.XXX". During the analysis of the network traffic of the "TURKCELL_eFATURA.exe" TorrentLocker ransomware, it was determined that the malicious software attempted to communicate with the IP addresses "171.25.XXX.X" and "194.109.XXX.XXX".

To identify the domain or sources of the malicious software, WHOIS records were queried through the www.domaintools.com website (Figure 3). WHOIS records provide extensive information about the owners of internet domain names or IP addresses and related information.

This analysis enables the determination of the origins and domains of the ransomware, understanding who or what is behind the attack, and taking appropriate steps for mitigation. Such information gathering and analysis processes significantly contribute to cybersecurity professionals in detecting and defending against attacks and tracing the footprint of the attacker.

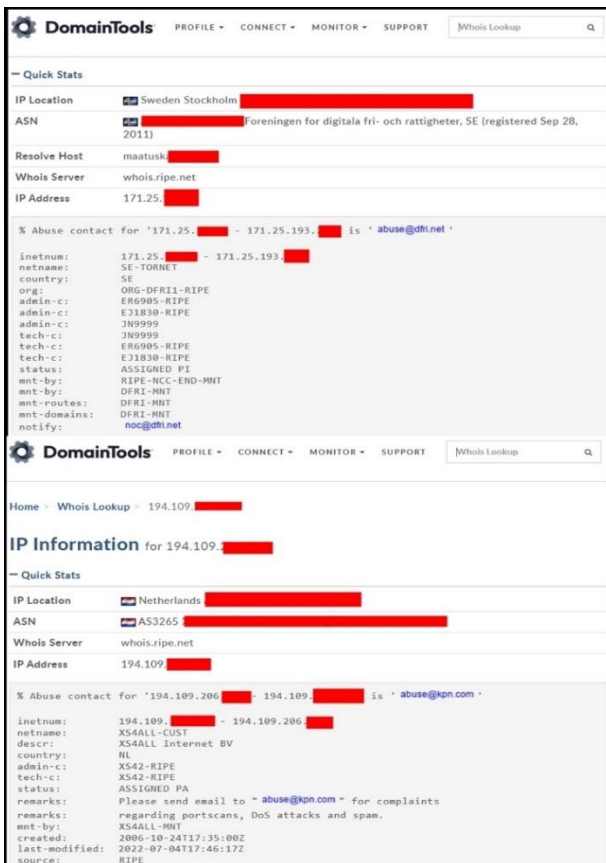


Figure 3. WHOIS records of the IP addresses contacted by the "TURKCELL_eFATURA.exe" file

4. Discussions

In this study, the "TURKCELL_eFATURA.exe" TorrentLocker ransomware has been extensively analyzed. The analyses provided an important step towards understanding the behavior of ransomware on computer systems and developing defense strategies.

As part of the analysis, file, directory, and registry movements of the "TURKCELL_eFATURA.exe" TorrentLocker ransomware, as well as network traffic analysis, were conducted. The results of these analyses allowed us to understand how the ransomware infiltrated the victim system, how it behaved on the victim system, and how it interacted. In particular, network traffic data recorded through Wireshark revealed that the ransomware attempted to communicate with specific IP addresses. By examining the WHOIS records of these IP addresses, potential information about the origins of the ransomware and the attackers was obtained.

Based on the analysis results, it is evident that the "TURKCELL_eFATURA.exe" TorrentLocker ransomware poses a serious cybersecurity threat. When such ransomware infiltrates computer systems, it can lead to significant data loss and financial damages.

On average, these types of ransomware demand approximately €1180 or \$1500 per attack, significantly harming the economic impact [4]. Furthermore, ransomware serves as an effective tool for cybercriminals to achieve their objectives, possessing the capacity to propagate by targeting vulnerable systems. The prevalence of these attacks has been particularly high in countries such as Canada, Australia, and New Zealand, indicating a targeted dissemination pattern by the perpetrators.

5. Conclusion

In recent years, TorrentLocker has emerged as a significant threat within the cybersecurity realm, posing a serious risk to the digital data of users and organizations. This study conducts a real-case analysis to understand the strategies and techniques of TorrentLocker-type ransomware attacks. The analysis meticulously examines the attack strategy and how to trace and identify the post-attack trails left by the attacker.

The findings of this study aim to raise awareness among cybersecurity professionals, organizations, and individuals regarding TorrentLocker ransomware attacks, providing crucial insights into preventing such attacks and outlining the steps to be taken post-incident. The results play a critical role in developing defense strategies against future ransomware attacks and contribute significantly to the research in this field.

In conclusion, this work presents a comprehensive analysis of TorrentLocker ransomware attacks, offering guidance on cybersecurity measures to counteract these threats. Moreover, it is significant for developing new preventative measures and strategies within the context of combating this threat, providing a perspective necessary for the enhancement of cybersecurity defenses.

Article Information Form

Acknowledgments

The authors thank Comodo Group, Inc. USA for providing the malware dataset.

Funding

The research was supported by the Cankiri Karatekin University.

The Declaration of Conflict of Interest/ Common Interest

No conflict of interest or common interest has been declared by the authors.

The Declaration of Ethics Committee Approval

This study does not require ethics committee permission or any special permission.

The Declaration of Research and Publication Ethics

The authors of the paper declare that they comply with the scientific, ethical and quotation rules of SAUJS in all processes of the paper and that they do not make any falsification on the data collected. In addition, they declare that Sakarya University Journal of Science and its editorial board have no responsibility for any ethical violations that may be encountered, and that this study has not been evaluated in any academic publication environment other than Sakarya University Journal of Science.

Copyright Statement

Authors own the copyright of their work published in the journal and their work is published under the CC BY-NC 4.0 license.


References

- [1] T. Meurs, E. Cartwright, A. Cartwright, M. Junger, A. Abhishta, "Deception in double extortion ransomware attacks: An analysis of profitability and credibility," *Computers & Security*, vol. 138, pp. 103670, 2024
- [2] A. Mukhopadhyay, S. Jain, "A framework for cyber-risk insurance against ransomware: A mixed-method approach," *International Journal of Information Management*, vol. 74, pp. 102724, 2024.
- [3] Malware Statistics, the AV-TEST Institute. [Online]. Available: <https://www.av-test.org/en/statistics/malware/>, 2024.
- [4] Malware Statistics, the eset. [Online]. <https://www.eset.com/za/about/newsroom/press-releases-za/research/torrentlocker-cracked-europe-in-the-sight-of-bitcoin-requesting-ransomware1/>, 2024.
- [5] P. O’Kane, S. Sezer, D. Carlin, "Countering cyber threats for industrial applications: An automated approach for malware evasion detection and analysis," *Journal of Network and Computer Applications*, vol. 7, no. 5, pp. 321-327, 2018.
- [6] P. Sharma, S. Zavar, S. B. Patil, "Ransomware analysis: Internet of Things (Iot) security issues challenges and open problems inthe context of worldwide scenario of security of systems and malware attacks," In *International conference on recent Innovation in Engineering and Management*, vol. 2, no. 3, pp. 177-184. 2016.
- [7] A. Alraizza, A. Algarni, "Ransomware detection using machine learning: A survey. *Big Data and Cognitive Computing*," vol. 7, no. 3, pp.143. 2023.
- [8] M. Cen, F. Jiang, X. Qin, Q. Jiang, R. Doss, "Ransomware early detection: A survey," *Computer Networks*, pp. 239, gmr.110138. 2024.
- [9] K. Begovic, A. Al-Ali, Q. Malluhi, "Cryptographic ransomware encryption detection: Survey," *Computers & Security*, pp. 103349, 2023.
- [10] T., Baker, A. Shortland, "The government behind insurance governance: Lessons for ransomware," *Regulation & Governance*, 2023, 17(4), pp. 1000-1020.
- [11] A. Mukhopadhyay, S. Jain, "A framework for cyber-risk insurance against ransomware: A mixed-method approach,"

International Journal of Information Management, pp. 74, gmr.102724, 2024.

- [12] S. A. Syed, "Industry trends in computer software. In Ethical hacking techniques and countermeasures for cybercrime prevention," pp. 54-59, 2021.
- [13] I. Kara, M. Aydos, "The rise of ransomware: Forensic analysis for windows based ransomware attacks. Expert Systems with Applications," pp.190, gmr.116198, 2022.

Determination of Potential Distribution Areas of *Quercus cerris* (Turkish oak) in Anatolia According to Climate Change Scenarios

Cercis İkiel Sakarya University, Faculty of Humanities and Social Sciences, Department of Geography, Sakarya, Türkiye, cikiel@sakarya.edu.tr

ARTICLE INFO

ABSTRACT

Keywords:

Quercus cerris
Turkish oak
Climate change
Species distribution model
Anatolia



Article History:

Received: 04.03.2024
Accepted: 30.05.2024
Online Available: 01.08.2024

The aim of this study is to determine the potential suitable distribution areas for *Quercus cerris* in the future depending on climate change scenarios. For this purpose, current spatial distribution data and 19 bioclimatic variable data downloaded from the WorldClim 2.1 database were used. The bioclimatic variable data consist of the climate data for the 2081-2100 period belonging to the SSP2-4.5 and SSP5-8.5 scenarios of the MIROC6 climate model with resolution of 2.5 arc-minutes. PCA was applied to bioclimatic variable data. MaxEnt 3.4.1 and ArcGIS 10.5 software were used to generate the models. The accuracy of the models was measured as 0.79 accuracy with the AUC test value. The variables that contributed the most to the model were BIO4 (temperature seasonality) with 39.8%, BIO9 (mean temperature of driest quarter) with 26.7%.

According to the results, it is predicted that the spatial distribution of this species unsuitable habitat areas, which is 25.9% today, will increase by 54.1% according to the SSP 245 scenario and by 80.2% according to the SSP 585 scenario. While the suitable habitat areas for *Q. cerris* in Anatolia are 33.2% today, they will change in a decreasing direction in the future by 11.6% according to the SSP 245 scenario and 14.0% according to the SSP 585 scenario. In addition to the direct impact of climate change scenarios on *Q. cerris*, when changes in land use are taken into account, the current distribution areas and suitable distribution areas of the species should be preserved with sustainable development goals.

1. Introduction

Environmental factors have significant effects on the distribution of species. Climate, being a major factor influencing the pattern, structure, and ecology of vegetation, plays a primary role in the spatial distribution of plants. Therefore, changes in plant distribution are expected in response to variations in climate conditions [1, 2].

Since the beginning of the 21st century, climate change has been recognized as one of the greatest threats to global biological diversity [3]. According to the latest report by the IPCC, the Mediterranean region, including the study area, is one of the most affected regions by climate

change. Predicting the effects of climate change on species distribution models is one of the most current topics in ecology and biogeography [4]. Species distribution models are essential tools for biogeographical researches. Some of the most widely used species distribution modelling software today include Genetic Algorithm for Rule-set Prediction (GARP) [5], Ecological Niche Factor Analysis (ENFA) [6], Bioclimatic Prediction System (Bioclim) [7], Maximum Entropy (MaxEnt) [8], Flexible Discriminant Analysis (FDA), Generalized Additive Model (GAM), Generalized Boosting Model (GBM), Generalized Linear Model (GLM), Random Forest (RF) [9-10].

Among software, MaxEnt is one of the most used [11-15]. MaxEnt has significant advantages due to its user-friendly interface and its ability to provide accurate predictions with a small number of species distribution data. MaxEnt predicts species probability distributions based on environmental constraints and identifies potential suitable distribution areas using the current distribution data of species [8].

One of the most pronounced consequences of global warming in the last decade is the increased occurrence of extreme weather events. The increasing climate variability predicts that severe rains, storms, floods, mass movements, severe heatwaves, droughts, and forest fires will be encountered, especially in the Mediterranean region [16-18]. Climate change will affect all biodiversity, including species distributed in Anatolia. Anatolia, habitat approximately 12.000 plant species due to its past exposure to climate change its unique geographical location, is one of the primary locations where these changes occur.

The natural distribution of oak trees has significantly diminished over time [19-21]. *Quercus cerris* is one of the tree species with high economic returns from wood/non-wood products, and it has been one of the most destroyed tree species over time. Although *Q. cerris* can sustain its existence as coppice due to its ability to regenerate, random cuts, inappropriate silvicultural management, fires, overgrazing (especially during rejuvenation), mining activities, and climate change threaten the presence of the species [22]. Rigo et al. (2016), who examined the distribution areas and suitability of *Q. cerris* in Europe, stated that *Q. cerris* is more drought-resistant than other oak species living in the same region [23].

Moricz et al. (2021) examined the sensitivity of *Q. cerris* to drought with rainfall datasets [24]. In their study, Mert et al. (2016) emphasized that *Q. cerris* is highly sensitive to forest fires and that it is necessary to study such species for the continuity of the ecosystem in the Mediterranean region, which is under the threat of climate change [25]. They also conducted a distribution suitability analysis for the Sütçüler basin in Türkiye as a sampling area. Filippo et al. (2010)

analysed the response of *Q. cerris* to climate change in Italy [26]. Stafasani and Toramani (2015) conducted dendroclimatological research on *Q. cerris* in Albania, assuming that *Q. cerris* is more sensitive to natural environmental conditions when it grows at different latitudes and ecological conditions [27]. Given the effects of climate change on biodiversity, determining the future status of *Q. cerris* is important. Therefore, the aim of this study is to determine the current and future potential distribution areas/distribution areas of *Q. cerris* in Anatolia.

Study Area:

The Anatolian Peninsula, which is located within the borders of Türkiye, which connects the continents of Asia and Europe, is situated between longitudes 26° and 45° East and latitudes 36° and 42° North. The average elevation of the study area is 1141 meters. The primary geomorphological unit that forms the study area are the Northern Anatolian Mountains, the Central Anatolian Mountains, the Taurus Mountains, and the Southeastern Anatolian Mountains. The Central Anatolia, Southeastern Anatolia, and Western Anatolia Plains cover extensive areas [28, 29]. Although there are various climate types in the study area, the dominant climate type is hot/dry summer and very hot Subtropical Mediterranean climate. [30, 31] (Figure 1).

2. General Methods

Quercus cerris, has two varieties (*Quercus cerris* var. *cerris* and *Quercus cerris* var. *austriaca*). *Q. cerris*, a member of the red oak group, is adaptable to different climate conditions. It can be distributed in areas dominated by the Black Sea climate as well as in regions with a Marmara and Mediterranean climate. It forms pure communities but can also be seen in mixed forests that include different oak species (*Quercus frainetto*, *Quercus pubescens*, *Quercus infectoria*, *Quercus petraea*, *Quercus libani*), other broad-leaved species (*Fagus*, *Castanea*, *Carpinus*), and coniferous trees (*Pinus nigra*, *Pinus brutia*, *Pinus pinea*) [32-35]. (Photo 1).

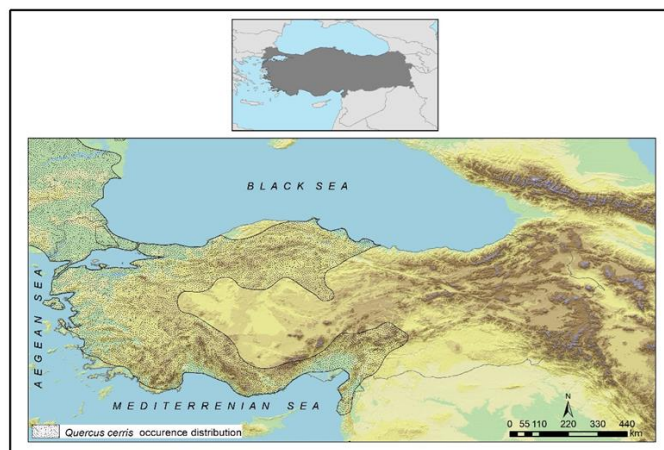


Figure 1. Location map of the study area



Photo 1. *Q. cerris*, natural distributed in Sakarya

It is a large, fast-growing, deciduous tree naturally found in Europe and Asia. In this region, it is one of the dominant deciduous tree species in mixed forest areas. It has a wide distribution range, stretching from central Europe southward to the Eastern Mediterranean countries. In this region, it forms extensive forests in Italy, the Balkan Peninsula, Türkiye, and Syria. The southern and eastern parts of Anatolia (up to Erzincan), the northern parts of Anatolia (up to Samsun) and the Aegean coast are the distribution areas of two different subspecies of *Q. cerris*. [32-36].

Current distribution data of the species in Anatolia and its surroundings were obtained from the Global Biodiversity Information Facility (GBIF) [37], and EUFORGEN databases [38], and by scanning the relevant sections of the work titled "Flora of Türkiye and the East

Aegean Islands" [33, 34]. While using the distribution data of the selected species from Anatolia and its surroundings (*Q. cerris*: 105 occurrence data), care was taken to ensure that the data had a homogeneous distribution. For this purpose, a spatial filter will be used on species distribution data using the "Spatially Rarefy Occurrence Data" tool in ArcGIS 10.5 SDM Toolbox.

For the development of current and future models for *Q. cerris*, climate data obtained from the WorldClim 2.1 database was used. Climate data for the present time covers the period of 1970-2000, while for future projections, the MIROC6 model and climate projection data for the 2081-2100 period under the SSP2-4.5 and SSP5-8.5 scenarios were used (Fick & Hijmans, 2017; [39, 40]). The climate data used for both current and future scenarios have a resolution of 2.5 arcminutes, approximately 5 km.

The SSP scenarios are consolidated by the IPCC 6th Assessment reports and used as 21st century scenarios. Among these scenarios, SSP1 and SSP5 scenarios foresee significant investments in education and health, rapid economic growth and well-functioning institutions. In terms of where they differ from each other, while there is a transition towards sustainable practices in SSP1, SSP5 assumes that it will be governed by an energy-intensive, fossil fuel-based economy [41].

As in many plants, climate is the most important ecological factor influencing the distribution of *Quercus cerris* in Anatolia [16, 42-48].

Therefore, other ecological factors were not included in the modelling. In this study, 19 bioclimatic variables were obtained from the WorldClim database. To understand the relationships between the 19 bioclimatic variables and to create a model with good performance, a PCA (Principal Component Analysis) analysis was applied to the bioclimatic variables. Highly correlated data were removed from the model to avoid multicollinearity problems.

For this purpose, Pearson correlation coefficient was calculated to look at the linear relation of bioclimatic variables with each other using PCA analysis. These bioclimatic variables that did not exhibit collinearity with a correlation coefficient less than 0.85 were used in the models. The following bioclimatic variables were used in the modelling: BIO2 (Mean Diurnal Range - Mean of monthly (max temperature - min temperature)), BIO3 (Isothermality), BIO4 (Temperature Seasonality), BIO8 (Mean Temperature of Wettest Quarter), BIO9 (Mean Temperature of Driest Quarter), BIO12 (Annual Precipitation), BIO13 (Precipitation of Wettest Month), BIO14 (Precipitation of Driest Month), BIO15 (Precipitation Seasonality) [14, 45, 46, 47, 48].

To create species distribution models for *Quercus cerris* using the current distribution data and climate data, the MaxEnt (Maximum Entropy) software was employed.

MaxEnt is one of the most widely used and important statistical techniques for species distribution modelling. MaxEnt is effectively used to predict and determine the current geographical areas of the species in question. In addition, future projections based on environmental changes help evaluate the effects of possible changes and niche shifts [49, 50].

During the run of the models, a 15 replicates cross-validation technique was used; where 70% of the species presence data was utilized as training data and 30% as test data, with the iteration fixed at 500 [1, 14, 49]. To evaluate model performance, the AUC (Area Under the Curve) obtained through the ROC (Receiver Operating Characteristic) curve analysis method with accuracy testing was used. The obtained AUC values range from 0.5 to 1. Values between

0.5-0.6 indicate poor performance, 0.6-0.7 weak performance, 0.7-0.8 moderate performance, 0.8-0.9 good performance, and 0.9-1 excellent performance. An AUC value close to 1 indicates that the results are far from random distribution, the correlation between environmental variables and the predicted geographic distribution of species is high, and the model performs accurately [15, 50]. To assess the contribution and importance of each bioclimatic variable used in the model, a Jackknife test (leave-one-out) was applied.

Using the obtained models, distribution suitability classes were determined in ArcGIS 10.5 software. As a result of the classification, values ranging from 0 to 0.2 represent unsuitable distribution, 0.2 to 0.4 represent partially suitable distribution, 0.4 to 0.6 represent suitable distribution, 0.6 to 0.8 represent highly suitable distribution, and 0.8 to 1 represent very highly suitable distribution [15, 51]. Additionally, spatial changes for the future were calculated with respect to current suitable distribution areas using ArcGIS 10.5 software.

3. Results and Discussion

The current and future (2100) potential distributions and changes of *Q. cerris* were determined using the MIROC6 climate model and the SSP245 and SSP585 climate scenarios with MaxEnt and ArcGIS 10.5 software.

The models achieved a high level of reliability, with an AUC test value of 0.79 (Figure 2). The percentage contribution of the bioclimatic variables in the models has been included in the model outputs. According to the Jackknife analyses, BIO4 has a contribution of 39.8%, BIO9 contributes 26.7%, and BIO14 contributes 15.8% (Table 1, Figure 3). When looking at the percentage contributions of the variables, it can be observed that drought is particularly important for *Q. cerris*. Considering the current distribution areas of the species, the conditions of temperature and precipitation are determinants.

When models produced for *Q. cerris* are examined, it is observed that the potential suitable distribution areas of the species are like the current distribution areas. These areas are

outside of eastern and southeastern Anatolia. When looking at the potential suitable distribution areas for the species in the future, under the SSP 245 scenario, it is possible that *Q. cerris* will have suitable distribution areas in the northern regions of Anatolia. According to the SSP 845 scenario, it is predicted that the species will lose most of its suitable habitat areas. It is possible that *Q. cerris*, which has a wide distribution in Anatolia today, will narrow down these areas in the future and find suitable/partially suitable habitat areas in the Black Sea and its surroundings. (Figure 4). Similar results to those obtained in the study were also found by Mert et al. (2016) in the analysis applied with different scenarios in the Sütçüler Basin in the southwest of Anatolia, predicted that the distribution area of the species will narrow in the coming years [23]. When we look at the temporal change in the suitable distribution areas for the species, it is

striking that unsuitable distribution areas will increase, and suitable distribution areas will decrease.

While the areal distribution of habitat areas that are not suitable for the growth of *Q. cerris* is 25.9% today, it is predicted that it will increase by 54.1% according to the SSP 245 scenario and 80.2% according to the SSP 585 scenario in the future. While the suitable habitat areas for *Q. cerris* in Anatolia are 33.2% today, they will change in a decreasing direction in the future by 11.6% according to the SSP 245 scenario and 14.0% according to the SSP 585 scenario. The areal change of highly suitable habitat areas for this species will decrease by 8.3% (present), 3.3% (SSP245) and 0.3% (SSP585), respectively, according to climate scenarios. It is predicted that very high suitable habitat areas will almost disappear. (Table 2).

Table 1. Contribution of bioclimatic variables obtained as a result of jackknife analysis (%)

	Bioclimatic variables	Percent contribution
<i>Quercus cerris</i>	BIO4 Temperature Seasonality	39.8
	BIO 9 Mean Temperature of Driest Quarter	26.7
	BIO14 Precipitation of Driest Month	15.8

Table 2. Temporal Change Rates of Potential Distribution Areas of *Quercus cerris*

	Present	SSP 245	SSP 585
Unsuitable distribution area (0–0.2)	25.9	54.1	80.2
Barely suitable distribution area (0.2–0.4)	32.5	31.1	5.5
Suitable distribution area (0.4–0.6)	33.2	11.6	14.0
Highly suitable distribution area (0.6–0.8)	8.3	3.3	0.3
Very highly suitable distribution area (0.8–1.0)	0.1		

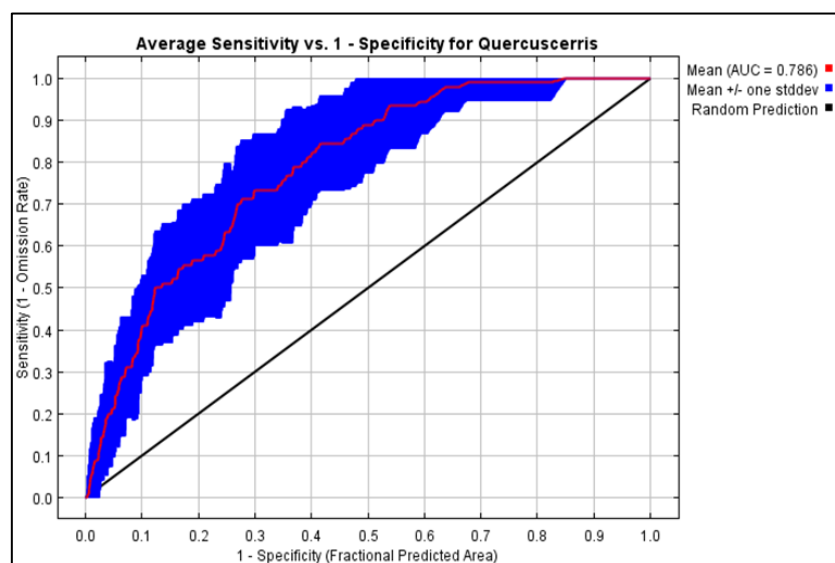


Figure 2. ROC curve and AUC values for MaxEnt model

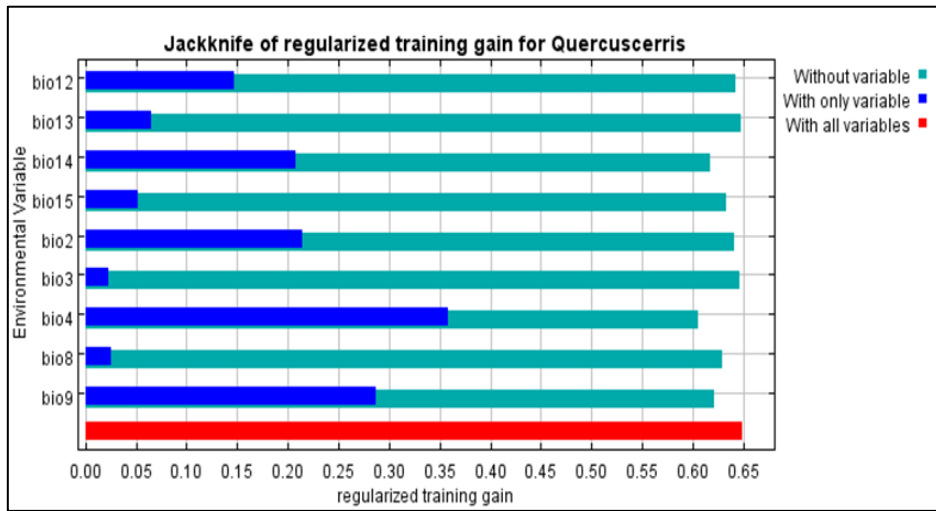


Figure 3. Jackknife test of variable importance of *Quercus cerris*

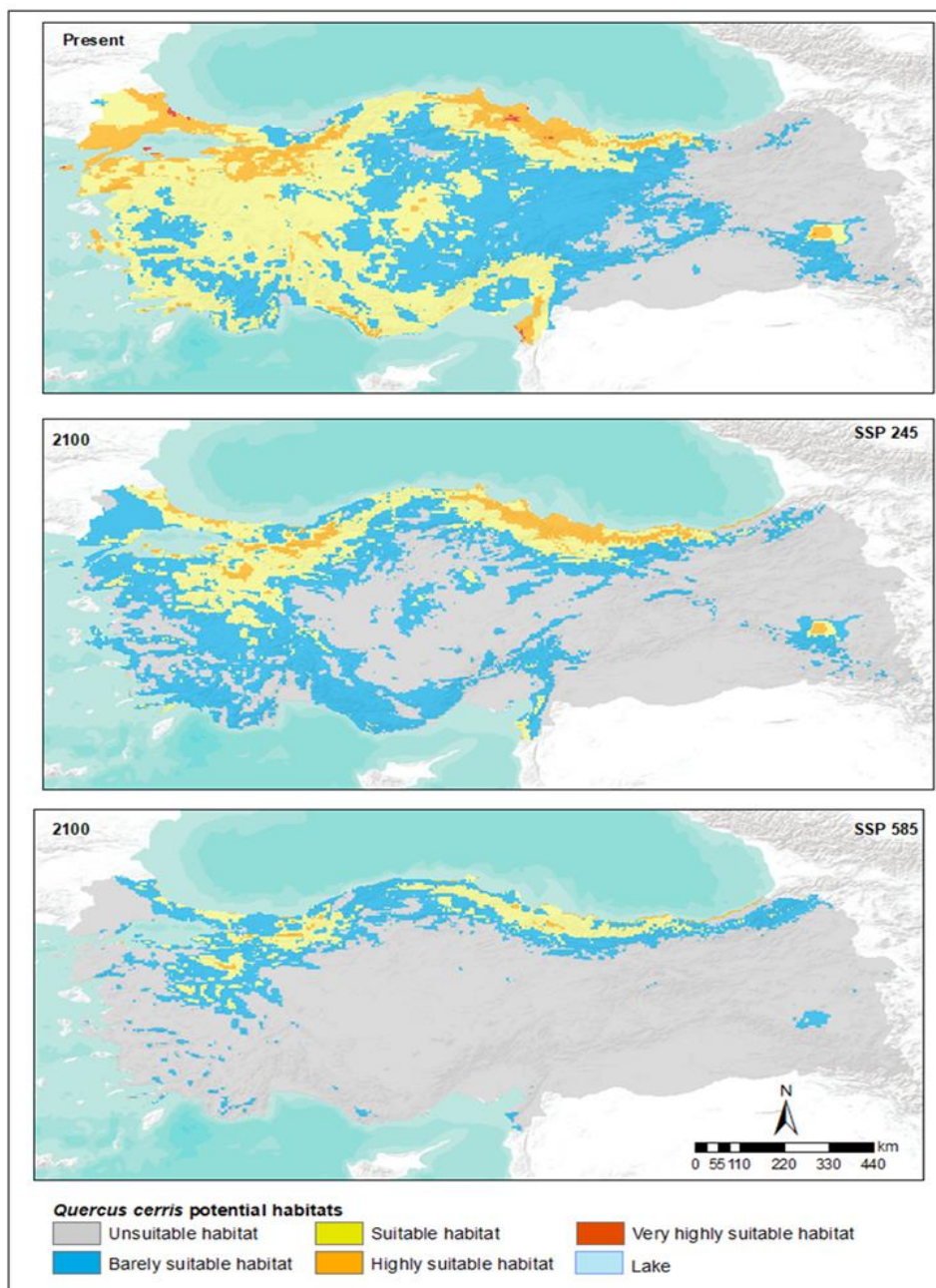


Figure 4. Current and future potential distribution areas of *Quercus cerris* in Anatolia

4. Conclusion

In this research, the current and future potential distribution areas of *Q. cerris* in Anatolia have been determined. The results obtained are model-based and contain predictions, therefore, the results are not definitive. Statistical methods have been used to ensure the validity of the models, and according to the results obtained, the model outcomes are accurate and usable. Although different ecological factors have an impact on the distribution of plants, when viewed on a broad scale, temperature and precipitation are the factors that affect species distribution. Theoretically, all ecological processes are required for detailed study in ecological niche modeling, but potential niches and potential distributions can only be predicted based on climatic variables [52-54].

As in many similar studies, the factors to be considered in species distribution modeling are bioclimatic variables [46-55-57]. The study was examined from a geographical perspective and "climatic conditions", one of the physical geography elements, were considered as independent variables. In this context, bioclimatic variables will be discussed primarily in the study since variable climatic conditions have the most impact on vegetation distribution. In addition, although present-day numerical data can be provided, future data (ecological, edaphic and topographic) limit the study because they cannot be modeled, especially since they are not in digital format and on a large scale, and therefore they were not used. Therefore, it was aimed to determine the possible effects of climate change on the distribution of *Q. cerris*.

According to the model results, the species currently has distribution in the regions around the Black Sea, Marmara, Aegean, and Mediterranean. However, in the future, suitable distribution areas in regions characterized by a Mediterranean climate, particularly around the Mediterranean and Aegean regions, are expected to decrease.

Recent studies focusing on the Mediterranean Basin indicate that species sharing distribution areas with *Q. cerris* in Anatolia or similar regions may likely reduce their ranges, experience shifts in distribution areas, or even face extinction due

to climate change [25]. This is especially relevant for dominant species in northern Anatolia, such as *Carpinus betulus*, *Tilia tomentosa*, *Tilia cordata*, *Tilia platyphyllos*, and *Fagus orientalis*, where it is probable that their distribution areas in the north will narrow, resulting in the loss of refuge areas [15, 58-60]. In addition, according to modeling studies carried out for some species such as *Laurus nobilis*, *Juniperus drupacea*, *Abies ciliccia*, *Cedrus libani*, *Quercus coccifera*, which are distributed in areas where *Q. cerris* is distributed and where characterized by a Mediterranean climate, it is predicted that the mentioned species will narrow their distribution areas and loss completely from some areas [15, 58-64].

Climate change has both direct and indirect effects on biodiversity. Changes in land use characteristics due to climate change are crucial factors that can significantly impact biodiversity. Shifts in areas such as settlements and agricultural fields can lead to the contraction of plant distribution areas. Therefore, for a sustainable ecosystem, it is imperative to preserve the current distribution areas and suitable distribution areas of *Q. cerris*.

Article Information Form

Funding

The author (s) has no received any financial support for the research, authorship or publication of this study.

The Declaration of Conflict of Interest/ Common Interest

No conflict of interest or common interest has been declared by the authors.

The Declaration of Ethics Committee Approval

This study does not require ethics committee permission or any special permission.

The Declaration of Research and Publication Ethics

The authors of the paper declare that they comply with the scientific, ethical and quotation rules of SAUJS in all processes of the paper and that they do not make any falsification on the data collected. In addition, they declare that Sakarya University Journal of Science and its editorial

board have no responsibility for any ethical violations that may be encountered, and that this study has not been evaluated in any academic publication environment other than Sakarya University Journal of Science.

Copyright Statement

Authors own the copyright of their work published in the journal and their work is published under the CC BY-NC 4.0 license.

References

- [1] P. Kumar, "Assessment of impact of climate change on *Rhododendrons* in Sikkim Himalayas Using Maxent Modelling: Limitations and Challenges," *Biodiversity and Conservation*, vol. 21, pp. 1251-1266, 2012.
- [2] D. W. McKenney, D. W., J. H. Pedlar, K. Lawrence, K. Campbell, M. F. Hutchinson, "Potential Impacts of Climate Change on the Distribution of North American Trees," *BioScience*, vol. 57, no. 11, pp. 939-948, 2007.
- [3] T. P. Dawson, S. T. Jackson, J., I. House, I. C. Prentice, G. M. Mace, "Beyond Predictions: Biodiversity Conservation in a Changing Climate," *Science*, vol. 332, no. 6025, pp. 53-58, 2011.
- [4] C. Bellard, C. Bertelsmeier, P. Leadley, W. Thuiller, F. Courchamp, "Impacts of Climate Change on the Future of Biodiversity". *Ecology Letters*, vol. 15, no. 4, pp. 365–377. 2012.
- [5] D. Stockwell, "The GARP Modelling System: Problems and Solutions to Automated Spatial Predictio,". *International Journal of Geographical Information Science*, vol. 13, pp. 143–158, 2010.
- [6] A. Hirzel, A. Guisan, "Which is the Optimal Sampling Strategy for Habitat Suitability Modeling." *Ecological Modelling*, Vol. 157, pp. 331–341, 2002.
- [7] J. R. Busby, "Bioclim, a Bioclimatic Analysis and Prediction System," in *Nature Conservation: Cost Effective Biological Surveys and Data Analysis*, CSIRO, C. R. Margules M. P. Austin, pp. 64–68, 1991.
- [8] S. J. Phillips, R. P. Anderson, R. E. Schapire, "Maximum Entropy Modeling of Species Geographic Distributions, *Ecological Modelling*," vol. 190, no. 3-4, pp. 231-259, 2006.
- [9] N. Anjum, Q. Ridwan, F. Akhter, M. Hanief, Predicting Current and Future Distribution Pattern of *Berberis lycium* Royle Concerning Climate Change Using an Ensemble Modelling Approach. *Geology, Ecology, and Landscapes*, pp. 1-10, 2023.
- [10] Y. P. Li, X. Gao, Q. An., Z. Sun, H. B. Wang, "Ecological Niche Modeling Based on Ensemble Algorithms to Predicting Current and Future Potential Distribution of African Swine Fever Virus in China", *Scientific Reports*, vol. 12, no. 1, 15614. 2022.
- [11] Y. Gebrewahid, S. Abrehe, E. Meresa, G. Eyasu, K. Abay, G. Gebreab, K. Kidanemariam, G. Adissu, G. Abreha, G. Darcha, "Current and Future Predicting Potential Areas of *Oxytenanthera abyssinica* (A. Richard) Using MaxEnt Model Under Climate Change in Northern Ethiopia,". *Ecological Processes*, vol. 9, no. 1, pp. 1-15, 2020.
- [12] Z. Cao, L. Zhang, X. Zhang, Z. Guo, "Predicting the potential distribution of *Hylomecon japonica* in China under current and future climate change based on Maxent model," *Sustainability*, vol 13, no. 20, 11253., pp.1-14, 2021.
- [13] G. Zhao, X. Cui, J. Sun, T. Li, Q. I. Wang, X. Ye, B. Fan, "Analysis of the Distribution Pattern of Chinese *Ziziphus jujuba* Under Climate Change Based on Optimized Biomod2 and MaxEnt Models." *Ecological Indicators*, vol. 132, 108256, pp. 1-11, 2021.

- [14] D. E. Koç, D. Biltekin, B. Ustaoglu, "Modelling Potential Distribution of *Carpinus betulus* in Anatolia and Its Surroundings from the Last Glacial Maximum to the Future," *Arabian Journal of Geosciences*, vol. 14, no. 12, 1186, pp. 1-13, 2021.
- [15] D. E. Koç, H. N. Dalfes, A. Meral, "Anadolu'da Konifer Ağaçların Yayılış Alanlarındaki Değişimler," *Coğrafya Dergisi*, vol. 44, pp. 81-95, 2022.
- [16] K. A. Baylan, B. Ustaoglu, "Emberger Biyoiklim Sınıflandırmasına Göre Türkiye'de Akdeniz Biyoiklim Katlarının ve Alt Tiplerinin Dağılışı," *Ulusal Çevre Bilimleri Araştırma Dergisi*, vol. 3, no. 3, pp. 158-174, 2020.
- [17] M Türkeş, E. Erlat, "Precipitation Changes and Variability in Türkiye Linked to the North Atlantic Oscillation During the Period 1930–2000," *International Journal of Climatology: A Journal of the Royal Meteorological Society*, vol. 23, no. 14, pp. 1771-1796, 2003.
- [18] B. Ustaoglu, K. A. Tunçat, D. E. Koç, "Impacts of Climate Change on Precipitation and Temperature Climatology in Türkiye from Present to Future Perspective," in *Urban Commons, Future Smart Cities and Sustainability*, Springer, pp. 403-426, 2023.
- [19] D. Aydınöz, A. Çoban, H. Tunç, "Tüylü Meşe'nin (*Quercus pubescens*) Türkiye'de Yeni bir Yayılış Alanı: Elmalı Dağı (Kayseri)," *Doğu Coğrafya Dergisi*, vol. 22, no. 37, pp.83-98, 2017.
- [20] T. Dünder, "Demirköy Yöresi Istranca Meşelerinin (*Quercus hartwissiana* Stev.) mekanik Özellikleri," *Journal of the Faculty of Forestry Istanbul University*, vol. 52, no. 2, pp. 159-176. 2002.
- [21] N. Günal, "Türkiye'de Sinirli Yayılışa Sahip Bir Meşe Türü: *Quercus ilex* (Pinal meşesi)," *Öneri Dergisi*, vol. 5, no. 19, pp. 191-197, 2003.
- [22] B. Gencal, "Bursa Orman Bölge Müdürlüğü Saçlı meşe (*Quercus cerris*) Meşcerelerindeki Büyüme İlişkileri," Master's thesis, Bursa Teknik Üniversitesi, 2019.
- [23] D. De Rigo, C. M. Enescu, T. Houston Durrant, G. Caudullo, "*Quercus cerris* in Europe: distribution, habitat, usage and threats," *European Atlas of Forest Tree Species*; Eds: J. San-Miguel-Ayanz, D de Rigo, G. Caudullo, T. Houston Durrant A. Mauri, pp. 148-149, 2016.
- [24] N. Móricz, G. Illés, I. Mészáros, B. Garamszegi, I. Berki, Z. Bakacsi, J. Kámpel, O. Szabó, E. Rasztovits, K. Cseke, K. Bereczki, T. M. Németh, "Different drought sensitivity traits of young sessile oak (*Quercus petraea* (Matt.) Liebl.) and Türkiye oak (*Quercus cerris* L.) stands along a precipitation gradient in Hungary," *Forest Ecology and Management*, 492, 119165, pp. 1-12, 2021.
- [25] A. Mert, K. Özkan, Ö. Şentürk, M. G. Negiz, "Changing the Potential Distribution of Türkiye Oak (*Quercus cerris* L.) Under Climate Change in Türkiye," *Polish Journal of Environmental Studies*, vol. 25, no. 4, pp.1633-1638, 2016.
- [26] A. Di Filippo, A. Alessandrini, F. Biondi, S. Blasi, L. Portoghesi, G. Piovesan, "Climate Change and Oak Growth Decline: Dendroecology and stand productivity of a Türkiye oak (*Quercus cerris* L.) old stored coppice in Central Italy," *Annals of Forest Science*, vol.67, pp. 706-706, 2010.
- [27] M. Stafasani, E. Toromani, "Growth-climate Response of Young Türkiye oak (*Quercus cerris* L.) Coppice Forest Stands Along Longitudinal Gradient in Albania," *South-East European Forestry: Seefor*, vol. 6, no. 1, pp. 25-38, 2015.

- [28] İ. Ketin, "Anadolu'nun Tektonik Birlikleri." Bulletin of the Mineral Research and Exploration, vol. 66, no. 66, pp. 20-37, 1966.
- [29] A. Tanoğlu, "Türkiye'nin İrtifa Kuşakları," Türk Coğrafya Dergisi, vol. 9, no. 10, pp. 37-63, 1947.
- [30] M. Türkeş, "Türkiye'nin İklimsel Değişkenlik ve Sosyo-Ekolojik Göstergeler Açısından Kuraklıktan Etkilenebilirlik ve Risk Çözümlemesi," Ege Coğrafya Dergisi, vol. 26, no. 2, pp. 47-70, 2017.
- [31] B. Ustaoglu, "Sakarya'nın İklim Özellikleri," in. Sakarya'nın Fiziki, Beşeri ve İktisadi Coğrafya Özellikleri, Sakarya Universtiy Press, Sakarya, C. İkiel, pp. 163-218, 2018.
- [32] N. Günal, "Türkiye'de Başlıca Ağaç Türlerinin Coğrafi Yayılışları, Ekolojik ve Floristik Özellikleri," Çantay Kitabevi. 1997.
- [33] I.C. Hedge, F. Yaltırık, "Quercus L.," in Flora of Türkiye and the East Aegean Islands, Vol.7 Edinburgh: Edinburgh University Press P. Davis, M. Coode, & J. Cullen, pp. 675-676, 1982.
- [34] F. Yaltırık, "Türkiye Meşeleri, Tarım Orman ve Köy İşleri Bakanlığı," Orman Genel Müdürlüğü Yayınları Yenilik Basımevi, İstanbul, 1984.
- [35] T. Sönmez, B. Gencal, "Bursa Orman Bölge Müdürlüğü Saçlı Meşe (*Quercus cerris*) Meşcerelerindeki Büyüme İlişkileri," Ormancılık Araştırma Dergisi, vol. 10 (Özel Sayı), pp. 92-104, 2023.
- [36] M. C. Simeone, P. Zhelev, Kandemir, G. (2019). Technical Guidelines for genetic conservation and use of Türkiye oak (*Quercus cerris*).
- [37] Global Biodiversity Information Facilit (GBIF), <https://doi.org/10.15468/dl.kb9wwr>, 02 August 2023.
- [38] European Forest Genetic Resources Programme (EUFORGEN), <https://www.euforgen.org/species/>, 02 August 2023.
- [39] S.E. Fick, R.J. Hijmans, "WorldClim 2: new 1km spatial resolution climate surfaces for global land areas," International Journal of Climatology 37 (12): 4302-pp. 4315, 2017.
- [40] WorldClim, https://www.worldclim.org/data/cmip6/cmip6_clim2.5m.html, 02 August 2023.
- [41] S. Özdemir, K. Özkan, A. Mert, "An Ecological Perspective on Climate Change Scenarios, Biodiversity and Conservation," vol. 13, no. 3, pp. 361-371, 2020.
- [42] D. E. Koc, J. C. Svenning, A. Meral, "Climate Change Impacts on the Potential Distribution of *Taxus baccata* L. in the Eastern Mediterranean and the Bolkar Mountains (Türkiye) from Last Glacial Maximum to the Future," Eurasian Journal of Forest Science, vol. 6, no. 3, pp. 69-82. 2018.
- [43] C. P. Osborne, P. L. Mitchell, J. E. Sheehy, F. I. Woodward, "Modelling the Recent Historical Impacts of Atmospheric CO2 and Climate Change on Mediterranean Vegetation". Global Change Biology, vol. 6, no. 4, pp. 445-458, 2000.
- [44] M. Toledo, L. Poorter, M. Peña-Claros, A. Alarcón, J. Balcázar, C. Leño, J. C. Licona, O. Llanque, V. Vroomans, P. Zuidema, F. Bongers, "Climate is a Stronger Driver of Tree and Forest Growth Rates Than Soil and Disturbance," Journal of Ecology, vol. 99, no. 1, pp. 254-264, 2011.
- [45] N. Bystriakova, M. Peregrym, R. H. Erkens, O. Bezsmertna, H. Schneider, "Sampling Bias in Geographic and Environmental Space and Its Effect on the

- Predictive Power of Species Distribution Models,” *Systematics and Biodiversity*, vol. 10, no. 3, pp. 305-315, 2012.
- [46] S. Özdemir, S. Gülsoy, M. Ahmet, “Predicting the Effect of Climate Change on the Potential Distribution of Crimean Juniper,” *Kastamonu University Journal of Forestry Faculty*, vol. 20, no. 2, pp. 133–142, 2020.
- [47] H. Su, M. Bista, M. Li, “Mapping Habitat Suitability for Asiatic Black Bear and Red Panda in Makalu Barun National Park of Nepal from Maxent and GARP Models,” *Scientific Reports*, vol. 11, no. 1, 14135, 2021.
- [48] A. M. Khan, Q. Li, Z. Saqib, N. Khan, T. Habib, N. Khalid, M. Majeed, A. Tariq, “MaxEnt Modelling and Impact of Climate Change on Habitat Suitability Variations of Economically Important Chilgoza Pine (*Pinus gerardiana* Wall.) in South Asia,” *Forests*, vol. 13, no. 5, 715, pp. 1-23, 2022.
- [49] K., İpekdal, D. Beton, “Model Predicts a Future Pine Processionary Moth Risk in Artvin and Adjacent Regions,” *Artvin Çoruh Üniversitesi Orman Fakültesi Dergisi*, vol. 15, no. 2, pp. 85-95, 2014.
- [50] G. Zhao, X. Cui, J. Sun, T. Li, Q. I. Wang, X. Ye, B. Fan, “Analysis of the Distribution Pattern of Chinese *Ziziphus Jujuba* Under Climate Change Based on Optimized Biomod2 and MaxEnt Models,” *Ecological Indicators*, vol. 132, 108256, pp. 1-11, 2021.
- [51] A. Qin, B. Liu, Q. Guo, R. W. Bussmann, F. Ma, Z. Jian, G. Xu, S. Pei, “Maxent Modeling for Predicting Impacts of Climate Change on the Potential Distribution of *Thuja sutchuenensis* Franch., an Extremely Endangered Conifer from Southwestern China,” *Global Ecology and Conservation*, vol., 10, pp. 139-146, 2017.
- [52] M. Bobrowski, L. Gerlitz, U. Schickhoff, “Modelling the Potential Distribution of *Betula utilis* in the Himalaya”, *Global Ecology and Conservation*, vol. 11, pp. 69–83.
- [53] M. Bobrowski, U. Schickhoff “Why Input Matters: Selection of Climate Data Sets for Modelling the Potential Distribution of a Treeline Species in the Himalayan Region”, *Ecological Modelling*, 359, pp. 92–102, 2017.
- [54] C. A. Drew, A. H. Perera, “Expert Knowledge as a Basis for Landscape Ecological Predictive Models”, *Predictive species and habitat modeling in landscape ecology: Concepts and applications*, Drew C. A., Wiersma Y. F., & Huettmann F., New York, NY: Springer.
- [55] A. Akyol, Ö. K. Örucü, E. S. Arslan, A. G. Sarıkaya, “Predicting of the Current and Future Geographical Distribution of *Laurus nobilis* L. Under the Effects of Climate Change,” *Environmental Monitoring and Assessment*, vol. 195, no. 4, 459, pp. 1-18, 2023.
- [56] H. Mirhashemi, M. Heydari, K. Ahmadi, O. Karami, A. Kavgaci, T. Matsui, B. Heung, “Species distribution models of Brant's oak (*Quercus brantii* Lindl.): The impact of spatial database on predicting the impacts of climate change”, *Ecological Engineering*, 194, pp. 107038, 2023.
- [57] R. Piwowarczyk, M. Kolanowska, “Predicting the Effect of Global Warming on the Distribution of a Polyphagous Tree Parasite, *Orobanche laxissima*, Based on Climatic and Ecological Data”, *Global Ecology and Conservation*, vol. 44, pp. e02486, 2023.
- [58] M. Lindner, J. B. Fitzgerald, N. E. Zimmermann, C. Reyer, S. Delzon, E. van der Maaten, M. Schelhaas, P. Lasch, J. Eggers, M. Maaten-Theunissen, F. Suckow, A. Psomas, B. Poulter, M. Hanewinkel, “Climate Change and European Forests: What Do We Know, What Are the Uncertainties, and What Are the Implications for Forest Management?”.

Journal of Environmental Management,
vol. 146, pp. 69–83, 2014.

- [59] S. Ayan, E. Bugday, T. Varol, H. B. Özel, E. A. Thurm, “Effect of Climate Change on Potential Distribution of Oriental Beech (*Fagus orientalis* Lipsky.) in the Twenty-First Century in Türkiye,”. Theoretical and Applied Climatology, vol. 148, no.1-2, pp.165-177, 2022.
- [60] U. Canturk, Ş. Kulaç, “The Effects of Climate Change Scenarios on *Tilia* ssp. in Türkiye,” Environmental Monitoring and Assessment, vol. 193, no. 12, 771, pp. 1-11, 2021.
- [61] A. A. Babalik, O. Sarikaya, O. K. Orucu, “The Current and Future Compliance Areas of Kermes Oak (*Quercus coccifera* L.) Under Climate Change in Türkiye,” Fresenius Environmental Bulletin, vol. 30, no. 01, pp. 406-413, 2021.
- [62] D. E. Koç, “Modeling of The Potential Distribution of *Laurus nobilis* in Anatolia from the Last Glacial Maximum to the Future,” International Conference on Agricultural, Biological and Life Science (AGBIOL 2022), pp. 248, Türkiye, 2022.
- [63] S. Ayan, E. Bugday, T. Varol, T., H.H. Özel, E.A. Thurm, Effect of climate change on potential distribution of oriental beech (*Fagus orientalis* Lipsky.) in the twenty-first century in Türkiye,” Theoretical and Applied Climatology, pp. 1-13, 2022.
- [64] A. U. Özcan, K. Çiçek, “How long do We Think Humans Have Been Planting Forests? A Case Study with *Cedrus libani* A. Rich,”. New Forests, vol. 54, no.1, pp. 49-65. 2023.

Forensic comparison of Soil Samples in Ömerli Dam Region by FTIR and ICP-OES

Soner Kızıl^{1,2*} , İkra Sedef Boler¹ , Sevil Atasoy^{1,2} 

¹ Uskudar University, Faculty of Engineering and Natural Sciences, Department of Forensic Science, İstanbul, Türkiye
soner.kizil@uskudar.edu.tr , ikrasedef.boler@st.uskudar.edu.tr , atasoy@uskudar.edu.tr

² Uskudar University, Institute of Addiction and Forensic Sciences, İstanbul, Türkiye

*Corresponding Author

ARTICLE INFO

ABSTRACT

Keywords:
Forensic soil
ICP-OES
Soil texture
FTIR
Crime scene

Article History:

Received: 15.03.2024

Accepted: 09.07.2024

Online Available: 01.08.2024

Soil is a one of the important physical evidence that could be encountered in any objects including car tire, shoes, or clothes. This study presents the comparison of the soils in Ömerli Dam, İstanbul-Türkiye. 35 of soil samples from 7 different regions have been collected around the lake. FTIR and ICP-OES have been utilized for structural analysis and detection of metal content in soil samples. Moreover, textural analysis, pH, sedimentation, color tests have been systematically investigated. The image of soil samples is also captured under different light of sources by VSC 8000. The outcome shows that discrimination of soil samples could be studied using various techniques including FTIR, textural analysis, metal concentrations and their color. ICP-OES analysis showed that the soil have various elements such as Si, Fe, Mg, Ca, Cu with a different amounts which provide discrimination for soil samples. The natural pH of the samples varied between 6.1 and 8.3 that are from slightly acidic to moderately alkaline character.

1. Introduction

Soil is a complex mixture that containing organic, inorganic and biological components in itself [1]. The characteristic feature of soils is generally affected by the natural events as a result of earth crust movement, rains, climate conditions and human made effect including industrialization, population growth, agriculture and livestock activities and so on [2]. Pedology which came from Greek words pedon- as soil and -logos as study refers to formation, classification, mapping and characterization of soil samples [3]. Due to the variance of samples as a result of natural and artificial dissimilarities, soil is considered as important evidence which can be transferred one environment to another when two surfaces come into physical contact [4].

Soil can be in the form of dust and mud on the clothes of individuals, as well as on different surfaces such as the soles of shoes, burial sites,

cars and tires. Therefore, it is encountered on crime scene which provide investigators to valuable evidence [5]. Detection of soil character could be the key information about spatial location and suspect's activities [6]. The first exploit of soil samples as forensic evidence is carried out by Georg Popp in 1904 who used soil on suspect's shoe to support the theory of the crime in the murder of Margarethe Filber [7].

Organic, inorganic and biological changes in the soil provide distinctive information about agricultural activities, population density and industrialization, poor management or inefficient disposal of waste in the region [6].

For instance, some synthetic chemicals such as pesticides could be found in the regions in which agricultural activities are carried out [8]. The percentage of dyes, polyaromatic hydrocarbons (PAHs) and heavy metals could be detected in industrial dense areas [9]. In addition, as a result

of natural processes such as the formation of the world, etc., regional differences may occur in the soil [10]. The oil accidents, asbestos from destroyed old buildings, gold mining operations, volcanic eruptions, agricultural irrigation, sewage systems are some significative natural and artificial parameters in terms of discriminative characteristics of soil samples [11]. Stern et al. examined the soil profiles of United States which have been collected over 20.000 fractions from 7534 sites [12].

It was demonstrated that soil mineral rarity could be important evidence in order to discriminate the soil samples from a region. Testoni et al. have collected various soil samples from different sites to develop and test a Standard Operating Procedure (SOP) for forensic soil sampling [13]. It was found that most of the samples were correctly grouped according to their location by using chemical characterization methods. Dong et al. have discriminated the soil samples according to their color by handheld spectrophotometer [14]. 0.02-0.04 g of fine soil samples was found to be enough for the accurate color determination by instrumental colorimetric equipment.

Discrimination of soils offers many benefits in forensic investigation because it can transfer from many materials, easy to storage, durable, may vary regional differences [15]. Forensic soil specimens could be discriminated according to their mineralogy, textural features, grain size, color, chemical composition, organic matter and so on [16, 17]. Therefore, it is very crucial to determine their divergent features using different characterization techniques. Distinctive features of soil as forensic evidence could be carried out by different methods in terms of color, pH of soil, the chemical and biological compositions, density, particle size [18]. The characterization of the soil evidence can be carried out by X-ray diffraction (XRD), Fourier Transform Infrared Spectroscopy (FTIR), Thermal gravimetric analysis (TGA), Scanning electron microscope (SEM), Transmission electron microscope (TEM), Inductively Coupled Plasma Optical Emission Spectroscopy (ICP-OES), Inductively Coupled Plasma Mass Spectroscopy (ICP-MS), Atomic Absorption Spectroscopy (AAS) [19].

For instance, decayed human remains can change the chemical structure of the soil by the emergence of various chemicals such as indole, carbon dioxide, hydrogen sulfide, ammonia. The determination of this change in the soil is of critical importance in terms of forensic events [20]. Focant et al. investigated the chemical changes in soil samples containing cadavers using two-dimensional gas chromatography time-of-flight mass spectrometry (GC/GC-TOF-MS). They have found that more than 20 specific compounds such as nitrile, ether, ketone, alcohol, aldehyde have been detected at different depths of the soil in the burial area [21].

In 2021, Chauhan et al. have used UV-Vis-NIR spectroscopy to discriminate the soil specimens which is collected from India. They have found the presence of some organic minerals in varying amounts [22]. Pirrie et al. have tested recovering soil trace evidence by using SEM-EDS techniques [23]. The study, published in 2020 by Sangwan et al., conducted many analyzes on soil. In this study, ATR-FTIR, pyGC-MS, SEM-EDX, ICP-MS/OES and XRD analyzes were also performed on the prepared soil samples, apart from physical analyzes such as determining the color, particle size and density of soil solutions [18]. Another study published by Marumo in 2003 revealed similar results and additionally the organic structure and mineral content of the soil were determined. In addition to these results, macroscopic and microscopic imaging of the soil content was also performed [24].

In another study published in 2014, in which soil was considered as trace evidence, ATR-FTIR spectroscopy was used to determine the organic and inorganic compounds of the soil. Soil samples, which were thoroughly crushed and homogenized, were separated according to their color using the Munsell chart, apart from spectroscopic methods [25, 26]. Dawson and Hillier's study in 2010 covered more than 70 soil samples, making it one of the publications that generated the largest sample group. In the study, besides the Energy dispersive spectroscopy (EDS) images, SEM images were also taken, and the inorganic compounds of the soil samples were determined. The structure of soil samples was tried to be fully elucidated by applying X-ray fluorescence (XRF), atomic absorption

spectroscopy (AAS), inductively coupled plasma (ICP) spectrometry, neutron activation analysis (NAA) and energy and wavelength dispersive X-ray (EDX and WDX) microanalysis [20]. The relevant section of the book, published by Fitzpatrick et al. in 2009, on soil investigations for forensic purposes, includes detailed physical analyses. SEM, XRF, ICP-MS, DSC, NMR analyzes were performed, especially IR spectroscopy and XRD analyzes, on soil samples separated according to particle size. The pH values of the soil samples strengthened with examples from real events were one of the first factors to be evaluated before all these analyzes [27].

The study which conducted in 1999 by Turner and Wiltshire examined changes in the soil after pig samples were buried in the ground for five months [28]. In this publication, the effect of soil acidity on the buried material after burial in an acidic pH area was evaluated. Although a limited region was chosen as the region, the study showing the change experienced by organic materials due to waiting in the soil has similar features to our current study.

Among these techniques; FTIR come to forefront to discriminate the distinguishing feature of unknown materials because it offers multiple advantage such as rapid, easy to use, portable, do not require further any pretreatment, suitable for different specimens including solid, liquid, paste, powders, films and even gases [29]. Xu et al. Investigated the soil samples from different regions of China by laser-induced breakdown spectroscopy (LIBS) and Fourier transform infrared total attenuated reflectance spectroscopy (FTIR-ATR). They have concluded that obtained soil samples can be easily separated according to their characteristic's differences including elemental, mineral and organic matter compositions via LIBS and FTIR-ATR [17].

This paper aims to characterize and discriminate the physical, chemical characteristics of different soil samples in which they are collected from Ömerli Dam which is one of the most important drinking water sources in the north-east of Istanbul.

The color of soil samples is determined according to the Munsell soil color chart. The structural analysis of soil samples is achieved by Fourier transform infrared spectroscopy (FTIR). The soils also classified according to the pH value of the soil suspensions and ranges between 6.1-8.3 for all regions. VSC 8000 are used to visualization of soil specimens under different light of sources.

Some heavy metals such as are studied by inductively coupled plasma optical emission spectrometry (ICP-EOS). The outlines show that FTIR is effective method to find out distinctive features in terms of forensic investigations. Moreover, the sedimentation character and textural analysis demonstrated that soil samples could be easily separated from each other which make it effective, cheap, and quick options for real crime scene.

Thanks to this study, a region that one of the important part of water source in Istanbul have been systematically explored by using FTIR, soil color test, textural analysis, ph and elemental analysis to discriminate the soil character in Ömerli Dam which provide significant data in crime scene investigation.

2. Material and Methods

2.1. Study area

Ömerli Dam is located in the north-east (approximately 30 km) of Istanbul and provides about 43% drinking water requirements of İstanbul which is engaged between 1968 and 1972. The map of region and places where the samples were taken are demonstrated in Figure 1. Google maps have been used to provide a location where soil samples were collected. All soil samples are taken on 5 November 2023. Before sampling, 1*1 m² of sampling area is determined. Then, four corner and one center of sampling area is excavated.

The coordinates of the collected soil samples was found to be 41°00'47.6"N 29°17'34.8"E, 40°57'59.8"N 29°20'56.3"E, 41°01'10.1"N 29°21'55.0"E, 41°01'24.4"N 29°22'39.1"E, 41°00'37.8"N 29°24'51.5"E, 41°03'49.8"N

29°21'30.9"E, and 41°04'29.0"N 29°23'20.8"E for S1, S2, S3, S4, S5, S6 and S7, respectively



Figure 1. The map of A) Marmara region, Türkiye B) Ömerli Dam in Istanbul

2.2. Sampling

A total of 35 soil samples from 7 region were collected from Ömerli Dam in autumn Figure 2. The samples are collected from 1 meter from the shore at a depth of 20 cm. 5 samples are collected within 1 square meter area (4 corner and 1 center) to get a homogeneous sampling. The collected samples were oven dried for 48 h at 100 °C then large structural such as rocks, leaves, twigs are gently separated from the soil samples. Then, the soil samples are gently grounded and filtered using <50 micron mesh sieve and then stored in a desiccator.

2.3. Color

The color of soil samples is detected according to the Munsell color system. Soil samples are wetted by spraying of water in order to be moist. White copy paper (A4 paper) was used as background for accurate reading of soil samples. To make a reliable color comparison, some parameter should be taken into consideration including soil comparison should be done under sunlight without using any sunglasses, a white ground should be used, and the soil should be

moist. For comparison of color, center of soil samples have been examined.



Figure 1. The images of Ömerli Dam region from different perspective

2.4. Textural analysis

Soil textures provides an information to proportion of sand, clay and silt particles. Different textures could be important evidence for the determination of the samples. For this, textural analysis of soil samples as forensic evidence has been investigated. The jar test method has been applied to S1, S6 and S7 samples for determining of silt, sand and rock compositions of samples. Briefly, a known amount of specimen has been added to the jar and water is added up to half of jar. 3 g of dishwashing detergent is added to the jar and the mixture was then vortex for 1 min. The sand, clay and silt compositions have been determined according to the textural triangle [30, 31].

2.5. Gravitational sedimentation of soil

Soil samples consist of sand, clay, silt, organic matter and so on. Depending on the composition, the soil textures can vary [12]. The sedimentation methods give an information on the analysis of gravitational settling of particles in a fluid. To compare the particle size distribution of soil samples, 5% of soil in water (g/mL) is prepared. the suspension first shaken and vortex for 1 min. After that, the suspensions was left tube holder to be rest of suspensions and allowed to sediment

against time. The images are captured at different time of intervals (from 1 min to 24 h) in order to observe the color of suspensions.

2.6. Instrumentation

The color of soil samples is classified according to the Munsell soil color chart. The color comparison was held on 19 December 2023 in the middle of the day, in clear weather and natural sunlight. The concentrations of selected elements were determined using Inductively coupled plasma atomic emission spectroscopy (ICP-OES, Thermo Fisher Scientific, Bremen, Germany).

An Attenuated Total Reflection (ATR)-Fourier Transform Infrared Spectroscopy (FTIR) was used to analyze structural characterization of soil specimens. Instrument settings used were 128 scans; 16 cm^{-1} resolution; range 4000-650 cm^{-1} . FTIR results is the average of 5 soil specimens. After analysis, the crystal was cleaned with ethanol. Video spectral comparator (VSC) 8000 have been used as light source which provide soil images in the different light sources including visible light, ultraviolet light and spot (fluorescence).

Inductively Coupled Plasma Optical Emission spectroscopy (ICP-OES) was used for quantifying of metals in soils. For preparation, a known amount (approximately 0.2 g) of soil sample which is used center of the soil samples is placed in vessel. Then, 8 mL of HNO_3 and 2 mL of HCl is added. The samples are microwaved for digestion (temperature program: heat to 200 °C in 15 min and hold to 200 °C for 15 min and cold to room temperature in 15 min). After digestion, samples in vessels are diluted to 50 mL by using ultrapure water.

3. Result and Discussion

3.1. The color of soil samples

The utilization of Munsell color investigation give a valuable information which enable visual comparison and discrimination of soil samples by investigators [32]. However, some parameters including moisture percentage of soils, lighting, ground color should be considered in order to get

a comparable result. For this, a white A4 paper is used for background and the soils are wetted by spraying to get moist samples. According to the Munsell color system, the color of soil samples is found to be 7.5 YR 4/4 (brown) for S1, 5 YR 4/4 (reddish brown) for S2, 7.5 YR 4/6 (strong brown) for S3, 10 YR 4/6 (red) for S4, 2.5 YR 3/4 (dark reddish brown) for S5, 7.5 YR 4/4 (brown) for S6, 5 YR 4/3 (reddish brown) for S7 Table 1.

Table 1. The color characteristics of soil samples

Sample	Color	Color name
S1	7.5YR 4/4	Brown
S2	5YR 4/4	Reddish brown
S3	7.5YR 4/6	Strong brown
S4	10YR 4/6	Red
S5	2.5YR 3/4	Dark reddish brown
S6	7.5YR 4/4	Brown
S7	5YR 4/3	Reddish brown

3.2. Soil images

Video Spectral Comparator 8000 (VSC-8000) was used to visualize the soil samples under different of light sources including visible light, ultraviolet, spot (fluorescence). Soil samples could be discriminated under visible light which confirms the Munsell color test, however, there was no difference under other light sources, even some organic particles could be seen under spot (fluorescence) which shines under fluorescence. The images of soil samples are shown in Figure 3.

3.3. FTIR

A total of 35 samples from 7 different region in the Ömerli Dam were analyzed by FTIR. Sieved and dried samples were used for FTIR analysis. In order to get homogeneity and repeatability, five different spectra are collected and compared which is given in Figure 4. The FTIR spectra of 7 different regions in the Ömerli Dam was demonstrated in Figure 1. According to the spectra, the peaks between 3700-3620 cm^{-1} represent the presence of kaolin mineral which can be especially seen S1-S5 samples. The bands at 1645 shows the C=O stretching of amides, and nitrate at 1380 cm^{-1} . The peaks between 3000-2800 cm^{-1} shows the aliphatic methyl and methylene groups [33].

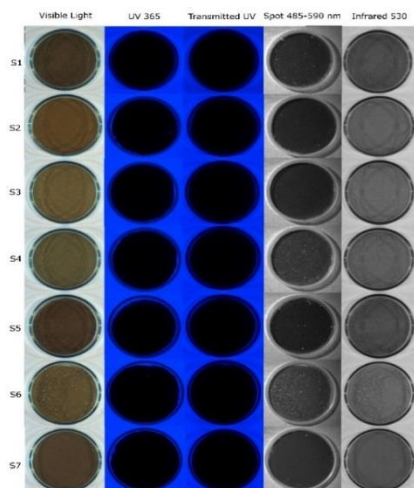


Figure 3. Soil samples under different light of sources

3.4. Textural analysis

A soil textural triangle is used to compare of soils according to their particle size compositions including silt, sand and clay. The relative percentages of components determine the soil texture. For this, some soil specimens are characterized by jar test to provide information about the soil texture. To do this, dried soil samples is placed to jar, and water is added up to half of the jar. Then, dish soap is added. The sediments are shaken and vortex for 1 min and allowed to be settled for 24 h. The bottom (first) phase shows the amount of the sand in the soil. Second phase demonstrated the presence of silt, and the third phase shows the clay composition. The organic matter on the top of water is not taken into account for the determination of soil texture.

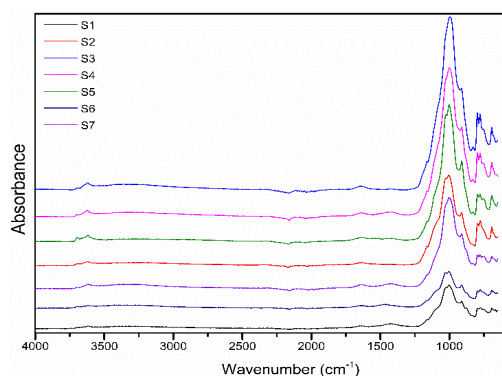


Figure 4. The FTIR spectra of soil samples

The sum of sand, silt and clay give the total amount of soil which assumed to be a 100. After then, Soil texture was determined by intersecting

the calculated percentages on the soil content scale. According to the textural analysis S1 samples were found to be sandy clay loam, S6 were found to be loamy sand and S7 were found to be sandy loam which is given in Figure 5. The outcomes show that sedimentation test could be applied for discrimination of soil samples which gives information about the silt, sand and clay composition in the unknown soil samples.

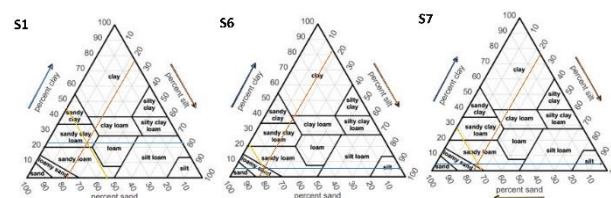


Figure 5. Textural analysis of soil samples

3.5. Sedimentation test

Sedimentation test is studied in order to investigate the stability and sedimentation behavior of soil sample in water [34]. For this, 5% of soil suspensions are prepared in falcon tube. Then, the suspension is shaken and vortex for 2 min. Then, all falcon tubes are allowed to rest, and images are taken at different time of intervals from 1 min to 24 h Figure 6. the color of all suspensions can vary which confirms the Munsell color results. At the end of 1 min, there was no obvious sediment at the bottom for all texture. To do this, dried soil samples is placed to jar, and water is added up to half of the jar. Then, dish soap is added. The sediments are shaken and vortex for 1 min and allowed to be settled for 24 h. The bottom (first) phase shows the amount of the sand in the soil.

Second phase demonstrated the presence of silt, and the third phase shows the clay composition. The organic matter on the top of water is not taken into account for the determination of soil texture. The sum of sand, silt and clay give the total amount of soil which assumed to be a 100. After then, Soil texture was determined by intersecting the calculated percentages on the soil content scale. According to the textural analysis S1 samples were found to be sandy clay loam, S6 were found to be loamy sand and S7 were found to be sandy loam which is given in Figure 5. The outcomes show that sedimentation test could be applied for discrimination of soil samples which

gives information about the silt, sand and clay composition in the unknown soil samples.

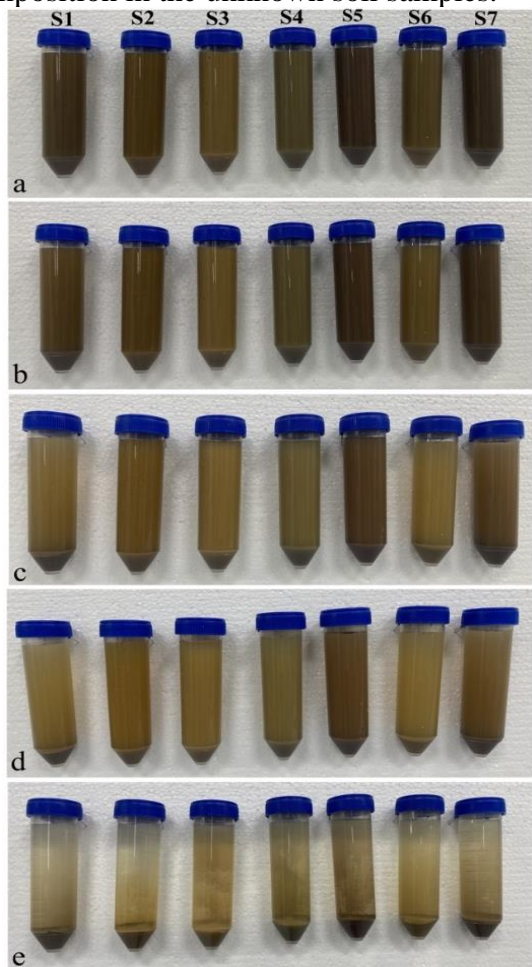


Figure 6. Sedimentation of soil suspensions against to time a) t:0 b) t:1 min c) t: 30 min d) t:1h e) t:24h

pH measurement of soil samples as a discriminant technique also gives a valuable information about the evidence and crime scene. For this, the pH value of soil samples from different region of Ömerli Dam is determined. It was found that the pH value of soil samples was ranged between 6.1 and 8.3. The pH value and description of the soil samples is given in Table 2. According to the results, S3 and S5 was found to be Neutral, while S1, S6, S7 is Moderately alkaline, and S2 is slightly acid. The difference in pH value could be discriminant character for forensic applications Table 2.

Table 2. pH of soil samples in Ömerli Dam region

Sample	pH	Description
S1	8.2	Moderately Alkaline
S2	6.1	Slightly Acid
S3	6.8	Neutral
S4	8.1	Moderately Alkaline
S5	6.6	Neutral
S6	8.3	Moderately Alkaline
S7	8.3	Moderately Alkaline

3.6. ICP-OES

The quantification of metal contents in the soil sample could be potential evidence for comparison of soils. The metal concentration of soil samples was shown in Table 3.

Table 3. Metal concentrations of soil samples by ICP-OES

	ppm				
	Si	Fe	Mg	Ca	Cu
S1	<1	139	39.5	265	0.5
S2	<1	229	33.4	22	0.35
S3	<1	268	79.9	30.8	0.60
S4	<1	265	80.2	548.5	0.97
S5	<1	161	22.5	41.4	0.21
S6	<1	94.9	7.5	240.7	0.20
S7	<1	166	62.0	273.2	0.36

The Fe content of soils was found to be 139 ppm for S1, 229 ppm for S2, 268 ppm for S3, 265 ppm for S4, 161 ppm for S5, 94.86 ppm for S6 and 166 ppm for S7. The Fe content was found to be between 94.86 and 268 ppm.

4. Conclusion

It is crucial that identifying the source of the evidence is gaining importance for crime scene investigation. In this study, the comparison of soils in Ömerli Dam which is one of the most important drinking water sources in the north-east of Istanbul have been explored. For this, various techniques including color test, structural analysis, pH, textural and metal analysis have been studied. The coordinates of studied area is detected by Google maps. The metal content including Si, Fe, Mg, Ca and Cu have been investigated which contains at different ratios.

35 of samples from 7 different regions for analyzed. The natural pH of the soils was varied from 6.1 to 8.3. The color comparison of soil samples is studied by Munsell color chart. The image analysis showed similarities and could not be discriminated from each other. Textural analysis of soil samples demonstrated that it could be effective, easy, and cheap method for studying of soil samples as forensic evidence. Moreover, the sedimentation studies could also be applied and show dissimilarity due to their sand, silt and clay composition which also influence the textural properties.

The outcomes showed that FTIR is inadequate by itself for discrimination of soil samples in Ömerli Dam region. pH of soil samples could give an crucial data for comparison of samples. Moreover, textural analysis and heavy metal analysis have discriminant results in order to compare the soil samples. VSC analysis is also not sufficient for comparing of soil samples. As a result, it is important for forensic sciences to use a combination of different methods to determine the source of the soil.

Article Information Form

Funding

We thank the Scientific and Technological Research Council of Turkey-TUBITAK for the support of this work through Grant **1919B012307270** (2209-A University Students Domestic Research Projects Support Program).

Authors' Contribution

S.K: writing, original draft, methodology, investigation, visualization, conceptualization, supervision, project administration, review, funding and editing I.S.B: writing, original draft, methodology, investigation, visualization, conceptualization, Project administration is added and funding S.A: writing, methodology, conceptualization, review and editing.

The Declaration of Conflict of Interest/ Common Interest

No conflict of interest or common interest has been declared by the authors.

The Declaration of Ethics Committee Approval

This study does not require ethics committee permission or any special permission.

The Declaration of Research and Publication Ethics

The authors of the paper declare that they comply with the scientific, ethical and quotation rules of SAUJS in all processes of the paper and that they do not make any falsification on the data collected. In addition, they declare that Sakarya University Journal of Science and its editorial board have no responsibility for any ethical violations that may be encountered, and that this study has not been evaluated in any academic publication environment other than Sakarya University Journal of Science.

Copyright Statement

Authors own the copyright of their work published in the journal and their work is published under the CC BY-NC 4.0 license.




References

- [1] S. C. A. Uitdehaag, T. H. Donders, I. Kuiper, F. Wagner-Cremer, M. J. Sjerps, "Use of Bayesian networks in forensic soil casework," *Science Justice*, vol. 62, no. 2, pp. 229–238, 2022.
- [2] N. A. N. B. Mohd Rosdi, N. Abd Hamid, S. F. Mohd Ali, H. Sino, L. C. Lee, "A Critical Review of Soil Sampling and Data Analysis Strategies for Source Tracing of Soil in Forensic Investigations," *Critical Reviews in Analytical Chemistry*, pp. 1–39, 2023.
- [3] A. Ruffell, "Forensic pedology, forensic geology, forensic geoscience, geoforensics and soil forensics," *Forensic Science International*, vol. 202, no. 1–3, pp. 9–12, 2010.
- [4] L. A. Dawson, R. W. Mayes, "Criminal and environmental soil forensics: soil as physical evidence in forensic investigations," *Forensic Sciences*, vol. 2 no.5 pp. 457–486, 2022.

- [5] L. C. Lee, A. A. Ishak, A. A. Nai Eyan, A. F. Zakaria, N. S. Kharudin, N. A. M. Noor, "Forensic profiling of non-volatile organic compounds in soil using ultra-performance liquid chromatography: a pilot study," *Forensic Science Research*, vol. 7, no. 4, pp. 761–773, 2022.
- [6] D. O. Carter, D. Yellowlees, M. Tibbett, "Moisture can be the dominant environmental parameter governing cadaver decomposition in soil," *Forensic Science International*, vol. 200, no. 1–3, pp. 60–66, 2010.
- [7] R. C. Murray, J. C. F. Tedwou, "Soil in trace evidence analysis," 13th Interpol Forensic Science Symposium, Lyon, France, 2001, pp. 75–78.
- [8] E.-J. Won, H.-Y. Yun, D.-H. Lee, K.-H. Shin, "Application of compound-specific isotope analysis in environmental forensic and strategic management avenue for pesticide residues," *Molecules*, vol. 26, no. 15, p. 4412, 2021.
- [9] A. Cachada, T. Rocha-Santos, A. C. Duarte, "Soil and pollution: an introduction to the main issues," in *Soil pollution*, Elsevier, 2018, pp. 1–28. Accessed: Jul. 01, 2024.
- [10] J. Rodrigo-Comino, J. M. Senciales, A. Cerdà, E. C. Brevik, "The multidisciplinary origin of soil geography: A review," *Earth-Science Reviews*, vol. 177, pp. 114–123, 2018.
- [11] A. Zwolak, M. Sarzyńska, E. Szyrka, K. Stawarczyk, "Sources of Soil Pollution by Heavy Metals and Their Accumulation in Vegetables: a Review," *Water, Air, Soil Pollution*, vol. 230, no. 7, p. 164, 2019.
- [12] L. A. Stern, J. B. Webb, J. Ingham, S. Monteith, I. Saginor, "Soil survey laboratory grain count data to substantiate the rarity of mineral grains in forensic soil reports of examination," *Journal of Forensic Sciences*, vol. 66, no. 6, pp. 2413–2423, 2021.
- [13] S. A. Testoni, V. F. Melo, L. A. Dawson, F. A. S. Salvador, P. A. Kunii, "Validation of a standard operating procedure (SOP) for forensic soils investigation in Brazil," *Revista Brasileira de Ciencia do Solo*, vol. 43, no.44, pp.1-30, 2019.
- [14] C. E. Dong, J. B. Webb, M. C. Bottrell, I. Saginor, B. D. Lee, L. A. Stern, "Strengths, limitations and recommendations for instrumental color measurement in forensic soil characterization," *Journal of Forensic Sciences*, vol. 65, no. 2, pp. 438–449, 2020.
- [15] M. A. S. Laidlaw, G. M. Filippelli, S. Brown, J. Paz-Ferreiro, S. M. Reichman, "Case studies and evidence-based approaches to addressing urban soil lead contamination," *Applied Geochemistry*, vol. 83, pp. 14–30, 2017.
- [16] U. Barman, R. D. Choudhury, "Soil texture classification using multi class support vector machine," *Agriculture*, vol. 7, no. 2, pp. 318–332, 2020.
- [17] X. Xu, C. Du, F. Ma, Y. Shen, J. Zhou, "Forensic soil analysis using laser-induced breakdown spectroscopy (LIBS) and Fourier transform infrared total attenuated reflectance spectroscopy (FTIR-ATR): Principles and case studies," *Forensic Science International*, vol. 310, p. 110-222, 2020.
- [18] P. Sangwan, T. Nain, K. Singal, N. Hooda, N. Sharma, "Soil as a tool of revelation in forensic science: a review," *Anal Methods*, vol. 12, no. 43, pp. 5150–5159, 2020.
- [19] B. G. Rawlins, S. J. Kemp, E. H. Hodgkinson, J. B. Riding, C. H. Vane, C. Poulton, K. Freeborough "Potential and pitfalls in establishing the provenance of earth-related samples in forensic investigations," *Journal of Forensic Sciences*, vol. 51, no. 4, pp. 832–845, 2006.
- [20] M. B. Alexander, T. K. Hodges, J. Bytheway, J. A. Aitkenhead-Peterson, "Application of soil in forensic science:

- residual odor and HRD dogs,” *Forensic Science International*, vol. 249, pp. 304–313, 2015.
- [21] C. Brasseur, J. Dekeirsschieter, E. M. J. Schotsmans, S. Koning, A. S. Wilson, E. Haubruge, J. F. Focant, “Comprehensive two-dimensional gas chromatography–time-of-flight mass spectrometry for the forensic study of cadaveric volatile organic compounds released in soil by buried decaying pig carcasses,” *Journal of Chromatography A*, vol. 1255, pp. 163–170, 2012.
- [22] R. Chauhan, R. Kumar, V. Kumar, K. Sharma, V. Sharma, “On the discrimination of soil samples by derivative diffuse reflectance UV–vis–NIR spectroscopy and chemometric methods,” *Forensic Science International*, vol. 319, p. 110–655, 2021.
- [23] D. Pirrie, “Testing the efficiency of soil recovery from clothing for analysis by SEM-EDS,” *Forensic Science International*, vol. 289, pp. 83–91, 2018.
- [24] Y. Marumo, “Forensic examination of soil evidence,” *Japanese Journal of Forensic Science* vol. 7, no. 2, pp. 95–111, 2003.
- [25] J. Sheffield, G. Goteti, F. Wen, E. F. Wood, “A simulated soil moisture based drought analysis for the United States,” *Journal of Geophysical Research: Atmospheres*, vol. 109, no. 24, p. 2004-5182, 2004.
- [26] Z. Fan, J. Herrick, J. Zee, “Measurement of Soil Color: A Comparison Between Smartphone Camera and the Munsell Color Charts,” *Soil Science Society America Journal*, vol. 81, no. 5, pp. 1139–1146, 2017.
- [27] R. W. Fitzpatrick, “Soil: forensic analysis,” *Wiley Encyclopedia Forensic of Science*, A. Moenssens, Forensic Consultant, USA, Wiley-Blackwell, 2009 pp. 1–14.
- [28] B. Turner, P. Wiltshire, “Experimental validation of forensic evidence: a study of the decomposition of buried pigs in a heavy clay soil,” *Forensic Science International*, vol. 101, no. 2, pp. 113–122, 1999.
- [29] Y. Tkachenko, P. Niedzielski, “FTIR as a method for qualitative assessment of solid samples in geochemical research: A review,” *Molecules*, vol. 27, no. 24, p. 88–109, 2022.
- [30] M. A. Shirazi, L. Boersma, “A Unifying Quantitative Analysis of Soil Texture,” *Soil Science Society America Journal*, vol. 48, no. 1, pp. 142–147, 1984.
- [31] P. A. Bull, A. Parker, R. M. Morgan, “The forensic analysis of soils and sediment taken from the cast of a footprint,” *Forensic Science International*, vol. 162, no. 1–3, pp. 6–12, 2006.
- [32] A. H. Munsell, *Munsell soil color charts*. New Windsor: Gretagmacbeth, 2000.
- [33] C. Peltre, E. G. Gregorich, S. Bruun, L. S. Jensen, J. Magid, “Repeated application of organic waste affects soil organic matter composition: evidence from thermal analysis, FTIR-PAS, amino sugars and lignin biomarkers,” *Soil Biology and Biochemistry*, vol. 104, pp. 117–127, 2017.
- [34] F. Gökmen, “Evaluation of the effect of tillage methods on soil quality,” Master’s Thesis, Institute of Science, 2011.

Investigation of Permeability of Thiocolchicoside Through Transdermal Drug Delivery System Using Franz Diffusion Cell

Hale Karagüzel^{1,2} , Sezen Sivrikaya Özak^{3*} , Aslıhan Dalmaz³ 

¹ Düzce University, Graduate Education Institute, Department of Chemistry, Düzce, Türkiye, halemanti@gmail.com

² Nobel Drug Pharmaceutical R&D Center (Nobel-İlac Ar-Ge Merkezi), Düzce, Türkiye

³ Düzce University, Faculty of Art and Science, Department of Chemistry, Düzce, Türkiye, sezensivrikaya@duzce.edu.tr, aslihandalmaz91@gmail.com

*Corresponding Author

ARTICLE INFO

ABSTRACT

Keywords:

Thiocolchicoside
Franz diffusion cell
Synthetic membranes
Transdermal drug
delivery system
HPLC

Article History:

Received: 21.03.2024

Accepted: 22.05.2024

Online Available: 01.08.2024

Recently, drug release applications through the skin have become very popular. One of the most remarkable of these drug release applications is transdermal drug release systems, which are drug release methods that allow the active substance to pass into the systemic circulation through the skin or artificial membranes. In this study, the optimization conditions required for the release and permeation tests of a gel drug containing the active substance thiocolchicoside were comparatively investigated using synthetic membranes without human or animal skin. For this purpose, the permeability of the gel drug in gel form and the active ingredient thiocolchicoside was carried out using Franz Diffusion Cell. As a result of the investigations, it was observed that the best synthetic membrane for the permeability of thiocolchicoside in the Franz Diffusion Cell was the Supor membrane. In addition, the method's relative standard deviation values, detection, and quantification limits were determined, and permeation studies were carried out. In this study, the correlation coefficient was found to be 0.9992, and the limits of detection and quantification were 0.026 and 0.078 µg/L. In this way, the sensitivity and reliability of the validation study were determined.

1. Introduction

Colchicoside is a glucoside found in the plant *Colchicum autumnale*. A semisynthetic sulfur derivative of colchicoside is called thiocolchicoside. Thiocolchicoside acts as a potent muscle relaxant by activating the GABA-nergic inhibitory pathways, which modify muscular contracture due to its particular affinity for -amino butyric acid (GABA) receptors (Figure 1). In clinical settings, the substance is used to treat neurological, rheumatic, muscular, and traumatic problems. In animal models, anti-inflammatory and analgesic effects have also been documented. Because of the hepatic first-pass effect and limited gastrointestinal absorption, the oral bioavailability of the medication is approximately 25%. Since its low

oral bioavailability limits its use, a different delivery method is preferred to achieve high blood concentrations for treatment management [1-8].

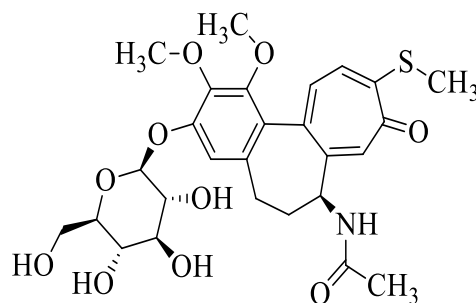


Figure 1. Chemical structure of thiocolchicoside

A transdermal drug delivery system (TDDS) is an effective system that provides controlled active drug delivery and is an alternative to

traditional drug delivery method treatments. TDDS ensures that the drug applied to the skin has a therapeutic effect and that the concentration of the active ingredient passes into the bloodstream systematically and is controlled. Essential advantages of TDDS: The aim is to reduce the side effects of the drug by avoiding the first pass effect in the liver, reducing the frequency of drug administration, and ensuring a constant and stable plasma level [9-13].

Thanks to these advantages, the development of TDDS has led to its approval by regulatory authorities for its increasing importance and commercialization in the pharmaceutical industry [14-18]. To observe and test the therapeutic efficacy of TDDS, *in vitro*, technical, and model systems that can measure drug release permeability and obtain reliable, reproducible, validated, and accurate predictive data are required [19-24]. In addition, the applicability of TDDS is made by *in vitro* tests on drugs in finished dosage form. The drug's performance can be tested with a permeation test study combined with an *in vitro-in vivo* [25-28].

Clinical trials for TDDS offer substantial chances to save time and money on development. Scale-up in drug production and extensive changes in the performance of approved products (e.g., changes in drug supplier, formulation and manufacturer, or raw materials. Comprehensive studies by companies should ensure reproducibility [29]. In the literature on *in vitro-in vivo* correlations (IVIVCs) for TDDS, the recommended drug by international guidelines formulation studies in topical and transdermal dosage forms are advised to measure release and penetration [30-37]. IVIVCs, Franz-type (static) diffusion cells with two compartments, are the most widely used technical (modifiable) diffusion cells. In the Franz Diffusion Cell test, a membrane that separates the donor and the receptor and can represent human skin is needed, and synthetic membrane studies are gaining importance for this purpose [30, 38, 39].

Synthetic membranes are frequently used in drug release and permeability studies on human or animal skin [31]. Synthetic membranes are the best topical *in vitro* model reported to date to predict skin status in Franz cells *in vivo*

penetration of products [40]. Regulatory authorities highly recommend them. However, the use of human skin and slaughtered animal skin is considered reasonable and is subject to national and international ethical guidelines [9, 41, 42]. Several studies have shown that pig ears can be used for testing because they have biochemical properties and structural similarities to human skin, and the ability to obtain results comparable to human skin has made them ideal for permeability studies [31, 43, 44].

Since biological skin is difficult to find and has different properties in each sample, an inexpensive and reproducible membrane model that mimics the skin barrier in terms of release and permeability is becoming very popular. In this study, the necessary optimization conditions for drug release and permeation tests were investigated by using synthetic membranes that do not contain human or animal skin. The effects of parameters such as membrane selection, membrane saturation, mixing time, mixing speed, and temperature on the permeability of the developed gel drug were investigated, and their similarity with the reference drug was proven. Fourier transform infrared spectroscopy and Differential scanning calorimetry analyses were performed to show the similarity between the developed gel drug and the reference drug.

2. Materials and Methods

2.1. Reagents and chemicals

All reagents used are of analytical purity. Potassium monobasic phosphate (KH_2PO_4), potassium chloride (KCl), sodium chloride (NaCl), disodium hydrogen phosphate (Na_2HPO_4), trifluoroacetic acid, high-performance liquid chromatography (HPLC) quality acetonitrile and methanol Merck quality 96% to 99.7%. It has varying degrees of purity. 0.45 mm polytetrafluoroethylene (PTFE) filters were used to filtrate the solutions (Millex Millipore, Istanbul, Türkiye). Ultrapure water was obtained using the Sartorius water purification (Sartorius Arium, USA). Thiocolchicoside standard (Batch No: M062300088) was purchased from INDIA GLYCOLS and used in working studies. The commercially available reference drug in gel

form containing the active ingredient thiocolchicoside was obtained from a pharmacy in Duzce (Türkiye). A drug in gel form with a new formulation was developed in the laboratory environment with the purchased thiocolchicoside standard. As a commercial membrane, PALL Supor 450 membrane disc filter 0.45 μ M 47 mm, plain (REF:60173), PALL HT-450 Tuffryn 100/PK Membrane Filter 0.45 μ M 47 m (Ref: T42575), Sartorius regenerated cellulose (RC) 0.45 μ M (Ref: 1122 18406 2201853) filters were used in Franz diffusion cell experiments.

2.2. Instruments

The study used Hanson Research MicroettePlus brand Franz cell 10-1522, serial number Franz Diffusion Cell, for in vitro permeation experiments. The quantification of thiocolchicoside in the samples obtained by permeation was validated with the WATERS 2487 Dual Absorbance Detector HPLC system.

2.3. Physico-chemical characterization

Fourier transform infrared (FT-IR) spectroscopy confirms the chemical characterization of two drugs developed in gel form and used as a reference, proving their similarity. The FT-IR analysis was performed using Agilent brand Digilab FTS-3500 model spectrophotometer equipped with an ATR to illuminate the structure in the wavelength spectrum range of 600-4000 cm^{-1} .

Differential scanning calorimetry (DSC) experiments were performed on two drugs developed in gel form and used as a reference. Calorimetric measurements were made using an Agilent brand DSC 200 F3 model differential scanning calorimeter. The samples were placed in tin pans and carried out in an N_2 atmosphere with a temperature increase of 10 $^\circ\text{C min}^{-1}$.

2.4. In vitro permeation method

The permeation of the active ingredient thiocolchicoside in the gel form of the commercially purchased and used reference drug through the Franz Diffusion Cell was compared with this developed drug. In vitro permeation studies were performed in a Franz Diffusion Cell

system with a receptor volume of 15 mL and a diffusion area of 1.77 cm^2 pH 7.4 media solution, representing the physiological region suitable for the receptor phase.

For permeability studies, three different membranes with different properties were kept in the media solution at pH 7.4, the most suitable pH for the skin, for 8 hours to saturate. Then, parameters affecting permeation, such as temperature, mixing speed, and sample amount, were changed, and the parameters that achieved the best efficiency were selected. All samples collected with the determined parameters were transferred to vials, and the amount of active ingredient was determined by the HPLC method and compared with the reference drug in the study. Permeation studies in each membrane and each parameter were performed in 3 repetitions. Thiocolchicoside permeation from a transdermal system using the Franz Diffusion Cell is shown in Figure 2.

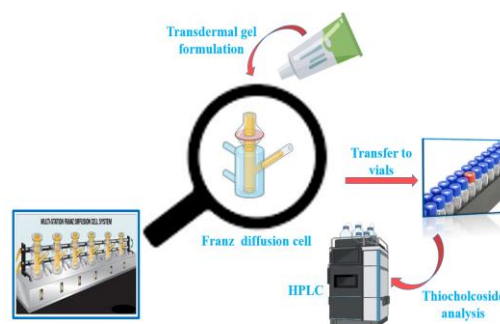


Figure 2. Thiocolchicoside permeation from a transdermal drug delivery system using the Franz Diffusion Cell

2.5. High-Performance Liquid Chromatography analysis

Waters 2487 model HPLC was used for the quantitative determination of thiocolchicoside. After filtering, standard thiocolchicoside solutions were analyzed at 280 nm with a Dual Absorbance Detector on an ACE5 C18 (4.6 mm; 150 mm; 5 μ m) column. HPLC analysis method conditions were performed at 25 $^\circ\text{C}$ temperature, 1.2 mL/min flow rate, and 50 μ L injection volume. The buffer solution contains pure water and trifluoroacetic acid. The mobile phase was prepared by adjusting acetonitrile and buffer solution in a ratio of 83:17, respectively. The dilution solution contains buffer solution and methanol in a 1:1 ratio.

3. Results and Discussion

3.1. FT-IR and DSC analysis

FT-IR spectroscopy is critical to determining the chemical interactions between thicolchicoside and excipients. The absorption bands seen in the FT-IR spectrum give us information about the functional groups present in the structure. FT-IR spectra of the reference and developed gel drug are shown in Figure 3. When the FT-IR spectrum was analyzed, all bands were present in the developed gel drug sample. In the spectrum, the fingerprint identification peaks of the functional groups that should be present in the structure of the gel drug are seen. These peaks can be observed in all characteristic interaction spectra. The characteristic fingerprint peaks at 1647 and 1525 cm^{-1} in the FT-IR spectrum correspond to C=O and amide groups in the tropane ring. In addition, the broadening band corresponding to the O-H stretching mode is observed between 3200 and 3600 cm^{-1} . Moreover, the peak at 2953 cm^{-1} indicates the presence of C-H groups in the structure.

DSC analysis provides information on endothermic/exothermic peaks, melting, release, and compatibility between thicolchicoside and the drug, thus providing rapid evidence. Figure 4 shows the DSC thermograms of the developed gel drug and the reference drug. The DSC thermograms show both the absence of a new peak and the presence of a characteristic endothermic peak. This peak indicates no incompatibility between the active ingredient thicolchicoside and the drug content. An endothermic peak with a maximum of 144.3 $^{\circ}\text{C}$ in the DSC thermograms is due to melting. When the analysis results are analyzed, it is seen that the thermograms of the developed gel drug and the reference drug are compatible [45-47].

3.2. HPLC method validation

This study developed an analytical method for in vitro permeation studies of a commercial reference drug and a gel containing the active ingredient thicolchicoside. The validation parameters of the developed method are given in Table 1. Linearity, precision, accuracy, limit of detection (LOD), and limit of quantification

(LOQ) parameters for the chromatographic method were validated. The results of the analysis will be determined by taking into account the ICH validation of analytical procedures: text and methodology Q2(R1) criteria [48-50]. For the linearity study, samples were prepared at six levels of thicolchicoside concentration ranging from 0.078 to 40.0 $\mu\text{g/mL}$. They were evaluated by linear regression analysis in line with the obtained areas. The regression equation and correlation coefficient are $y=56699572.93x+4514.39$ and 0.9992, respectively.

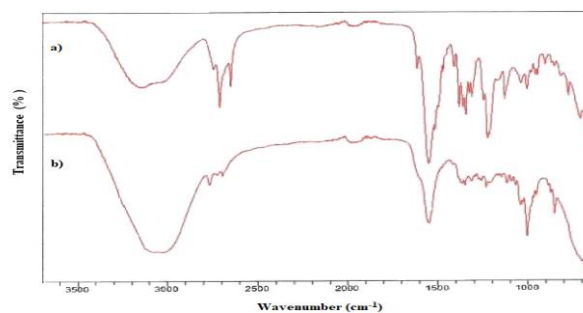


Figure 3. FT-IR spectra of a) reference drug and b) developed drug sample

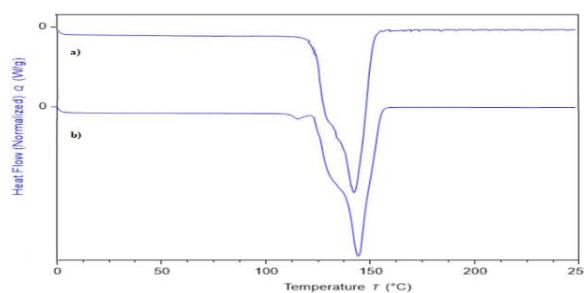


Figure 4. DSC thermograms of a) reference drug and b) developed drug sample

For the precision of this analytical method, the relative standard deviation (%RSD) value between the results of 5 different sample solutions prepared at the same concentration was determined to be less than 3%. To prove the accuracy of the analytical method, the % recovery values of the sample solutions prepared at four different concentrations in the linear region were calculated. The concentration of the value determined as 100% in accuracy and recovery studies is 26 $\mu\text{g/mL}$. Other concentration values were determined by proportioning the percentages of this value. The data obtained from 100%-102% proves the method's accuracy. Signal/noise (S/N) was used to determine LOD and LOQ values. The

signal/noise ratio determines it by comparing the result of the thiocolchicoside containing the lowest concentration of analyte with the result of the blank solution. S/N refers to 3 times the LOD

and ten times the LOQ of the noise. LOD and LOQ values were calculated as 0.026 $\mu\text{g/mL}$ and 0.078 $\mu\text{g/mL}$.

Table 1. Validation parameters of the developed method

Validation parameters	Level	Results	Level	Results	
Accuracy	50%	101.2 \pm 0.3%	Recovery	30%	98.9 \pm 0.3%
	80%	101.8 \pm 0.5%		80%	99.9 \pm 0.1%
	100%	101.1 \pm 0.9%		100%	100.1 \pm 0.1%
	120%	100.4 \pm 0.6%		120%	100.2 \pm 0.2%
	150%	100.2 \pm 0.5%		Repeatability	100%

3.3. Effect of membranes on Thiocolchicoside permeation

Three different membranes with different properties specified in “Section 2.1. Reagents and chemicals” were used. It was determined how similar results were obtained with the reference drug by using a pH 7.4 media solution, 600 rpm mixing speed, 32.0 °C temperature, and 400 mg thiocolchicoside as optimum parameters in the in vitro permeability of these membranes. When Figure 5 is examined, when the permeability of thiocolchicoside in the drug whose formulation was developed from Cellulose, Tuffryn, and Supor membranes is compared with the reference drug, the permeability differences between the membranes are seen. It can be seen from the figure that the best permeability was achieved when the Supor membrane was used, so the study continued using the Supor membrane.

3.4. Effect of membrane saturation on Thiocolchicoside permeation

One of the most critical parameters in Franz cell studies is saturation of the membrane with sufficient media solution. After the membrane selection is determined as “Supor”, the similarity of the membrane with the reference drug, both with and without saturation with the ambient solution under the selected optimum conditions, is shown in Figure 6.

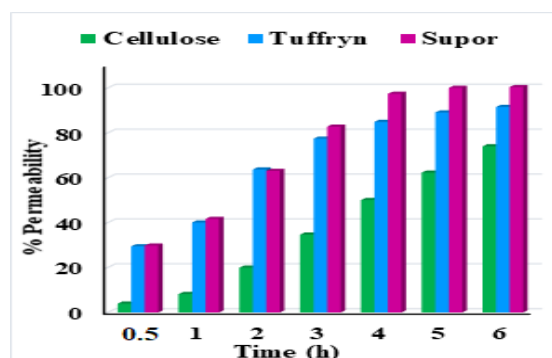


Figure 5. Effect of different membranes on thiocolchicoside permeation (Optimization conditions: solution pH: 7.4, mixing speed: 600 rpm, mixing time: 6 hours, temperature: 32.0 °C, thiocolchicoside amount: 400 mg)

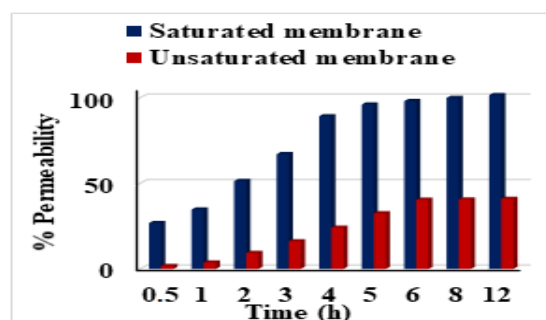


Figure 6. Effect of saturated and unsaturated membranes on thiocolchicoside permeation. (Optimization conditions: Supor membrane, solution pH: 7.4, mixing speed: 600 rpm, mixing time: 6 hours, temperature: 32.0 °C, thiocolchicoside amount: 400 mg)

It can be seen in Figure 6 that the saturated membrane is more similar to the reference drug. The study conducted with a saturated membrane showed that 6 hours of saturation time was sufficient. For this reason, the membrane saturation time in the study was determined as 6 hours.

3.5. Effect of sample amount on Thiocolchicoside permeation

Another parameter whose effect is examined is the amount of sample placed in the Franz Diffusion Cell. Sample amounts ranging from 300 to 500 mg were inducted into the cell, questioning whether it affected thiocolchicoside permeation. A minimum of 300 mg of gel drug is required to completely cover the area of the membrane placed on the Franz Diffusion Cell and to spread the drug evenly on the membrane [51]. Examining this parameter determined that the amount of sample placed in the Franz Diffusion Cell had no effect (Figure 7). Therefore, a 400 mg thiocolchicoside sample was selected and used as an optimum sample amount in the study.

3.6. Effect of mixing time on Thiocolchicoside permeation

The amount to which the mixing time affected the permeability of thiocolchicoside in the Franz Diffusion Cell was evaluated to achieve the best resemblance with the reference drug. Under the identified ideal conditions, the amount of thiocolchicoside was measured various times, ranging from 0.5 to 8 hours, and its resemblance to the reference drug was ascertained.

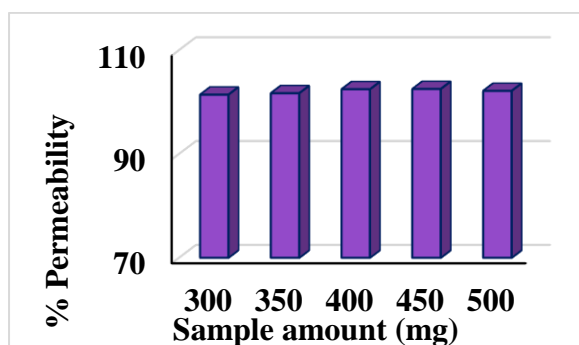


Figure 7. Effect of sample amount on thiocolchicoside permeation. (Optimization conditions: solution pH: 7.4, mixing speed: 600 rpm, mixing time: 6 hours, temperature: 32.0 °C)

As seen in Figure 8, the amount of thiocolchicoside passing from the Franz Diffusion Cell to the environment did not vary in 6 hours or longer. Since it was similar to the reference drug, 6 hours was sufficient for the study's mixing time. The mixing time was determined to be 6 hours.

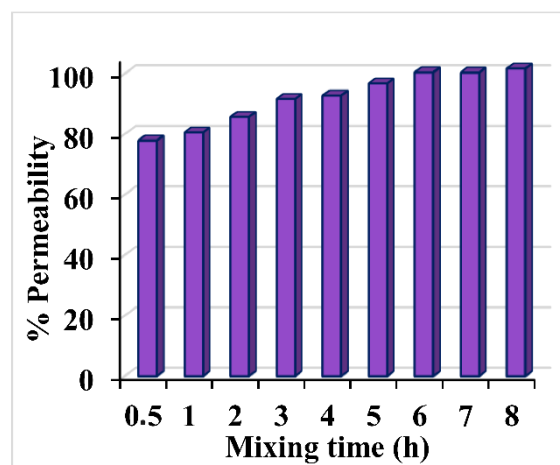


Figure 8. Effect of mixing time on thiocolchicoside permeation. (Optimization conditions: solution pH: 7.4, mixing speed: 600 rpm, temperature: 32.0 °C, and thiocolchicoside amount: 400 mg)

3.7. Effect of mixing speed on Thiocolchicoside permeation

After determining the mixing time, another parameter is to examine the effect of mixing speed. For this parameter, the change in the permeability of thiocolchicoside was investigated by changing the mixing speed between 500 and 660 rpm. When Figure 9 is reviewed, it is seen that the similarity with the reference drug reaches 100% when mixing at 600 rpm. For this reason, 600 rpm was preferred as the working mixing speed.

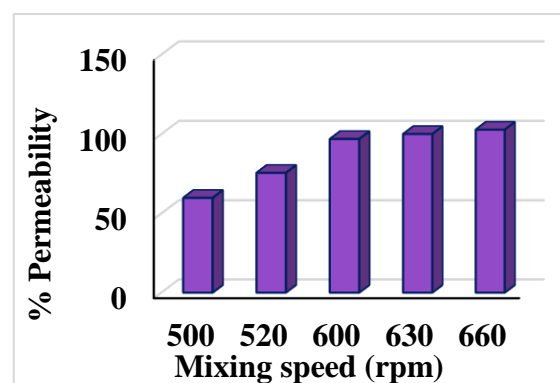


Figure 9. Effect of mixing speed on thiocolchicoside permeation. (Optimization conditions: solution pH: 7.4, mixing time: 6 hours, temperature: 32.0 °C, and thiocolchicoside amount: 400 mg)

3.8. Effect of temperature on Thiocolchicoside permeation

In the study examining the effect of temperature on the permeation of thiocolchicoside, the

required temperature was 32.0 °C, which is the body temperature. The experiment on permeation rate is conducted at 32 ± 1 °C, except for vaginal drug products, which require a temperature of 37 ± 1 °C [52]. The permeation of thiocolchicoside was carried out at different temperatures by varying the temperatures between 30.0 and 36.0 °C. Figure 10 shows that the best permeability to the reference drug was obtained at 32.0 °C body temperature. For this reason, 32.0 °C was determined as the optimum temperature and used in the study. The temperature optimization study is to observe the permeation of thiocolchicoside at temperatures other than 32.0 °C and prove that 32.0 °C has the highest permeation.

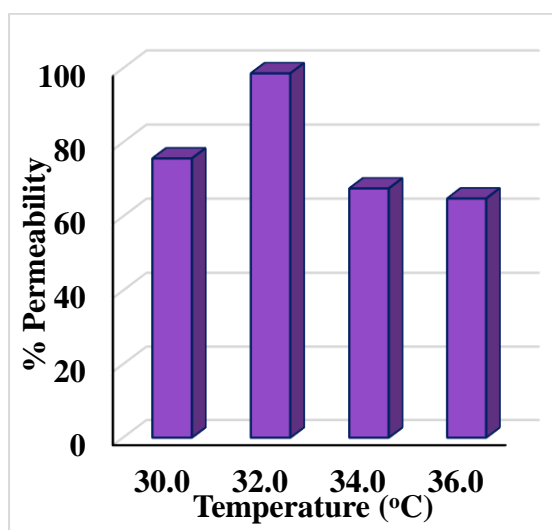


Figure 10. Effect of temperature on thiocolchicoside permeation. (Optimization conditions: solution pH: 7.4, mixing speed: 600 rpm, mixing time: 6 hours, and thiocolchicoside amount: 400 mg)

3.9. Comparison of the method with other studies

When the results obtained from the literature data are examined, it is seen that the Franz Diffusion Cell is frequently used to investigate the use of transdermal drug carrier systems and it is one of the important methods due to its originality. In a study reported by Shioh-Fern Ng and colleagues, Franz Diffusion Cells were used and their effect on the applied method was examined. For this purpose, they used ibuprofen as a model drug and synthetic membranes as a barrier. When they examined the study results, they found that it positively affected the validation [53].

In another study, Alice Simon et al. used different synthetic polymeric membranes and pig ear skin and evaluated the rivastigmine transdermal drug delivery system by performing in vitro permeation experiments in Franz Diffusion Cells. They performed a series of studies to identify the best-performing model membranes [30]. In the study examining the passage of niacinamide from different formulations into human skin, traditional Franz Diffusion Cells were used and investigated both in vitro and in vivo using a quantitative Confocal Raman Spectroscopy method including finite dose conditions. They emphasized that it is a valuable study for both actives and excipients [54].

4. Conclusions

One of the increasingly essential systems in the pharmaceutical industry is the transdermal drug delivery system, which constitutes an innovative and successful research area. In this study, the permeation of thiocolchicoside, the active ingredient taken into the body through various drug applications, with Franz Diffusion Cell, the permeability of the drug developed in gel form, and the reference drug was evaluated comparatively using the "Supor" membrane. Validation studies were carried out to evaluate the accuracy and reliability of the results obtained from the samples. In addition, although there are different studies with the thiocolchicoside agent, it will be the first comparative study with the reference drug gel. As a result of the injection of sample and reference solutions, it was determined that the linearity of the chromatograms obtained for thiocolchicoside with a correlation coefficient of 0.9992 was satisfactory for the established method.

Moreover, it was observed that the detection limit was 0.026 µg/mL, the relative standard deviation values were less than 3%, and the accuracy values were between 100% and 102%. These values obtained prove the accuracy and reliability of the study. In addition, the method is environmentally friendly in that it can be applied rapidly because it does not require many process steps, consumes few materials, and requires no toxic solutions.

Article Information Form

Acknowledgments

The authors want to thank Düzce University.

Funding

This research was supported by the Düzce University Scientific Research Projects Fund (Project No: 2023.05.03.1406) for contributing to the financial portion of the project.

Authors' Contribution

Hale Karagüzel Investigation, Methodology; **Aslihan Dalmaz** Methodology, Writing-Writing-review & editing; **Sezen Sivrikaya Özak** Writing-review & editing, Supervision. All authors have read and agreed to the published version of the manuscript.

The Declaration of Conflict of Interest/ Common Interest

No conflict of interest or common interest has been declared by the authors.

The Declaration of Ethics Committee Approval

This study does not require ethics committee permission or any special permission.

The Declaration of Research and Publication Ethics

The authors of the paper declare that they comply with the scientific, ethical, and quotation rules of SAUJS in all processes of the paper and that they do not make any falsification on the data collected. In addition, they declare that Sakarya University Journal of Science and its editorial board have no responsibility for any ethical violations that may be encountered, and that this study has not been evaluated in any academic publication environment other than Sakarya University Journal of Science.

Copyright Statement

The authors own the copyright of their work published in the journal and their work is published under the CC BY-NC 4.0 license.

References

- [1] F. Bigucci, A. Abruzzo, B. Saladini, M. C. Gallucci, T. Cerchiara, B. Luppi, "Development and characterization of chitosan/hyaluronan film for transdermal delivery of thiocolchicoside," *Carbohydrate Polymers*, vol. 130, pp. 32-40, 2015.
- [2] M. Artusi, P. Santi, P. Colombo, H. E. Junginger, "Buccal delivery of thiocolchicoside: in vitro and in vivo permeation studies," *International Journal of Pharmaceutics*, vol. 250, pp. 203-213, 2003.
- [3] G. C. Ceschel, P. Maffei, S. Porzio, G. Melillo, G. F. Caselli, M. C. Dragani, G. Clavenna, "In vitro permeation screening of a new formulation of thiocolchicoside containing various enhancers," *Drug Delivery*, vol. 9, pp. 259-263, 2002.
- [4] M. Artusi, S. Nicoli, P. Colombo, R. Bettini, A. Sacchi, P. Santi, "Effect of chemical enhancers and iontophoresis on thiocolchicoside permeation across rabbit and human skin in vitro," *Journal of Pharmaceutical Sciences*, vol. 93, pp. 2431-2438, 2004.
- [5] C. Aguzzi, S. Rossi, M. Bagnasco, L. Lanata, G. Sandri, F. Bona, et al., "Penetration and distribution of thiocolchicoside through human skin: comparison between a commercial foam (Miotens®) and a drug solution," *AAPS PharmSciTech*, vol. 9, pp. 1185-1190, 2008.
- [6] S. Bhamburkar, S. Khandare, S. Patharkar, S. Thakare, "Thiocolchicoside: An Updated Review," vol. 12, pp. 213-218, 2022.
- [7] M. Carta, L. Murru, P. Bota, G. Talani, G. Sechi, P. Riu, et al., "The muscle relaxant Thiocolchicoside is an antagonist of GABA-A receptor in the central nervous system," *Neuropharmacology*, vol. 51, pp. 805-815, 2006.
- [8] M. Trellu, A. Filali-Ansary, D. Françon, R. Adam, P. Lluet, C. Dubruc, et al., "New metabolic and pharmacokinetic characteristics of thiocolchicoside and its

- active metabolite in healthy humans,” *Fundamental & Clinical Pharmacology*, vol. 18, pp. 493-50, 2004.
- [9] Y. Yang, P. Manda, N. Pavurala, M. A. Khan, Y. S. Krishnaiah, “Development and validation of in vitro–in vivo correlation (IVIVC) for estradiol transdermal drug delivery systems,” *Journal of Controlled Release*, vol. 210, pp. 58-66, 2015.
- [10] A. Arunachalam, M. Karthikeyan, D. V. Kumar, M. Prathap, S. Sethuraman, S. Ashutoshkumar, et al., “Transdermal drug delivery system: a review,” *International Journal of Current Pharmaceutical Research*, vol. 1, pp. 70-75, 2010.
- [11] A. D. Mali, “An updated review on transdermal drug delivery systems,” *Skin*, vol. 1, pp. 244-254, 2015.
- [12] G. M. Shingade, “Review on: recent trend on transdermal drug delivery system,” *Journal of Drug Delivery and Therapeutics*, vol. 2, pp. 62-75, 2012.
- [13] A. V. Patel, B. N. Shah, “Transdermal drug delivery system: a review,” *Pharma Science Monitor*, vol. 9, pp. 378-390, 2018.
- [14] P. Chinchole, S. Savale, K. Wadile, “A novel approach on transdermal drug delivery system [TDDS],” *World Journal of Pharmacy and Pharmaceutical Sciences*, vol. 5, pp. 932-958, 2016.
- [15] D. D. Biradar, N. Sanghavi, “Technologies in transdermal drug delivery system: a review,” *Small*, vol. 6, pp. 528-541, 2014.
- [16] P. M. Satturwar, S. V. Fulzele, A. K. Dorle, “Evaluation of polymerized rosin for the formulation and development of transdermal drug delivery system: a technical note,” *AAPS PharmSciTech*, vol. 6, pp. E649-E654, 2005.
- [17] M. A. Kassem, M. H. Aboul-Einien, M. M. El Taweel, “Dry gel containing optimized felodipine-loaded transferosomes: A promising transdermal delivery system to enhance drug bioavailability,” *AAPS PharmSciTech*, vol. 19, pp. 2155-2173, 2018.
- [18] D. A. Davis, P. P. Martins, M. S. Zamloot, S. A. Kucera, R. O. Williams, H. D. Smyth, et al., “Complex drug delivery systems: Controlling transdermal permeation rates with multiple active pharmaceutical ingredients,” *AAPS PharmSciTech*, vol. 21, pp. 1-11, 2020.
- [19] N. Thakur, B. Kaur, C. Sharma, M. Goswami, “Evaluation of the Dermal Irritation and Skin Sensitization Due to Thiocolchicoside Transdermal Drug Delivery System,” *International Journal of Health Sciences*, (III), pp. 3057-3066, 2022.
- [20] M. Paradkar, S. Vaghela, “Thiocolchicoside niosomal gel formulation for the pain management of rheumatoid arthritis through topical drug delivery,” *Drug Delivery Letters*, vol. 8, pp. 159-168, 2018.
- [21] Y. M. Rao, P. Gayatri, M. Ajitha, P. P. Kumar, “Chemical Permeation Enhancers for Transdermal Delivery of Thiocolchicoside: Assessment of Ex-vivo Skin Flux and In-vivo Pharmacokinetics,” *International Journal of Pharmaceutical Sciences and Nanotechnology (IJPSN)*, vol. 10, pp. 3827-3835, 2017.
- [22] P. Panda, A. Sahu, “Permeation Enhancers for Transdermal Drug Delivery: Strategies and Advancements Focusing Macromolecules,” *International Journal of Advanced Pharmaceutical Sciences and Research*, vol. 3, pp.1-11, 2023.
- [23] L. Allen, H. C. Ansel, “Ansel's pharmaceutical dosage forms and drug delivery systems,” Tenth ed., Lippincott Williams & Wilkins, Philadelphia, 2013.
- [24] R. B. Saudagar, P. A. Gangurde, “Formulation, development and evaluation of film-forming gel for prolonged dermal

- delivery of miconazole nitrate,” *Research Journal of Topical Cosmetic Sciences*, vol. 8, pp. 19-29, 2017.
- [25] Y. Yang, R. Ou, S. Guan, X. Ye, B. Hu, Y. Zhang, et al., “A novel drug delivery gel of terbinafine hydrochloride with high penetration for external use,” *Drug Delivery*, vol. 22, pp. 1086-1093, 2015.
- [26] M. M. Patel, Z. M. Vora, “Formulation development and optimization of transungual drug delivery system of terbinafine hydrochloride for the treatment of onychomycosis,” *Drug Delivery and Translational Research*, vol. 6, pp. 263-275, 2016.
- [27] S. T. Tanriverdi, Ö. Özer, “Novel topical formulations of Terbinafine-HCl for treatment of onychomycosis,” *European Journal of Life Sciences*, vol. 48, pp. 628-636, 2013.
- [28] L. Sun, D. Cun, B. Yuan, H. Cui, H. Xi, L. Mu, et al., “Formulation and in vitro/in vivo correlation of a drug-in-adhesive transdermal patch containing azasetron,” *Journal of Pharmaceutical Sciences*, vol. 101, pp. 4540-4548, 2012.
- [29] A. K. Gupta, M. Venkataraman, N. H. Shear, V. Piguet, “Onychomycosis in children—review on treatment and management strategies,” *Journal of Dermatological Treatment*, vol. 3, pp. 1213-1224, 2022.
- [30] A. Simon, M. I. Amaro, A. M. Healy, L. M. Cabral, V. P. de Sousa, “Comparative evaluation of rivastigmine permeation from a transdermal system in the Franz cell using synthetic membranes and pig ear skin with in vivo-in vitro correlation,” *International Journal of Pharmaceutics*, vol. 512, pp. 234-24, 2016.
- [31] B. Godin, E. Touitou, “Transdermal skin delivery: predictions for humans from in vivo, ex vivo and animal models,” *Advanced Drug Delivery Reviews*, vol. 59, pp. 1152-1161, 2007.
- [32] L. N. R. Katakam, N. K. Katari, “Development of in-vitro release testing method for permethrin cream formulation using Franz Vertical Diffusion Cell apparatus by HPLC,” *Talanta Open*, vol. 4, pp. 100056, 2021.
- [33] I. Neri, S. Laneri, R. Di Lorenzo, I. Dini, G. Russo, L. Grumetto, “Parabens permeation through biological membranes: a comparative study using Franz cell diffusion system and biomimetic liquid chromatography,” *Molecules*, vol. 27, pp. 4263, 2022.
- [34] E. Abd, J. Gomes, C. C. Sales, S. Yousef, F. Forouz, K. C. Telaprolu, et al., “Deformable liposomes as enhancer of caffeine penetration through human skin in a Franz diffusion cell test,” *International Journal of Cosmetic Science*, vol. 43, pp. 1-10, 2021.
- [35] R. D. Kirk, T. Akanji, H. Li, J. Shen, S. Allababidi, N. P. Seeram, et al., “Evaluations of Skin Permeability of Cannabidiol and Its Topical Formulations by Skin Membrane-Based Parallel Artificial Membrane Permeability Assay and Franz Cell Diffusion Assay,” *Medical Cannabis and Cannabinoids*, vol. 5, pp. 129-137, 2022.
- [36] I. Pulsoni, M. Lubda, M. Aiello, A. Fedi, M. Marzagalli, J. von Hagen, et al., “Comparison between Franz diffusion cell and a novel micro-physiological system for in vitro penetration assay using different skin models,” *SLAS Technology*, vol. 27, pp. 161-171, 2022.
- [37] M. J. Reese, G. D. Bowers, J. E. Humphreys, E. P. Gould, S. L. Ford, L. O. Webster, et al., “Drug interaction profile of the HIV integrase inhibitor cabotegravir: assessment from in vitro studies and a clinical investigation with midazolam,” *Xenobiotica*, vol. 46, pp. 445-456, 2016.
- [38] S. F. Ng, J. Rouse, D. Sanderson, G. Eccleston, “A comparative study of transmembrane diffusion and permeation

- of ibuprofen across synthetic membranes using Franz diffusion cells,” *Pharmaceutics*, vol. 2, pp. 209-223, 2010.
- [39] S. F. Ng, J. J. Rouse, F. D. Sanderson, G. M. Eccleston, “The relevance of polymeric synthetic membranes in topical formulation assessment and drug diffusion study,” *Archives of Pharmacal Research*, vol. 35, pp. 579-593, 2012.
- [40] T. J. Franz, P. A. Lehman, S. G. Raney, “Use of excised human skin to assess the bioequivalence of topical products,” *Skin Pharmacology and Physiology*, vol. 22, pp. 276-286, 2009.
- [41] A. S. Silva, J. M. Cruz Freire, R. Sendón, R. Franz, P. Paseiro Losada, “Migration and diffusion of diphenylbutadiene from packages into foods,” *Journal of Agricultural and Food Chemistry*, vol. 57, pp. 10225-10230, 2009.
- [42] D. Ramsden, “Bridging in vitro and in vivo metabolism and transport of faldaprevir in human using a novel cocultured human hepatocyte system, HepatoPac,” *Drug Metabolism and Disposition*, vol. 42, pp. 394-406, 2014.
- [43] A. M. Barbero, H. F. Frasc, “Pig and guinea pig skin as surrogates for human in vitro penetration studies: a quantitative review,” *Toxicology in Vitro*, vol. 23, pp. 1-13, 2009.
- [44] G. A. Simon, H. I. Maibach, “The pig as an experimental animal model of percutaneous permeation in man: qualitative and quantitative observations—an overview,” *Skin Pharmacology and Physiology*, vol. 13, pp. 229-234, 2000.
- [45] H. Annepogu, H. A. Ahad, D. Nayakanti, “Determining the best poloxamer carrier for thiocolchicoside solid dispersions,” *Turkish Journal of Pharmaceutical Sciences*, vol. 17, pp. 372-377, 2020.
- [46] N. Thakur, B. Kaur, M. Goswami, C. Sharma, “Compatibility studies of the Thiocolchicoside with Eudragit RLPO, Eudragit E100 and Eudragit L100 using thermal and non-thermal methods,” *Drug Combination Therapy*, vol. 4, pp. 1-10, 2021.
- [47] R. R. Joshi, K. R. Gupta, “Solid-state characterization of thiocolchicoside,” *International Journal of Advanced Pharmaceutical Sciences and Research*, vol. 4, pp. 1441-1450, 2013.
- [48] G. A. Shabir, “Validation of high-performance liquid chromatography methods for pharmaceutical analysis: Understanding the differences and similarities between validation requirements of the US Food and Drug Administration, the US Pharmacopeia and the International Conference on Harmonization,” *Journal of Chromatography A*, vol. 987, pp. 57-66, 2003.
- [49] USP. Validation of Compendial Procedures. In: *The United States Pharmacopeia and National Formulary*, (2015b).
- [50] ICH. International Conference on Harmonisation of Technical Requirements for Registration of Pharmaceuticals for Human Use. *Validation of Analytical Procedures: Text and Methodology Q2(R1)*, (2005).
- [51] F. CDER, “Guidance for Industry, Nonsterile Semisolid Dosage Forms,” US Department of Health and Human Services May 1997.
- [52] Chapter, U. S. P. “1724> Semisolid Drug Products—Performance Tests.” *USP: Rockvill, MD, USA*, 2014.
- [53] S. F. Ng, J. J. Rouse, F. D. Sanderson, V. Meidan, G. M. Eccleston, “Validation of a static Franz diffusion cell system for in vitro permeation studies,” *AAPS Pharmscitech*, vol. 11, pp. 1432-1441, 2010.

- [54] F. Iliopoulos, P. J. Caspers, G. J. Puppels, M. E. Lane, “Franz cell diffusion testing and quantitative confocal raman spectroscopy: In vitro-in vivo correlation,” *Pharmaceutics*, vol. 12, pp. 887-899, 2020.

Improved Automatic Migraine Classification Performance with Naive Bayes

Arzum Karataş 

Bandırma Onyedi Eylül University, Faculty of Engineering and Natural Sciences, Department of Computer Engineering, Balıkesir, Türkiye, akaratas@bandirma.edu.tr

ARTICLE INFO

ABSTRACT

Keywords:
Migraine type diagnosis
Naive Bayes
Classification



Article History:
Received: 26.07.2023
Accepted: 03.06.2024
Online Available: 01.08.2024

The expertise of the physician and the patient's ongoing observation are the two primary contributing factors in diagnosing migraines. However, individuals who experience migraines in the early stages frequently visit emergency rooms or different outpatient clinics, such as internal medicine, ophthalmology, and family medicine. Additionally, the type of migraine is frequently misdiagnosed due to the severity of the symptoms being misjudged or because the five-to-ten-minute examination period is insufficient for achieving an accurate diagnosis. Incorrect treatment of this type can have adverse effects on the patient's health. The majority of research in this field has concentrated on the study of brainwaves, leading to the development of complex tests that are only available to a small proportion of the population. However, one study has made progress in automatic migraine classification. The study, which demonstrates 97% classification performance above that of previous studies and produces findings in a timely manner, provides a decision support mechanism that will assist clinicians in the proper classification of migraine type. Given that over 20% of Turkey's population suffers from migraines, our study concentrated on the same issue to enhance classification performance in terms of accuracy and training time. The Naive Bayes model was employed in the study to categorize the various types of migraines, and the performance of the model was evaluated using data from actual migraine sufferers. The classification model utilized exhibited superior classification performance compared to previous studies, with 99% accuracy and precision. Additionally, the model's training time in the same dataset was the shortest when compared to other benchmarked classifier models. The application of the Naive Bayes classifier to the classification of migraines represents a highly effective technique that can facilitate rapid, accurate clinical diagnoses, thereby enabling physicians to provide their patients with precise diagnoses.

1. Introduction

Migraine is a neurological pain illness that affects millions of people worldwide [1]. It is thought of as a long-term nerve system problem [1, 2]. The International Headache Society (IHS) describes a migraine as a recurrent headache with or without aura, lasting 4–72 hours in adults and 2–72 hours in children. It is frequently accompanied by nausea, vomiting, or sensitivity to light, sound, or movement [3-6]. The illness has a high rate of impairment and a significant financial cost [3,7], and is influenced by genetic, hormonal, environmental, dietary, sleep, and

psychological factors [8-10]. According to a press release from the Turkish Neurological Society in Turkey, one in five women and one in ten males, or around 20% of the population, suffer from migraines in 2019 [11]. Globally, more than a billion people were impacted by migraine in 2019 [2]. Additionally, migraine is a significant contributor to disability and job loss [1]. A substantial body of evidence indicates that migraine has a profound impact on a country's economy and health [1, 7, 12-15].

The illness burden and the rate of disability can be reduced through the early, accurate

identification and treatment of the condition [1, 3, 7, 16]. Decision support systems can facilitate the accurate diagnosis of each patient's migraine type during the official examination process, thereby improving their quality of life. Such a strategy benefits social well-being and indirectly aids in the restoration of the nation's workforce, which has been affected by migraines.

The revised second edition of the IHS's International Classification of Headache Disorders [16] is divided into six basic categories: migraine without aura, migraine with aura, retinal migraine, complications of migraine, probable migraine, and frequently occurring childhood periodic syndromes [17]. However, the actual dataset employed for this investigation was divided into three subgroups, comprising patients with migraines with aura, migraines without aura, and other migraines.

A correct diagnosis of the type of migraine is of critical importance, given that 20% of Turkey's population suffers from this illness [11]. In general, individuals who experience migraines in the early stages of their illness frequently seek medical attention in emergency rooms or other outpatient clinics, such as those specializing in internal medicine, ophthalmology, and family medicine. Nevertheless, some symptoms are also associated with other illnesses. It is therefore evident that diagnosis requires expertise.

In order to diagnose and detect migraines in a traditional manner, medical images obtained via machines such as CT (computed tomography), MRI (magnetic resonance imaging), and PET (positron emission tomography) are utilized in hospitals. Nevertheless, individuals may lack the financial resources to utilize these services in private hospitals or may not have timely access to them in state hospitals. For instance, in state hospitals in Turkey, it may take several months to obtain an appointment for the use of these machines. Furthermore, the interpretation of these medical images necessitates the expertise of highly trained medical professionals. However, the short examination periods of five to ten minutes in state hospitals frequently result in misdiagnosis of migraine types due to the inability to adequately assess the severity of the symptoms. The majority of research on the

subject has been concentrated on the study of brainwaves, which has led to the development of complex tests that are only available to a very small portion of the population [18].

Consequently, an affordable, fast, accessible, accurate, and user-friendly approach is indispensable in the classification of migraine types. Only Sanchez-Sanchez's study [19] employed a machine learning-based methodology on symptoms rather than medical images for automatic migraine type classification, which achieved an accuracy rate of 97%. The aforementioned study employed traditional machine learning techniques, including k-nearest neighbor, decision trees (CART classification and regression tree), support vector machines (SVM), logistic regression, and artificial neural networks (ANN).

The objective of our study was to investigate whether the classification accuracy could be increased while the classification time was decreased. This would be beneficial in the context of migraine diagnosis, as an accurate diagnosis could help to reduce the potential consequences that patients may be susceptible to. To this end, we proposed a machine learning-based solution that was fast, accessible, accurate, and easy to use for clinicians who may wish to use it in their decision-making.

In this study, we used the Naive Bayes classifier, a machine learning approach, to analyze the data. In this study, we propose that Naive Bayes can enhance classification performance, particularly when the predictors are categorical. This is despite the naive assumption that the predictors are independent and identically distributed, as discussed in [20]. Furthermore, Naive Bayes can be applied to the solution of multi-class classification issues. Additionally, it is straightforward, rapid, and easy to implement. The research findings have enhanced the existing literature on the automatic migraine-type classification and have provided support for our initial intuition.

The remainder of this document will proceed as follows: The methodology employed in this research is outlined in the subsequent section, along with the workflow. Then, the dataset,

classifier model, implementation environment, and performance assessment metrics utilized in the experimental investigation are described in detail. Later, the findings of the experiment will be presented. The results and contributions of the research are then discussed. The final section of the paper presents a conclusion to the research.

2. Methodology

In this study, we propose a Naive Bayes-based model to enhance the classification performance of earlier efforts. The methodology employed in this investigation is illustrated in Figure 1, which represents a straightforward supervised classification approach. First, the "Migraine dataset," as detailed in the 3.2 Dataset section, was divided into two subsets: a training set (representing 80% of the dataset) and a test set (representing 20% of the dataset). The training set was then used to train the classification model, Naive Bayes, while the test set was used to evaluate the classification performance of the trained classifier. Finally, the performance of the classifier is evaluated by means of performance metrics, such as accuracy and precision, as detailed in Section 3.3 Measures for Performance Evaluation.

This approach is designed for medical practitioners to assist them in their decision-making regarding the classification of migraine types in their patients. This method is designed to be user-friendly, requiring only the entry of migraine symptoms as specified in Section 3.2 of the dataset by the doctor or medical staff. The method then automatically predicts the migraine type.

3. Experimental Study

3.1. Naïve Bayes classifier

The Bayes theorem, a formula for calculating conditional probability, was developed by Thomas Bayes in 1812 for use in statistics. This theorem elucidates the relationship between conditional probabilities and marginal probabilities in the probability distribution for a random variable. The calculation is performed using Equation (1).

$$P(E_1|E_2) = \frac{P(E_1|E_2) \times P(E_1)}{P(E_2)} \tag{1}$$

where the components of the formula as is defined below.

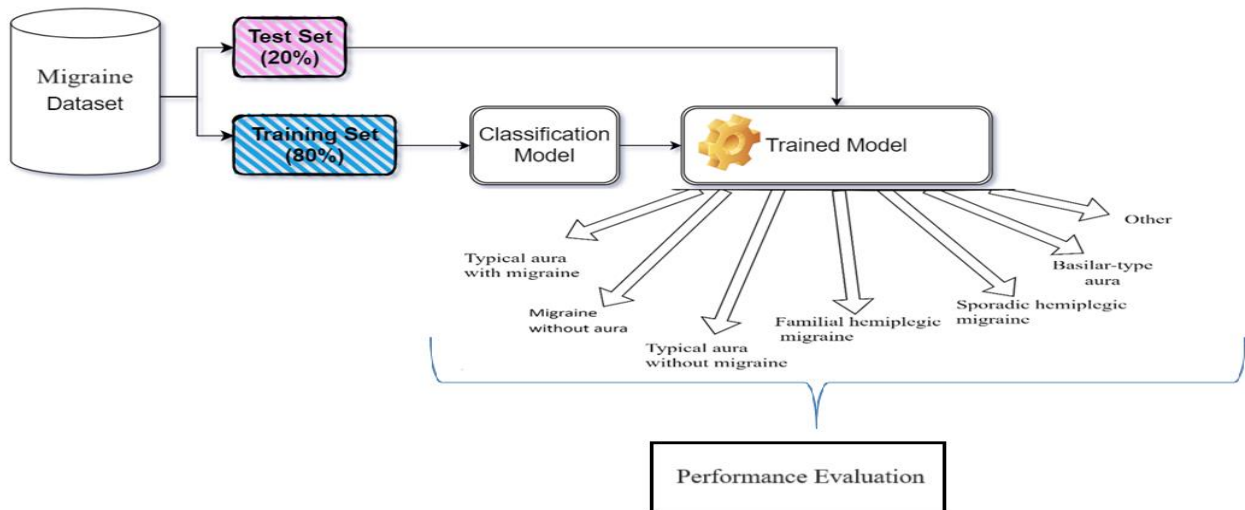


Figure 1. Methodology used in this work

- E_1 and E_2 are events.
- The probabilities of events E_1 and E_2 , respectively, are represented by $P(E_1)$ and $P(E_2)$.
- $P(E_1|E_2)$ is the probability of event E_1 occurring when event E_2 occurs.

$P(E_2|E_1)$ is the probability of event E_2 occurring when event E_1 occurs.

The Naive Bayes classifier is based on the application of Bayes' theorem with the naive assumption that each pair of features will have a conditional dependency given the value of the

class variable. In other words, the classifier first creates a Naive Bayes probability model and then combines it with a typically maximum posterior decision rule. In conclusion, a Bayes classifier, represented by Equation (2), can be conceptualized as a function that assigns class labels to data item properties.

$$class = \arg \max_{class} \times P(class) \prod_{i=1}^n P(feature_i|class) \quad (2)$$

The probability function P, the class label to be assigned, and the i^{th} attribute of the data point are all shown in Equation (2).

3.2 Dataset

The "Migraine" dataset created by Sanchez-Sanchez is publicly available on CodeOcean [21]. The data was collected during the course of a master's thesis research project. In 2013, a medical professional maintained records at the Hospital Materno Infantil de Soledad. The dataset comprises 400 individuals' medical records and contains no personal data that could be used to identify the patients. The dataset comprises 24 variables, including both migraine symptoms and diagnoses. The variables are listed in Table 1 and have natural number values.

Furthermore, the dataset is free of missing values. The diagnosis of the patient, as indicated by the variable "Type," is based on the patient's symptoms and medical history. One of the seven forms of migraines is indicated, including "1. Typical aura with migraine", "2. Migraine without aura", "3. Typical aura without migraine", "4. Familial hemiplegic migraine", "5. Sporadic hemiplegic migraine", "6. Basilar-type aura" and "7. Other". Figure 2 presents the percentage of cases in the dataset by type of migraine. It should be noted that migraine types that can develop without headache, such as acephalgic migraine or silent

migraine, are represented under other categories. Consequently, this particular type is not fully represented in the study.

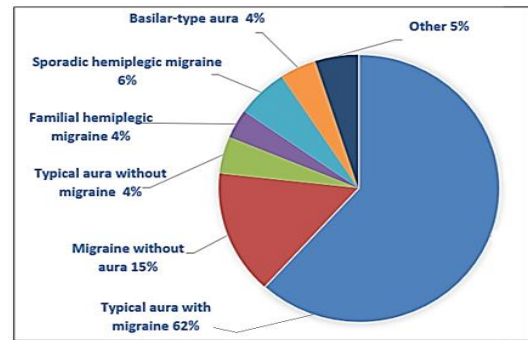


Figure 2. A pie chart illustrating the relative prevalence of different types of migraines within the dataset

3.3 Measures for performance evaluation

In this study, precision and accuracy metrics are employed to assess the performance of machine learning models. To facilitate comprehension of these measurements, it is essential to present a number of factors, including true positive (TP), true negative (TN), false positive (FP), and false negative (FN). These parameters are employed to assess precision, recall, and accuracy. As illustrated in Figure 3, a confusion matrix, which is a table for a binary classifier, is a valuable tool in the classification process, which allows for the comparison of actual values with predicted values by a machine learning model.

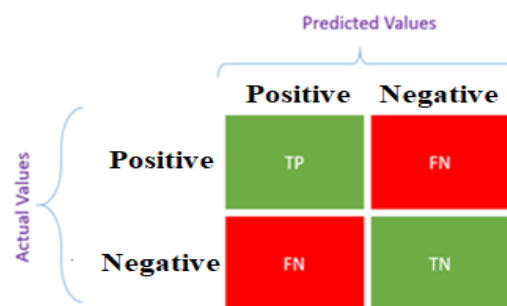


Figure 3. A confusion matrix for assessing classification performance

Table 1. Description of the Migraine dataset

#	Identified Variable	Value Range	Description
1	Age	15-77	Age of the patient
2	Duration	1-3	Duration of symptoms last episode in days
3	Frequency	1-8	Frequency of episodes per month
4	Location	0-2	Unilateral/bilateral pain location {0: None, 1: Unilateral, 2: Bilateral}
5	Character	0-2	Throbbing or constant pain {0: None, 1: Throbbing, 2: Constant}
6	Intensity	0-3	Pain intensity {0: None, 1: Mild, 2: Medium, 3: Severe}
7	Nausea	0-1	Nauseous feeling {0: Not, 1: Yes}
8	Vomit	0-1	Existence of vomiting {0: Not, 1: Yes}
9	Phonophobia	0-1	Noise sensitivity {0: Not, 1: Yes}
10	Photophobia	0-1	Light sensitivity {0: Not, 1: Yes}
11	Visual	0-4	Reversible visual symptoms
12	Sensory	0-2	Reversible sensory symptoms
13	Dysphasia	0-1	Lack of speech coordination {0: Not, 1: Yes}
14	Dysarthria	0-1	Disarticulated sounds and words {0: Not, 1: Yes}
15	Vertigo	0-1	Dizziness {0: Not, 1: Yes}
16	Tinnitus	0-1	Ringing in the ears {0: Not, 1: Yes}
17	Hypoacusis	0-1	Hearing loss {0: Not, 1: Yes}
18	Diplopia	0-1	Double vision {0: Not, 1: Yes}
19	Visual_defect	0-1	Simultaneous frontal eye field and nasal field defect and in both eyes {0: Not, 1: Yes}
20	Ataxia	0-1	Lack of muscle control {0: Not, 1: Yes}
21	Conscience	0-1	Jeopardized conscience {0: Not, 1: Yes}
22	Paresthesia	0-1	Simultaneous bilateral paresthesia {0: Not, 1: Yes}
23	DPF	0-1	Family background {0: Not, 1: Yes}
24	Type	1-7	Diagnosis of migraine type

True positives (TP) represent the number of outcomes that were correctly identified as positive by the machine learning model. True negatives (TN), on the other hand, refer to the number of outcomes that were correctly identified as negative. False positives (FP) are instances where a negative result was erroneously classified as a positive. Similarly, false negatives (FN) are instances where a favorable outcome was erroneously projected as a negative one. The metrics employed in this study for evaluating the performance of the model are outlined below.

Precision is defined as the degree of agreement between the predicted and actual values. The precision of the learning model's positive predictions is evaluated by measuring its accuracy. Equation (3) specifies that this metric is calculated as the ratio of true positives to all positive predictions. This is calculated as the sum of the model's true positives and false positives.

$$Precision = \frac{TP}{TP + FP} \quad (3)$$

Accuracy is a metric used to evaluate the quality of predictions. It determines the percentage of accurate predictions made by the machine learning model. For instance, if 95% of the predictions are correct, the model's accuracy is 95%. The accuracy of the model is calculated using the following equation:

$$Accuracy = \frac{TP + TN}{TP + TN + FP + FN} = \frac{\text{Number of correct predictions}}{\text{Number of total predictions}} \quad (4)$$

4. Results and Discussion

In this study, we utilize the recommended methodology to categorize the migraine dataset. The dataset encompasses information on adults who have been diagnosed with migraines. The classification process makes use of every detected variable. To provide a fair comparison of Sanchez-Sanchez's work [19], a

Python 3 script utilizing the "Scikit-learn" [22] and "Pandas" [23] libraries was employed, as these were used in the implementation of Sanchez-Sanchez's work [19].

The precision and accuracy figures that Sanchez-Sanchez published for their studies, those of their opponents, and those that we empirically discovered for our work are presented in Table 2.

Table 2. Comparative performance outcomes in terms of accuracy and precision

Study	Classifier Model	Precision (%)	Accuracy (%)
Sanchez-	kNN	87.19	78.75
Sanchez	CART	81.00	81.25
[20]	SVM	95.31	86.25
	Logistic Regression	95.63	87.50
	ANN	97.00	97.50
Our Study	Naive Bayes	99.00	98.75

Table 2 presents the performance values for the same dataset when employing various machine learning classifier models. The weighted average of all migraine types was derived from precision calculations that were conducted independently for each form of migraine.

One of the objectives of this study is to develop a rapid and automated classification system for migraine types. To demonstrate the efficiency of the Naïve Bayes classifier in comparison to other classifiers, we quantified the training times of the classifiers. This is because the majority of the time consumed by machine learning algorithms is spent on the training stage. Table 3 presents the average training time, in seconds, required by machine learning classifiers. Training times are expressed in seconds and represent the average of ten separate executions. For the purposes of the experimental analysis, a laptop with the following configuration was utilised: The processor is an Intel Core i7 CPU @ 2.30 GHz. The processor is 64-bit and runs on the Windows 10 operating system, which has 16 GB of main memory.

Table 3. Comparative outcomes for the classification models' training times

Works	ML Classifier	Training Time (in seconds)
Sanchez-	kNN	0.041
Sanchez	CART	0.035
[20]	SVM	0.026
	Logistic Regression	29.856
	ANN	5.216
Our Study	Naive Bayes	0.002

Furthermore, this study does not encompass the full spectrum of migraine types, including vestibular migraine, menstrual migraine, abdominal migraine, and acephalgic migraine (or silent migraine), which are all classified as "others" in the dataset. Consequently, the dataset utilized in this study must be augmented in order to facilitate the identification of these migraine subtypes and other subtypes of migraines like retinal migraine.

5. Conclusion

It is a priori assumed that Naive Bayes may enhance the prediction accuracy on classification of the migraine dataset. This is based on the observation that Naive Bayes can perform well on relatively less data, can be trained in a short amount of time, and can provide highly accurate results on categorical variables, regardless of whether the variables are conditionally dependent or not. The objective of this study is to examine the potential of the Naive Bayes machine learning model to enhance the precision and accuracy of diagnosing the various types of migraine in migraine sufferers. The outcomes demonstrate that, when compared to numerous models employed for the classification of migraine types in the literature, the Naive Bayes model outperforms all other reference works in terms of precision, accuracy, and model training time.

Future studies may expand the dataset to include additional migraine types that are currently underrepresented, such as vestibular migraine, menstrual migraine, abdominal migraine, and acephalgic migraine (or silent migraine). These migraine types are all categorized as "others" in the dataset. Additionally, the dataset may be extended by other migraine subtypes like retinal migraine.

Article Information Form

Funding

The author has not received any financial support for the research, authorship or publication of this study.

The Declaration of Ethics Committee Approval

This study does not require ethics committee permission or any special permission.

The Declaration of Conflict of Interest/ Common Interest

No conflict of interest or common interest has been declared by the author.

The Declaration of Research and Publication Ethics

The authors of the paper declare that they comply with the scientific, ethical and quotation rules of SAUJS in all processes of the paper and that they do not make any falsification on the data collected. In addition, they declare that Sakarya University Journal of Science and its editorial board have no responsibility for any ethical violations that may be encountered, and that this study has not been evaluated in any academic publication environment other than Sakarya University Journal of Science.

Copyright Statement

Authors own the copyright of their work published in the journal and their work is published under the CC BY-NC 4.0 license.

References

- [1] M. Ashina, Z. Katsarava, T. P. Do, D. C. Buse, P. Pozo-Rosich, A. Özge, A. V Krymchantowski, E. R. Lebedeva, K. Ravishankar, S. Yu, S. Sacco, S. Ashina, S. Younis, T. J Steiner, R. B Lipton, "Migraine: epidemiology and systems of care," *The Lancet*, vol. 397, no. 10283, pp. 1485-1495, 2021.
- [2] J. Gupta, S. S. Gaurkar, "Migraine: An Underestimated Neurological Condition Affecting Billions," *Cureus*, vol. 14, no.8, Art no. e28347, 2022.
- [3] J. Berg, L. J. Stovner, L. J., "Cost of migraine and other headaches in Europe," *European Journal of Neurology*, vol. 12, no. June 2005, pp. 59-62, 2005.
- [4] P. J. Goadsby, "Recent advances in understanding migraine mechanisms, molecules and therapeutics," *Trends in Molecular Medicine*, vol. 13, no. 1, pp. 39-44, 2007.
- [5] P. Parisi, A. Verrotti, M. C. Paolino, A. Ferretti, F. D. Sabatino, F.D., "Obesity and Migraine in Children," in *Omega-3 Fatty Acids in Brain and Neurological Health*, R.R. Watson and F. D. Meester, Eds. Cambridge, UK: Cambridge Academic Press, 2014, pp. 277-286.
- [6] Headache Classification Committee of the International Headache Society, "The International Classification of Headache Disorders, 3rd edition," *Cephalalgia*, vol. 38, no.1, pp.1-211, 2018
- [7] T. Shimizu, F. Sakai, H. Miyake, T. Sone, M. Sato, S. Tanabe, Y. Azuma, D. W. Dodick, "Disability, quality of life, productivity impairment and employer costs of migraine in the workplace," *The Journal of Headache and Pain*, vol. 22, no. 29., Art no. 29, 2021.
- [8] C. Wöber, W. Brannath, K. Schmidt, M. Kapitan, E. Rude, P. Wessely, Ç. Wöber-Bingöl, the PAMINA Study Group, "Prospective Analysis of Factors Related to Migraine Attacks: The PAMINA Study," *Cephalalgia*, vol. 17, no. 4, pp. 304-314, 2007.
- [9] P. T. Fukui, T. R. T. Goncalves, C. G. Strabelli, N. M. F. Lucchino, F. C. Matos, C. Fernanda, J. P. M. D. Santos, E. Zukerman, V. Zukerman-Guendler, J. P. Mercante, M. R. Masruha, "Trigger factors in migraine patients," *Arquivos de Neuro-Psiquiatria*, vol. 66, no. September 2008, pp. 494-499, 2008 .
- [10] J. M. Pavlovic, D. C. Buse, C.M. Sollars, S. Haut, R.B. Lipton, "Trigger Factors

- and Premonitory Features of Migraine Attacks: Summary of Studies,” *Headache The Journal of Head and Face Pain*, vol. 54, no. 10, pp. 1670-1679, 2014.
- [11] Turkish Neurological Society. (2019, Jun. 23). Türk Nöroloji Derneği Basın Bülteni 22 Temmuz “Dünya Beyin Günü - Migren”[Online]. Available: <https://www.noroloji.org.tr/haber/586/turk-noroloji-dernegi-basin-bulteni-22-temmuz-dunya-beyin-gunu-migren>.
- [12] R. Agosti, “Migraine burden of disease: From the patient's experience to a socio-economic view,” *The Journal of Headache and Pain*, vol. 58, pp. 17-32, 2018.
- [13] M. Bonafede, S. Sapra, N. Shah, S. Tepper, K. Cappell, P. Desai, “Direct and indirect healthcare resource utilization and costs among migraine patients in the United States,” *The Journal of Headache and Pain*, vol. 58, no.5, pp. 700-714, 2018.
- [14] T. Takeshima, Q. Wan, Y. Zhang, M. Komori, S. Stretton, N. Rajan, T. Treuer, K. Ueda, “Prevalence, burden, and clinical management of migraine in China, Japan, and South Korea: a comprehensive review of the literature,” *The Journal of Headache and Pain*, vol. 20, Art no. 111, 2019.
- [15] L. P. Wong, H. Alias, N. Bhoo-Pathy, I. Chung, Y. C. Chong, S. Kalra, Z. U. B. S. Shah, “Impact of migraine on workplace productivity and monetary loss: a study of employees in banking sector in Malaysia,” *The Journal of Headache and Pain*, vol. 21, no. 68, 2020.
- [16] Headache Classification Subcommittee of the International Headache Society, “The International Classification of Headache Disorders: 2nd edition,” *Cephalalgia*, vol. 24 (Suppl 1), pp. 9-160, 2004.
- [17] S. Tarantino, A. Capuano, R. Torriero, M. Citti, C. Vollono, S. Gentile, F. Vigevano, M. Valeriani, “Migraine Equivalents as Part of Migraine Syndrome in Childhood,” *Pediatric Neurology*, vol. 51, no. 5, pp. 645-649, 2014.
- [18] S. B. Akben, D. Tuncel, A. Alkan, “Classification of multi-channel EEG signals for migraine detection,” *Biomedical Research*, vol. 27, no.3, pp. 743-748, 2016.
- [19] P. A. Sanchez-Sanchez, J. R. García-González, J. M. R. Ascar, “Automatic migraine classification using artificial neural networks”, *F1000 Research*, vol. 16, no. 9, Art no. 618, 2020.
- [20] P. Domingos, M. Pazzani, “On the Optimality of the Simple Bayesian Classifier under Zero-One Loss,” *Machine Learning*, vol. 29, pp. 103-130, 1997.
- [21] P. A. Sánchez-Sánchez, J. R. García-González, J. M. R. Ascar. (2020). Migraine Classification Model [Online]. Available: <https://codeocean.com/capsule/1269964/tree/v1>.
- [22] F. Pedregosa, G. Varoquaux, A. Gramfort, V. Michel, B. Thirion, “Scikit-learn: Machine Learning in Python,” *Journal of Machine Learning Research*, vol. 12, no.85, pp. 2825-2830, 2011.
- [23] Zenodo.(2020). Pandas [computer software library] [Online]. Available: <https://pandas.pydata.org/>.

Evaluating the Impact of Building Materials on Indoor Air Quality: A Critical Analysis

Tuğçe Pekdoğan 

Adana Alparslan Türkeş Science and Technology University, Faculty of Architecture, Department of Architecture, Adana, Türkiye, tpekdogan@atu.edu.tr

ARTICLE INFO

ABSTRACT

Keywords:

Indoor air quality
Indoor pollution
Building materials
Bibliometrics

Article History:

Received: 23.03.2024

Accepted: 02.07.2024

Online Available: 01.08.2024

It is known that people generally spend 90% of their time indoors. Therefore, indoor air quality is a major concern for many people. Building materials play an important role in indoor air quality. Therefore, this study evaluates the role of building materials in IAQ by conducting a bibliometric analysis of articles from the Web of Science Core Collection and utilizing VOSviewer software to analyze publications from 2010 to 2023, focusing on the citation, year, country, and keywords co-occurrence. The analysis reveals key trends and gaps in the literature, highlighting the predominance of specific materials and pollutants. It also highlights that variability in building parameters makes attributing pollution sources difficult and underlines the need for context-specific assessments. These findings underscore the critical need to prioritize IAQ in building design and management to ensure safe and healthy indoor environments. This study manifests by methodologically mapping the research landscape on building materials and IAQ, guiding future empirical research.

1. Introduction

We all know that air quality greatly impacts our health and well-being. However, it is known that the building materials used in houses and buildings can also play a role in indoor air quality (IAQ). A successful building design requires a good indoor environment that not only impacts energy consumption but also affects the comfort of the inhabitants. Building environments vary in size, design, and function, influenced by the available building materials, climate, and culture. Building spaces are thermally conditioned to provide indoor and thermal comfort suitable for different weather conditions. The indoor environment is frequently contaminated with dangerous compounds and biological pollution sources, which can cause various health issues. IAQ is influenced by chemical, biological,

building materials, furnishing, design, and mechanical systems. Poor IAQ can greatly impact occupant health. Figure 1 illustrates the various sources and types of contaminants (chemical, biological, and physical) that impact users, leading to a range of diseases.

IAQ and the comfort of occupants are closely intertwined. The indoor environmental conditions include four major factors. These are thermal comfort, indoor air quality, visual comfort, and acoustic comfort. Frontczak et al. [2] found that IAQ significantly impacts occupants' satisfaction, with factors such as visual, thermal, acoustic, and indoor air quality contributing to overall satisfaction. Additionally, Astolfi and Pellerey [3] found that satisfaction with indoor environments is related to thermal, acoustic, visual, and air quality conditions.

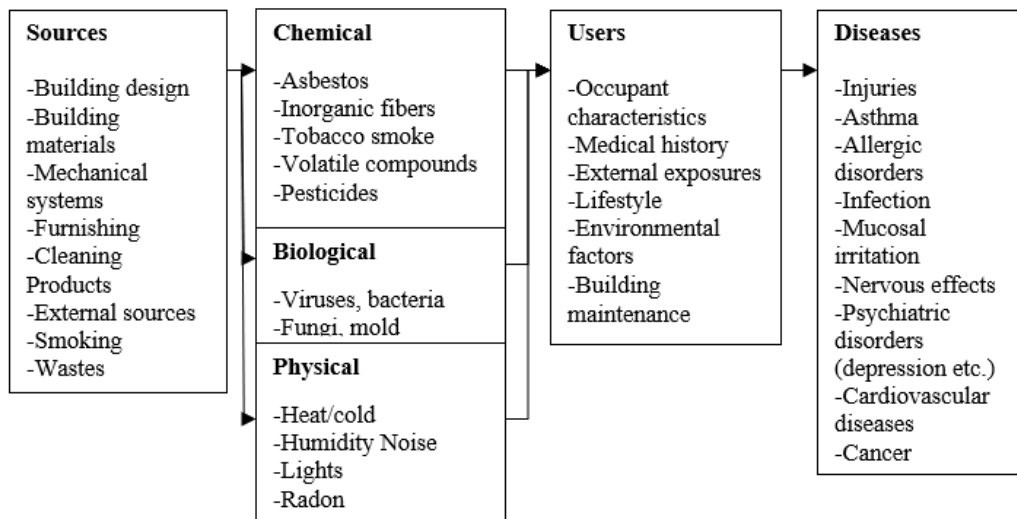


Figure 1. The built environment to health effects pathway [1]

Control of pollutant sources, removing contaminants from the air using effective filters, and dilution ventilation are important techniques for IAQ management. Architects must consider IAQ as a part of human-centered design strategies, requiring adequate ventilation systems, air filtration, humidity regulation, and temperature control [4]. Studies have shown that outdoor/indoor temperature, wind velocity, humidity, ventilation, and occupancy influence IAQ and thermal comfort.

According to the literature, Indoor Air Quality (IAQ) is crucial in minimizing Sick Building Syndrome (SBS) symptoms. IAQ is a significant concern for human health, and many studies have been conducted to address this issue. Numerous studies have focused on indoor air pollutants' sources, concentrations, and health risks, such as VOCs, PM, and biological pollutants (Table 1). Experimental studies, such as those conducted by [5] and [6], have specifically examined the impact of certain pollutants like viruses. Both studies aimed to provide architects with solutions to reduce the risk of disease transmission through effective air disinfection techniques, engineering controls, and design methods.

Related studies, such as Ma et al. [7], investigated the correlations among thermal comfort, IAQ, and human health and well-being factors. The study identified factors like outdoor and indoor temperature, wind velocity, relative humidity, physical features of the room, ventilation, and air exchange rates as contributing to IAQ. To improve IAQ and reduce

exposure to pollutants, studies proposed using green materials, plants, and nanomaterials [8-13]. For example, nanomaterials have been recommended to detoxify indoor air using heterogeneous photocatalysis [9]. In another case, houseplants reduced formaldehyde, a poisonous substance, in indoor air environments [13]. Green adhesives from renewable natural resources include tannin and cashew nutshell liquid. With the ability to have low formaldehyde release from wood products, they can hence boost indoor air quality [12].

Moreover, much better regulation is essential, enhancing the IAQ integrity [14]. Various researchers have indicated the importance of controlling of emission of volatile organic compounds (VOCs) due to their toxicity, especially from building material formaldehyde and other toxic substances [15-22].

Megahed et al. [23] studied design strategies in post-pandemic architecture to address IAQ challenges related to COVID-19. Their work aimed to provide architects with solutions to reduce the risk of disease transmission through effective air disinfection techniques, engineering controls, and design methods. Their conceptual model discusses the need for human-centered design through holistic IAQ management strategies like ventilation systems, air filtration, humidity control, and temperature regulation.

Building materials can release various pollutants, which can cause indoor air-related health problems [24]. Kozielska et al. [25] monitored

indoor pollutants in a residential building in Poland and found that CO₂ concentrations and BTEX were higher in homes with more people and fewer rooms, while NO₂ levels increased during cooking. The highest exposure risks were associated with PM₄ (with a diameter of $\leq 4 \mu\text{m}$), which poses significant health risks. Poor ventilation contributed to high pollutant levels.

Riaz et al. [8] explore the impact of microbial colonies in wet and damp indoor environments on human health. The authors discuss Building-associated illness (BRI) and SBS as significant health issues caused by indoor biological pollutants or bioaerosols such as bacteria, fungi, and viruses like coronavirus. They argue for using nanomaterials in heterogeneous photocatalysis for indoor air detoxification. They also stress the importance of cost-effective and safer materials to address indoor air quality and public health issues. Aydoğan et al. argue that biological methods based on plants and their associated microorganisms offer a promising solution to eliminate toxins from indoor environments. They discuss the psychological, physiological, and cognitive benefits of incorporating vegetation into indoor environments and cleaning the air [26].

Radon gas exposure raises lung cancer risk. Community-level data is vital to prioritize testing and remediation, conserve public health resources, and involve building owners [27]. Popa et al. emphasize that because of inadequate ventilation and the widespread use of new building materials that emit organic chemicals, indoor environments risk human discomfort and harm to health. It notes that several VOCs, some of which are known to be hazardous, mutagenic, or carcinogenic, have been found in indoor air [14].

To forecast PM_{2.5} conditions, Saini et al. suggest an IAQ monitoring system using Internet of Things-based sensors. The Vayurveda system was evaluated using a variety of datasets from both urban and rural areas, and updates were made available to users via an online portal. To establish the optimal model for real-time IAQ assessment, the authors evaluated various approaches at each stage of the development process [28]. When the relationships between

PM concentrations are examined, it is emphasized that location affects the results and that a uniform approach cannot effectively combat air pollution [29].

A dangerous pollutant with a large global production and consumption rate, formaldehyde, is discussed by Wang et al. as a source of pollution in Chinese homes. The study aimed to assess home formaldehyde pollution in 11 cities and investigate potential contributing factors. The findings indicate that northern cities, bedrooms, and warm seasons had higher pollution levels [15].

The BTEX group of hazardous organic chemicals, which includes benzene, toluene, ethylbenzene, and xylenes, is the paper's subject by Mokammel et al. The study evaluated the health hazards and factors of BTEX levels in indoor and outdoor air in rural communities in Ardebil, Iran. According to the findings, indoor air contained higher levels of BTEX than outdoor air. According to the report, tobacco smoke was a prominent temporary source of indoor BTEX, and using kerosene fuel for heating systems resulted in higher concentrations of BTEX [10].

Alfuraty discusses using eco-friendly materials in the design of interior decorations. The paper explores the current issues of the decoration materials, the idea, and the value of environmental protection together with the analysis of relevant information on modern green design, providing sustainable development of environmentally friendly material for interior design. The study observes that environmental protection materials help improve IAQ and include outdoor spaces in continuity with indoor spaces [30].

Mareş et al. evaluate the IAQ and energy efficiency of a single-family house in Cluj-Napoca County, Romania. Past research studies have found that with increased energy efficiency, there is reduced IAQ due to more energy efficiency, and there tends to be less natural ventilation. The research also observed that their installation caused a higher IAQ at low energy costs and significant energy savings compared to conventional ventilation [31].

The emissions of VOC and PAHs and their impact on IAQ were studied by Pineiro et al. The study looked at both primary and secondary emissions. The study found that an original coal-tar membrane used to waterproof the terrace was a possible source of contaminants. The article suggested that the contaminated materials should be removed, and ventilation systems should be installed to force the emitted gases from the rest of the contaminated slab outside to remediate the emission problem [16].

Adam et al. researched personal exposure to particulate-bound black carbon (BC) in urban areas of Trivandrum, India. The study aimed to quantify the levels of exposure to BC in a home-based and mobility-based scenario. The study found that BC concentrations were highest during transportation, such as using motorcycles and cars. The inhaled dose of BC was relatively larger in the mobility-based scenario. The study highlights the need to reduce personal exposure to fossil fuel-related particulate emissions in cities for public health reasons [11]. The article highlights the need for better legislation to improve household IAQ. It discusses sources of indoor air pollution, health impacts, and groups affected by COVID-19 and poor IAQ [17].

The emissions of VOCs and SVOCs and the presence of mold were examined by Gallon et al. at various stages of construction. According to the study, the entire implementation process is closely linked to the future indoor air quality of a building. During construction, mold spore measurements can reach high levels. They argue that SVOC and VOC emissions must be regulated due to their toxicity [18].

Alenezi et al.'s study in Kuwait measured the precise concentrations of VOCs and the associated risks in homes near fuel dispensing stations. The study found that BTEX has mutagenic and carcinogenic characteristics, leading to high health risks for the neighboring community [32].

In winter in Xi'an, China, Huang et al. measured harmful VOCs and carbonyls in typical apartments. The study discovered significant indoor levels of formaldehyde, acetone, naphthalene, methylene chloride, and

acetaldehyde in Chinese households. According to the study, the main sources of indoor VOCs and carbonyls are household items, smoking, cooking, paints and adhesives, furniture and building materials, and paints and adhesives [33]. Skaar et al. evaluated indoor emissions of toxic substances from products and their impact on human health, which is typically not considered in life cycle assessments (LCAs). They developed a method based on measured emission rates to calculate the impact on human health during the use stage of products that emit VOCs [34].

Building materials are significant sources of VOCs and Formaldehyde, which can pose health risks to occupants. With the increasing use of composite wood products in Korea, efforts are being made to reduce formaldehyde emissions in indoor environments using green adhesives from natural materials [35]. Toxic substances like Formaldehyde and VOCs released from building materials and wood composite products can be the cause of SBS symptoms. The placement of indoor plants in newly built apartment houses in Seoul has been shown to reduce SBS symptoms and ventilation [13].

Fungal metabolites such as beta-D-glucan, mycotoxins, and VOCs that induce ill health in susceptible occupants are strongly associated with indoor humidity and IAQ [19]. The use of composite wood products in indoor environments in Korea has increased, causing problems related to human health due to the emission of toxic substances such as Formaldehyde and VOCs. Green adhesives from natural materials such as tannin and cashew nutshell liquids reduce formaldehyde emissions and improve IAQ [20].

When combined with ventilation, indoor plant placement in newly constructed apartment buildings in Korea was proven to improve the mental and physical health of the occupants. The planting of indoor plants alone proved insufficient to minimize indoor hazardous chemical compounds despite improvements in mental health and some physical parameters [21]. This study used houseplants to examine the signs of SBS in 82 households in a recently constructed apartment building in Korea. The study proved

that houseplants positively impacted indoor air quality and formaldehyde levels. Some toxic chemical substances that cause SBS were quantitatively reduced by using houseplants [22].

Table 1. Overview of the past reviews

Ref.	Method	Sources	Pollutants
[8]	Review	TiO ₂ nanomaterials-based air filters and building coatings	Bioaerosols
[10]	Experimental	Heating systems, paints, building materials, smoking, cooking appliances, furnishings, and cleaning products	BTEX (benzene, toluene, ethylbenzene, and xylene)
[11]	Experimental	Black carbon	PM, PAHs
[13]	Experimental	For VOCs: paints, varnishes, waxes, conservation materials, solvents of anti-mold agents, and detergents. For benzene: plastics, resins, and detergents For formaldehyde and acetaldehyde: chipboards, various resins, paints, disinfectants For Terpenes: household detergents and perfumes	VOCs
[14]	Experimental	Construction materials	VOCs
[15]	Experimental+ Survey	Household characteristics (building age, distance from a traffic road, residence duration, window glass layers, decoration, furniture, and type of AC)	Formaldehyde
[16]	Experimental +Numerical	Coal-tar membrane for insulation	VOCs, PAHs
[17]	Analytical	-	Biological pollutants: Virus (COVID-19)
[18]	Experimental	Construction material	VOCSs, tVOCs
[19]	Analytical	Building materials (mineral wool, plasterboard, cardboard), cigarette smoke	Fungal metabolites, mycotoxins, and VOCs
[20]	Analytical	The wood-based panel, furniture, engineered flooring, and construction adhesive	Formaldehyde and VOCs
[21]	Experimental	-	Formaldehyde, CO, CO ₂
[22]	Experimental+ Survey	-	Toxic chemical
[24]	Experimental	MDF	VOCs, Formaldehyde
[25]	Experimental	For NO ₂ : gas-fired appliances (stoves, ovens, cookers, and water heaters) For VOCs: (installations, odors, room furnishings, furniture, carpets, electronics, etc.)	CO ₂ , VOCs, PM, NO ₂ , and BTEX
[21]	Experimental	-	Formaldehyde, CO, CO ₂
[26]	Review	-	-
[27]	Survey	Bedrock-penetrates building foundation and cracks	Radon
[28]	Experimental +IoT	Biomass fuels such as wood, cow dung, and kerosene	PM _{2.5} , PM ₁₀ , CO ₂ , CO, NO ₂ , and tVOC
[30]	Analytical	Surface finishing, furnishing, lighting system, equipment, and electrical devices	-
[31]	Experimental +Numerical	-	Radon
[32]	Experimental	Fuel dispensing station near the residential area	VOCs and BTEXs (benzene, toluene, ethyl benzene and xylenes)
[33]	Experimental	Furniture and building materials, paints and adhesives, household products, smoking, and cooking	Formaldehyde, acetaldehyde acetone, naphthalene, and methylene chloride
[34]	Experimental+ Numerical	Room furnishing	VOCs
[35]	Numerical	Building and furnishing materials (paint, coating, wood-based panels, plywood)	VOCs, Formaldehyde
[36]	Experimental	Floor/wall coverings, furniture, and the use of cleaning products, heating system	VOCs, benzene, ethylbenzene, o-xylene, and formaldehyde
[37]	Analytical	Indoor coal smoke	Formaldehyde
[38]	Experimental	House dust	Macromolecular organic compounds (MOC) and VOCs

Aldehyde compounds are the most common chemical group in the indoor air of atopy patients and control households in Korea. Atopic dermatitis and allergic asthma patients' homes

had considerably higher indoor air benzene, ethylbenzene, xylene, styrene, and formaldehyde substances. Higher quantities of formaldehyde and other VOCs were associated with house age,

floor or wall coverings, and the type of heating system [36].

The article reviews energy-saving in building and IAQ-related standards in China. It discusses how the two systems of building energy-saving and IAQ-related standards have been established separately. The article also explains the importance of formaldehyde as a pollution index in the IAQ control strategy in China [37]. Molhave et al. describe the composition of floor dust from Danish offices collected and analyzed to be used in an exposure experiment. The study found that the dust contained microorganisms, microfungi, endotoxins, allergens, macromolecular organic compounds (MOD), and VOCs. The article emphasized that sediments of dirt and dust resulted in airborne dust, which causes exposure and soiling problems [38].

These studies discuss IAQ, focusing on pollutants, ventilation, humidity control, and temperature regulation. Several studies emphasize the correlations between thermal comfort and human health. The use of green materials and houseplants to improve IAQ is also discussed. Common pollutants such as VOCs and Formaldehyde, as well as their potential health risks, are explored in multiple studies. Many studies recommend the adoption of better legislation and building standards to promote and ensure healthy IAQ. Controlling IAQ is crucial for mitigating SBS. Effective ventilation can maintain IAQ below set pollutant limits, but perceptions of air quality and ventilation rates are correlated. Therefore, adequate ventilation should be central to design or remediation efforts.

Although extensive research has investigated the impact of building materials on indoor air quality (IAQ), a gap exists in synthesizing this body of work through bibliometric analysis. This study was necessitated by consolidating and analyzing existing literature to identify common trends, methodologies, and gaps. Using a bibliometric approach using VOSviewer to review articles in the WoSCC systematically, this research provides a data-driven perspective on the impact of building materials on IAQ. Unlike previous reviews that qualitatively discuss the effects of specific materials, our study maps the research

landscape quantitatively. It provides insight into the most frequently studied materials, contaminants, and their associated health effects.

2. Methodology/Bibliometric Analysis

This study aimed to conduct a thorough literature review on IAQ in residential buildings by searching for relevant articles on the Web of Science (WoS) using various keywords. All data were obtained from the Web of Science Core Collection between 2010 to 2023. English-only document types were articles, letters, and reviews from the following indexes: SCI-EXPANDED, SSCI, ESCI and A&HCI, CPCI-S. Data from different sources were collected and analyzed. VOSviewer [39] software version 1.6.18 was used to display the literature on indoor air quality and building materials. The relevant publications were selected based on specific criteria such as publication year, language, journal, title, author, institution, keywords, document type, abstract, and citation counts. The data from these publications were entered into the software manually in text format [4].

In this software, analysis types such as citation analysis, co-citation analysis and bibliographic matching are frequently preferred. In addition to these traditional methods, this study incorporates an approach by analyzing keyword co-occurrences, specifically within word mining, enhancing the understanding of the field's thematic structures and semantic networks. The types of analysis in Table 2 show the types of bibliometric analyses used in this study. In the study conducted with VOSviewer, 4059 publications were found with the keyword "IAQ." In this analysis, the minimum frequency of occurrence of terms was chosen as 10, and there are 50,840 terms in total. 3264 of these terms meet the determined threshold value. As a rule of thumb in analysis, 60% of the terms were selected as the most relevant.

A bibliometric study examined the development of IAQ within scholarly articles and its correlation with environmental factors, reflecting its increasing prominence in academic research. This study utilized a systematic bibliographic review of literature central to the theme,

following a structured methodology: (1) establishing search parameters, keywords, and timeframes; (2) utilizing the Web of Science database for data retrieval; (3) refining and adjusting the search criteria; (4) comprehensive exportation of the data; (5) analyzing the gathered data and discussing the findings with five analysis.

Table 2. Types of bibliometric analysis used

Analysis Type	Characteristics Analyzed
Citation	
Bibliographic coupling	
Publication numbers (year)	Documents, Sources, Authors, Numbers,
Publication numbers (country)	Countries
Keyword Co-occurrence	

2.1. Findings

This section details the principal findings from a comprehensive examination of published articles, focusing on the correlation between

various building materials and their contributions to IAQ. Advanced bibliometric tools have allowed for a nuanced data analysis, revealing key materials and pollutants that play pivotal roles in indoor air environments. The five analyses, which are citation analysis, publication number according to year and country, bibliographic analysis and keyword co-occurrence analysis methods mentioned above, are examined below.

2.1.1. Citation analysis

Many researchers have made significant contributions to the field of indoor air quality. The analysis from WoSCC highlights the top ten authors with the most citations for their work and the titles of their publications. This comprehensive overview demonstrates the depth of research and the critical insights these scientists provide to understanding and improving indoor air quality.

Table 3. Citation analysis of top ten publications between 2010 to 2023

Ref. No.	Authors	Title	Doc. Type	Total Times Cited
[40]	Liu, C; Hsu, PC; Lee, HW; Ye, M; Zheng, GY; Liu, NA; Li, WY; Cui, Y	Transparent air filter for high-efficiency PM2.5capture	Article	816
[41]	Cao, XD; Dai, XL; Liu, JJ	Building energy-consumption status worldwide and the state-of-the-art technologies for zero-energy buildings during the past decade	Article	805
[42]	Rupp, RF; Vásquez, NG; Lamberts, R	A review of human thermal comfort in the built environment	Review	562
[43]	Sundell, J; Levin, H; Nazaroff, WW; Cain, WS; Fisk, WJ; Grimsrud, DT; Gyntelberg, F; Li, Y; Persily, AK; Pickering, AC; Samet, JM; Spengler, JD; Taylor, ST; Weschler, CJ	Ventilation rates and health: multidisciplinary review of the scientific literature	Article	510
[44]	Sarigiannis, DA; Karakitsios, SP; Gotti, A; Liakos, IL; Katsoyiannis, A	Exposure to major volatile organic compounds and carbonyls in European indoor environments and associated health risk	Review	434
[45]	Schober, W; Szendrei, K; Matzen, W; Osiander-Fuchs, H; Heitmann, D; Schettgen, T; Jörres, RA; Fromme, H	Use of electronic cigarettes (e-cigarettes) impairs indoor air quality and increases FeNO levels of e-cigarette consumers	Article	387
[46]	Schripp, T; Markewitz, D; Uhde, E; Salthammer, T	Does e-cigarette consumption cause passive vaping?	Article	374
[47]	Wolkoff, P	Indoor air humidity, air quality, and health - An overview	Review	366
[48]	Pacheco-Torgal, F; Jalali, S	Earth construction: Lessons from the past for future eco-efficient construction	Review	348
[49]	Vakiloroaya, V; Samali, B; Fakhar, A; Pishghadam, K	A review of different strategies for HVAC energy saving	Review	331

Table 3 below lists these influential authors and their seminal work, demonstrating the scope of the study and the impact of their research on the academic community and beyond. The most cited publication was the most cited publication between 2010 and 2023, with 816 citations. This study is a study on PM2.5, a particularly important air pollutant.

2.1.2. Bibliographic coupling

In this analysis, there are five clusters with ten or more authors. This analysis does not generally represent all 11610 authors who contributed to this topic, but only those who contributed to the central research network. Accordingly, the total power of co-authorship resources with other authors was calculated for one of the 45 authors.

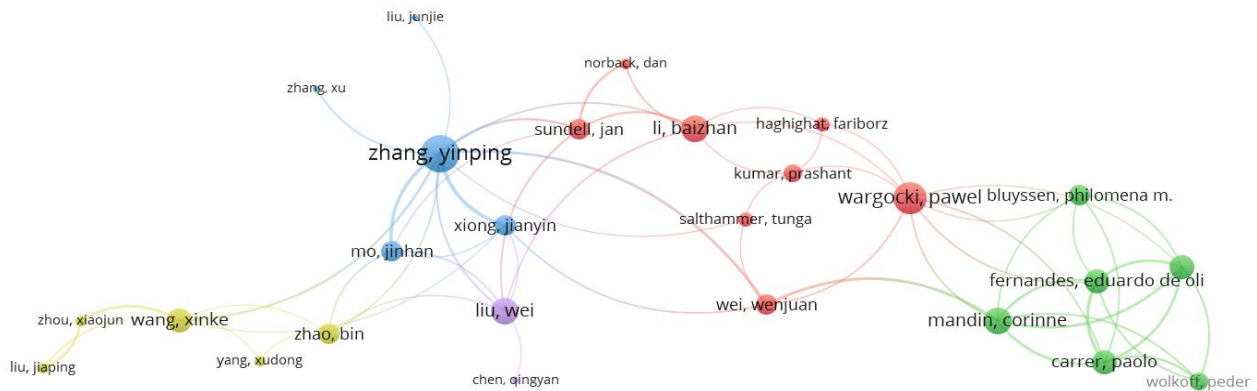


Figure 2. Network map visualization of IAQ keyword search

2.1.3. Year analysis

Figure 3 shows that there has been significant growth in research on indoor air quality over the years, reaching a peak in 2022, the highest number of publications at 1004, between 2010 to 2023.

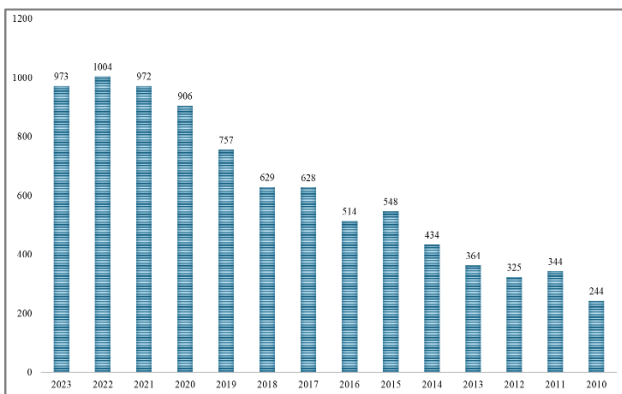


Figure 3. Number of publications related to IAQ between 2010 and 2023

Figure 2 shows a network map visualizing co-author affiliations within 4059 publications with IAQ keyword search. The network map reveals collaborations and relationships among scientists conducting IAQ research. Clusters of different colors represent specific research groups or authors who collaborate extensively. While each link represents at least one joint publication between the two authors, the links' density and thickness indicate this collaboration's frequency and strength.

The strongest connections within this central network of writers are Zhang Yinping, Wei Wenjuan, Li Baizhan, and Pawel Wargocki. Almost all of the strongest links are between the same authors.

The general trend shows a steady increase in publications, with some fluctuations, since 2010. This trend reflects the increasing awareness and importance of IAQ in recent years.

2.1.4. Country analysis

Figure 4 shows the number of publications on indoor air quality (IAQ) in different countries between 2010 and 2023. The USA is the country with the most publications in the field of indoor air quality, with 1605 publications. China ranks second with 778 publications. South Korea ranks third with 597 publications, while England ranks fourth with 550 publications. It is included in this ranking in Turkiye and ranks twenty-fourth with 133 publications.

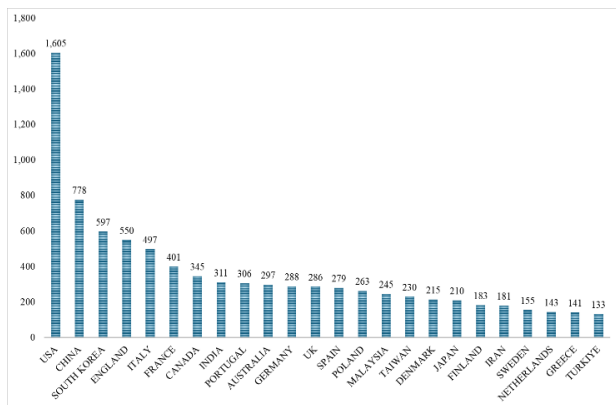


Figure 4. Number of publications on IAQ in different countries between 2010 and 2023

2.1.3. Keyword Co-occurrence

The distribution of the relationships between words or terms in documents based on indoor air quality is determined by keyword co-occurrence analysis. The color distributions on the map show that current and basic publications are clustered separately.

Figure 5 shows the flowchart maps the structured process of bibliometric analysis, which focuses on examining the impact of building materials on indoor air quality (IAQ). The first phase begins with bibliometric analysis, in which a search is performed using specified keywords in the Web of Science database. After the search, the data is downloaded and carefully analyzed.

Three different sets of keywords form the basis of our analysis:

Figure 6a corresponds to articles on "Building Materials OR Construction Materials" and

"Indoor Air Quality" OR "IAQ" representing the first broad search. In this figure a network with 4059 references and related with 3264 keywords in WoS.

Figure 6b narrows the scope by focusing on articles covering a more specific subset of the literature, 'Building Materials, Indoor Air Quality and Toxic Chemicals.' A search on WoS for "toxic chemicals" OR "chemicals" added to 'Building Materials and Indoor Air Quality,' resulted in a network with 2160 references and 2256 keywords, as seen in Figure 6b.

Figure 6c represents a further refined search covering "Building Materials OR Construction Materials" and "Indoor Air Quality" OR "IAQ," "Toxic Chemicals" OR "Chemicals," "Residential," and "Health" targeting articles. In addition to the previous keywords, a search for "residential" and "health" produced a network consisting of 34 references and 50 keywords, displayed in Figure 6c.

In Figures 6a, 6b and 6c, the size of the nodes in the graphs represents the frequency of occurrence, with keywords that commonly appear together and are linked by curves. The font size also indicates the prevalence of the keyword [50]. From this analysis, primary concepts like "environment," "health," and "building material" emerged as the most relevant, with secondary concepts closely linked to these primary ideas. These major themes emerge as focal points of research in the collected literature.

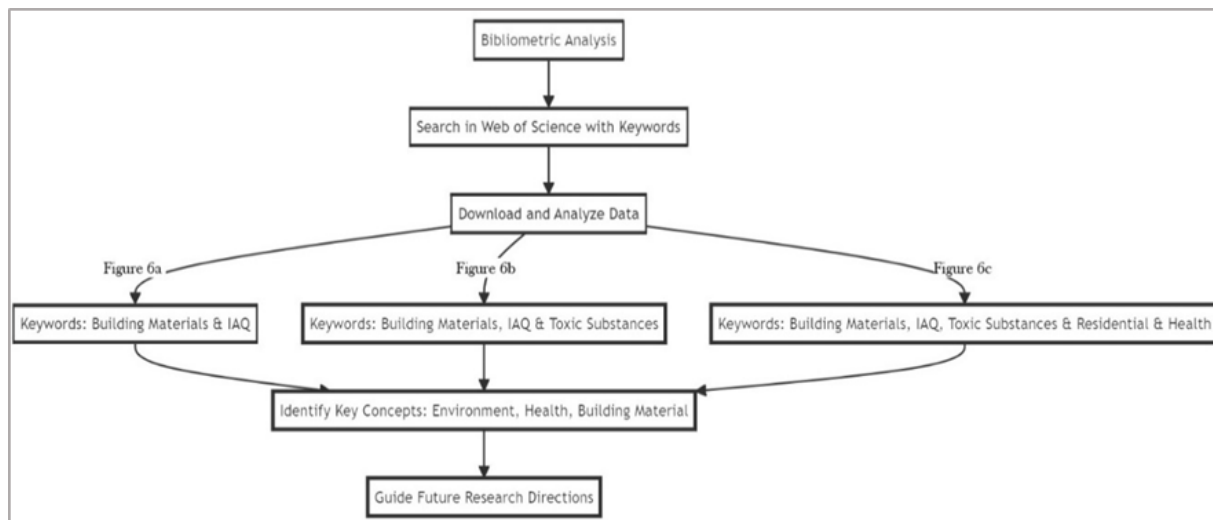


Figure 5. Flowchart of the Bibliometric Analysis

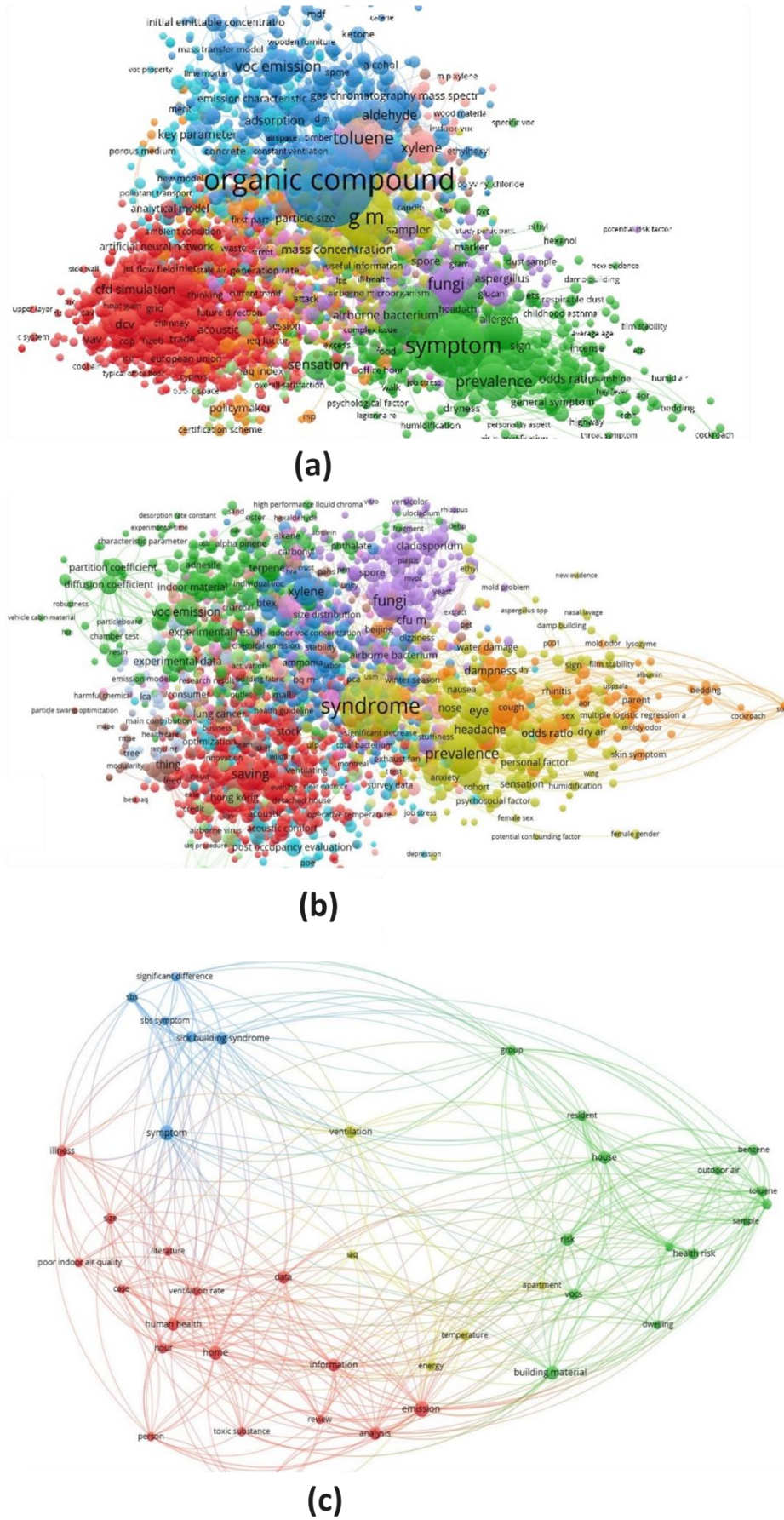


Figure 6. (a) Building materials and IAQ keyword co-occurrence analysis network visualization, (b) toxic substances keyword co-occurrence analysis network visualization, (c) Network visualization based on

analysis of the co-occurrence of the keywords building materials, IAQ, toxic substances, residential, and health

This bibliometric analysis helps understand IAQ's complex dynamics better and guides future research directions by highlighting under-researched areas and emerging trends. This article, therefore, contributes to the field by providing a comprehensive, methodologically novel approach to assessing the role of building materials in influencing indoor air environments. This study has some inherent limitations that should be considered. First is the database. The analysis is limited to articles from the WoSCC. Studies published in languages other than English or journals not indexed by this database are not included in this analysis. The second is time. The study examines the literature of a specific period (2010-2023). This provides insights into the latest trends. And keywords the results obtained from this bibliometric analysis are based on the assumed relevance and accuracy of the data of the resulting keywords. Thus, the selected keywords reflect trends and patterns in the academic literature.



Figure 7. Word cloud of the keywords in the selected papers

The bibliometric analysis conducted here focused on the effects of building materials on indoor air quality and the most common and mentioned pollutants, and in particular, studies in the literature examined the prevalence of total volatile organic compounds (TVOCs) and formaldehyde (CH₂O). Textometric analysis of the last 34 sampled articles reveals keywords repeated at least five times [51-52]. The word 'IAQ' was the most frequently used keyword 19 times. The word 'VOC' was the most frequently used keyword 12 times. This figure is graphically organized according to their frequency (Figure 7) in a word cloud obtained from an online word cloud generator – the size of each word is related to the frequency of its appearance. This analysis

prominence of terms like "pollutants," "IAQ," "health," and "building material" visually conveys the focal points of the literature on IAQ.

Analysis of scientific articles in the WoSCC, dating from 2010 to 2023, has led to some relevant discoveries outlined below:

Building Material Emissions: The literature reviewed consistently reported that various building materials are significant sources of indoor air pollutants. TVOC and formaldehyde emissions, particularly from materials such as paints, adhesives, and insulation materials, are of great concern due to their prevalence and impact on IAQ.

Health and Exposure Considerations: The relationship between exposure to indoor air pollutants from building materials and health outcomes is an issue addressed in all studies. Articles have highlighted the importance of IAQ management in residential environments, focusing on how pollutants such as formaldehyde and VOCs can affect health.

Emerging Trends: Incorporating new methodologies, such as in-home measurements and detection, to enable home testing of pollutants such as formaldehyde, CO₂, VOCs, etc., indicates a trend toward more accessible and user-friendly IAQ monitoring techniques.

Legal and Regulatory Insights: The articles reviewed call for improved regulatory standards and legislation to reduce the impact of indoor pollutants. Some studies include using green-certified materials and improved building practices for a healthier indoor environment.

These findings highlight the impact of building materials, construction practices, and IAQ, affecting health, environmental policy, and material use. According to this analysis, it has been observed that some pollutants and several factors directly affect IAQ. These can be grouped under 3 main headings according to the literature review.

Chemical pollutants

These substances are released into the air from various sources, including household and

industrial chemicals. Some of the most common chemical pollutants that affect IAQ include cigarette smoke, VOCs found in interior paints and varnishes, chemicals used in cleaning products and furniture, and scented products such as incense and deodorizers [53]. VOC concentration in indoor environments can increase due to ventilation in areas with high traffic [54]. Studies have found that bedrooms have the highest levels of TVOCs compared to other areas, such as kitchens, living rooms, and workplaces, with emissions from furniture and carpeting being possible contributors [55].

Biological pollutants

These living organisms can be found in the air and can cause allergic reactions, infections, and other health concerns. For instance, ultrafine particles were significant risk factors for dermal symptoms [56]. The most common biological pollutants that affect IAQ are mold, fungi and bacteria, pet dander and soil, pollen, and other allergens.

Environmental factors

The quality of air indoors can be affected by environmental factors. Air pollution from external sources can significantly impact indoor air quality. Polluted outdoor air will create indoor air pollution. Therefore, the IAQ affects the indoor environment, location, climate, temperature, and light. High temperatures cause mold and bacteria to grow, while low light levels create a suitable environment for them to thrive and multiply. Also, low humidity can cause respiratory problems, while high humidity can encourage mold growth and other biological contaminants.

It is known that people, in general, spend 90% of their time indoors. This is why the IAQ is a major concern for many people. Building materials can adversely affect indoor air quality by releasing VOCs and Formaldehyde, which can cause respiratory irritation and trigger allergic reactions in some people. According to an article published by Artiola et al., all respiratory symptoms, such as coughing and throat irritation, are responsible for all VOC cases released by paint, carpet, furniture, insulation, and similar building materials [57]. VOC release can damage the respiratory system and affect immunity, leading

to chronic diseases such as asthma or allergies later in life.

Improving IAQ is important in creating a safe and healthy living space. It is necessary to know how the building materials used in the construction of buildings affect health and the precautions and requirements to be taken in this regard.

2.2. IAQ requirements

Ensuring that the quality of IEQ is good for the occupants' overall mental and physical well-being is crucial. Achieving this involves considering factors such as IAQ, lighting, acoustics, and thermal comfort. National and international organizations have established building standards, regulations, and guidelines to promote good IAQ and thermal comfort. These standards ensure that occupants of indoor environments are healthy and comfortable.

Indoor air that is of low quality can have negative effects on both health and comfort. It can also have a detrimental impact on performance in a variety of settings, from offices to schools and healthcare facilities. Global guidelines and standards exist for indoor air pollutants. Various studies have been conducted on the IAQ, following the regulations and standards of different countries. Information regarding the distribution of global deaths caused by indoor and outdoor air pollution, and annual CO₂ emissions can be found in Table 4. The table also provides data on the relative percentage contribution of publications in Indoor Air Quality for various countries.

Most deaths per 100,000 people are due to indoor air pollution in India and China. India and China are the two countries that have the highest fatalities resulting from outdoor air pollution. Türkiye, South Korea, and Greece follow these countries. This information is based on statistics from 1990 to 2019. The United States contributed the most publications regarding IAQ, followed by China, the United Kingdom, Italy, South Korea, Canada, and India, according to a keyword search of the literature databases. The Scopus literature database identified 16.245 papers between 2010 and 2023 when the term

"indoor air quality" was used in a search. Looking at the table, the highest contribution was made by the United States, 14.66%, and China, 13.14%, while the United Kingdom, South Korea, Italy, and Canada followed with 5.31%, 4.28%, respectively, 4.27%, and 3.19%.

Table 4. Compared mortality due to indoor/outdoor air pollution, annual tons of CO₂, and contributions to the overall number of IAQ publications for the respective countries [58]

Country	Share of deaths from indoor/outdoor air pollution (per 100,000) in 1990		Share of deaths from indoor/outdoor air pollution (per 100,000) in 2019		Annual CO ₂ emissions tonnes		Contributions to the total amount of publications IAQ	National/ International bodies involved in setting air quality guidelines and standards		
	Indoor	Outdoor	Indoor	Outdoor	Start in 1860	End in 2021		%	2010-2023	%
Australia	0.76	12.42	0.03	4.06	509,296 t	391,187,420 t	669,637	40.9	2.52	NHMRC
Belgium	0.29	45.21	0.02	13.08	16,458,689 t	95,722,280 t	1,425	16.1	0.99	AIVC, SHC
Canada	0.28	18.52	0.01	5.35	458,000 t	545,634,500 t	15,587.75	51.9	3.19	Health
China	195.56	77.15	20.73	81.28		11,472,369,000 t	9.84 b.t.	21.35	13.14	AIVC,
Denmark	0.17	44.26	0.02	10.07	784,096 t	29,576,956 t	25,577	31.4	1.93	DICL
France	0.25	26.85	0.02	8.73	41,241,984 t	305,963,700 t	14,994	45.4	2.79	ANSES,

2.3. International standards for IAQ

There are different standards for IAQ across the world, with some countries having national regulations or international standards and others having their own guidelines. The WHO and the EPA guidelines are generally followed in the European Community. IAQ is a major concern for many governments and health organizations due to its impact on human health, and the European Union has encouraged its members to act against air pollution. National organizations and the WHO have set standards and guidelines to reduce the air pollutants people are exposed to. Table 5 summarizes the indoor air contaminant standards and guidelines set by different international organizations. CO₂ concentration is a crucial aspect of IAQ and is often used to indicate air exchange rates and whether fresh air is being provided sufficiently. Various organizations suggest different CO₂ concentration limit values, with ASHRAE and OSHA recommending no more than 700-1000 ppm above outdoor concentrations, the EPA suggesting 800 ppm, and WHO and CIBSE suggesting 1000 ppm.

Table 5. WHO and some national agencies stipulate the primary IAQ standards and guidelines

Organization	Reference
American Society of Heating, Refrigerating, and Air Conditioning Engineers (ASHRAE Standard-55)	[59]
Chartered Institution of Building Services Engineers (CIBSE)	[60]
Occupational Safety and Health Administration (OSHA)	[61]
US Environmental Protection Agency (EPA)	[62]
World Health Organization (WHO)	[63]

2.4. Strategies to improve indoor air quality

Ensuring good IAQ is crucial for maintaining good health and well-being. As most individuals spend around 90% of their lives indoors, it is important to prioritize indoor air quality. Therefore, you should be aware of the dangers indoors. As can be seen in the literature review above, building materials have a great impact on IAQ's various pollutants and VOCs. Improving IAQ is important in creating a safe and healthy living space. Construction, rebuilding, remodeling, extensions, collapse, infrastructure maintenance, and other activities generate 10 billion tons of waste products annually [64]. As

these materials enter our air, their use adversely affects IAQ.

Understanding the different building materials and how they affect IAQ is key to maintaining a healthy environment. IAQ can be adversely affected by the presence of various building materials. For example, wood is a common building material that releases PM over time. Building materials such as concrete, mortar, and stone emit particles over time. Certain building materials and chemicals can contribute to indoor air contamination, worsened by increased building airtightness. Petroleum distillates and VOCs are a particular concern as they continue to emit toxins after installation [65].

Strategies to improve indoor air quality include: Using ventilation and air filtration systems: A well-ventilated home or office can help minimize air pollutants. Using proper ventilation, fresh outdoor air can be circulated throughout the building. Air filtration systems can also help remove dust, pollen, and other airborne contaminants. In addition, more advanced innovative products can be used. Using decentralized ventilation systems [66] instead of central ventilation systems is a good choice both in terms of energy saving and improving indoor air quality.

Banning the smoking of any tobacco product: Cigarette smoke contains various toxic chemicals that can harm smokers and non-smokers. Banning smoking in homes, workplaces, and public places can reduce the risk of respiratory and other health problems from second-hand smoke.

Using low-emission materials in product selection: When choosing products for our homes or workplaces, it is essential to consider the impact of chemical emissions. Furniture, wall paint, flooring, etc., materials may contain chemicals that may cause eye and respiratory tract irritation. Studies have shown that some of the tested furniture has a high emission rate. It has been determined that some furniture used indoors can cause high concentrations of formaldehyde. Therefore, by choosing materials with low emissions, we can reduce the risk of indoor air pollution [67].

Regular maintenance of building damage: Proper maintenance of buildings can help prevent mold and fungus growth. Structural damage can create leaks and dampness, providing a breeding ground for bacteria, mold, or other harmful substances. Repairing any damage to the structure can prevent the increase of indoor pollutants.

Using natural cleaning products: Many traditional cleaning products contain toxic chemicals that can cause skin and respiratory irritation and allergies. Natural cleaning products can be used as a good alternative for cleaning while affecting health less negatively [68].

Controlling the humidity level: High humidity levels can cause respiratory problems and allergic reactions. To prevent these problems, the growth of algae, mold and harmful mites can be prevented by preventing the increase in indoor humidity of houses and workplaces, especially in the bathroom and kitchen [34].

Providing natural light: While natural light positively affects people, especially psychologically, it is also important for health. Good lighting can reduce the risk of indoor air pollution and improve indoor conditions.

Using plants: Plants are natural air filters that add a decorative touch while removing toxins. We can improve IAQ and support a healthy environment by including plants in our living and working spaces [25].

3. Conclusion

IAQ has gained significant attention in the past few years due to various factors, such as the COVID-19 outbreak and increased awareness of the health hazards linked with inadequate IAQ. The need of the hour is to have efficient and effective solutions to improve IAQ to mitigate its associated health risks. That is why researchers and developers are working on several solutions. These include technologies such as ventilation systems, air cleaners, etc. In addition, various international organizations are developing guidelines and standards to meet the requirement.

The extensive bibliometric analysis in this study has examined indoor air pollutants and their

health effects, as well as current standards and guidelines, and the studies in the literature and related keywords have been analyzed with VOSviewer with citation, bibliographic coupling, publication numbers (year), publication numbers (country) and keyword co-occurrence analysis. According to these network visualizations that have been made, documents, sources, authors, numbers and countries with the keyword of building materials, which are especially related to the main issues such as health, emissions, viruses, and bacteria. The studies generally focus on parameters such as Formaldehyde, PM, volatile compounds, CO₂, and CO. It has been emphasized that allergic reactions and respiratory problems are seen due to these pollutants.

This study also emphasizes the necessity of considering furnishings and construction materials as potential sources of indoor air pollution. Additionally, since the parameters differ in each situation, it is impossible to identify the sources of pollution that are liable for every building. Every study needs to be judged on its terms, considering its environment. IAQ must be prioritized as a fundamental building design and management component to guarantee everyone a secure and healthy indoor environment.

Considering the shortcomings illuminated by this comprehensive literature analysis study, future research efforts should focus on this topic:

Development of Low Emission Building Materials: Research of new building materials that significantly reduce or eliminate the emission of harmful pollutants and the necessity of green-certified interior materials.

Health Effect Studies: Conduct comprehensive studies to understand the health effects of continuous exposure to various IAQ pollutants, especially in different climatic situations.

Technology-Assisted IAQ Monitoring: Development of real-time IAQ monitoring technologies to provide immediate and accurate assessments.

Holistic IAQ Management Models: Creating models that integrate IAQ management with

sustainable building practices, considering emerging phenomena such as climate change and urbanization.

Policy Development and Regulatory Frameworks: Development of comprehensive policies and regulatory frameworks that can govern the selection, use and disposal of construction materials about IAQ.

Harmonization of Global IAQ Standards: Considering the inequality in IAQ standards in different countries, achieving a global consensus by researching harmonizing international IAQ guidelines.

Article Information Form

Acknowledgments

The author would like to thank all who offered indirect support and contributions to this study. Their valuable insights and perspectives have been instrumental in completing this research.

Funding

The author has not received any financial support for this study's research, authorship, or publication.

The Declaration of Conflict of Interest/ Common Interest

The author has declared no conflict of interest or common interest.

The Declaration of Ethics Committee Approval

This study does not require ethics committee permission or any special permission.

The Declaration of Research and Publication Ethics

The author of the paper declares that it complies with the scientific, ethical and quotation rules of SAUJS in all processes of the paper and that do not make any falsification of the data collected. In addition, the author declares that Sakarya University Journal of Science and its editorial board have no responsibility for any ethical violations that may be encountered and that this study has not been evaluated in any academic publication environment other than Sakarya University Journal of Science.

Copyright Statement

The author owns the copyright of work published in the journal, which is published under the CC BY-NC 4.0 license.

References

- [1] F. Wu, D. Jacobs, C. Mitchell, D. Miller, M. H. Karol, “Improving indoor environmental quality for public health: impediments and policy recommendations,” *Environmental health perspectives*, vol. 115, no. 6, pp. 953–957, 2007.
- [2] M. Frontczak, S. Schiavon, J. Goins, E. Arens, H. Zhang, P. Wargoeki, “Quantitative relationships between occupant satisfaction and satisfaction aspects of indoor environmental quality and building design,” *Indoor air*, vol. 22, no. 2, pp. 119–131, 2012.
- [3] A. Astolfi, F. Pellerey, “Subjective and objective assessment of acoustical and overall environmental quality in secondary school classrooms,” *The Journal of the Acoustical Society of America*, vol. 123, no. 1, pp. 163–173, 2008.
- [4] T. Pekdoğan, “Design of learning spaces in the post-pandemic era,” *International Journal of Sustainable Building Technology and Urban Development*, vol. 13, no. 4, pp. 500 – 513, 2022
- [5] S. Mentese, N. A. Mirici, T. Elbir, E. Palaz, D.T. Mumcuoglu, O. Cotuker, C. Bakar, S. Oymak, M. T. Otkun, “A long-term multi-parametric monitoring study: Indoor air quality (IAQ) and the sources of the pollutants, prevalence of sick building syndrome (SBS) symptoms, and respiratory health indicators,” *Atmospheric Pollution Research*, vol. 11, no. 12, pp. 2270–2281, 2020.
- [6] Y. S. Lee, S. Kim, “Indoor environmental quality in LEED-certified buildings in the U.S.,” *Journal of Asian Architecture and Building Engineering*, 2008
- [7] N. Ma, D. Aviv, H. Guo, W. W. Braham, “Measuring the right factors: A review of variables and models for thermal comfort and indoor air quality,” *Renewable and Sustainable Energy Reviews*, vol. 135, no. March 2020, p. 110436, 2021
- [8] N. Riaz, M. S. Khan, M. Bilal, S. Ullah, A.G. Al-Sehemi, “Photocatalytic Inactivation of Bioaerosols: A Short Review on Emerging Technologies,” *Current Analytical Chemistry*, vol. 17, no. 1, 2020
- [9] J. Saini, M. Dutta, G. Marques, “Indoor air quality monitoring systems based on internet of things: A systematic review,” *International Journal of Environmental Research and Public Health*, vol. 17, no. 14. 2020.
- [10] A. Mokammel, R. Rostami, S. Niazi, A. Asgari, M. Fazlzadeh, “BTEX levels in rural households: Heating system, building characteristic impacts and lifetime excess cancer risk assessment,” *Environmental Pollution*, vol. 298, 2022
- [11] M. G. Adam, P. T. M. Tran, D. K. W. Cheong, S. Chandra Sekhar, K. W. Tham, R. Balasubramanian, “Assessment of home-based and mobility-based exposure to black carbon in an urban environment: a pilot study,” *International Journal of Environmental Research and Public Health*, vol. 18, no. 9, p. 5028, 2021.
- [12] H. Guo, L. Huang, W. Song, X. Wang, H. Wang, X. Zhao, “Evaluation of the summer overheating phenomenon in reinforced concrete and cross-laminated timber residential buildings in the cold and severe cold regions of China,” *Energies*, 2020


- [13] C. Patkó, I. Patkó, Z. Pásztor, "Indoor air quality testing in low-energy wooden houses: Measurement of formaldehyde and VOC-s," *Acta Polytechnica Hungarica*, vol. 10, no. 8, 2013
- [14] M. Popa, M. S. Popa, "Use of volatile organic compounds as an indicator in indoor air quality investigations," in *Seventh International Symposium on Laser Metrology Applied to Science, Industry, and Everyday Life*, 2002, pp. 1090–1093.
- [15] X. Wang, X. Han, L. Fan, L. Li, C. Wang, S. Gong, J. Qi, T. Ge, H. Liu, X. Li, Y. Cao, M. Liu, Q. Wang, L. Su, X. Yao, X. Wang, "The relationship of residential formaldehyde pollution in 11 Chinese cities to schoolchildren pneumonia prevalence in actual living condition," *Environmental Research*, vol. 214, 2022
- [16] R. Piñeiro, E. Jimenez-Relinque, R. Nevshupa, M. Castellote, "Primary and secondary emissions of VOCs and PAHs in indoor air from a waterproof coal-tar membrane: Diagnosis and remediation," *International Journal of Environmental Research and Public Health*, vol. 18, no. 23, 2021
- [17] J. C. Nwanaji-Enwerem, J. G. Allen, P. I. Beamer, "Another invisible enemy indoors: COVID-19, human health, the home, and United States indoor air policy," *Journal of Exposure Science and Environmental Epidemiology*, vol. 30, no. 5. 2020.
- [18] V. Gallon, P. Le Cann, M. Sanchez, C. Dematteo, B. Le Bot, "Emissions of VOCs, SVOCs, and mold during the construction process: Contribution to indoor air quality and future occupants' exposure," *Indoor Air*, vol. 30, no. 4, 2020
- [19] E. Piecková, "Adverse health effects of indoor moulds," *Arhiv za Higijenu Rada i Toksikologiju*, vol. 63, no. 4. 2012.
- [20] J. Lee, J. Jeon, S. Kim, "Green Adhesives Using Tannin and Cashew Nut Shell Liquid for Environment-friendly Furniture Materials," *Journal of the Korea furniture Society*, vol. 22, no. 3, 2011.
- [21] H. H. Kim, J. W. Park, J. Y. Yang, K. J. Kim, J. Y. Lee, D. C. Shin, Y. W. Lim, "Evaluating the relative health of residents in newly built apartment houses according to the presence of indoor plants," *Journal of the Japanese Society for Horticultural Science*, vol. 79, no. 2, 2010
- [22] Y. W. Lim, H. H. Kim, J. Y. Yang, K. J. Kim, J. Y. Lee, D. C. Shin, "Improvement of indoor air quality by houseplants in new-built apartment buildings," *Journal of the Japanese Society for Horticultural Science*, vol. 78, no. 4, 2009
- [23] N. A. Megahed, E. M. Ghoneim, "Antivirus-built environment: Lessons learned from Covid-19 pandemic," *Sustainable Cities and Society*, 2020
- [24] J. H. Lee, S. G. Jeong, S. Kim, "Performance evaluation of infrared bake-out for reducing VOCs and formaldehyde emission in MDF panels," *BioResources*, vol. 11, no. 1, 2016
- [25] B. Kozielska, A. Mainka, M. Żak, D. Kaleta, W. Mucha, "Indoor air quality in residential buildings in Upper Silesia, Poland," *Building and Environment*, vol. 177, p. 106914, 2020.
- [26] A. Aydogan, R. Cerone, "Review of the effects of plants on indoor environments," *Indoor and Built Environment*, vol. 30, no. 4. 2021.

- [27] S. B. Henderson, T. Kosatsky, P. Barn, "How to ensure that national radon survey results are useful for public health practice," *Canadian Journal of Public Health*, vol. 103, no. 3, 2012
- [28] J. Saini, M. Dutta, G. Marques, "Modeling indoor PM2.5 using Adaptive Dynamic Fuzzy Inference System Tree (ADFIST) on Internet of Things-based sensor network data," *Internet of Things (Netherlands)*, vol. 20, 2022
- [29] T. Pekdoğan, M. T. Udriștioiu, H. Yildizhan, A. Ameen, "From Local Issues to Global Impacts: Evidence of Air Pollution for Romania and Turkey," *Sensors*, vol. 24, no. 4, p. 1320, 2024.
- [30] A. B. Alfuraty, "Sustainable Environment in Interior Design: Design by Choosing Sustainable Materials," in *IOP Conference Series: Materials Science and Engineering*, 2020.
- [31] I. C. Mareș, T. Catalina, M. A. Istrate, A. Cucuș, T. Dicu, B. D. Burghel, K. Hening, L. L. Popescu, R. S. Popescu, "Research on best solution for improving indoor air quality and reducing energy consumption in a high-risk radon dwelling from Romania," *International Journal of Environmental Research and Public Health*, vol. 18, no. 23, 2021
- [32] R. A. Alenezi, N. Aldaihan, "Impact of fuel dispensing stations in the vicinity residential homes on the indoor and outdoor air quality," *International Journal of Environmental Science and Technology*, vol. 16, no. 6, 2019
- [33] Y. Huang, T. Su, L. Wang, N. Wang, Y. Xue, W. Dai, S. C. Lee, J. Cao, S. S. H. Ho, "Evaluation and characterization of volatile air toxics indoors in a heavy polluted city of northwestern China in wintertime," *Science of the Total Environment*, vol. 662, 2019
- [34] C. Skaar, R. B. Jørgensen, "Integrating human health impact from indoor emissions into an LCA: A case study evaluating the significance of the use stage," *International Journal of Life Cycle Assessment*, vol. 18, no. 3, 2013
- [35] C. W. F. Yu, J. T. Kim, "Material emissions and indoor simulation," *Indoor and Built Environment*, vol. 22, no. 1, 2013
- [36] D. W. Choi, K. W. Moon, S. H. Byeon, E. Il Lee, D. G. Sul, J. H. Lee, E. H. Oh, Y. H. Kim, "Indoor volatile organic compounds in atopy patients' houses in South Korea," *Indoor and Built Environment*, vol. 18, no. 2, 2009
- [37] Z. Wang, Z. Bai, H. Yu, J. Zhang, T. Zhu, "Regulatory standards related to building energy conservation and indoor-air-quality during rapid urbanization in China," in *Energy and Buildings*, 2004.
- [38] L. Mølhave, T. Schneider, S. K. Kjærgaard, L. Larsen, S. Norn, O. Jørgensen, "House dust in seven Danish offices," *Atmospheric Environment*, vol. 34, no. 28, 2000
- [39] N. J. Van Eck, L. Waltman, "Software survey: VOSviewer, a computer program for bibliometric mapping," *Scientometrics*, 2010
- [40] W. Liang, Y. Xu, X. Li, X. X. Wang, H. Di Zhang, M. Yu, S. Ramakrishna, Y. Z. Long, "Transparent Polyurethane Nanofiber Air Filter for High-Efficiency PM2.5 Capture," *Nanoscale Research Letters*, vol. 14, no. 1, 2019
- [41] X. Cao, X. Dai, J. Liu, "Building energy-consumption status worldwide and the state-of-the-art technologies for zero-energy buildings during the past decade," *Energy and Buildings*, vol. 128, 2016

- [42] R. F. Rupp, N. G. Vásquez, R. Lamberts, “A review of human thermal comfort in the built environment,” *Energy and Buildings*, vol. 105. 2015.
- [43] J. Sundell, H. Levin, W. W. Nazaroff, W. S. Cain, W. J. Fisk, D. T. Grimsrud, F. Gyntelberg, Y. Li, A. K. Persily, A. C. Pickering, J. M. Samet, J. D. Spengler, S. T. Taylor, C. J. Weschler, “Ventilation rates and health: Multidisciplinary review of the scientific literature,” *Indoor Air*, vol. 21, no. 3, 2011
- [44] D. A. Sarigiannis, S. P. Karakitsios, A. Gotti, I. L. Liakos, A. Katsoyiannis, “Exposure to major volatile organic compounds and carbonyls in European indoor environments and associated health risk,” *Environment International*, vol. 37, no. 4. 2011.
- [45] W. Schober, K. Szendrei, W. Matzen, H. Osiander-Fuchs, D. Heitmann, T. Schettgen, R. A. Jörres, H. Fromme, “Use of electronic cigarettes (e-cigarettes) impairs indoor air quality and increases FeNO levels of e-cigarette consumers,” *International Journal of Hygiene and Environmental Health*, vol. 217, no. 6, 2014
- [46] T. Schripp, D. Markewitz, E. Uhde, T. Salthammer, “Does e-cigarette consumption cause passive vaping?,” *Indoor Air*, vol. 23, no. 1, 2013
- [47] P. Wolkoff, “Indoor air humidity, air quality, and health – An overview,” *International Journal of Hygiene and Environmental Health*, vol. 221, no. 3. 2018.
- [48] F. Pacheco-Torgal, S. Jalali, “Earth construction: Lessons from the past for future eco-efficient construction,” *Construction and Building Materials*, vol. 29. 2012.
- [49] V. Vakiloroyaya, B. Samali, A. Fakhar, K. Pishghadam, “A review of different strategies for HVAC energy saving,” *Energy Conversion and Management*, vol. 77, 2014
- [50] Y. Yu, Y. Li, Z. Zhang, Z. Gu, H. Zhong, Q. Zha, L. Yang, C. Zhu, E. Chen, “A bibliometric analysis using VOSviewer of publications on COVID-19,” *Annals of Translational Medicine*, 2020
- [51] A. Fonseca, I. Abreu, M. J. Guerreiro, C. Abreu, R. Silva, N. Barros, “Indoor air quality and sustainability management study in three Portuguese healthcare units,” *Sustainability (Switzerland)*, 2018
- [52] H. Ali, G. Yilmaz, Z. Fareed, F. Shahzad, M. Ahmad, “Impact of novel coronavirus (COVID-19) on daily routines and air environment: evidence from Turkey,” *Air Quality, Atmosphere and Health*, vol. 14, no. 3, 2021
- [53] I. Sakellaris, D. Saraga, C. Mandin, Y. de Kluizenaar, S. Fossati, A. Spinazzè, A. Cattaneo, V. Mihucz, T. Szigeti, E. de Oliveira Fernandes, K. Kalimeri, R. Mabilia, P. Carrer, J. Bartzis, “Association of subjective health symptoms with indoor air quality in European office buildings: The OFFICAIR project,” *Indoor Air*, vol. 31, no. 2, 2021
- [54] C. R. de O. Nunes, B. Sánchez, C. E. N. Gatts, C. M. S. de Almeida, M. C. Canela, “Evaluation of volatile organic compounds coupled to seasonality effects in indoor air from a commercial office in Madrid (Spain) applying chemometric techniques,” *Science of the Total Environment*, vol. 650, 2019
- [55] X. Chen, F. Li, C. Liu, J. Yang, J. Zhang, C. Peng, “Monitoring, human health risk assessment and optimized management for

- typical pollutants in indoor air from random Families of University staff, Wuhan City, China,” *Sustainability (Switzerland)*, vol. 9, no. 7, 2017
- [56] Y. Sun, J. Hou, R. Cheng, Y. Sheng, X. Zhang, J. Sundell, “Indoor air quality, ventilation and their associations with sick building syndrome in Chinese homes,” *Energy and Buildings*, vol. 197, pp. 112–119, Aug.2019
- [57] J. F. Artiola, K. A. Reynolds, M. L. Brusseau, “Urban and Household Pollution,” in *Environmental and Pollution Science*, 2019.
- [58] OurWorldInData, “{CO₂} emissions per capita vs {GDP} per capita,” *Our World in Data*. 2016.
- [59] S. C. Turner, G. Paliaga, B. M. Lynch, E. A. Arens, R. M. Aynsley, G. S. Brager, J. J. Deringer, J. M. Ferguson, J. M. Filler, J. J. Hogeling, D. Int-hout, A. G. Kwok, H. F. Levy, E. M. Sterling, J. L. Stoops, S. T. Taylor, R. W. Tinsley, K. W. Cooper, K. W. Dean, F. Myers, J.C. Peterson, “ASHRAE STANDARD 55,” *American Society of Heating, Refrigerating and Air-Conditioning Engineers, Inc.*, 2010.
- [60] CIBSE, “TM36: Climate change and the indoor environment: impacts and adaptation,” *The Chartered Institution of Building Service Engineers*, 2005.
- [61] “OSHA Technical Manual (OTM) | Section IV: Chapter 4 - Industrial Robots and Robot System Safety | Occupational Safety and Health Administration,” *United States Department of Labor*.
- [62] U. Epa, “A Standardized Epa Protocol for Characterizing Indoor Air Quality in Large Office Buildings,” *Indoor Environment Division US EPA, Washington, DC*, 2003.
- [63] “WHO global air quality guidelines,” 2021.
- [64] O. Singh, “Forecasting trends in the generation and management of hazardous waste,” in *Hazardous Waste Management: An Overview of Advanced and Cost-Effective Solutions*, 2021.
- [65] J. Kim, B. Rigdon, “Sustainable Architecture Module : Qualities , Use , and Examples of Sustainable Building Materials,” in *Sustainable Building Materials*, no. December 1998, 1998.
- [66] T. Pekdoğan, A. Tokuç, M. A. Ezan, T. Başaran, “Experimental investigation on heat transfer and airflow behavior of latent heat storage unit in a facade integrated ventilation system,” *Journal of Energy Storage*, 2021
- [67] H. V. Andersen, H. B. Klinke, L. W. Funch, L. B. Gunnarsen, “Emission of formaldehyde from furniture: Test results and assesment of impact on indoor air quality,” 2016.
- [68] I. Ayri, M. Genisoglu, H. Gaygisiz, A. Sofuoglu, S. C. Sofuoglu, “Bleach-containing automatic toilet-bowl cleaners as sources of VOCs, associated indoor air concentrations and carcinogenic risk,” *Atmospheric Pollution Research*, vol. 11, no. 12, 2020.

Impact of Iron Clamps and Dowels on the Vulnerability of Ancient Masonry Walls

Funda Gençer Manisa Celal Bayar University, Faculty of Fine Arts, Design and Architecture, Department of Architecture, Manisa, Türkiye, funda.gencer@cbu.edu.tr

ARTICLE INFO

Keywords:

Ashlar masonry
Failure mechanisms
Metal connectors
Tilt analysis
Conservation



Article History:

Received: 03.04.2024

Accepted: 04.06.2024

Online Available: 01.08.2024

ABSTRACT

Various masonry wall organization techniques were used in ancient Anatolian buildings depending on the local characteristics and the kind of stone used in the region. Traces of iron clamps or dowels can be seen on numerous ancient walls. This study's main goals are to ascertain the impact of iron clamps and dowels on the vulnerability of various ancient wall organizations in Anatolia and investigate potential relationships between wall organization types and clamp or dowel usage. Another study objective is to gather information about using metal connectors for restoration or anastylosis studies in archaeological sites.

First, a site analysis was performed on ancient cities to document various types of masonry. Four types of walls, namely *isodomum*, *isodomum* with header and stretcher, pseudo *isodomum*, and *isodomum* in alternation header and stretcher row were determined. Quasi-static tilt analysis was performed on 3D models of walls without clamps and dowels, with clamps, and with dowels to compare the failure mechanisms of the wall types.

As a result, the wall type with the highest strength gain when metal connectors were utilized in the analysis was *isodomum* organization, which also includes numerous traces of clamps and dowels in ancient cities. This indicates that knowledge was gained because of experiences against lateral loads at that time. This information is not only significant in terms of understanding the history of architecture but also provides data to reinforce ancient walls during conservation work.

1. Introduction

In the past, builders were aware of the earthquake risks and had tried to develop techniques to minimize their impact on their constructions. They tried to use different methods to improve the resistance of masonry walls and prevent the horizontal shifting of blocks. For instance, they used iron elements such as dowels and clamps of various shapes between blocks. Iron clamps and dowels were typically used to fasten together the blocks of stone in *ashlar* dry masonry construction.

Throughout history, various cultures and regions have given rise to a diverse range of masonry styles. Initially, walls were constructed with dry-jointed stones, while for defensive purposes,

such as polygonal Cyclopean structures. First, polygonal masonry became common, however, the processing of stones and construction of the walls in polygonal masonry had been difficult and time-consuming. Then, the *Ashlar* technique composed of finely cut and worked stones became common due to its advantage of simple construction.

There were different *Ashlar* technique applications. *Isodomum ashlar* technique, involved uniform height courses in construction. These different techniques were illustrated in Figure 1. When rows had different heights but continuous horizontal joints, it was called *Pseudisodomum*. Another way to arrange stone courses is by altering the block orientation, header, and stretcher position [1]. This header

and stretcher style of masonry was discussed by Vitruvius (1914) in his book "De Architectura" (first century B.C.) [1]. Headers were used to strengthen walls that were constructed with trapezoidal or rectangular masonry [2-3]. The headers, which are arranged perpendicular to the course wall, reinforce the wall, and hold the wall leaves together (Figure 1).

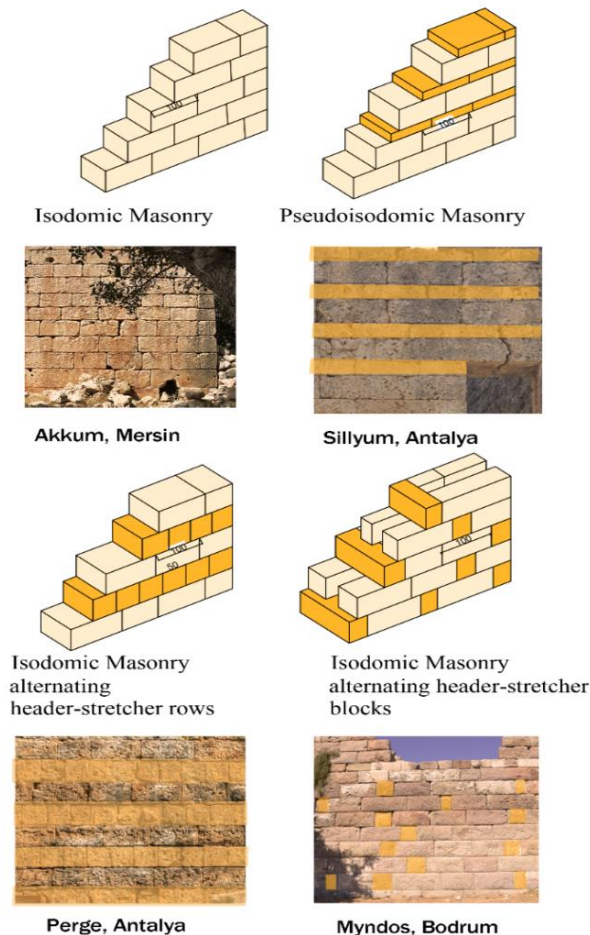


Figure 1. Examples of masonry organizations (drawings were drawn and photos taken by the author in 2017)

According to historical sources by Vitruvius (1914), Ceradini (1992), and Saner (1995) [1, 4, 5], the wall's thickness increases as there is a gap between the parallel stretchers. For thicker walls, three leaves were used, with a space in the middle of two parallel stretchers. To fill this space, stone fragments were used, or it was left unfilled. In some cases, headers were used to provide flexibility in the block arrangement. Throughout the third century BC, alternating layers of headers and stretchers were favored in most of Greece. In these wall sections, stretchers alternate with headers in all courses [6].

The primary requirement for *ashlar* building techniques was the organization of the stones to provide integrity. This type of organization was commonly employed in classical studies by scholars [7-10].

In the past, construction involved merely placing dry-jointed blocks together. However, the Romans also adopted the Greek technique of using metal or wooden clamps and dowels to strengthen the components of a stone block construction. These were designed to prevent joints from enlarging due to potential movements caused by shifts in foundation settlement or seismic shocks [11]. Various metallic connections, including dowels and clamps, were used between the stone blocks to prevent horizontal movement in *ashlar* dry masonry construction. Iron clamps and dowels were commonly used to fasten stone blocks together. The blocks were joined horizontally with an iron clamp that slid into grooves cut into the ends of the stone blocks. Similarly, iron dowels were used to fasten the drums of columns or blocks vertically to prevent sliding under shear. Clamps and dowels were also utilized to prevent any stone movements caused by earthquakes or foundation settlements [12-13].

Due to their ability to provide the building with plasticity and allow for energy dissipation through plastic deformation, metal connectors decrease friction forces even before the blocks begin to move relative to each other [14]. Structural analysis, simulations, etc. have been used in conservation studies of cultural heritage in recent years [14-19]. Numerous studies have been conducted to examine the structural strength of various masonry arrangements, in addition to typological examinations [4, 16-20]. There are studies demonstrating types of iron connectors in historical buildings [20-21].

Kurugöl, Küçük (2015) discuss the various forms and applications of iron in traditional architecture, as well as the production techniques and shaping methods used throughout history. The paper also highlights some of the problems that have arisen with iron materials over time [20]. Also, in some studies, the effect of the size and position of the iron clamps and dowels on the behavior of the masonry walls is investigated

[22-33]. Tanrıverdi, Çelik, Ural, Fırat (2022) investigated the effect of clamps with different widths on lateral load behavior and determined the ideal seam width [22]. The study by Tanrıverdi, Çelik, Ural, Fırat (2022) investigates the impact of clamp immersion points on the shear strength of stones [23]. In a study by Uslu (2013), walls that were constructed using metal clamps and dowels were subjected to the diagonal pressure effect to examine their behavior under the shear effect [24].

Additionally, Smoljanovic, Nikolic, Zivaljic (2015) analyzed the seismic performance of a historical masonry structure strengthened with steel clamps and bolts [25]. Karabork, Kocak (2014) conducted a study on stone masonry walls supported by various iron clamps and dowels to test their structural integrity under diagonal compression and investigate failure modes [26]. Nikolić, Krstevska, Marovic (2017) investigated the behavior of the model of the stone masonry structure in Diocletian's Palace in Split, Croatia under lateral loading [27]. There are some studies discussing the development of the usage of iron clamps and dowels in ancient temples and monuments. The effect of iron connectors on the strength of the monuments and conservation studies were discussed [28-33].

These studies investigate the potential impact of the size, position, and type of clamps and dowels within the same masonry structure. However, considering the variety of masonry organization types found in Anatolia, figuring out the optimal size and placement of metal connectors has proven to be difficult. Although clamps and dowels have been used in various wall types, there is a need for research on how these metal elements contribute to the strength of different wall types and how they affect damage mechanisms. The primary objective of this study is to determine the effect of iron clamps and dowels on different ancient wall organizations in Anatolia and investigate if there is any correlation between wall organization types and the usage of clamps and dowels. The study explores whether iron clamps and dowels were used intentionally. Results should be used as a base for restoration or anastylosis applications in archaeological sites.

1.1. Clamps and dowels

The Egyptians were the first to use strong hardwood clamps shaped like double dovetails to provide integrity to masonry walls. Bronze clamps, shaped like a double T, were also used in pre-Columbian Andean construction in the eighth century AD. Roman builders used fewer double-T clamps than Greek architects, who extensively used them in Greek constructions up until the Hellenistic era. The double-T clamps were first utilized in Athens at the beginning of the fifth century BC. The stones in the course were firmly attached using clamps. Occasionally, and more frequently among the Greeks than the Romans, a vertical bonding was added to the horizontal bonding [34]. Clamps are typically made of iron flats that have tails, forks, and other shapes that are created through the shaping process. Types of clamps were demonstrated in Figure 2. To reinforce the connection, lead was poured on the curved ends that entered the holes made in the stone [20].

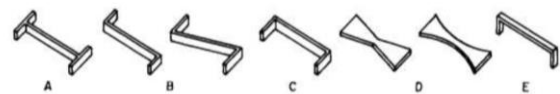


Figure 2. Clamp types [35]

The clamping method involves placing two blocks side by side in the slots on the connecting edges, which are only 3-4 mm wide. Iron pieces are inserted, and molten lead is poured over them to secure the irons tightly into the stone slot and prevent rusting. To facilitate the lead flow, channels may be created that extend to the edge of the block, and the molten lead is poured into clay chambers at the end of these channels to cover the seam with lead. Clamps and dowels were typically made of iron, rarely bronze, and placed in rectangular cuttings in stone. They were fixed with lead to ensure cohesion of courses, to prevent the connection from breaking due to any possible movement, and to isolate the metal element inside from air [13, 34]. The size of the clamps used depends on the size of the stones being connected.

Traces of iron connectors were widely observed in *isodomic* masonry structures consisting of single-walled stretcher blocks, such as Cnidus, Sard, Lairbenos, Pergamon, and Gölyazı, etc. in the site surveys. However, their use was rare in

isodomic structures with headers and stretchers and *pseudoisodomic* masonry. Clamps and dowels were primarily used in the walls of temples, bouleuterions, stadiums, etc., rather than in the city walls. Their use on the ground levels of buildings, such as the Priene Athena Temple and Theater, the foundation of a grave building in Pergamon was particularly noteworthy.

The walls of the Sard Artemis Temple had clamps and dowels in both *isodomic* and *isodomic* with header and stretcher block wall types. In the ancient city of Cnidus, both *pseudoisodomic* and *isodomic* walls had traces of clamps and dowels. However, no clamps were found on the *isodomic* walls with alternating header and stretcher blocks, which are commonly used in Mediterranean ancient cities such as Perge and Side. The traces of clamps and dowels from Anatolian ancient cities were given in Figure 3.



Figure 3. Traces of clamps and dowels in different ancient Anatolian cities (photos taken by the author in 2024)

2. General Methods

First, a site analysis was performed on ancient cities such as Perge, Side, Pergamon, Aigai, Sillyum, and Sardes, to document various types of masonry. The relationships between stone blocks were examined. To analyze why they were employed or not, wall types with and without iron connecting traces have both been chosen. The study has focused on four types of walls, namely *isodomic*, *isodomic* with header and stretcher, pseudo *isodomic*, and *isodomic* in alternation header and stretcher rows. Only the

isodomic wall with alternation header and stretcher rows exhibited no traces, whereas the other three types have traces. Table 1 demonstrates different wall types and usage of clamps and dowels in different ancient cities.

In the second phase, 3D models were created for different types of walls. These walls are 500 cm tall and 560 cm long and were modeled with clamps and dowels separately. Connectors, clamps, and dowels were used to connect two blocks. Clamps have dimensions of 20 cm in length and 6 cm in width. They are arranged in the stones' center axes of width. Dowels have dimensions of 5 by 5 cm. One dowel was placed in the center of the header blocks, and two dowels were placed on each stretcher block. The 3D models of the wall types and the position of metal connectors were given in Figure 4 and 5 respectively. The clamps and dowels were modeled as Hinge Joint.

Then, quasi-static analysis was performed on wall types with and without metal connectors, as well as those with clamps and dowels to analyze the effect of metal connectors on the lateral load behavior of the walls. Using SketchUp 2017, the walls were modeled as distinct rigid blocks arranged in a certain order without any connecting elements. Next, a quasi-static tilt analysis simulation based on the equilibrium state was conducted using MS Physics 1.0.3. This made it possible to simulate discrete elements physically in real time, giving each piece unique attributes like shape, density, and friction, among others. The equilibrium problem was solved using a static rigid body method (Figure 4).

Initial analyses were performed to verify the accuracy of the MS Physics software. The literature's experimental results and the simulation's results were compared. Using SketchUp software, 3D models were generated based on the wall sizes and material properties reported by Restrepo Velez, Magenes, Griffith (2014) [36].

Table 1. Wall types observed in ancient cities

Ancient Cities	Wall types	Clamps	Dowels
Aigai	Isodomic	√	
	Isodomic header and stretcher blocks		
Pergamon	Isodomic	√	
Silyum	Pseudoisodomic		
Sard	Isodomic	√	√
	Isodomic Header and Stretcher blocks	√	√
Lairbenos	Isodomic		√
Aiolis	Isodomic		√
Cnidus	Isodomic header and stretcher blocks	√	√
	Isodomic	√	√
	Pseudoisodomic	√	√
Perge	Isodomic header and stretcher rows		
Side	Isodomic header and stretcher rows		
Myndos	Isodomic header and stretcher blocks	√	
Akkum	Isodomic header and stretcher blocks	√	

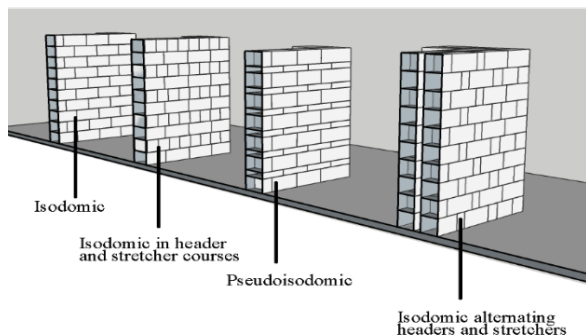


Figure 4. Ashlar masonry types (drawn by the author via SketchUp 2017)

The failure mechanisms were examined by tilting these models using a virtual table in MsPhysics. Using marble units, Restrepo Velez, Magenes, Griffith (2014) carried out an extensive quasi-static testing program that considered 1:5 scale models of dry-joint stone masonry walls and structures [36]. Their marble blocks measured 80 mm by 40 mm by 30 mm. Blocks' unit weight

was 2680 kg/m³, and their friction coefficient was calculated to be 0.77 [37].

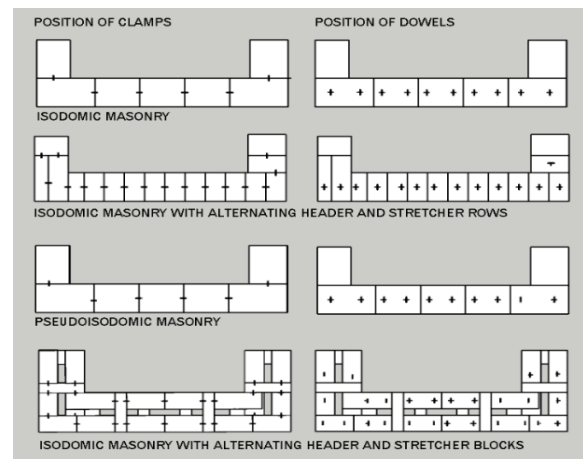


Figure 5. Position of clamps and dowels (modeled by the author via SketchUp 2017)

In this quasi-static testing regimen, 0.6 m, or 21 courses, was the average height of a specimen. The examples featured a two-story building with openings, as well as one-, two-, or three-sided walls with or without openings. The iterative value of 16 was selected, and an update time step of 1/120 was used to guarantee accuracy in the computer simulations of the 3D models. It was discovered that the real verses of the virtual models' damage mechanisms and collapse angles were nearly equivalent. The simulation results were compared in Figure 6.

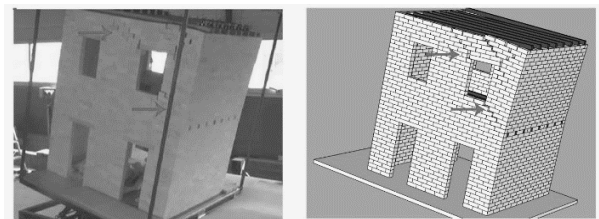


Figure 6. Wall behavior observed from experimental analysis [36] and simulation

Rigid block, group, and component densities are provided by MS Physics software, which is based on physical simulations and connection states. The modulus of elasticity is disregarded in the simulations, but the friction coefficient is considered. Since a smaller update time step yields more accurate simulation results and keeps collisions from getting worse, 1/120 was chosen as the update time step. Given that the towers were made up of numerous movable blocks, 16 was chosen as the iterative value [38].

By tilting the ground plane of each 3D model, the lateral acceleration applied to each model could be changed. Until complete collapse, the tilt value was raised by one degree. The component that is parallel to the gravitational acceleration's tilted ground plane at the collapse level can be understood to represent the maximum ground acceleration that the structure must be able to withstand. According to DeJong (2009) and Jimenez (2011), the lateral component of the gravitational acceleration equals the horizontal acceleration (λ), where $\lambda = mg \times \sin \theta$.

Although the impacts of dynamics as shown by seismic loading are not represented by this equivalent static loading, it does allow one to quantify the structure's lateral load-bearing capability in terms of acceleration [39-40]. Every designed wall has an in-plane and an out-of-plane tilt. When evaluating, the smallest collapse angle was always considered.

3. Results and Discussion

When the damages of different wall organizations were compared, the wall with the

highest structural strength was the *isodomic* wall with headers and stretchers, followed by the *isodomic* wall and *pseudoisodomic* walls, which had similar strengths. The walls alternating header and stretcher rows had the lowest strength under lateral loading.

When the lateral load was in the in-plane direction, the use of clamps or dowels increased the strength of the wall significantly. Dowel additions improved resistance more than clamp additions. Moreover, in the *isodomic* wall, the contribution of both the clamps and the dowels to the structure strength was found to be the highest. The usage of clamps resulted in a 35% increase in strength, whereas using dowels resulted in an 80% increase in strength. The analysis results were given in Table 2.

The strength of the walls increased by about 25% when clamps were used, and by up to 60% when dowels were used. But dowels, used in the walls alternating header and stretcher courses, contributed only 5% of the wall's strength.

Table 2. Collapse angles of walls under lateral force in the in-plane direction.

	Without clamps	With clamps	Percentage of increase in resistance	With dowels	Percentage of increase in resistance
<i>Isodomic</i> masonry	20°-collapse	28°-crack 29°-collapse	35 %	36°-collapse	80 %
<i>Isodomic</i> with alternating header and stretcher courses	18°-collapse	23°-collapse	28 %	19°-crack 20°-collapse	5.5 %
<i>Pseudoisodomic</i> masonry	20°-collapse	24°-crack 25°-collapse	20 %	35°-collapse	75 %
<i>Isodomic</i> alternating header and stretcher blocks	22°-collapse	27°-crack 28°-collapse	27 %	36°-collapse	68 %

The contribution of clamps and dowels to wall strength was less when the lateral load occurred in an out-of-plane direction. The strongest wall, *isodomic* alternating stretchers and headers, increased in structural strength by 15% when dowels were used. On the other hand, the use of dowels did not affect the resistance of walls with alternating header and stretcher rows. The analysis results were given in Table 3.

Four different types of failures were observed in the walls based on analysis results: flexural

failure, diagonal/stair-stepped cracking, vertical cracking, and sliding failure (Figure 7), [41]. Diagonal cracks or stair-stepped cracks occurred in *isodomic*, *isodomic* alternating header stretcher, and *pseudoisodomic* walls when clamps or dowels were not used, and when the lateral load came in the in-plane direction. On the other hand, both vertical and diagonal cracks were observed on the walls alternating header stretcher rows.

Table 3. Collapse angles of walls under lateral force in the out-of-plane direction

	Without clamps	With clamps	Percentage of increase in resistance	With dowels	Percentage of increase in resistance
<i>Isodomic</i> masonry	13° -collapse	15° -collapse	15%	15° -collapse	15%
<i>Isodomic</i> with alternating header and stretcher courses	14° -collapse	15° -collapse	7%	14° -collapse	0%
<i>Pseudoisodomic</i> masonry	14° -collapse	15° -collapse	7%	15° -collapse	7%
<i>Isodomic</i> alternating header and stretcher blocks	18° -collapse	21° -collapse	17%	23° -collapse	28%

When clamps were used, flexural failures and diagonal cracking were observed in the walls connected with clamps. The walls presented both sliding and cracking along the length of the wall. The study by Karabork, Kocak (2014) was supported by the results obtained. The study found that a failure mechanism like the *isodomic* wall developed with clamps when tested for shear strength under diagonal compression [26]. However, it is worth noting that block sliding in the upper parts was not observed since the walls were mortared. The failure mechanisms were given in Figure 8.

The use of dowels did not result in flexural failure like clamps did. However, cracks (approximately 1 cm) were observed in *isodomic* and *pseudoisodomic* walls due to sliding, while partial collapse was seen in the *isodomic* walls that used alternating header and stretcher without any diagonal cracking. Dowels considerably strengthened the walls when headers and stretchers were used (Figure 8).

Isodomic walls consist of alternating header and stretcher rows, wherein the vertical joints are situated close to each other in the upper and lower rows. The blocks on top of one another displayed a monolithic behavior and created vertical cracks when dowels were used to join them. Therefore, the use of dowels did not affect the structure's behavior and strength in the walls with alternating header stretcher courses. Clamps reduced the vertical cracking of the close-jointed blocks stacked on top of one another, hence increasing the strength of the walls. Stair-stepped cracks began to form in place of vertical

cracking. The failure mechanisms were given in Figure 9.

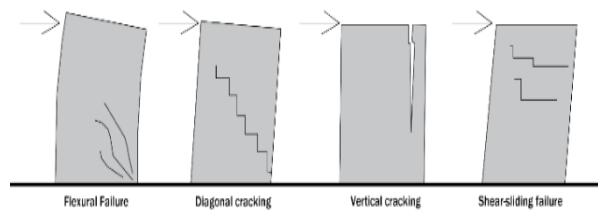


Figure 7. Determined failure types in the walls (drawn by the author via Autocad 2024)

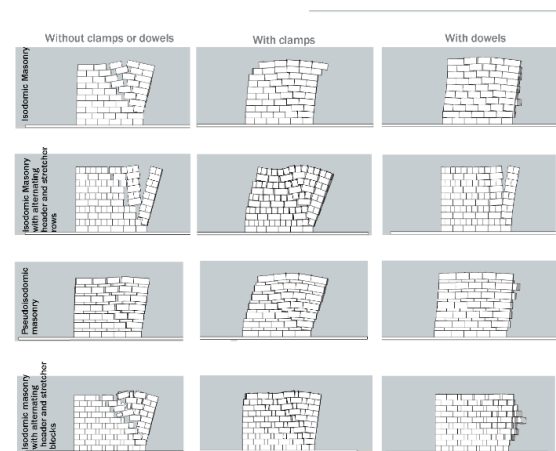


Figure 8. Failure types when the lateral load at the in-plane direction (modeled by the author via SketchUp 2017 and MsPhysics 1.0.3.)

Similar failure mechanisms were observed in the models when the walls were tilted in an out-of-plane direction. However, bending shear was observed when dowels were used in alternating header and stretcher rows. In cases where clamps and dowels were used in alternating header and stretcher blocks, bending shear formation was also observed. Shear cracking was observed in other wall types, as well as in dowel usage. The failure mechanisms were given in Figure 10.

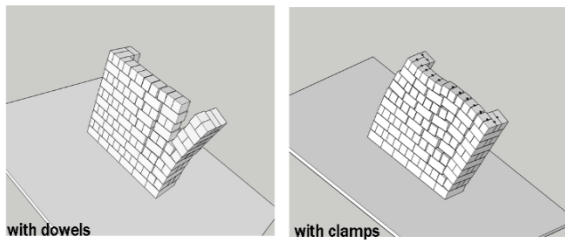


Figure 9. Different behavior of walls alternating header and stretcher rows connected with dowels and clamps (modeled by the author via SketchUp 2017 and MsPhysics 1.0.3.)

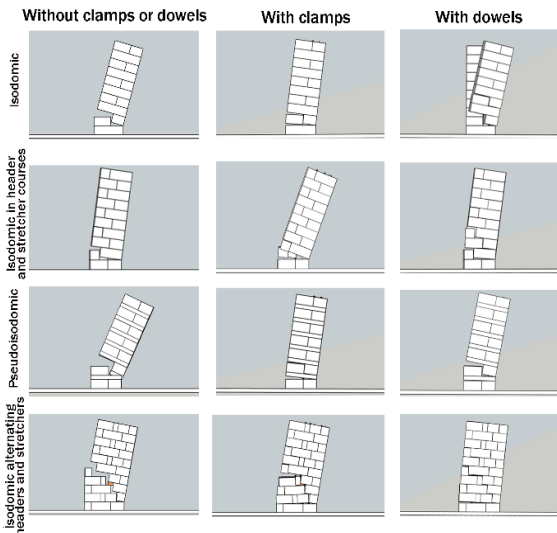


Figure 10. Different behavior of walls connected with dowels and clamps (modelled by the author via SketchUp 2017 and MsPhysics 1.0.3.)

4. Conclusion

The impact of metal connections on different types of masonry walls was investigated through research. As a result, the wall type with the highest utilization of clamps and dowels in ancient cities was isodomic organization, which also offered the greatest strength gain when metal connectors were tested in the analysis.

The use of dowels in *isodomic*, *isodomic* header stretcher blocks, and *pseudoisodomic* walls significantly increased the strength of the structure. However, it also caused shifts in horizontal rows between the blocks and changes in failure types. Stair-stepped cracks in the structure were reduced to a minimum.

In *isodomic* alternating header and stretcher rows, the vertical joints in the upper and lower rows were near to one another thus, vertical cracks were seen. Clamps prevented vertical

cracks by connecting blocks horizontally. Thus, using clamps was crucial to maintaining the structural integrity of walls with narrow vertical joint distances. However, the blocks, on top of each other, connected with dowels behaved monolithically, and vertical cracks were observed right away. In the site surveys, no traces of dowels were observed on the walls alternating header and stretcher rows commonly used in the Side and Perge regions. This led to the question of whether stonemasons made a conscious decision regarding this.

Consequently, results are crucial for comprehending the evolution of structural design, and they show which types of ancient walls should be supported by clamps or dowels while doing conservation works. Rather, distinct safety measures ought to be implemented to augment the structural robustness of disparate wall types.

Article Information Form

Funding

The author has not received any financial support for the research, authorship, or publication of this study.

The Declaration of Conflict of Interest/ Common Interest

No conflict of interest or common interest has been declared by the authors.

The Declaration of Ethics Committee Approval

This study does not require ethics committee permission or any special permission.

The Declaration of Research and Publication Ethics

The authors of the paper declare that they comply with the scientific, ethical, and quotation rules of SAUJS in all processes of the paper and that they do not make any falsification on the data collected. In addition, they declare that Sakarya University Journal of Science and its editorial board have no responsibility for any ethical violations that may be encountered and that this study has not been evaluated in any academic publication environment other than Sakarya University Journal of Science.

Copyright Statement

Authors own the copyright of their work published in the journal and their work is published under the CC BY-NC 4.0 license.




References

- [1] Vitruvius, *The Ten Books on Architecture*, Translated by Morgan M. H. Cambridge: Harvard University Press, 1914.
- [2] A. Orlandos, *Les Matériaux de Construction: Et la Technique Architecturale des Anciens Grecs*, Paris: E. de Boccard, 1968.
- [3] S. K. Nossov, *Greek Fortifications of Asia Minor 500-130 BC: From the Persian Wars to the Roman Conquest*, UK: Osprey Publishing, 2012.
- [4] V. Ceradini, "Modellazione, Sperimentazione per lo Studio della Struttura Muraria Storica," Ph.D. Dissertation, Department of Architecture, University of Rome, Rome, Italy, 1992.
- [5] T. Saner, "Some Remarks on the Hellenistic Masonry Techniques in Asia Minor," in *Archéomatériaux Marbres et autres roches*, Actes de la IV^e Conférence internationale ASMOSIA IV, University of Bordeaux, France, 1995, pp. 347-350.
- [6] L. Karlsson, "Fortification Towers and Masonry Techniques in the Hegemony of Syracuse, 405-211 B.C," in *Acta Instituti Romani Regni Sueciade*, 40, XLIX, B. Alroth, Ed. Stockholm: Minab, 1992.
- [7] S. Clarke, R. Englebach, *Ancient Egyptian Masonry*, London: Oxford, 1930.
- [8] R. L. Scranton, *Greek Walls*, Cambridge: Harvard University Press, 1941.
- [9] A. W. Lawrence, *Greek Architecture*. England: Penguin, 1957
- [10] R. Martin, *Living Architecture-Greek*. London: Oldbourne, 1967.
- [11] J. P. Adam, *Roman Building, Materials, and Techniques*, translated by Anthony Mathews, London, and New York: Routledge, 2005.
- [12] R. Mark, *Architectural Technology up to the Scientific Revolution. The Art and Structure of Large-Scale Buildings*. Cambridge: The MIT Press, 1993.
- [13] O. Bingöl, *Arkeolojik Mimaride Taş*, İstanbul: Homer Yayınevi, 2004.
- [14] S. Alaçam, İ. Karadağ, O. Z. Güzelci, "Reciprocal style and information transfer between historical Istanbul Pervititch Maps and satellite views using machine learning," *Journal of the Faculty of Architecture and Urbanism of University of Cuenca*, vol.11, no.22, pp. 71-81, 2022.
- [15] K. A. Papadopoulos, "The restoration study of the connections between the stone blocks in the steps of the temple of Apollo Epikourios," in *5th International Conference on Structural Analysis of Historical Constructions*, New Delhi, India, 2006, pp. 1389-1396.
- [16] A. Giuffrè, *Lecture sulla meccanica delle murature storiche*, Rome: Kappa, 1991.
- [17] P. Fuentes, S. Huerta, "Geometry, Construction and Structural Analysis of the Crossed-Arch Vault of the Chapel of Villaviciosa, in the Mosque of Córdoba," *International Journal of Architectural Heritage*, vol.10, no.5, pp. 589-603, 2016.
- [18] S. Huerta, "The Analysis of Masonry Architecture: A Historical Approach," *Architectural Science Review*, vol.51, no.4, pp. 297-328, 2008.
- [19] M. A. Keller, "The early Phrygian gate at Gordion, Turkey: An investigation of dry-stone masonry in seismic regions and recommendations for stabilization," Master Thesis, Department of Historic Preservation, University of Pennsylvania, USA, 2009.

- [20] S. Kurugöl, S. G. Küçük, “Tarihi eserlerde demir malzeme kullanım ve uygulama teknikleri,” in 5. Tarihi Eserlerin Güçlendirilmesi ve Geleceğe Güvenle Devredilmesi Sempozyumu, Erzurum, 2015, pp. 521-536.
- [21] İ. E. Usta, H. İ. Alpaslan, “Batı Anadolu'daki Antik Yapılarda Taş ve Taşçı İzleri,” in IV. Uluslararası Taş Kongresi, İzmir, 2017, pp. 615-637.
- [22] Ş. Tanrıverdi, T. Çelik, A. Ural, F. K. Fırat, “Kenet Genişliğinin Yığma Taş Bloklarının Kayma Davranışı Üstündeki Etkisinin İncelenmesi,” Düzce Üniversitesi Bilim ve Teknoloji Dergisi, vol.10, pp. 1811-1825, 2022.
- [23] T. Çelik, Ş. Tanrıverdi, A. Ural, F. K. Fırat, “Yığma Yapılarda Kullanılan Kenetlerin Yapı Davranışına Etkilerinin İncelenmesi,” Afyon Kocatepe University Journal of Sciences and Engineering, vol. 21, pp. 650-659, 2021.
- [24] S. Uslu, “Tarihi yığma yapılarda kullanılan metal bağlantı elemanlarının deneysel metotlarda incelenmesi,” M.S. Dissertation, Aksaray University, Aksaray, Turkey, 2013.
- [25] H. Smoljanovic, A. Nikolic, N. Zivaljic, “A finite-discrete element model for dry stone masonry structures strengthened with steel clamps and bolts,” Engineering Structures, vol.90, pp. 117–129, 2015.
- [26] T. Karabork, Y. Kocak, “New metal connectors developed to improve the shear strength of stone masonry walls,” Structural Engineering and Mechanics, vol. 50, no.1, pp. 121–135, 2014.
- [27] Z. Nikolić, L. Krstevska, P. Marovic, H. Smoljanović, “Shaking table test of scaled model of Protiron dry stone masonry structure,” Procedia Engineering, vol.199, pp. 3386-3391, 2017.
- [28] G. Varoufakis, “The iron clamps and dowels from the Parthenon and Erechtheion,” The Journal of Historical Metallurgy Society, vol. 26, 1992.
- [29] K. Papadopoulos, “The Restoration Study of the Connections Between the Stone Blocks in the Steps of the Temple of Apollo Epikourios,” in 5th International Conference on Structural Analysis of Historical Constructions, New Delhi, India, 2006, pp.1389-1396.
- [30] S. Kourkoulis, E. Pasiou, “Epistyles connected with "I" connectors under pure shear,” Journal of the Serbian Society for Computational Mechanics, vol.2, pp. 81-99, 2009.
- [31] E. E. Toumbakari, “Analysis and Interpretation of the Structural Failures of the Orthostate in the Northern Wall of the Athens Parthenon,” Strain, vol. 45, pp. 456-467, 2009.
- [32] G. Varoufakis, “The rapid Development of Technology in making iron Clamps of three Ancient Temples in the Archaic and Classical Period,” Journal of Chemistry and Chemical Engineering, vol.6, pp. 1136-1141, 2012.
- [33] D. Triantis, I. Stavrakas, E. Pasiou, G. Hloupis, S. Koukoulis, “Innovative Experimental Techniques in the Service of Restoration of Stone Monuments - Part II: Marble Epistyles under Shear,” Procedia Engineering, vol.109, pp. 276-284, 2015.
- [34] Masonry. (2024, March 20). Available: http://www.ime.gr/chronos/04/en/culture/314arts_arch_masonry.html
- [35] W. B. Dinsmoor, Ancient Athenian Building Methods, Vermont: American School of Classical Studies at Athens, 1984.
- [36] L. F. Restrepo Velez, G. Magenes, M. C. Griffith, “Dry Stone Masonry Walls in Bending—Part I: Static Tests,” International Journal of Architectural Heritage: Conservation, Analysis, and Restoration, vol.8, no.1, pp.1-28, 2014.

- [37] T. Bui, A. Limam, V. Sarhosis, M. HJiaj, “Discrete Element Modelling of the In-Plane and Out-Of-Plane Behavior of Dry-Joint Masonry Wall Constructions,” *Engineering Structures*, vol.136, pp. 277-294, 2017.
- [38] A. Synytsia, (2017, March 15). MSPhysics 1.0.3 [Online] Available: <https://sketchucation.com/forums/viewtopic.php?f=323&t=56852&start=660>.
- [39] M. J. DeJong, “Seismic Assessment Strategies for Masonry Structures,” Ph.D. dissertation, Department of Architecture, Massachusetts Institute of Technology, United States, 2009.
- [40] D. D. Jimenez, “Empirical Analysis of Masonry Walls: Structural Design and Seismic Reinforcement through Tilting Experiments,” M.S. Dissertation, Department of Civil and Environmental Engineering, Massachusetts Institute of Technology, United States, 2011.
- [41] I. Calì, Ivo, M. Marletta, B. Pantò, “A Simplified Model for the Evaluation of the Seismic Behaviour of Masonry Buildings,” in *The Tenth International Conference on Civil, Structural and Environmental Engineering*, pp.2-17.

Validating the Credibility of Photovoltaic Systems Simulation Tools with a Case Study

Barış Alaçam¹ , Hatice Vural^{2*} , Metin Orbay³ 

¹ Amasya University, Institute of Science, Department of Renewable Energy and Applications, Amasya, Türkiye, barissanelk@gmail.com

²Amasya University, Faculty of Engineering, Department of Electrical-Electronics Engineering, Amasya, Türkiye, hatice.vural@amasya.edu.tr

³Ankara Hacı Bayram Veli University, Polatlı Faculty of Science and Letters, Department of Mathematics, Ankara, Türkiye, metin.orbay@hbv.edu.tr

*Corresponding Author

ARTICLE INFO

ABSTRACT

Keywords:

Renewable energy
Photovoltaic system
Solar energy
Simulation

Article History:

Received: 10.05.2024

Accepted: 06.07.2024

Online Available: 02.08.2024

In this study, a photovoltaic system with an installed power of 10 kW_p, which was built on the roof of a school cafeteria in Gümüşhacıköy district of Amasya, was modeled using the PVsyst software and PVSOL software. The real-life data of the system and the production data calculated from the software used were compared. While the actual total electricity production data of this photovoltaic system for 2021 was determined as 12.473 MWh, this value was obtained as 12.912 MWh using PVsyst software and 13.556 MWh using PVSOL software. While there was a 3.40% difference between the estimated production value and the real-life data with the PVsyst software, it was determined that there was a 7.99% difference between the estimated production value and the actual production value of the system as a result of the simulation made with PVSOL. From the production estimates made with two different simulation software, it was seen that the PVsyst software gave results closer to the real-life data.

1. Introduction

In today's conditions, countries are turning to renewable energy sources in electricity generation due to the limited fossil resources, geographical reserves only in certain regions, economic cost, supply security, use as a means of sanction between countries, and negative effects on the environment [1].

As in the rest of the world, Türkiye's increasing energy demand along with its growing population increases the demand for renewable energy [2]. To reduce external dependence on energy and energy imports, studies on determining the potential of renewable energy resources and expanding their use continue to increase [3]. Türkiye has a significant amount of renewable energy resources (wind, solar, water,

geothermal, etc.) and the optimum use of these resources is of great importance [4]. Aware of these natural resources, Türkiye's share of renewable energy-based electricity generation is continuously increasing [4]. While in 2009, the electricity generated from wind, solar, and geothermal energy was quite low, according to December 2022 data, the total electricity generated from these three energy sources increased to 22 512.9 MW. According to March 2024 Turkish Electricity Transmission Corporation (TEİAŞ) data, Türkiye's installed capacity reached 107 799 MW. While the installed wind capacity was 11 961 MW, the installed solar capacity increased to 12 639 MW [5].

In the study titled "Modeling and Simulation of 30 kW Grid Connected Photovoltaic System with

PVsyst Software", modeling and simulation studies were carried out on a school roof in Batman province with PVsyst Software for a 30 kW grid-connected photovoltaic system using 300 Wp polycrystalline PV panels facing full south direction with 34° panel slope and 0° azimuth angle. What kind of results will be encountered in case of realization of this PV system was evaluated with the PVsyst simulation program. As a result of the simulation, it was planned that 35.31 MWh/year of electricity could be generated at the school and 35.31 MWh/year of energy generated could be sold to the grid to generate income for the school. Considering the energy needs of the places where the system is designed, it is concluded that the system can meet how much of this need and cost analyzes can be made [6].

In their study titled "Analysis of the Lebit Energy Solar Power Plant with Pvsyst Program", Demiryürek et al. [7] analyzed the data of Lebit Energy solar power plant in Siirt province, which has an installed capacity of 200 kWp, by comparing them with PVsyst software. They compared the actual production values for one year with the simulation values obtained with the PVsyst program and observed that the program reflects the reality with a very small error margin of 0.56 %. As a result of the analysis and investigations, they concluded that more energy production can be achieved if regular dust and snow cleaning is carried out.

In a study, the real-life data of 3 different solar power plants in Kilis province for the years 2018, 2019, and 2020 were compared with the system data designed with PVsyst 7.1. software using the same system features. As a result of the analysis, it was observed that the data obtained were close to each other, but the power plant energy production values were less [8].

Thailand is rapidly moving towards sustainable electricity generation using renewable energy systems, especially solar photovoltaic systems and wind turbines. Four renewable energy modeling tools (SAM, PVsyst, HOMER and RETScreen) were used to model solar photovoltaic systems (PVS), wind turbine systems (WTS) and solar photovoltaic-wind turbine hybrid systems (PVWHS) in different

regions of Thailand. The results of the analysis using PVsyst software were reported to be close to the real data with an error rate of 6.9 % [9].

In the study conducted by Altınkök et al. [10], a 3D photovoltaic system design was carried out on the roofs of Giresun University Faculty of Engineering in Türkiye using the PVSol program. When the analysis of the simulation results was evaluated, it was stated that the Faculty would contribute to the production of approximately 138.054 MWh of electricity and in this case, approximately 52% of the annual consumption could be met.

Dirlik et al. [11] investigated the real data of 7 solar power plants (SPP) in different geographical regions in Türkiye are compared with the results of PVSyst, PVSOL and HOMER software. As a result of the study, it was stated that the most suitable software for these analyzed power plants was HOMER.

In this study, PVsyst V.7.1.0 DEMO and PVSOL Premium 2022 DEMO software were used to design an on-grid photovoltaic (PV) system with an installed capacity of 10 kWp on the roof of the cafeteria of a school in Gümüşhacıköy district of Amasya province.

2. Material and Methods

2.1. Solar energy potential of Amasya province

Amasya province is located in the inner part of the Central Black Sea region (34° 57' 06" - 36° 31' 53" East Longitude and 41° 04' 54" - 40° 16' 16" North Latitudes). According to the data of the General Directorate of Meteorology, the solar energy potential of Amasya is given in Figure 1 [12]. Compared to other regions, the solar energy potential of the Black Sea region is low. It is seen that the average solar radiation of the districts of Amasya province is between 1400-1550 KWh/m²-year and this value is lower than Türkiye's average annual total irradiance of 1527.46 kWh/m²-year [13].

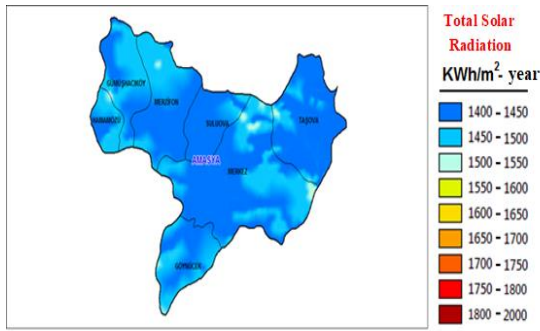


Figure 1. Solar energy potential atlas of Amasya province [12]

Gümüşhacıköy district is located in the northwest of Amasya. The average daily sunshine duration of the district is 6.63 hours, which is lower than Türkiye's average daily sunshine duration of 7.5 hours. When we look at the global radiation values of Gümüşhacıköy district given in Figure 2, it is seen that the highest radiation intensity is reached in July with 6.19 kWh/m²-day. The lowest radiation intensity is observed in December with 1.34 kWh/m²-day.

As seen in Figure 3, the highest efficiency per square meter is obtained from monocrystalline silicon PV panels. Monocrystalline panels are preferred in order to obtain more intense energy in a small area, especially where there is insufficient space to install panels.

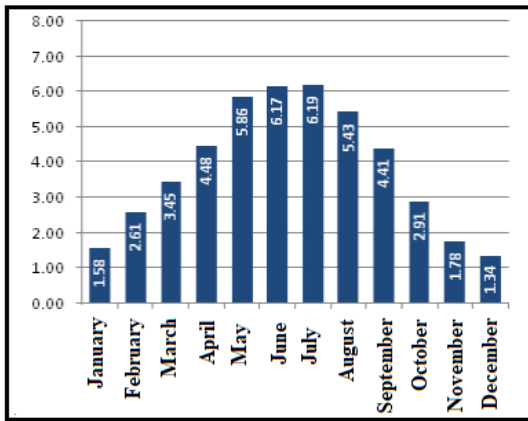


Figure 2. Gümüşhacıköy global radiation values (kWh/m²-day) [12]

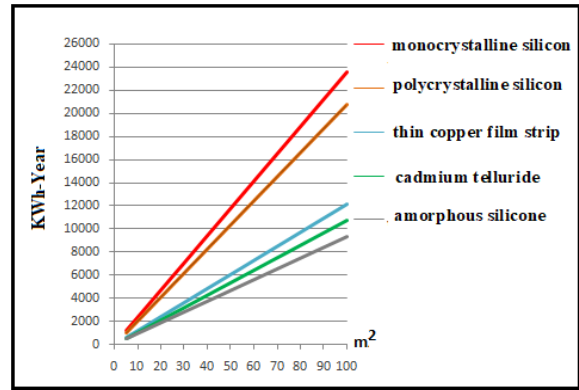


Figure 3. Comparison of energy densities of photovoltaic panel types (kWh/year) [12]

2.2. Rooftop photovoltaic system

In the photovoltaic system installed on the roof of the school cafeteria, 28 pieces of 395 Wp monocrystalline PV panels were placed according to the roof slope. Total installed power is 395 Wp x 28 = 11.060 kWp. Growatt 10000-TL3-S brand inverter with 3-phase 2 MPPT input and 10 kW power is used in the power plant. PV panels are arranged in 2 strings (chains) with 14 panels in each string (Figure 4). The roof slope is 11° vertically (N-S). The azimuth angle of the roof where the PV panels are located is 40° in the south-east direction, not exactly south. The system is grid-connected (on grid) and fully supplies the electricity it generates to the grid. The electricity generated by the system is mutually offset by the distributor company.



Figure 4. Installation of PV Panels on the roof in 2 chains

In this project, the orientation of the roof where the PV panels are located is deviated from south to east by 40°, so the azimuth angle is -40°. The azimuth angle can be easily found with various interactive maps and websites using satellite images.

2.3. PVsyst software

One of the most preferred programs for designing PV solar systems is PVsyst software. PVsyst program is a simulation program developed by the University of Geneva, Switzerland, where solar energy systems such as PV field irrigation systems, grid-connected, off-grid PV systems can be designed in 3D and the results can be obtained as reports and graphics. PVsyst program provides the opportunity to make calculations using detailed specifications for the system [14].

The program allows us to obtain the solar radiation data of the region where we will apply, by entering the coordinates of the region where the solar power plant (SPP) will be established, through various software, or by entering it manually. PVsyst accesses the solar radiation and meteorological data of the selected location using Meteonorm, NASA or PVGIS databases.

2.4. System design with PVsyst software

When designing the photovoltaic system, factors such as panel orientations, panel properties, inverter properties and shading effect are fully entered into the system. If desired, an economic evaluation is made. After marking the geographical coordinates of the roof where the PV panel is installed on the interactive map, the meteorological data of Gümüşhacıköy district in the PVsyst database is retrieved via Meteonorm 7.3. As a result, monthly global radiation, wind speed and temperature values falling on the horizontal plane of the location where the PV panels were installed were obtained. When Solar Energy Potential Atlas (SEPA) and Meteonorm 7.3. data are compared, it is seen that the data are close to each other and while Meteonorm annual average is 3.86 kWh/m²/day, this value is 3.865 kWh/m²/day according to SEPA [15].

Panel inclination and orientation directly affect the efficiency of the photovoltaic system. The roof on which the PV panels are installed does not face directly towards the south and faces 40° east from the south. This caused the azimuth angle to deviate 40° from the south direction and this caused a decrease in efficiency. Again, the angle of the panels with the vertical is 11°, which is considerably smaller than the optimum angle

of 33° according to the latitude of the building. This causes a decrease in efficiency compared to the optimum slope. According to the slope and azimuth angles where the system is installed, the total loss is around 7.9 %.

The values where the panel inclination is 33° and the panel direction is exactly facing south, i.e. the azimuth angle is 0°, give us the optimum situation. In this case, PVsyst shows 0 % losses. The surface radiation rate also increases from FT=1.06 to FT=1.15. If the panel slope was 33° and the azimuth angle was 0° in the photovoltaic system installed on the roof, the system would be operating at the highest efficiency. If the panel slope was 33° and the panel direction was in the same direction as the roof as in the real situation, that is, if the azimuth angle was -40°, the loss would be 3.8 % compared to the optimum situation. This shows us how important the panel tilt alone is in the performance of the system. If the panel tilt is 11° as in the real photovoltaic system and we change the panel orientation and ignore the deviation of 40° and make the azimuth angle 0°, the loss compared to the optimum case is 6.2 %.

In roof applications, in sloping roofs, PV panels are generally installed according to the slope of the roof and additional construction costs are avoided. This way is used because the installation construction is a little more difficult and costly on sloping roofs. Determining the panel inclination and azimuth angle that can achieve maximum efficiency before starting the project and assembling according to these values will significantly increase the amount of energy produced by photovoltaic systems that will operate with a constant inclination for many years.

In the real photovoltaic system, a total of 28 PV panels of 395 Wp were placed in 2 arrays and connected to several 14 panels per MPPT. The power of the system was selected as 11.06 kWp independently of the area since there is enough roof space (Table 1).

Since the 10 kW Growatt 10000-TL3-S inverter used in the system is available in the Pvsyst program, inverter selection is made here (Table 2).

Table 1. Characteristics of the PV panel used
ELNPLUS6612M-395

Characteristics	Value
Voc	49.12 V
Vmpp	40.28 V
Isc	10.14 A
Impp	9.81 A
Maximum power at STC (Pmax)	395 Wp
Number of Panels Used	28

Since the PV panel used in our study is not readily available in the database of PVsyst software, PV panel specifications were found in the manufacturer's catalogs and added to the component library of PVsyst program.

Table 2. Specifications of the inverter used in the system

GROWATT 10000-TL3- S Inverter	
Characteristics	Value
Max. Recommended PV Power	12000W
Max. DC Voltage	1000V
Start Voltage	160V
Nominal Voltage	600V
Max. Input Current	13A/13A
Rated AC Output Power	10 kW
Max. AC apperent Power	11kVA
Max. Output Current	16.7A
AC Nominal Voltage	230V/400V; 320V/438V

2.5. PVSOL premium 2022 software

Valentin Software Simulation Software, based in Berlin, Germany, launched PVSOL Photovoltaic Systems Design Software in 1998. PVSOL is a dynamic software that enables professional design for photovoltaic systems. It allows the 3D design of many photovoltaic systems such as grid-connected, off-grid, DC pumping, rooftop systems, battery storage systems and field applications. Single and dual-axis solar tracking systems can be designed. With PVSOL, the shading effect of field applications, rooftop parallel and elevated mounting angle systems can be designed in 3D and shading effects can be calculated. The software provides the opportunity to include satellite maps in 3D design [16].

2.6. System design with PVSOL software

The system specifications installed on the roof were defined in the same way. Electrical parameters, temperature coefficient data and

dimensions of 395 Wp panel specifications, which are not readily available in the PVSOL program, were entered into the panel data section in the system. The Growatt 10000TL3-S inverter used in the system was selected exactly as it is available in the software. In the system, a total of 28 panels were placed in 2 arrays. The building location was selected from the map and the azimuth angle was automatically output and the roof slope value was entered as 11°.

The main building and the tree near the power plant were placed in the field according to their exact location. Considering that the tree is a deciduous tree, solar transmittance values were selected. These choices are important in finding shading losses.

3. Results and Discussion

3.1. Design results with PVsyst software

The system installed on the roof of the school was designed with PVsyst software together with the actual panel, inverter, tilt, location, angle and shading effect, and it was calculated that the total annual electrical energy to be supplied to the grid would be 12.91 MWh. The system performance ratio was found to be 78.74%. When the economic data for the system is entered, it is seen that the system covers the installation cost after approximately 6.64 years due to the effects such as the ownership of the land, rent expenses and the absence of taxes.

As a result of the simulation made with PVsyst software without shading objects, it was calculated that the system would produce 13.650 MWh of electricity annually, and because of the simulation using shading objects, it could produce 12.912 MWh of electricity annually. This result shows that there is an annual loss of 738 kWh of electricity due to shading, causing a loss of 5.40 % in the system. Looking at the monthly estimated production results, it is seen that the highest production is reached in July and the lowest electricity production is realized in December (Figure 5).

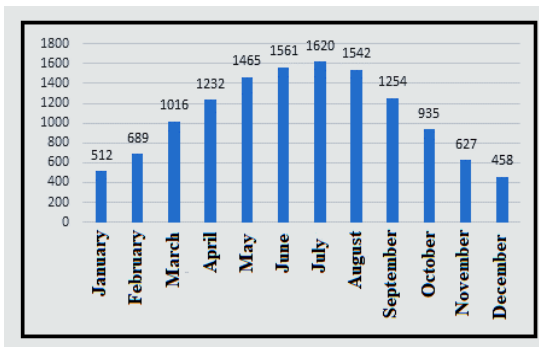


Figure 5. Estimated monthly production amounts (kWh) of the design made with the PVsyst

When the loss diagram obtained as a result of the simulation is examined, the annual global radiation amount coming to the horizontal plane in the area where the panels are installed is 1.408 MWh/m² (Figure 6). As a result of azimuth angle, panel inclination and shading objects, the effective radiation amount hitting the panels decreased to 1.346 MWh/m². The radiation loss due to close shading objects is 4.68 % and the loss due to reflection is 3.77 %.

When the contamination loss of the panels is accepted as 1%, the effective irradiation amount reaching the panels is 1.346 MWh/m² when the optical losses to the panels are subtracted. Since the area covered by the panels is 56 m², the energy that can be produced with the total incoming 1.346 MWh/m² radiation will be 1.346 MWh/m² * 56 m² = 75.376 MWh. Since the STC (Standard Test Conditions) efficiency of the PV panels used in the solar power plant is 20.01 %, the amount of energy converted will be 14.95 MWh.

The PV loss due to irradiance level is 1.12 % as the panels receive less radiation than they should. The loss in the panels due to temperature is 7.95%, the main reason for this situation is that the panels are installed fully integrated on the roof without leaving enough air space. For the existing installed power plant, PVsyst calculated the estimated annual production result as 13.642 MWh when we selected the installation type as "Free modules with air circulation" in the calculations made under the thermal parameters tab in the detailed losses section while keeping all system features the same. When "Semi-integrated with rear air duct" is selected, the production value is calculated as 13.296 MWh. However, when the installation type of the

photovoltaic system is selected as "Integrated with rear insulation", where the photovoltaic system is fully integrated on the roof, the estimated annual production is lower at 12.912 MWh. This result shows us to what extent the roof mounting type affects the thermal losses.

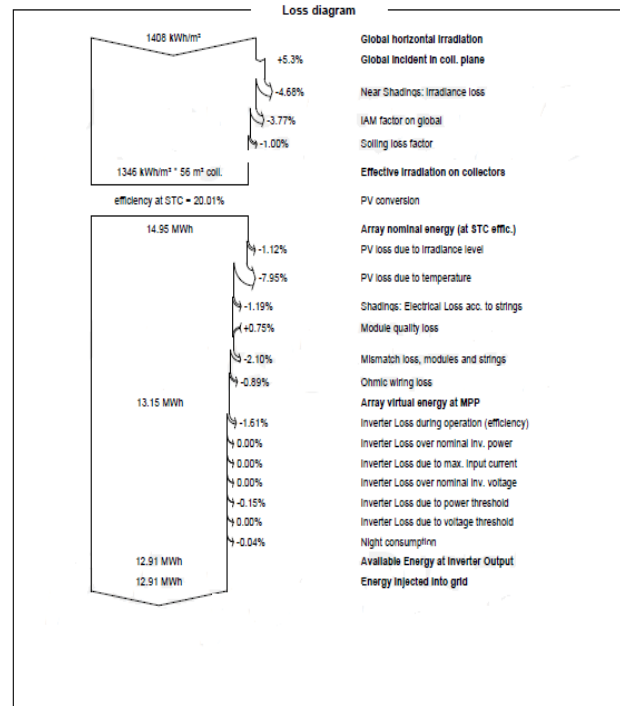


Figure 6. Loss diagram of the design with the PVsyst

According to the module chains, the electrical loss due to shadowing is 1.19 %. According to the power tolerance and quality of the modules determined during production, no loss was observed. Additionally, a gain of 0.75% was observed. Mismatch losses due to the connection type of panels and arrays were calculated as 2.10%. Mismatch losses also increase due to shadowing on the panels. The ohmic wiring loss was calculated as 0.89%. As a result of the array losses, the total energy at the panel outputs was 13.15 MWh.

The loss due to the inverter efficiency is 1.61%. The loss due to the inverter exceeding the required power limits is 0.15%. The loss due to the inverter's electricity consumption at night is calculated as 0.04%. In total, 1.80% loss is foreseen in the inverter. After the losses in the inverter, the energy generated by the photovoltaic system at the output of the inverter and supplied to the grid is calculated as 12.91 MWh.

3.2. Design results with PVSOL program

As a result of the calculations, while the PVSOL software finds the annual production amount to be 14.910 MWh without the shading effect of the main building and tree, it is seen that it decreases to 13.556 MWh when the shading effect is included. According to the PVSOL program, the shading effect causes an annual loss of approximately 9.08%.

With PVSOL software, it was concluded that the system can generate 13.556 MWh of electrical energy per year. The performance of the system was calculated as 78.66%. With the PVSOL software, it is estimated that the highest electricity production will occur in June and the lowest production will occur in December (Figure 7).

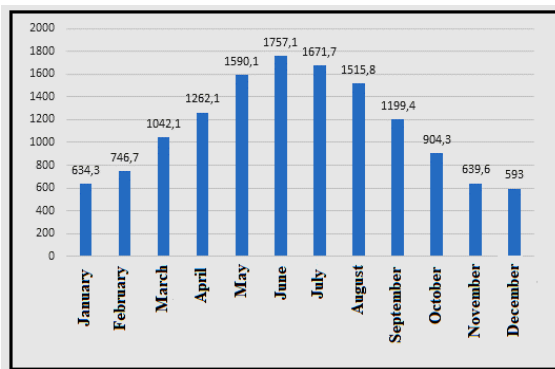


Figure 7. Monthly production amounts (kWh) found as a result of the PVSOL design

3.3. Economic analysis

The photovoltaic system installed on the roof of the school cafeteria was installed in November 2020 with an installation cost of approximately 85 000 TL (\$10 193 - dollar exchange rate: 8.34 TL). A total of 28 panels cost \$6 799.52, the inverter cost \$1 798.56, and a total of \$1595 was spent on project costs, metal rails, cabling, installation and labor costs. Since the system land belongs to the public, no rent or tax is paid. With PVsyst software, it was concluded that the system would operate for 25 years and generate 12.9 MWh of electricity per year, and since the Renewable Energy Resources Support Mechanism (YEKDEM) solar energy purchase price is determined as 13.3 cents/kWh with a 10-year purchase guarantee for Renewable Energy Resources (YEK) certified facilities that have

entered into operation until 06.30.2021, when the sales tariff for the system installed in November 2020 is entered as 13.3 cents/kWh, the system will pay for itself after approximately 6.0 years. However, since the photovoltaic system installed on the roof cannot meet the self-consumption of the school, the offset is realized in kWh, not in money. When the amount of electricity produced by the system is read and deducted from the two-way meter, the remaining kWh amount is paid to the distributor company [17].

In November 2020, when the electricity bills received by the school are examined, the distributor company sells electricity to the institutional consumer with a tariff of 0.99154 TL/kWh, including consumption cost, taxes and funds [18]. Considering that the PVsyst software will generate 12.912 MWh of electricity per year, the amount of the invoice that the school will pay to the distributor company will decrease by $12\,912 \times 0.99154 \text{ TL} = 12\,802.76 \text{ TL}$ per year. It is seen that the photovoltaic system will reduce the amount of electricity bills that the school will pay annually by 12 802.76 TL and will amortize the total installation cost of 85 000 TL in November 2020 within 6.64 years.

Due to the COVID-19 Pandemic, distance education was partially or completely switched to distance education in some months during the 2019-2020 and 2020-2021 academic years. Since there were no students in the school during these periods, electricity consumption data for 2018 was used to understand the full capacity of consumption. The school's electricity consumption in 2018 was 44. 072,73 MWh per year and the photovoltaic system produced a total of 12.473 MWh of electricity throughout 2021. This shows that the photovoltaic system alone cannot meet the electricity consumption.

As can be seen in Table 3, production covered consumption only in July. In July and August, it was seen that the system could meet the consumption as a result of the decrease in electricity consumption due to the school's summer vacation, the department workshops not working, and the heaters not burning.

Table 3. Electricity consumption of the school by month

Months	Electricity Consumption of the School in 2018 (MWh)	Production Values of Photovoltaic System in 2021 (MWh)
January	5.94159	0.460
February	3.44331	0.664
March	4.66566	0.924
April	4.35849	1.181
May	3.81063	1.451
June	2.82501	1.520
July	1.62702	1.633
August	1.51572	1.501
September	2.5617	1.252
October	5.78322	0.939
November	2.61693	0.559
December	4.92345	0.389
Total	44.07273	12.473

It was observed that the difference between the production and consumption amounts increased with the increase in electricity consumption especially in winter months and the decrease in sunshine duration and solar radiation values.

The photovoltaic system installed on the roof produced a total of 12.473 MWh of electrical energy during the 1-year in 2021. Table 4 shows the comparison of the amount of electricity generated by the system with the simulation results of the software.

For 2021, it is seen that the production forecast values of the PVSOL software are higher than the real-life data of the system. It is seen that the closest forecast of the PVSOL software to the real-life data was realized in August 2021. For 2021, the forecast values of PVSOL software deviated the most from the real-life data in June and December.

PVsyst software, on the other hand, made its closest prediction for 2021 in September and October, and showed the most deviation from the real-life data in March and December for 2021. For 2021, the estimated production value of the software is generally higher than the real-life

data. In 2021, the real-life data was lower than the production results predicted by both software (Table 4).

Table 4. Monthly comparison of simulation results with the real-life data of the photovoltaic system

Months	PVsyst (MWh)	PVSOL (MWh)	The real-life data in 2021 (MWh)
January	0.512	0.6343	0.460
February	0.689	0.7467	0.664
March	1.016	1.0421	0.924
April	1.232	1.2621	1.181
May	1.465	1.5901	1.451
June	1.561	1.7571	1.520
July	1.620	1.6717	1.633
August	1.542	1.5158	1.501
September	1.254	1.1994	1.252
October	0.935	0.9043	0.939
November	0.627	0.6396	0.559
December	0.458	0.593	0.389
Total (MWh/year)	12.912	13.556	12.473

During 2021, the rooftop photovoltaic system produced a total of 12.473 MWh of electricity. PVsyst software estimated the total amount of energy that can be produced for 2021 as 12.912 MWh/year and PVSOL software estimated it as 13.556 MWh/year. There was a difference of 0.439 MWh with PVsyst software and 1.083 MWh with PVSOL software between simulation results and the real-life data for 2021. There is an annual difference of 3.40% with PVsyst software and 7.99 % with PVSOL software.

PVSOL software shows the annual average global solar radiation value of the region where the panels are installed as 1.504 MWh/m² and makes calculations according to this value, while PVsyst software shows the annual global solar radiation value of the same region as 1.408,4 MWh/m² and makes production calculations according to this value. According to the SEPA map, the global solar radiation value of most of Gümüşhacıköy district is between 1400-1450 kWh/m².

The photovoltaic system installed on the examined roof does not work with optimum efficiency due to the low roof slope and the roof not facing exactly south. According to the calculations made with PVsyst software, the most suitable panel inclination for the location where the panels are installed is 33° and the panel directions are oriented exactly to the south (azimuth angle = 0°). However, the panel slopes of the fully integrated (non-ventilated) panels on the roof are 11° and the panel orientations are deviated from the south direction to 40° east direction. This significantly reduced the amount of electricity generated by the system.

With the calculation made with PVsyst software, if the main building and the tree had remained in place and all photovoltaic features were used in the same way without changing the panels and inverters used in the system, if the azimuth direction had remained the same (azimuth = -40°) and only the panel vertical slope had been placed at 33° , the estimated annual production of PVsyst software would be 13.317 MWh/year. This would be 0.405 MWh/year more than the 12.912 MWh/year calculated by the PVsyst software with panel inclinations of 11° . If the panels were installed in the most optimum situation with the panel orientations facing full south and the panel slope was 33° , the PVsyst software estimated annual production would be 13.943 MWh/year.

4. Conclusion

In this study, the real electricity production data of the 10 kWp Photovoltaic Solar Energy System installed on the roof of the school cafeteria in Gümüşhacıköy district of Amasya province was compared with the results obtained using PVsyst and PVSOL software. Comparison of the real-life data with the computational results given by the software is important data for measuring the degree of accuracy and analyzing the extent to which shading losses affect the photovoltaic system. At the same time, these comparison results can also be characterized as a feasibility study to understand whether solar power plants can be invested in Gümüşhacıköy district and for future photovoltaic applications.

As a result of the evaluations made on the 10 kWp Photovoltaic solar energy system, it was

determined that the software used gave approximate results to the real production data.

As a result of the calculations made by entering all the parameters of the system, it was concluded that a total of 12.912 MWh of electrical energy could be produced annually with the PVsyst software, and 13.556 MWh of energy could be produced annually with the PVSOL software. During 2021, the actual amount of energy produced by the photovoltaic system was determined as 12.473 MWh. The amount of electrical energy produced is lower than the simulation results with both software for 2021. It was observed that there was a total annual deviation of 3.40 % from the real-life data with the PVsyst software and 7.99 % annually with the PVSOL software.

According to the Turkish National Electricity Grid Emission Factor Information Form prepared by the Ministry of Energy and Natural Resources, the system prevented 12.473 MWh * 0.6482 tons = 8.085 tons of CO₂ emissions for 2021, considering that it prevented 0.6482 tons of CO₂ emissions for every 1 MWh of electricity generated from solar or wind energy [19]. Considering that the system will operate for 25 years, it is calculated that it will reduce a total of 202.125 tons of CO₂ emissions.

Article Information Form

Funding

The author received no financial support for the research, authorship, and/or publication of this paper.

The Declaration of Conflict of Interest/ Common Interest

The authors declare that there is no conflict of interest between them. This research is based on a part of Barış ALAÇAM's Master's Thesis.

Authors' Contribution

The authors contributed equally to the study.

The Declaration of Ethics Committee Approval

This study does not require ethics committee permission or any special permission.

The Declaration of Research and Publication Ethics

The authors of the paper declare that they comply with the scientific, ethical and quotation rules of SAUJS in all processes of the paper and that they do not make any falsification on the data collected. In addition, they declare that Sakarya University Journal of Science and its editorial board have no responsibility for any ethical violations that may be encountered, and that this study has not been evaluated in any academic publication environment other than Sakarya University Journal of Science.

Copyright Statement

Authors own the copyright of their work published in the journal and their work is published under the CC BY-NC 4.0 license.

References

- [1] E. Koç, K. Kaya, "Enerji Kaynakları-Yenilenebilir Enerji Durumu," *Mühendis ve Makina*, 56(668), pp 36-47, 2015.
- [2] N. Yılankırkan, H. Doğan, "Türkiye'nin Enerji Görünümü ve 2023 Yılı Birincil Enerji Arz Projeksiyonu," *Batman Üniversitesi Yaşam Bilimleri Dergisi*, 10(2), pp.77-92, 2020.
- [3] S. Özbektaş, M. C. Şenel, B. Sungur, "Dünyada ve Türkiye'de Yenilenebilir Enerji Durumu ve Kurulum Maliyetleri," *Mühendis ve Makine*, 64, 711, pp. 317-351, 2023.
- [4] Ç. F. Kılıç, "Güneş Enerjisi Türkiye'deki Son Durumu ve Üretim Teknolojileri," *Mühendis ve Makina*, 56 (671), pp. 28-40, 2015.
- [5] Turkish Electricity Transmission Corporation (TEİAŞ). <https://www.teias.gov.tr/kurulu-guc-raporlari>. Last Access Date: 22.04.2024.
- [6] E. Akcan, M. Kuncan, M. R. Minaz, "Pvsyst Yazılımı ile 30 kW Şebekeye Bağlı Fotovoltaik Sistemin Modellenmesi ve Simülasyonu," *Avrupa Bilim ve Teknoloji Dergisi*, 18, pp. 248-261, 2020.
- [7] H. K. Demiryürek, U. Arifoğlu, M. Bolat, "Lebit Enerji Güneş Santralının Pvsyst Programı ile Analizi," *BEÜ Fen Bilimleri Dergisi*, 9 (3), pp.1351-1363, 2020.
- [8] M. S. Çınaroğlu, M. Nalbantoğlu, "Şebekeye Bağlı Üç Adet Fotovoltaik Enerji Santralının PVsyst Programı ile Analizi; Kilis Örneği," *ECJSE*, 8(2), pp. 675-687, 2021.
- [9] S. Komrit, F. Zabihiyan, "Comparative analyses of solar photovoltaic, wind turbine, and solar photovoltaic and wind turbine hybrid systems: Case study of Thailand," *Energy Conversion and Management*, 293, pp. 117479, 2023.
- [10] S. Altınkök, S. Karadeniz, A. Altınkök, "Photovoltaic System Design and Analysis at Faculty Scale," *Journal of Naval Sciences and Engineering*, 18(1), pp. 91-120, 2022.
- [11] E. E. Dirlik, C. Gezeğin, S. A. D. Mohammadi "Comparison of PVsyst, PVSOL and HOMER Simulation Software Results with Real Production Data of Solar Power Plants in Different Provinces of Türkiye," *Journal of Engineering Research and Applied Science*, 12(2), pp. 2357-2364, 2023.
- [12] (SEPA, Solar Energy Potential Atlas) Güneş Enerjisi Potansiyel Atlası, GEPA (2021). <https://gepa.enerji.gov.tr/MyCalculator/> Last Access Date: 25.04.2024.
- [13] N. Kan Kaynar, "Yenilenebilir Enerji Kaynaklarından Güneş Enerjisinin Amasya İlindeki Potansiyeli," *Bilge International Journal of Science and Technology Research*, 4 (2), pp. 48-54, 2020.
- [14] PVsyst Program Interface. <https://www.pvsyst.com>. Last Access Date: 22.06.2021.
- [15] Meteonorm 7.3 https://www.pvsyst.com/help/meteo_sourc

e_meteororm.htm. Last Access Date:
22.06.2021

- [16] Valentin Software, <https://valentin-software.com/en/products/custom-software/>. Last Access Date: 06.12.2021.
- [17] YEKDEM, Yenilenebilir Enerji Kaynakları Destekleme Mekanizması.
- [18] <https://www.epdk.gov.tr/Detay/Icerik/3-0-72-3/elektrikyekdem> Last Access Date: 22.06.2021.
- [19] ETBK, Enerji ve Tabii Kaynaklar Bakanlığı. <https://enerji.gov.tr/evced-cevre-ve-iklim-turkiye-ulusal-elektrik-sebekesi-emisyon-faktoru/>. Last Access Date: 23.03.2022

Elemental Impurity Analysis in Five Different Types of Coffee: Assessment of Carcinogenic and Non-carcinogenic Risks

Fadime Canbolat 

Department of Pharmacy Services, Vocational School of Health Services, Çanakkale Onsekiz Mart University, Çanakkale, Türkiye, fadime.canbolat@comu.edu.tr

ARTICLE INFO

ABSTRACT

Keywords:
Coffee
Elemental impurity
Risk assessment

In the study, the levels of Cd, Pb, As, and Hg elemental impurities potentially present in coffee bean samples from Indonesia, Kenya, Colombia, Guatemala, and Türkiye were determined using chromatographic analysis, and the analysis results were utilized to assess the risks on human health. The risk assessment of coffee was calculated for one or three servings per day for 365 days a year. Exposure to coffee consumption was calculated according to age groups of young adults and middle-aged adults (20-65 years). When Cd, Pb, As and Hg levels in coffee samples were analyzed, Cd in coffee samples was found to be in the range of approximately 3.70 - 5.89 µg/kg, Pb in the range of 25.68-41.11 µg/kg, As in the range of 1.45-6.64 µg/kg and Hg in the range of 1.06-5.06 µg/kg. Hazard Index (HI) values for all elements in the assessment of non-carcinogenic risks were found to be <1.0. When the cancer risk (CR) value was calculated for Cd, Pb, and As, it was found that the CR value did not exceed the United States Environmental Protection Agency (USEPA) criteria in all coffee samples in both scenarios. Considering the assessment of the health risks of elemental impurities in five different coffee bean samples, it was concluded that all samples' CR and HI values did not exceed the USEPA criteria.



Article History:
Received: 22.05.2024
Accepted: 26.07.2024
Online Available: 06.08.2024

1. Introduction

The spread of coffee worldwide gained momentum with its origins in Northeast Africa, then transitioned to the Middle East in the 15th century and subsequently to Europe. Coffee consumption has become a part of daily life on a global scale. The average annual consumption per capita in America and Europe is 5.1 kg/year [1]. The botanical family of coffee plants comprises approximately 500 genera and over 6000 species. The commercially most significant genus is *Coffea* (Rubiaceae family). Among the prominent species within this genus are *Coffea arabica* (Arabica) and *Coffea canephora* (Robusta) [2, 3].

However, all types of coffee have pharmacologically bioactive ingredients [4].

Coffee serves as a significant source of essential elements required daily, such as copper (Cu), manganese (Mn), magnesium (Mg), calcium (Ca), iron (Fe), potassium (K), phosphorus (P), and zinc (Zn). However, some heavy metals found in coffee, such as cadmium (Cd), lead (Pb), arsenic (As), and mercury (Hg), can be harmful to health [5]. The type and level of elements in plants are directly related to factors such as the geographical area where the plant grows, climate, altitude, soil properties, and crop cultivation methods [5, 6].

The accumulation of heavy metals in plants is also affected by these processes. Therefore, heavy metal levels in coffee content may vary depending on these factors. These heavy metals have the risk of being accumulated in coffee and reaching the consumer directly [6].

Various guidelines exist for the risk assessment of metal toxicity in foods like coffee [7, 8]. These guidelines direct the assessment of heavy metal content to ensure food safety and protect consumer health. For instance, the U.S. Food and Drug Administration (USFDA) provides specific guidelines (USP <232>, USP <233>) for assessing metal content in foods [9]. These USFDA guidelines establish permissible levels of toxic elements in foods and provide food producers with appropriate testing methods and monitoring strategies.

The European Food Safety Authority (EFSA) also sets guidelines and standards for evaluating metal content in foods [8]. EFSA's guidelines rely on scientific data to identify risks of metal toxicity in foods and offer food producers suitable testing methods and monitoring strategies. These guidelines serve as fundamental sources used to assess metal toxicity in foods. Risk assessments conducted by these guidelines are crucial for ensuring consumers consume safe and healthy foods. Elemental impurities in foods are classified into specific categories based on their toxic effects and potential risks to human health. These classifications are often based on the type of element, its toxicity, and the routes of exposure to the human body.

Organizations like the USFDA and EFSA generally use three classes when determining the permissible maximum levels of metal elements in foods. Class 1: This class typically includes elements with the highest toxicity and pose the greatest risk to human health. Elements such as Cd, Pb, As, and Hg may be included in this category. Class 2: This class includes elements that pose a lower risk to human health. Class 3: This class generally includes elements with low risk to human health. These elements typically do not have any significant toxic effects on human health at typical levels of food-related exposure or have very low toxicity [10].

These classifications are used to assess the risk of elements for food safety and are monitored by the food industry, regulators, and researchers. The detection of one or more elemental impurities, such as Cd, Pb, As, and Hg, particularly in coffee ingredients consumed globally, and the evaluation of their potentially harmful effects on

health have increased the importance of elemental impurity analyses and risk assessments in the literature [11-13]. Exposure to these heavy metals is a silent threat to human life. They have the potential to damage almost every organ and body system. Excessive Cd exposure causes kidney, lung, liver, skeletal structure damage and cancer [14].

Target organs where Cd can accumulate in the body are bones, brain, blood, kidneys and thyroid gland. Pb exposure can cause high blood pressure, muscle weakness and headaches [15]. Inorganic As is acutely toxic and ingestion of large amounts can lead to peripheral vascular disease, severe central nervous system (CNS) disorders and cardiovascular disease. Long-term exposure to As increases the risk of lung, bladder and kidney cancer [16]. Long-term exposure to Hg compounds in humans and animals can cause toxic effects on the skin, cardiovascular, pulmonary, urinary, gastrointestinal and neurological systems [17].

In order to minimize these risks, it is important to ensure the continuity of metal risk assessment studies on foods, to share analysis results on the necessary platforms, to support field-based experiments and tests, and to develop risk management strategies. Therefore, the detection of elemental impurities in coffee, which has an important place in food consumption, and the evaluation of their potential toxic effects on health are of great importance for consumer awareness and quality control processes in the coffee industry.

In this study, it was aimed to determine the heavy metal concentrations in Turkish coffee, which is widely consumed in Türkiye, and coffees from Indonesia, Kenya, Colombia, Guatemala in the markets, to provide up-to-date data to the literature and to provide a perspective on the risk that coffee consumers may be exposed to through coffee consumption. Therefore, the levels of Cd, Pb, As, and Hg elemental impurities potentially present in coffee beans from Indonesia, Kenya, Colombia, Guatemala, and Türkiye were determined using chromatographic analysis, and the analysis results were used to evaluate the carcinogenic and non-carcinogenic risks on human health.

2. Materials and Methods

2.1. Material

Five different coffee beans (*Coffea Arabica* L.) samples were bought at grocery stores (Ozbek Kahvecisi, Çanakkale) in Türkiye, in April 2024.

2.2. Chemical analysis

Analyses were carried out by considering Inductively coupled plasma–mass spectrometry (ICP-MS) methods used in the literature for heavy metal analysis [10, 13, 18-20]. 0.3 g sample was weighed into polytetrafluoroethylene (PTFE) tubes, followed by the addition of 8 mL nitric acid (60% HNO₃) and 2 mL hydrogen peroxide (H₂O₂). After waiting for gas evolution for a while in a fume hood, the Teflon tubes were sealed, and the samples were digested for 30 minutes using a microwave digestion system (Ethos Easy, Milestone Srl., IT) (Table 1).

Table 1. The microwave digestion program

Time (minute)	Power (W)	Temperature (°C)
15	0 - 1800	30 - 200
15	1800	200

After the microwave digestion, the sample solutions were diluted to 30 mL with ultrapure water.

2.3. Inductively coupled plasma–mass spectrometry (ICP–MS) parameter

The ICP-MS analyses were conducted at İzmir Katip Çelebi University Central Research Laboratories Application and Research Center (İzmir, Türkiye). For the analyses, ICP–MS instrument (7800, Agilent Technologies Inc., US, CA) combined with a chiller (Agilent G3292A), autosampler (Agilent SPS4), vacuum pump system, and Mass Hunter 4.4 software was utilized. The device parameters are provided in Table 2.

2.4. Calculations

The safety of coffee was assessed based on consuming either one serving or three servings daily throughout the year [11]. Exposure to coffee consumption was calculated according to

age groups of young adults and middle-aged adults (20-65 years) [21]. One portion was defined as the amount of the instant product advised by the manufacturers, as stated on the packaging. For one cup of Turkish coffee, 0.007 kg of Turkish coffee and 0.015 kg of coffee were prepared in 240 mL for other types of coffee. Calculations were made accordingly. The values utilized in assessing and evaluating carcinogenic and non-carcinogenic risks associated with elemental impurities are provided in Table 3.

Table 2. The device parameters

Parameter	Value
RF Power	1500 W
RF Voltage	1.80 V
S/C Temperature	2 °C
Skimmer Diameter	10 mm
Nebulizer Gas Flow Rate	1 L/min
Nebulizer Pump	0.10 rps
Internal standards	⁶ Li, ⁴⁵ Sc, ⁷² Ge, ⁸⁹ Y, ¹¹⁵ In, ¹⁵⁹ Tb, ²⁰⁹ Bi
Tune solution	⁷ Li, ⁸⁹ Y, ²⁰⁵ Tl

Table 3. Oral Reference dose factor (RfD), maximum permitted dose (PDE), and the cancer slope factor (CSF) limits for elemental impurities

Element	RfD (mg/kg/day)	PDE (mg/kg)	CSF (mg/kg/day) ⁻¹	Reference
Cd	0.001	0.3	0.38	[12]
Pb	0.0035	10.0	0.0085	[11, 12]
As	0.0003	5.0	1.5	[12]
Hg	0.0005	0.2	-	[12]

RfD; Oral reference dose; mg/kg/day, PDE; maximum permitted dose (mg/kg), CSF; the cancer slope factor values ((mg/kg/day)⁻¹)

2.5. Health risks assessment

Many studies have examined how humans may be exposed to harmful substances by consuming contaminated food [10, 13]. In this study, the estimated daily intake (EDI), the target hazard quotient (THQ), the hazard index (HI), and the target cancer risk (CR) were determined to quantify the potential adverse health effects.

THQ was employed to assess the non-carcinogenic health risks associated with elemental impurities in adult populations during

non-carcinogenic risk evaluations. To compute the THQ, the first step was establishing each element's EDI value. The EDI value was determined using Equation 1, assuming a body weight of 70 kg for a typical adult [10].

$$\text{EDI (mg/kg/day)} = (\text{EF} \times \text{ED} \times \text{IR} \times \text{MC}) \times \text{CF} / (\text{BW} \times \text{AT}) \quad (1)$$

EF: Exposure frequency (365 days/year) [22], ED: Exposure duration (45 years for young adults and middle-aged adults) [10, 21], IR: The amount of coffee recommended by the manufacturer when preparing one cup or one serving of coffee, MC: Amount of elemental impurity in the coffee; $\mu\text{g/kg}$, BW: Body weight; 70 kg for adults [10], AT: Average time (days), which is $\text{ED} \times \text{EF}$ [22], CF: Conversion coefficient (from μg to mg ; 10^{-3})

The THQ value was determined by calculating each elemental impurity's EDI and RfD values (Equation 2), according to Winiarska-Mieczan et al. [11].

$$\text{THQ} = \text{EDI/RfD} \quad (2)$$

THQ: The target hazard quotient
EDI: Estimated daily intake dose (mg/kg/day)
RfD: Oral reference dose (mg/kg/day)

The $\text{THQ} \geq 1$ suggests that the exposed element risks human health [2].

Equation 3 calculated the HI of the combined risk related to the metals examined by totaling the THQs for Cd, Pb, As, and Hg in each sample [10].

$$\text{HI} = \text{THQ (Cd)} + \text{THQ (Pb)} + \text{THQ (As)} + \text{THQ (Hg)} \quad (3)$$

HI: The hazard index

THQ: The target hazard quotient

An HI value of 1 or lower indicates no harmful effects will occur due to metal exposure [2].

Regular contact with certain substances that may cause cancer can raise the risk of cancer in individuals. Equation 4 can calculate the cancer risk (CR) from chronic exposure to toxic elements over a lifetime [23].

$$\text{CR} = \text{EDI} \times \text{CSF} \quad (4)$$

CR: cancer risk

EDI: Estimated daily intake dose (mg/kg/day)

CSF: The cancer slope factor (mg/kg/day) $^{-1}$

CSF for carcinogenic metals, including Cd, Pb, and As, are 0.38, 0.0085, and 1.5 (mg/kg/day) $^{-1}$, respectively (Table 3) [11, 12, 23]. According to the USEPA, human exposure to CR values within 1×10^{-6} to 1×10^{-4} is acceptable. However, it is imperative that the CR value does not exceed 1×10^{-4} [10-12, 23].

2.6. Statistical evaluation

The statistical analysis of the MC in coffee samples was analyzed three times using the IBM SPSS 23 software. A normality test was conducted, and all data showing a normal distribution underwent intergroup comparison using One-Way ANOVA followed by Tukey's post-hoc test at 0.05 significance level.

3. Results

3.1. Heavy metals and toxicity levels

The microwave sample preparation method was used in the ICP-MS device to analyze four elemental impurities (Cd, Pb, As and Hg), classified as Class 1 elements in the USP <232> guideline. The samples were readied, assessed, and judged based on the standards outlined in the USP <232> and USP <233> regulations [9]. The quantification parameter data in Table 4 includes the calibration curve details for ICP-MS and the limit of detection (LOD) values derived from the calibration standards for the four elements. The method had a calibration range of 0.5-1000 $\mu\text{g/L}$ for Cd, Pb, As. The range of calibration for Hg was 1.5-100 $\mu\text{g/L}$. The regression (R^2) value for each element was $R^2 \geq 0.9995$.

Table 4. Quantification parameters for elemental impurities

Element	Isotop	LOD ($\mu\text{g/L}$)	Calibration range ($\mu\text{g/L}$)	Calibration curve regression (R^2) value
Cd	111	0.005	0.5-1000	1.0000
Pb	208	0.02	0.5-1000	0.9996
As	75	0.02	0.5-1000	0.9998
Hg	201	1.168	1.5-100	0.9995

LOD; Limit of dedection

When Cd, Pb, As and Hg levels in coffee samples were analyzed, Cd was detected in coffee samples in the range of approximately 3.70 - 5.89 $\mu\text{g}/\text{kg}$. Colombian coffee beans were found to have the highest Cd level (Table 5). Colombia is followed by Indonesia, Kenya, Turkish, and Guatemala coffee beans. Statistically significant differences were observed among the Cd levels in all coffees ($p < 0.05$) (Table 5).

The Pb level in the coffee samples was approximately 25.68-41.11 $\mu\text{g}/\text{kg}$. The coffee with the highest Pb levels was Indonesian coffee.

The Pb levels in the other coffee beans ranged from highest to lowest in Türkiye, Guatemala, Colombia and Kenya, respectively. The Pb level in Indonesia was statistically different ($p < 0.05$) from Kenya, Colombia and Guatemala (Table 5).

The As level in coffee samples was approximately 1.45-6.64 $\mu\text{g}/\text{kg}$. The highest As level was found in Indonesian coffee. Other coffees had trace levels of As. The As level in Indonesian coffee was statistically different ($p < 0.05$) from the As level in Kenyan, Colombian and Guatemalan as well as Turkish coffees (Table 5).

Table 5. Levels of elemental impurities and carcinogenic and non-carcinogenic results in five different coffee beans

Sample	MC ($\mu\text{g}/\text{kg}$) (mean \pm std. dev.)			
	Cd	Pb	As	Hg
Indonesia	4.95 \pm 0.02 ^a	41.11 \pm 3.22 ^a	6.64 \pm 0.71 ^a	5.06 \pm 0.32 ^a
Kenya	4.38 \pm 0.03 ^b	25.68 \pm 1.70 ^b	1.99 \pm 0.03 ^b	2.12 \pm 0.43 ^{b,c}
Colombia	5.89 \pm 0.02 ^c	26.53 \pm 1.41 ^b	1.45 \pm 0.02 ^b	3.11 \pm 0.21 ^b
Guatemala	3.70 \pm 0.04 ^d	30.05 \pm 1.70 ^b	1.74 \pm 0.01 ^b	1.06 \pm 0.02 ^c
Turkish	4.21 \pm 0.03 ^e	33.85 \pm 1.00 ^{a,b}	2.66 \pm 0.09 ^b	2.05 \pm 0.30 ^{b,c}

Sample	Element	Risk assessment							
		EDI (mg/kgbw/day)	THQ	HI	CR	EDI (mg/kgbw/day)	THQ	HI	CR
Indonesia	Cd	1x10 ⁻⁶	11x10 ⁻⁴	104x10 ⁻⁴	6.7 x10 ⁻⁶	5x10 ⁻⁶	53x10 ⁻⁴	524x10 ⁻⁴	3.3 x10 ⁻⁵
	Pb	9x10 ⁻⁶	25x10 ⁻⁴		7.5 x10 ⁻⁸	44x10 ⁻⁶	126x10 ⁻⁴		3.7x10 ⁻⁷
	As	1x10 ⁻⁶	47x10 ⁻⁴		2.1 x10 ⁻⁶	7x10 ⁻⁶	237x10 ⁻⁴		1.1x10 ⁻⁵
	Hg	1x10 ⁻⁶	21x10 ⁻⁴		NC	5x10 ⁻⁶	108x10 ⁻⁴		NC
Kenya	Cd	1x10 ⁻⁶	9x10 ⁻⁴	48x10 ⁻⁴	5.9 x10 ⁻⁶	5x10 ⁻⁶	47x10 ⁻⁴	212x10 ⁻⁴	3.0 x10 ⁻⁵
	Pb	6x10 ⁻⁶	16x10 ⁻⁴		4.7 x10 ⁻⁸	28x10 ⁻⁶	79x10 ⁻⁴		2.3x10 ⁻⁷
	As	4x10 ⁻⁷	14x10 ⁻⁴		6.4 x10 ⁻⁷	2x10 ⁻⁶	71x10 ⁻⁴		3.2 x10 ⁻⁶
	Hg	4x10 ⁻⁷	9x10 ⁻⁴		NC	2x10 ⁻⁶	45x10 ⁻⁴		NC
Colombia	Cd	1x10 ⁻⁶	13x10 ⁻⁴	52x10 ⁻⁴	7.9 x10 ⁻⁶	6x10 ⁻⁶	63x10 ⁻⁴	233x10 ⁻⁴	4.0 x10 ⁻⁵
	Pb	6x10 ⁻⁶	16x10 ⁻⁴		4.8 x10 ⁻⁸	28x10 ⁻⁶	81x10 ⁻⁴		2.4 x10 ⁻⁷
	As	3x10 ⁻⁷	10x10 ⁻⁴		4.7 x10 ⁻⁷	2x10 ⁻⁶	52x10 ⁻⁴		2.3 x10 ⁻⁶
	Hg	1x10 ⁻⁶	13x10 ⁻⁴		NC	3x10 ⁻⁶	67x10 ⁻⁴		NC
Guatemala	Cd	1x10 ⁻⁶	8x10 ⁻⁴	42x10 ⁻⁴	5 x10 ⁻⁶	4x10 ⁻⁶	40x10 ⁻⁴	217x10 ⁻⁴	2.5 x10 ⁻⁵
	Pb	6x10 ⁻⁶	18x10 ⁻⁴		5.5 x10 ⁻⁸	32x10 ⁻⁶	92x10 ⁻⁴		2.7 x10 ⁻⁷
	As	3x10 ⁻⁷	12x10 ⁻⁴		5.6x10 ⁻⁷	2x10 ⁻⁶	62x10 ⁻⁴		2.8 x10 ⁻⁶
	Hg	2x10 ⁻⁷	4x10 ⁻⁴		NC	1x10 ⁻⁶	23x10 ⁻⁴		NC
Turkish	Cd	4x10 ⁻⁷	4x10 ⁻⁴	26x10 ⁻⁴	2.6 x10 ⁻⁶	2x10 ⁻⁶	21x10 ⁻⁴	134x10 ⁻⁴	1.3 x10 ⁻⁵
	Pb	3x10 ⁻⁶	9x10 ⁻⁴		2.9 x10 ⁻⁸	17x10 ⁻⁶	48x10 ⁻⁴		1.4 x10 ⁻⁷
	As	2x10 ⁻⁷	9x10 ⁻⁴		3.9 x10 ⁻⁷	1x10 ⁻⁶	44x10 ⁻⁴		2.0 x10 ⁻⁶
	Hg	2x10 ⁻⁷	4x10 ⁻⁴		NC	1x10 ⁻⁶	21x10 ⁻⁴		NC

MC; Amount of elemental impurity in the coffee ($\mu\text{g}/\text{kg}$), EDI; Estimated daily intake dose (mg/kg/day), THQ; The target hazard quotient, HI; The hazard index, CR; Cancer risk, NC; Not calculated. The mean MC of samples followed by different letters in the same column are significantly different ($p < 0.05$).

The Hg level in the coffee samples was approximately 1.06-5.06 $\mu\text{g}/\text{kg}$. Hg levels were highest in Indonesian coffee. Hg levels in the other coffees were trace levels. The Hg level in Indonesian coffee was statistically different from that in all other coffees. A difference was also found between Colombian and Guatemalan coffees ($p < 0.05$) (Table 5).

3.2. The health risk assessment

In the study, the age range covering young adults and middle-aged adults (20-65 years) was considered as the exposure age range, and according to two different coffee consumption scenarios (one cup or three cups per day), EDI, THQ, and HI values were calculated (Table 5). The HI for the combined risk related to the examined metals was computed by adding the

THQs for Cd, Pb, As, and Hg in every coffee sample (Equation 3). When examining the HI values for all samples considering both scenarios in Table 5; the HI values for the first and second scenarios were respectively 104×10^{-4} and 524×10^{-4} in Indonesian coffee, 48×10^{-4} and 212×10^{-4} in Kenyan coffee, 52×10^{-4} and 233×10^{-4} in Colombian coffee, 42×10^{-4} and 217×10^{-4} in Guatemalan coffee, and 26×10^{-4} and 134×10^{-4} in Turkish coffee.

Since the HI value was less than one for all coffees, consuming one or three cups of coffee between the ages of 20-65 is not expected to cause adverse non-carcinogenic effects due to metal exposure. However, Turkish coffee has the lowest HI value among all coffee types. It has been determined that Guatemalan and Turkish coffees are more reliable than others in terms of metal levels and HI values. The level of the HI value for each coffee sample is directly affected by the IR amount of the coffee samples (For one cup of Turkish coffee, 0.007 kg of Turkish coffee and 0.015 kg of coffee were prepared in 240 mL for other types of coffee). The IR level of Turkish coffee was almost half of the IR level of other coffees.

When examining the carcinogenic risk assessment of the elements, it is observed that the CR values of Cd, Pb, and As elements in all samples are less than 10^{-4} . Considering the criteria, as the metal levels in the samples are within acceptable limits, no carcinogenic risk seems to be present due to the heavy metal content.

4. Discussion

Elemental impurities, common in nature, can accumulate in plants through soil, water, air, or other means. Since these elemental impurities can cause various health problems in the human body, non-toxic limits for these elements are specified in the guidelines [13]. Assessing the accumulation of elemental contaminants in coffee samples, one of the most widely consumed foods is very important to ensure human safety due to its widespread global consumption [24, 25]. In our study, the amounts of Cd, Pb, As, and Hg heavy metals classified as Class 1 in USP <232> in five different ground coffee beans grown in different geographical

regions were determined by ICP-MS, and risk assessments were made according to the values obtained.

Monitoring elemental impurities potentially present in foods due to contamination is crucial for health purposes. Class 1 elements are toxic, and their levels should not exceed PDE limits. Cd is typically found at low levels in nature [10]. In our study, the range of Cd in all coffee samples was below the permitted limit set by the World Health Organization (WHO) of 0.3 mg/kg [12]. The mean Cd levels in the five different coffee beans included in the study ranged from 3.70 to 5.89 $\mu\text{g}/\text{kg}$. Cd levels were found to be in the order of Colombia > Indonesia > Kenya > Turkish > Guatemala. Cd levels were statistically different among all coffee samples (Table 5).

Our study showed a statistically significant difference in Cd levels between Colombia and Kenya coffee beans (Table 5). In the Albals et al. (2021) study, Cd levels in coffee beans originating from Colombia and Kenya were found to be 150 $\mu\text{g}/\text{kg}$ and 140 $\mu\text{g}/\text{kg}$, respectively [24]. In the study by Kowalska (2021), Cd levels in eight different Arabica coffee bean varieties were found to be an average of 58 $\mu\text{g}/\text{kg}$ [23]. In the study by Ali (2024), the average Cd level in 42 coffee samples collected from local markets in Iraq was 35 $\mu\text{g}/\text{kg}$ [25]. Upon examination of the literature and our analysis results, it was determined that Cd levels are below the permitted range set by the WHO.

Pb is considered a toxic environmental pollutant, and its toxicity in humans has been associated with mental disorders, behavioral abnormalities, seizures, and other health issues. This metal can accumulate in tea leaves and coffee plants, raising consumer concerns [25]. The mean Pb level in our study's five different coffee beans ranged from 25.68 to 41.11 $\mu\text{g}/\text{kg}$. Pb levels were found to be in the order of Kenya > Colombia > Guatemala > Turkish > Indonesia. While the Pb level in Indonesian and Turkish coffee beans did not show a statistically significant difference, the Pb level in Indonesian coffee beans was statistically different from that in Kenya, Colombia, and Guatemala coffee samples (Table 5). In the study by Nędzarek et al. (2013), Pb levels in infusion coffee samples from Bosnia

and Herzegovina, Brazil, Lebanon, and Poland were found to be 710-1050 $\mu\text{g}/\text{kg}$ [4]. In the Albals et al. (2021) study, Pb levels in coffee beans originating from Colombia and Kenya were 1040 $\mu\text{g}/\text{kg}$ and 1380 $\mu\text{g}/\text{kg}$, respectively [24]. Similarly to the literature, our study did not find a statistically significant difference in Pb levels between Colombia and Kenya coffee beans (Table 5). In the study by Guadalupe et al. (2023), Pb levels in parchment coffee beans obtained from the Peru region were between 640-670 $\mu\text{g}/\text{kg}$ [2]. Our study and analytical data from the literature revealed that all samples contained low levels of Pb. These values were below the permitted limit of 10.0 mg/kg set by the WHO [12].

As is among the toxic elements capable of entering organisms via the consumption of water and food. As is a toxic element, and its chronic ingestion can cause many adverse health effects [10]. Among the coffee samples, As had concentrations ranging from 1.45-6.64 $\mu\text{g}/\text{kg}$, lower than the PDE (5 mg/kg) [12]. The mean As concentration in our study's five different ground coffee beans was determined to be in the order of Indonesia > Turkish > Kenya > Guatemala > Colombia. The As level in Indonesian coffee samples differed statistically from all other coffee samples (Table 5). In the study by Omer et al. (2019), the highest As level in coffee samples sold in Saudi markets was 0.107 mg/kg [26]. In the study by Taghizadeh et al. (2023), the highest As level among 29 different coffee samples was found to be 0.32 mg/kg [12]. Our study and analytical data from the literature revealed that all samples contained low levels of As. These values were below the permitted limit set by the WHO.

Hg is commonly present in various forms in the natural environment. Metallic and inorganic mercury are commonly found in nature. Mercury salts are naturally occurring forms of inorganic mercury. Microorganisms generate organic mercury through biological processes. Inorganic mercury is frequently utilized in the medical field, as well as in disinfectants and ointments. All types of Hg can lead to harmful effects [10]. The mean Hg level in our study's five different ground coffee beans ranged from 1.06–5.06 $\mu\text{g}/\text{kg}$. The Hg level was determined to be in the

order of Indonesia > Colombia > Kenya > Turkish > Guatemala. The Hg level in Indonesian coffee beans differed statistically from all other coffees. The Hg level in Colombian and Guatemalan coffee beans was also statistically different (Table 5). In the study by Massoud et al. (2022), the Hg level in roasted coffee powder samples sold in Iran and Turkish markets was below 0.3 $\mu\text{g}/\text{kg}$ [27]. In the study by Taghizadeh et al. (2023), the highest Hg level among 29 different coffee samples was found to be 0.94 mg/kg [12]. Our study and analytical data from the literature revealed that all samples contained low levels of Hg. These values were below the permitted limit set by the WHO [12].

Our study conducted carcinogenic and non-carcinogenic risk assessments considering consumption scenarios of one or three cups of coffee per day for individuals aged 20-65. The EDI, THQ, HI, and CR calculations were performed for all investigated metals in coffee. The calculated EDIs for all examined metals through the consumption of one or three cups of coffee are summarized in Table 5. According to the results, the EDI values for all elements were below the RfD, indicating no health risk associated with our samples. The THQ values for all samples were less than one, indicating no potential consumer health effects.

The HI, which represents the combined non-carcinogenic effects of the investigated heavy metals in coffee, was less than one in our samples. HI values of less than one indicate no significant health risks related to our samples. However, the HI values for coffee samples were determined to be in the order of Indonesia > Colombia > Kenya > Guatemala > Turkish. In a study by Winiarska-Mieczan et al. (2023) on the elemental impurity analysis of coffee beans, the THQ and HI values were found to be less than one for Cd and Pb, indicating that the risk of disease due to Cd and Pb exposure through coffee consumption could be considered very low [11]. Similarly, in another study by Taghizadeh et al. (2023) on coffee and tea, the THQ and HI values for Cd, Pb, As, and Hg were below 1.0 [12], consistent with our findings. When the risk assessment of heavy metal exposure in terms of human health is associated with coffee consumption, it is clear that no health

risk is associated with the consumption of one or three cups of the coffees in our study. Considering that the recommended doses in coffee consumption directly affect the HI value, it is predicted that any health risk that may occur due to heavy metal exposure will not occur for the coffee types included in the study if the usage dose is not exceeded.

In our study, when the CR value was calculated for Cd, Pb, and As, it was found that the CR value did not exceed 1×10^{-4} in all coffee samples in both scenarios, meeting the USEPA criteria. Considering the risk assessment of elemental impurities in the five different ground coffee beans included in our study, it can be concluded based on our data that the consumption of Indonesia, Kenya, Colombia, Guatemala, and Turkish coffee varieties does not pose a health risk, as the CR and HI values for all samples did not exceed the USEPA criteria.

5. Conclusion

This study evaluated the risks associated with oral ingestion of four elemental impurities classified under Class 1 in USP<232> in five different ground coffee beans. The levels of elemental impurities in each sample were determined by chromatographic means, followed by risk calculations. In the assessment of non-carcinogenic risks, all elements had HI values <1.0. Therefore, elemental impurities in the coffee samples analyzed in our study do not pose non-carcinogenic health risks in terms of the heavy metals. For the carcinogenic risk calculation, the CR values of Cd, Pb and As elemental impurities were calculated and no health risks for coffee consumers were identified based on the CR values. The results of our analysis show that the level of elemental impurities that can enter the human body with the consumption of one to three cups of coffee does not pose a health risk. However, the cumulative assessment of elemental impurity levels from other foods in the diet is important for expanding the risk analysis. For this reason, planning and conducting comprehensive risk assessment studies that take into account individual differences and the presence of metal levels in other consumed foods will contribute to the literature in order to determine the levels of

heavy metals that may be exposed through diet and to perform risk calculations.

Article Information Form

Acknowledgments

We would like to thank Asst. Prof. Ayşe Özçetin.

Funding

The author has no received any financial support for the research, authorship or publication of this study.

The Declaration of Conflict of Interest/ Common Interest

No conflict of interest or common interest has been declared by the author.

The Declaration of Ethics Committee Approval

This study does not require ethics committee permission or any special permission.

The Declaration of Research and Publication Ethics

The author of the paper declares that she complies with the scientific, ethical, and quotation rules of SAUJS in all processes of the paper and that they do not make any falsification on the data collected. In addition, he declares that Sakarya University Journal of Science and its editorial board have no responsibility for any ethical violations that may be encountered and that this study has not been evaluated in any academic publication environment other than Sakarya University Journal of Science.

Copyright Statement

The author owns the copyright of their work published in the journal, and their work is published under the CC BY-NC 4.0 license.

References

- [1] A. Ornek, "Kahve ve Türkiye'de kahve kültürü," in *Gastronomi Alanında Tematik Araştırmalar I*, Y. Ogan, Ed. İstanbul: Çizgi Kitapevi, 2022, pp. 38-46.
- [2] G. A. Guadalupe, S. G. Chavez, E. Arellano, E. Doménech, "Probabilistic Risk Characterization of Heavy Metals in Peruvian Coffee: Implications of Variety,

- Region and Processing,” *Foods*, vol. 12, no. 17, pp. 1-13, 2023.
- [3] M. D. S. G. Barbosa, M. B. dos Santos Scholz, C. S. G. Kitzberger, M. De Toledo Benassi, “Correlation between the composition of green Arabica coffee beans and the sensory quality of coffee brews,” *Food Chemistry*, vol. 292, pp. 275-280, 2019.
- [4] A. Nędzarek, A. Tórz, B. Karakiewicz, J. S. Clark, M. Laszczyńska, A. Kaleta, G. Adler, “Concentrations of heavy metals (Mn, Co, Ni, Cr, Ag, Pb) in coffee,” *Acta Biochimica Polonica*, vol. 60, no. 4, pp. 623-627, 2013.
- [5] A. Rahimi, E. Talebi-Ghane, A. Heshmati, A. Ranjbar, F. Mehri, “Content of potentially toxic elements (PTEs) in coffee and coffee-based products: a meta-analysis study, systematic review, and health risk assessment,” *Drug and Chemical Toxicology*, vol. 47, no. 3, pp. 356-364, 2024.
- [6] A. Gure, B. S. Chandravanshi, T. W. Godeto, “Metals in green coffee beans from major coffee-growing regions of Ethiopia,” *Chemistry International*, vol. 3, no. 4, pp. 458-468, 2017.
- [7] World Health Organisation (WHO), “WHO Environmental Health Criteria 240: Principles and methods for the risk assessment of chemicals in food. IPCS International Programme on Chemical Safety,” World Health Organization, Geneva, 2009.
- [8] W. Koch, M. Czop, K. Iłowiecka, A. Nawrocka, D. Wiącek, “Dietary intake of toxic heavy metals with major groups of food products—results of analytical determinations,” *Nutrients*, vol. 14, no. 8, pp. 1-17, 2022.
- [9] A. J. DeStefano, K. Zaidi, T. L. Cecil, G. I. Giancaspro, E. I. A. P. USP, “Elemental Impurities-Information,” *In Pharmacopeial forum*, vol. 36, no. 1, pp. 2-9, 2010.
- [10] F. Canbolat, “Analysis of non-carcinogenic health risk assessment of elemental impurities in vitamin C supplements,” *Iranian Journal of Basic Medical Sciences*, vol. 26, no. 2, pp. 216-227, 2023.
- [11] A. Winiarska-Mieczan, K. Jachimowicz, S. Kislova, M. Kwiecień, Z. Zasadna, D. Yanovych, “Cadmium and lead concentration in drinking instant coffee, instant coffee drinks and coffee substitutes: safety and health risk assessment,” *Biological Trace Element Research*, vol. 201, no. 1, pp. 425-434, 2023.
- [12] S. F. Taghizadeh, M. Azizi, G. Hassanpourfard, R. Rezaee, G. Karimi, “Assessment of carcinogenic and non-carcinogenic risk of exposure to metals via consumption of coffee, tea, and herbal tea in Iranians,” *Biological Trace Element Research*, vol. 201, no. 3, pp. 1520-1537, 2023.
- [13] B. Yüksel, F. Ustaoglu, M. M. Yazman, M. E. Şeker, T. Öncü, “Exposure to potentially toxic elements through ingestion of canned non-alcoholic drinks sold in Istanbul, Türkiye: A health risk assessment study,” *Journal of Food Composition and Analysis*, vol. 121, pp.1-17, 2023.
- [14] F. Zhu, L. Qu, W. Fan, M. Qiao, H. Hao, X. Wang, “Assessment of heavy metals in some wild edible mushrooms collected from Yunnan Province, China,” *Environmental Monitoring and Assessment*, vol. 179, pp. 191-199, 2011.
- [15] A. Quarcoo, G. Adotey, “Determination of heavy metals in *Pleurotus ostreatus* (Oyster mushroom) and *Termitomyces clypeatus* (Termite mushroom) sold on selected markets in Accra, Ghana,” *Mycosphere*, vol. 4, no. 5, pp. 960-967, 2013.
- [16] Fu, Z., Liu, G., Wang, L. (2020). Assessment of potential human health risk of trace element in wild edible mushroom species collected from Yunnan Province,

- China. *Environmental Science and Pollution Research*, 27 (23), 29218-29227
- [17] K. H. Kim, E. Kabir, S. A. Jahan, "A review on the distribution of Hg in the environment and its human health impacts," *Journal of Hazardous Materials*, vol. 306, pp. 376-385, 2016.
- [18] M. Jarošová, D. MilDe, M. Kuba, "Elemental analysis of coffee: a comparison of ICP-MS and AAS methods," *Czech Journal of Food Sciences*, vol. 32, no. 4, pp. 354-359, 2014.
- [19] C. Voica, A. Dehelean, M.H. Kovacs, "The use of inductively coupled plasma massspectrometry (ICP-MS) for the determination of toxic and essential elements in differenttypes of food samples," *Food Chemistry*, vol. 112, no. 3, pp. 727-732, 2015.
- [20] B. Girma, K. Wale, "Analytical Methods for Determining Metals Concentrations in Coffee (*Coffea arabica* L.) in Ethiopia: A Review," *American Journal of Applied Chemistry*, vol. 11, no. 4, pp. 95-102, 2023.
- [21] M. E. Lachman, "Development in midlife," *Annual Review of Psychology*, vol. 55, pp. 305-331, 2004.
- [22] M. Pirsahab, M. Hadei, K. Sharafi K, "Human health risk assessment by Monte Carlo simulation method for heavy metals of commonly consumed cereals in Iran-Uncertainty and sensitivity analysis," *Journal of Food Composition and Analysis*, vol. 96, pp.1-10, 2021.
- [23] G. Kowalska, "The safety assessment of toxic metals in commonly used herbs, spices, tea, and coffee in Poland," *International Journal of Environmental Research and Public Health*, vol. 18, no. 11, pp. 1-19, 2021.
- [24] D. Albals, I. F. Al-Momani, R. Issa, A. Yehya, "Multi-element determination of essential and toxic metals in green and roasted coffee beans: A comparative study among different origins using ICP-MS," *Science Progress*, vol. 104, no. 2, pp. 1-17, 2021.
- [25] H. S. Ali, "Evaluation of heavy metal concentration in black tea and coffee marketed in Arbil, Iraq: A consumer health risk assessments," *International Journal of Environmental Analytical Chemistry*, pp. 1-11, 2024.
- [26] E. O. M Omer, O. A. Labib, M. Zafar, "Physicochemical parameters and toxic heavy metals concentration in coffee," *Development*, vol. 3, no. 3, pp.1-8, 2019.
- [27] R. Massoud, F. MirMohammadMakki, S. F. MirMohammadMakki, N. MirMohammadMakki, A. Massoud, "Evaluation of heavy metals in Roasted Coffee powder in Iran and Turkey," *Coffee Science*, pp. 1-8, 2022.

A Novel Compact GNSS Antenna with Plasma Frequency Selective Surface

Olca Yigit¹, Fadil Kuyucuoglu^{2*}, Yavuz Ozturk³

¹ Ünüvar Elektronik A.Ş., İstanbul, Türkiye, olcyygt@gmail.com

² Manisa Celal Bayar University, Faculty of Engineering and Natural Sciences, Department of Electrical-Electronics Engineering, Manisa, Türkiye, fadil.kuyucuoglu@cbu.edu.tr

³ Ege University, Faculty of Engineering, Department of Electrical and Electronics Engineering, İzmir, Türkiye, yavuz.ozturk@ege.edu.tr

*Corresponding Author

ARTICLE INFO

ABSTRACT

Keywords:

Gnss
Pfss
Spiral antenna
Plasma array

In this study, a plasma frequency selective surface (PFSS) was designed with an array of ordinary fluorescent lamps backed by a conducting plate. The proposed PFSS structure was used as a reflector with the spiral two arms Archimedean type Global Navigation Satellite System (GNSS) antenna to reduce the overall size of the antenna system. Characteristics and the performance of the proposed system were presented by using the results of simulations and experiments in the GNSS band. The optimum distance between antenna and PFSS was found to be around 35 mm to achieve a maximum gain in the simulation which is a lower profile than antenna with conventional conductive plate (66 mm at the GNSS center frequency). Experimental results show that the antenna system has mean values of around 6.7 dBiC gain, 1.27 dB axial ratio and less than -10 dB return loss in the range of 1.14 and 1.61 GHz. All these results show that the proposed novel antenna system is suitable for the reception of the GNSS signals with the advantage of its low profile design.

Article History:

Received: 29.04.2023

Accepted: 05.07.2024

Online Available: 06.08.2024

1. Introduction

Global Navigation Satellite System (GNSS) has been a key element of significant technological devices and finds an important role in many areas of the life including navigation, transportation, mining, mapping, and road pricing [1-3]. This technology has been subject to research studies in terms of new antenna designs, anti-jamming, and improving positioning performance in recent years [4-6].

The emergence of the multiple GNSS service providers GPS L1 (1575.42 ± 1.023 MHz), BDS B1 (1561.098 ± 5 MHz), and GLONASS L1 (1602.5 ± 4 MHz) for the navigation systems has made antennas, covering all GNSS bands, to play an indispensable role [4]. All-band GNSS antennas should cover the range between 1146

MHz-1610 MHz band, have high front to back ratio, and acceptable axial ratio with a large beam-width for a better satellite coverage [7-9]. In addition, high accuracies, and low profile characteristics are needed for many high precision applications [9]. Spiral antennas, which satisfy the necessary electrical properties, are widely used in GNSS applications [10].

In general, one of the major factor which prevents designing low profile antennas is the use of high electric conductor materials. These materials are placed $\lambda/4$ away from the antenna, to increase the gain of the receiver and to improve the directivity of the radiating antennas. In this type of directive antennas, $\lambda/4$ value is the optimum distance between the antenna and high electric reflector, due to the ($\lambda/2$) out of phase reflected wave. There is no design flexibility in

such systems. However, the use of a modified reflector [9] or plasma frequency selective surface (PFSS), which was proposed in this study, can be used to decrease the $\lambda/4$ distance value. The PFSS is an artificial magnetic conductor that gives a design flexibility, and it can be used in many novel applications such as radar cross section reduction, wide band absorber, and photonic band gap devices because of its adjustable electrical characteristics [11-13].

PFSS structures can be formed by using energized fluorescent lamps which are also plasma medium. The fluorescent lamp has frequency dependent adjustable electrical conductor properties. In other words, by applying variable electric potential to the fluorescent lamps, collision and plasma frequencies can be changed. Consequently, the optical and the electrical properties can be adjusted. In this way, a band pass filter mechanism can be achieved to transmit and reflect some of the frequency band region of the radiation.

For instance, in our previous study, the PFSS structure for GNSS frequency band with high impedance and in-phase reflection characteristics were presented [14]. Plasma antennas also are widely studied in research studies such as development of intelligent reflective surfaces [15-16], and corner reflectors [17] to improve the performance of the systems. Although the plasma and electromagnetic radiation interaction investigated in many studies as mentioned or used as reflector or antenna structures [14-17]. Best to our knowledge, the utilization of a plasma structure to minimize the antenna system size without compromising the radiation performance has not been published yet and we believe that the results of this study can contribute to the research on both plasma and electromagnetic wave interaction.

In this paper, the design of a two arm Archimedean antenna with PFSS structure realized by fluorescent lamps array and a conductor plane was presented.

The fluorescent lamp array, as a low cost plasma source, which is placed under the antenna behaves like a plasma frequency selective surface (PFSS) since its refractive index, and so

reflectivity depends on the plasma parameters of the gas in the energized lamps. The simulation and the experimental measurement outcomes of the antenna for the parameters of the return loss, axial ratio, and gain were investigated by considering plasma properties of PFSS structure. To the best of our knowledge, this is the first time shown that such PFSS surfaces can be used to reduce the size of the system without compromising the radiation performance of the antenna.

2. Theory and Experimental Results

2.1. Experimental design

The designed system consists of a GNSS antenna, a PFSS structure, assembled of the florescent lamp array and a metal reflector, is illustrated in Figure 1 (a). Circular polarized antennas are generally used with a reflector surface to detect the radiation especially by satellites in GNSS applications. The main reason to choose these types of antennas is that the circularly polarized signals are less affected while passing through the ionosphere. In this study, one of the circular polarized antennas, the two arm Archimedean type was used because of providing stable results in terms of gain and axial ratio values in a certain bandwidth.

The parameters of the antenna were determined for the GNSS band of 1.146-1.610 GHz. The physical dimensions of the antenna were calculated using well known antenna equations [18]. Thereafter the antenna was simulated using CST software by using calculated parameters and the target parameters were found for the fabrication. The designed antenna was fabricated to have 12 turns of copper lines width of 1 mm and the line spacing of 1 mm by using 1 mm thick FR4 material of the relative dielectric constant of 4.5 and the loss tangent of 0.02 (Figure 2 (a)).

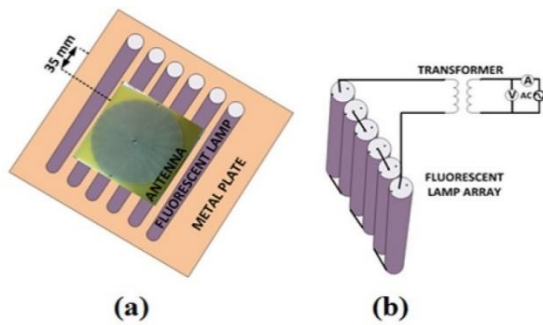


Figure 1. a) The illustration of the proposed system, b) the illustration of fluorescent lamp array

The PFSS structure was designed by integrating an array of easy access fluorescent lamps and a conducting surface. In the system, serially connected lamps were excited by a transformer system (Figure 1(b)). Alternative voltage of 220 Vrms and 50 Hz was applied to the transformer input. The transformer primary and secondary windings were selected as 500 and 10000 turns respectively to obtain around 4400 Vrms. The plasma was formed in the lamps by applying this voltage to the lamp array. The PFSS structure was placed 35 mm (Figure 1 (a) and Figure 2 (b)) below the antenna. A network analyzer (Rohde Schwarz NWA ZVA-24) was used for the S parameters measurements, a signal generator (Rohde Schwarz model) (10 kHz-12 GHz) and Rohde Schwarz model spectrum analyzer (100 kHz-30 GHz) were used for the gain and axial ratio measurements.

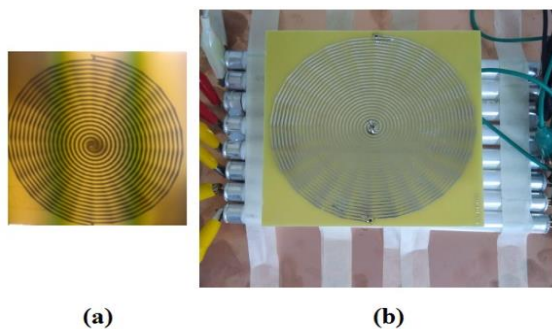


Figure 2. a) Radiator part of the GNSS antenna, b) the actual experiment setup

The array was formed with 6 identical fluorescent lamps which emit white light and each has 6 W power (Global T5/6W, RPC). The diameter, length, and glass thickness of each lamp are 16 mm, 225 mm, and 0.8 mm respectively. These lamps were placed 5 mm apart from each other as shown in Figure 2(b).

2.2. Plasma characteristics

Dielectric constant is a parameter which determines the electrical properties of the materials in theoretical and experimental physics. Electrical and optical properties such as conductivity, reflection, transmission, and absorption can be calculated by using the dielectric constant. The dielectric constant and optical properties can be tuned by using applied voltage in plasma mediums like fluorescent lamps. Relative dielectric constant ϵ_r of a plasma medium can be characterized by using the Drude model as given in equation (1).

$$\epsilon_r = 1 + \frac{w_p^2}{jw(jw + v_c)} \quad (1)$$

where w is electromagnetic wave frequency, v_c is collision frequency and w_p is the plasma frequency. The plasma frequency is defined as:

$$w_p = \sqrt{\frac{n_e e^2}{m_e \epsilon_0}} \quad (2)$$

Here, n_e is the electron concentration, e is the charge of an electron, m_e is the electron mass, ϵ_0 is the dielectric constant of the vacuum. It can be seen in Eq (1), if an electromagnetic wave frequency is less than the plasma frequency, there will be a high reflection from the lamps. If $w > w_p$, the reflectivity decreases and the transmissivity increases. Therefore, when the electromagnetic wave frequency ω is smaller than ω_p , it will be reflected with a high reflectivity. However, the phase difference between the incident and reflected waves will be different from $\pi/2$ when the reflected medium is the PFSS which is a combination of the dielectric, plasma and metallic components [19]. This effect is exploited in our study to design a low profile antenna system.

The summary of experimental antenna parameters and plasma simulation parameters are summarized in Table 1.

3. Results and Discussion

The Archimedean antenna and PFSS structure were designed and studied to present the

reduction the size of the system without compromising the radiation performance.

Table 1. The antenna and plasma parameters

Antenna Parameters		Plasma Parameters	
r1	40 mm	w _p :	48.4 GHz
H (antenna height)	35 mm	v _c :	287 GHz
Turn number	12		
Width of the arm	1 mm		
Spacing between arms	1 mm		
Distance between lamps	5 mm		

The measurement and simulation results of the proposed antenna system were presented in this section. In order to analyze the influence of the plasma structure on the antenna characteristics, the return loss S_{11} , the axial ratio AR, and the right hand circular polarized RHCP gain parameters were investigated. During all measurement and simulations, the two arm Archimedean spiral antenna and PFSS structure were used together. The study was first started with the simulation and measurement of the S_{11} parameter to determine the signal ratio returning from the antenna and 50Ω compatibility.

The return loss values in the range of 1.05 GHz - 1.70 GHz frequency band with the plasma and without the plasma cases were shown in Figure 3. The number of the resonance frequencies and ripples were decreased in plasma cases. These results can be attributed to the change of the reflected electric field which affects the power on the antenna and input impedance in the presence of plasma. The S_{11} parameters were expected to be lower than -10 dB to satisfy the requirement of low return loss condition.

All the results of the measurements of the antenna with and without plasma correlate this condition except some frequency bands in the simulation. The S_{11} parameter of the measurement results with plasma presented in

Figure 3 show that the S_{11} lies between -10.32 and -17.17 dB. Especially at GPS frequency 1.575 GHz, the values were approximately -17.00 dB. Measured and simulated results of S_{11} parameters have differences as can be seen in Figure 3. The possible reasons for these differences can be SMA connector losses, fabrication tolerances and external disturbances which are not considered in the simulations. For this study these differences are ignored and only checked if S_{11} values are below -10 dB. The S_{11} values below -10 dB in this frequency range indicate that the input impedance value of the antenna is compatible with 50Ω and the antenna system can be used in the GNSS band.

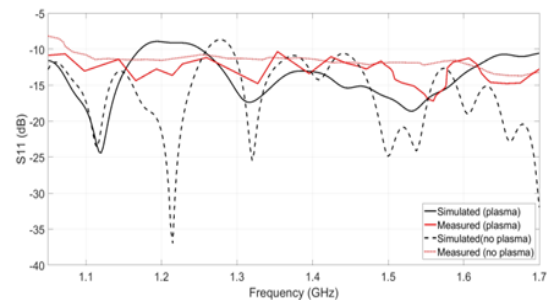


Figure 3. The S_{11} parameter of antenna with PFSS

The AR value gives the information about the polarization of an antenna. The axial ratio values were determined by measuring the difference of power values of two orthogonal components. The orthogonal components obtained by rotating a linearly polarized transmitter antenna in 90 degrees in azimuth. Figure 4 shows the measured and simulated AR characteristics of the proposed antenna system. Although the axial ratio value was higher than 3 dB at low frequencies of the GNSS band in simulation, it was found that the AR value was observed to lie below the limit value of 3 dB in measurements. Hereby, it was understood that the deviation from circular polarization is less than 3 dB and the antenna can be assumed to be circularly polarized.

Especially at the GPS center frequency (L1 Band) that is the 1575.42 MHz, the measured axial ratio values were in the range between 0-1 dB (measured with plasma 0.6 dB, measured without plasma 0.45, simulated with plasma 1.63, simulated without plasma 1.52). This means that the desired circularly polarized antenna characteristic was obtained very closely for the antenna at GPS L1 frequency band.

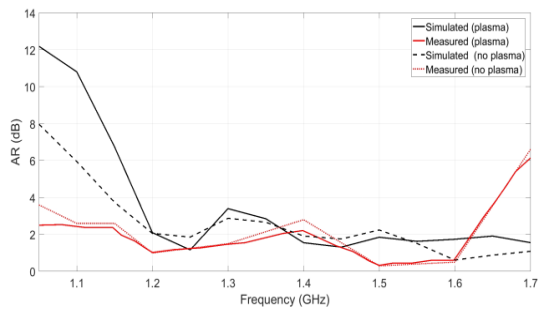


Figure 4. The AR of the antenna with PFSS

The antenna gain, one of the most important parameter was measured and simulated with and without plasma conditions in Figure 5. When the plasma lamps were energized, it was observed that the gain value was highly increased in the whole in the GNSS frequency range both in experimental and also simulation cases. At the GPS center frequency (L1 Band), the measured gain values were as follows. The measured plasma 7.01 dBic, the measured without plasma: 3.94 dBic, The simulation plasma 6.97 dBic, the simulated no plasma 4.18 dBic. The obtained gain showed that the reflection from PFSS surface was near to the inphase component.

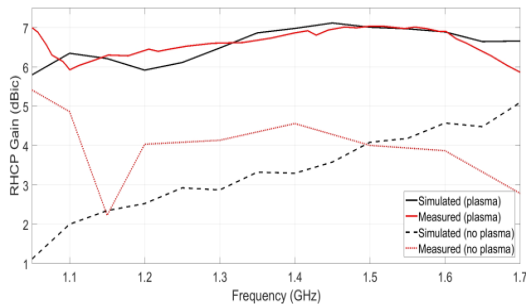


Figure 5. The RHCP gain of the antenna with PFSS

Radiation patterns in CST simulation of the proposed system are given in Figure 6. As it is seen that, when plasma is activated, the radiation pattern is changed for all degrees. Half power beam width (HPBW) of the radiation pattern of the antenna which has PFSS is 88.5 degree and it is larger than the no plasma version of the antenna which has the HPBW is 72 degrees. Both of them have hemispherical shapes that radiate toward the upper side of the atmosphere. In addition, there is a difference between radiation strength of the antennas because of the inconsistent heights of the radiation part of the antennas.

The height must be 66 mm which is the quarter wavelength of the resonant frequency for the no

plasma version. Because reflected waves from the reflector must be in phase with the radiation of the radiator. In the plasma case, PFSS behaves as a high impedance surface so reflected signals are not out of phase. So it does not need a larger air gap. Detailed information of the antenna without lamps can be found in [20].

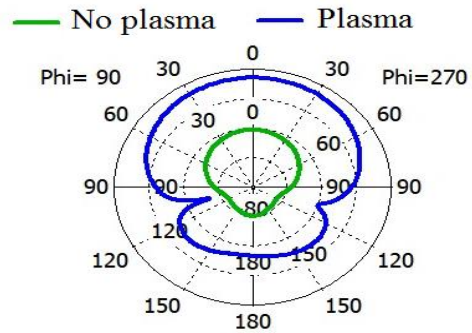


Figure 6. Radiation patterns of the proposed system

Several GNSS antennas dimensions and operating frequencies were presented in Table 2 to compare them with the proposed antenna. Designed metamaterials were used as a reflector for the other antennas presented in Table 2 [21-24]. As can be seen, except the single frequency antenna in reference [24] all the other ones have larger volume than our antenna. The antenna presented in this work, being wideband and also low profile has advantages over the antennas in Table 2.

The simulation results show that the optimum distance of the conductor is around 66 mm. For the ideal case, when the conducting plate is $\lambda/4$ (66 mm for 1.14 GHz) apart from the antenna, the mean values of S_{11} , axial ratio, gain are -17.50 dB (max: -26.70 dB, min: -11.80 dB), 1.20 dB (max:2.10 dB, min:0.25) and 6.90 dBic (max:7.05 dBic min:6.45 dBic) are obtained in GNSS band respectively. The measured performance of the antenna without lamps and when a metal reflector is placed under the antenna (66 mm below) is summarized as follows: the S_{11} parameter was lower than -10 dB, the gain was between 6.0 dBic and 6.2 dBic, axial ratio was between 0.9 dB and 1.4 dB at 1.1-16 GHz range [20]. The detailed results can be found in the study of Yiğit [20].

Table 2. The antenna and plasma parameters

REF.	Dimensions	Operating Frequency
[21]	130 mm x 30 mm (RxH)	Wideband (1.1-1.6 Ghz)
[22]	200 x 200 x55 mm (WxLxH)	Single frequency (1.575 GHz)
[23]	280x280x29 mm (WxLxH)	L1 and L2 band
[24]	44x44x19 mm (WxLxH)	Single frequency (1.575 GHz)
This work	80x80x35 mm (WxLxH)	Wideband (1.1-1.6GHz) Reconfigurable

*RxH: RadiusxHeight; WxLxH:WidthxLengthxHeight

The mean values of S_{11} , axial ratio, and gain are -12.86 dB (max: -17.08 dB, min: -10.35 dB), 1.27 dB (max:2.37 dB, min:0.36) and 6.70 dBic (max:7.04 dBic min:6.29 dBic) are measured for the proposed system respectively. These results show that the system performance is close to that of the ideal case. It is worth mentioning that the proposed antenna system can be utilized in small GNSS platform applications when it is upgraded to a portable one. It is possible to make the system portable with a miniature 36 W high voltage source since there are 6 lamps with 6W rating. This kind of high voltage source can be designed or commercially available ones can be used [25]. As a conclusion, the proposed wide band GNSS antenna system with low profile is realized with the proposed PFSS.

4. Conclusion

The performance of an Archimedean type GNSS antenna with a PFSS structure, formed via fluorescent lamp array as a plasma source and conducting plate, was investigated. The proposed antenna parameters showed promising results such as having a low axial ratio and a high gain in all GNSS band. In addition, a smaller size compared to the antenna with a single conducting plane was obtained by exploiting the reflection properties of the PFSS.

Article Information Form

Funding

The authors have not received any financial support for the research, authorship, or publication of this study.

Authors' Contribution

The authors contributed equally to the study.

The Declaration of Conflict of Interest/ Common Interest

No conflict of interest or common interest has been declared by the authors.

The Declaration of Ethics Committee Approval

This study does not require ethics committee permission or any special permission.

The Declaration of Research and Publication Ethics

The authors of the paper declare that they comply with the scientific, ethical and quotation rules of SAUJS in all processes of the paper and that they do not make any falsification on the data collected. In addition, they declare that Sakarya University Journal of Science and its editorial board have no responsibility for any ethical violations that may be encountered, and that this study has not been evaluated in any academic publication environment other than Sakarya University Journal of Science.

Copyright Statement

Authors own the copyright of their work published in the journal and their work is published under the CC BY-NC 4.0 license.


References

- [1] J. Yu, X. Meng, B. Yan, B. Xu, Q. Fan, Y. Xie, "Global Navigation Satellite System-Based Positioning Technology for Structural Health Monitoring: A Review," *Structural Control and Health Monitoring*, vol. 27, no. 1, pp. e2467, 2020.
- [2] X. Lian, Z. Li, H. Yuan, H. Hu, Y. Cai, X. Liu, "Determination of the Stability of High-Steep Slopes by Global Navigation Satellite System (GNSS) Real-Time Monitoring in Long Wall Mining,"

- Applied Sciences, vol. 10, no. 6, pp. 1952, 2020.
- [3] S. Shankar, M. Roth, L.A. Schubert, J.A. Versteegen, "Automatic Mapping of Center Line of Railway Tracks Using Global Navigation Satellite System, Inertial Measurement Unit and Laser Scanner," *Remote Sensing*, vol. 12, no. 3, pp. 411, 2020.
- [4] J. Yuan, J. Zheng, Z.D. Chen, "A Compact Meandered Ring Antenna Loaded with Parasitic Patches and a Slotted Ground for Global Navigation Satellite Systems," *IEEE Transactions on Antennas and Propagation*, vol. 66, no. 12, pp. 6835-6843, 2018.
- [5] T. E. Humphreys, M. J. Murrian, L. Narula, "Deep-Urban Unaided Precise Global Navigation Satellite System Vehicle Positioning," *IEEE Intelligent Transportation Systems Magazine*, vol. 12, no. 3, pp. 109-122, 2020.
- [6] O. Yigit, İ. Sisman, Y. Asci, K. Yegin, "Beam Switched Antenna Design for Jamming Mitigation of Legacy GPS Receivers," in *24th Telecommunications Forum (TELFOR)*, Belgrade, Serbia, 2016, pp. 494-497.
- [7] Y. D. Yan, Y. C. Jiao, Z. Weng, C. Zhang, "An Umbrella-Shaped Broadband Circularly Polarized Antenna with Wide Beamwidth for Global Navigation Satellite Systems Applications," *Microwave and Optical Technology Letters*, vol. 61, no. 11, pp. 2455-2462, 2019.
- [8] X. S. Li, L. L. Cheng, X. Y. Liu, Q.H. Liu, "Wideband Gns Antenna Covered by a Double-Sided Metasurface," *AEU-International Journal of Electronics and Communications*, vol. 96, pp. 170-177, 2018.
- [9] J. Yuan, Y. Li, Z. Xu, J. Zheng, "A Compact Cpw-Fed Low-Profile Wideband Circularly Polarized Slot Antenna with a Planar Ring Reflector for Gns Applications," *International Journal of Antennas and Propagation*, pp. 1-12, 2019.
- [10] L. Guo, P. Zhang, F. Zeng, Z. Zhang, C. Zhang, "A Novel Four-Arm Planar Spiral Antenna for GNSS Application," *IEEE Access*, vol. 9, pp. 168899-168906, 2021.
- [11] A. Ghayekhloo, A. Abdolali, S. H. M. Armaki, "Observation of Radar Cross Section Reduction Using Low Pressure Plasma Arrayed Coating Structure," *IEEE Transactions on Antennas and Propagation*, vol. 65, no. 6, pp. 3058-3064, 2017.
- [12] M. Z. Joozdani, M. K. Amirhosseini, "Wideband Absorber with Combination of Plasma and Resistive Frequency Selective Surface," *IEEE Transactions on Plasma Science*, vol. 44, no. 12, pp. 3254-3261, 2016.
- [13] O. Sakai, T. Sakaguchi, K. Tachibana, "Photonic Bands in Two Dimensional Microplasma Arrays. I. Theoretical Derivation of Band Structures of Electromagnetic Waves," *Journal of Applied Physics*, vol. 101, no. 7, pp. 073304, 2007.
- [14] O. Yigit, K. Yegin, I. Akkaya, Y. Ozturk, "Plasma Frequency Selective Surface for Gns Applications," in *25th Telecommunication Forum (TELFOR)*, Belgrade, Serbia, 2017, pp. 1-3.
- [15] M. Magarotto, L. Schenato, P. De Carlo, A. D. Capobianco, "Feasibility of a Plasma-Based Intelligent Reflective Surface," *IEEE Access*, vol. 10, pp. 97995-98003, 2022.
- [16] M. Magarotto, L. Schenato, P. De Carlo, A. D. Capobianco, "Plasma-Based Intelligent Reflective Surfaces for Beam Steering Operations," in *17th European Conference on Antennas and Propagation (EuCAP)*, Florence, Italy, 2023, pp. 1-5.
- [17] M. T. Jusoh, F. Colombel, O. Lafond, M. Himdi, "Realization of a Dual Dihedral

- Corner-Reflector Antenna by Using Low Cost Plasma," in 8th European Conference on Antennas and Propagation (EuCAP 2014), Hague, Netherlands, 2014, pp. 2340-2344.
- [18] C. A. Balanis, "Frequency Independent Antennas, Antenna Miniaturization, and Fractal Antennas," in *Antenna Theory - Analysis and Design*, 3rd ed., New Jersey, USA: John Wiley & Sons, 2005, pp. 611-652.
- [19] S. H. Zainud-Deen, H. A. E. A. Malhat, N. A. Shabayek, "Reconfigurable Rcs Reduction from Curved Structures Using Plasma Based FSS," *Plasmonics*, vol. 15, no. 2, pp. 341-350, 2020.
- [20] O. Yiğit, "Uydudan Küresel Konumlama Sistemleri Alıcıları için Karıştırmaya Dayanıklı Ön-Uç Elektroniği ve Anten Tasarımı," M.S. Dissertation, Dept. Electrical-Electronics Eng., Ege University, Izmir, Türkiye, 2017.
- [21] J. Wei, S. Liao, Q. Xue, W. Che, "A Lightweight Low-Profile GNSS Antenna Based on Wideband Multipath Mitigation Strategy," *IEEE Antennas and Wireless Propagation Letters*, vol. 22, no. 9, pp. 2150-2154, 2023.
- [22] A. Konforta, S. Horn, T. Bertuch, P. Knott, "A Miniaturized GNSS Controlled Reception Pattern Antenna Array with AMC Virtual Ground Plane," in 13th European Conference on Antennas and Propagation (EuCAP), Krakow, Poland, 2019, pp. 1-4.
- [23] M. K. Emara, S. Gupta, J. Hautcoeur, G. Panther, J. Wight, "A Low-Profile Dual-Band Tunable AMC Structure for GNSS Antennas and Its Performance Trade-Offs," in 18th International Symposium on Antenna Technology and Applied Electromagnetics (ANTEM), Waterloo, ON, Canada, 2018, pp. 1-4.
- [24] M. Sumi, "A Circularly Polarized Metasurface Antenna Comprising Rectangular Loops with Gaps for Gns Receivers," in *International Workshop on Antenna Technology (iWAT)*, Miami, FL, USA, 2019, pp. 133-134.
- [25] S. Park, A. Goldin, J. Rivas-Davila, "Miniature High-Voltage Dc-Dc Power Converters for Space and Micro-Robotic Applications," in *IEEE Energy Conversion Congress and Exposition (ECCE)*, Baltimore, MD, USA, 2019, pp. 2007-2014.

Characterization of Micro-seismic Activity in Northern Cyprus Using Complexity and Corner Frequency Methods

Evrım Yavuz 

İstanbul Metropolitan Municipality, Department of Earthquake Risk Management and Urban Improvement, Directorate of Earthquake and Ground Research, İstanbul, Türkiye, evrim.yavuz@ibb.gov.tr

ARTICLE INFO

ABSTRACT

Keywords:

Discrimination functions
Complexity
Cyprus
Corner frequency
Seismic event



Cyprus is an island country located in the eastern Mediterranean, to the south of Türkiye and the western of Syria and Lebanon, and is a popular tourist destination. Due to being surrounded by seas on all four sides, meticulous planning of rescue, assistance, and evacuation plans is necessary in the face of disasters such as earthquakes and tsunamis. Tectonically, the southern part of the island is controlled by the Cyprus Arc, while the northern part is dominated by the Kyrenia Range. The demand for raw materials for construction and industry is met through controlled quarry blasting operations carried out by open-pit quarry companies in the districts of Kyrenia and Nicosia. As a result, both natural and artificial seismic events occur in the region, and these quakes are documented in seismic catalogs by seismology centers. However, due to the low energy content of micro-seismic events and the inadequacy of seismic stations on the island, the source types of these seismic events can be misidentified in the catalogs. In this context, the study focuses on 122 seismic events with magnitudes between $0.9 \leq M_l \leq 2.7$ that occurred in Northern Cyprus during the January 2018 - December 2021 period (4 years). The seismic events recorded by the station LFK, operated by Boğaziçi University Kandilli Observatory and Earthquake Research Institute Regional Earthquake-Tsunami Monitoring Center (KOERI-RETMC), were classified using Linear and Quadratic Discriminant Functions based on complexity and corner frequency methods. According to the results obtained, 10 of the 122 seismic events were identified as natural, and 96 were determined to be artificial, resulting in a general success rate of 86.89%. However, classification results for 16 seismic events were inconclusive with the methods used. As a result, more detailed secondary analyses should be conducted to accurately determine the source types of micro-seismic events, and the seismic catalogs should be updated accordingly.

Article History:

Received: 29.08.2023

Accepted: 30.07.2024

Online Available: 06.08.2024

1. Introduction

Cyprus is an island country located in the Mediterranean, which is not only rich in historical and cultural heritage but also draws significant attention in terms of tourism. Particularly due to the impact of tourism, there is an increase in construction and, consequently, a demand for industrial raw materials driven by the expansion of the intra-island road transportation infrastructure. The provision of material needs from its own internal resources is facilitated by

certain quarry operations located on the island. These quarry operations, where materials are obtained using explosive and combustible substances, exhibit micro-scale ground vibrations during their activities. These vibrations are recorded by seismic stations and documented in earthquake catalogs.

The tectonic control of the region is mainly provided by the Cyprus Arc, which passes through the southern part of the island in general; it is also supported by the Kyrenia Range (Girne-

Beşparmak Ridge) to the north and partially oblique-slip faults developing to the east and west. As a result, it is observed that not only micro-scale artificial vibrations but also tectonic events of similar scales are recorded in the region. The low energy content of these micro-scale activities, the limited number of recording stations, their small size resulting in noisy recordings, and the fact that they are not subjected to detailed analysis by the seismology center responsible for cataloging, sometimes lead to their omission from earthquake catalogs, or they are inaccurately categorized under the wrong source type. Erroneous micro-seismic catalogs mislead researchers and can even result in secondary studies, causing both time and workload burdens.

Due to these reasons, various methods have been employed to distinguish natural and artificial vibrations from the past to the present. The initial studies on this subject were conducted mainly in the United States [1-4]. While simple methods like amplitude ratio and complexity provide some direction, results obtained in the frequency domain also offer reliable information about source type identification based on signal characteristics. One of the first examples of the complexity method was conducted by [5] to differentiate underwater explosions. The same method was applied to short-period seismograms by [6]. In Türkiye, complexity analysis has been applied through earthquake stations located in various cities, such as Istanbul, Eastern Black Sea Region, Sakarya, Yalova-Bursa Gaziantep-Kahramanmaraş and Edirne [7-12].

In the US, discrimination analysis using high-frequency waves was conducted by [13], natural and artificial vibrations around the Vertes Mountains in Hungary were studied by [14], and seismic events of two different types in various regions of Egypt were analyzed using the complexity method by [15, 16]. Furthermore, in recent years, corner frequency methods are being employed worldwide to characterize natural and artificial vibrations. [17] determined source type using corner frequency-magnitude relationship on 2430 events at the Israel-Lebanon border. [18] discriminated earthquakes from controlled explosions near Mount St. Helens using corner frequencies of P and S waves. [19] applied a

similar method in the western US. [20] tested tree-based machine learning methods using the complexity approach. [21] combined the corner frequency and magnitude relationship with deep learning for source type identification. In seismic active regions of Egypt, [22-24] applied discrimination analysis based on the spectra of P and S waves.

In the study, complexity and corner frequency methods were employed using vertical components of events recorded at the seismic station LFK operated by the Boğaziçi University Kandilli Observatory and Earthquake Research Institute Regional Earthquake-Tsunami Monitoring Center (KOERI-RETMC) with local magnitudes of $M \leq 2.7$ that occurred in the northern part of Cyprus. In order to classify the obtained parameters, Linear Discriminant Function (LDF) and Quadratic Discriminant Function (QDF) were employed to determine the source types of these seismic events. The obtained results, along with statistical approaches, can be used to update the existing earthquake catalogs and will serve as a key in classifying future seismic events. Consequently, aiming for the emergence of more reliable earthquake catalogs, this will reduce the need for secondary analyses, leading to a decrease in time loss and workload.

2. Geological and Tectonic Structure

Northern Cyprus consists of three main geological belts from south to north, which are respectively Troodos Ophiolite, Troodos Surrounding Sedimentary Sequence, and the Beşparmak Region [25]. While Quaternary alluvial forms shape the northern coast of the region, as one moves southward from the coast, the dominance of Oligocene sedimentary rock units belonging to the Degirmenlik Group, including sandstones, conglomerates, and mudstones, can be observed. Within this group, Eocene-aged carbonate deposits running parallel to the east/northeast-west Girne-Beşparmak Ridge (Degirmenlik Fault), Mesozoic-aged dolomitized carbonate rocks forming the main elevation of the Beşparmak Mountains, known as the Tripa Group, and Late Cretaceous-Eocene-aged mudstones, limestone, and volcanics

forming the Lapta Group are present [26-29] (Figure 1).

To fulfill the industrial raw material needs of the region, some open quarry operations in certain areas of these formations carry out their activities through controlled explosions. Thus, micro-scale ground vibrations are also documented in seismic centers' earthquake catalogs.

The island is tectonically controlled by the Cyprus Arc, extend to the south, an area where the African and Anatolian Plates collide at a rate of 10 mm/year, generating both destructive and tsunami-generating earthquakes in the past [30-33]. The northern part of the island, which is the study area, is dominated by the Degirmenlik Fault (Girne-Beşparmak Ridge), extending parallel to the Beşparmak Mountains and producing earthquakes on a smaller scale [29, 34] (Figure 1).

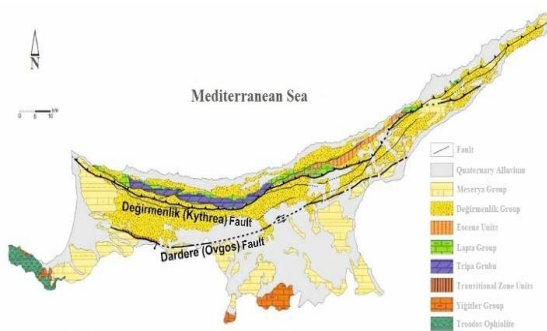


Figure 1. Simplified geological map of Northern Cyprus (Adapted from [29])

In the study area, micro-scale natural and anthropogenic-induced vibrations are recorded and cataloged by seismology centers. However, due to their low energy content, difficulties can arise in determining both the epicenter and source types of these vibrations. As a result, incorrect identifications in catalogs become prominent, leading to erroneous outcomes in new endeavors such as seismology, seismotectonics, hazard analysis, and more. This can either result in misleading conclusions or necessitate secondary analyses, leading to time loss and added workload for researchers.

3. Data Set

In the study, a GURALP-3ESP sensor-equipped seismic station with the station code LFK, operated by KOERI-RETMC, located at

coordinates 35.2832°N - 33.5335°E in the vicinity of Nicosia, at an elevation of 690 meters above sea level, and configured to sample at a rate of 100 samples per second was used. Vertical component seismograms of 122 seismic events with magnitudes ranging from $0.9 \leq M_l \leq 2.7$, characterized by high signal quality, absence of digitization errors, and reliable phase readings, were employed for the analysis of micro-seismic activity (Figure 2).

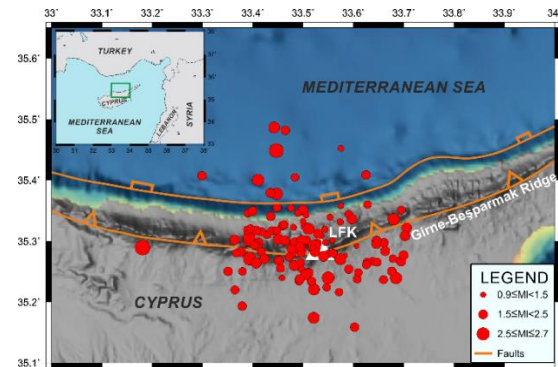


Figure 2. Tectonic structure of the study area and epicentral distribution of the seismic events. Faults are adapted from [34]

The events exhibit distances to the station ranging from 1 to 30 km, surrounding the station LFK from various directions. The epicenters for the 122 seismic events obtained by KOERI-RETMC are generally determined using 3 to 18 seismic stations and 4 to 19 phase picks (*P*, *S*), with azimuthal gap values varying between 70 and 349 degrees (Figure 3, Appendix A). Consequently, it has been determined that the low number of stations and phase readings, as well as the partially substantial azimuthal gap, play a role in locating micro-seismic activity. In the region where quarry blasts are frequent, records of a thorough analysis can be observed only for the station LFK, and a reliable assessment has been made with only one station.

Therefore, taking into consideration the potential location and depth errors that could arise due to the low number of existing stations on the island and the low energy content of micro-seismic events, along with the possibility of unauthorized explosions, seismic records were examined over a 4-year period from January 2018 to December 2021 (continuing in current open-pit quarry operations).

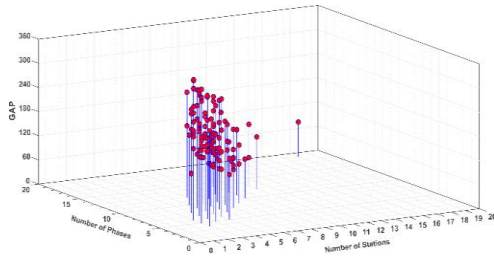


Figure 3. Azimuthal gap (GAP) along with the numbers of stations and phases used in the epicentral solution of the 122 events

4. Method

In the study, a total of 122 events with magnitudes ranging from $0.9 \leq M_l \leq 2.7$, recorded at the seismic station LFK operated by KOERI-RETMC, were analyzed using complexity and corner frequency methods. For both methods, Linear Discriminant Function (LDF) and Quadratic Discriminant Function (QDF) were employed to classify the results.

In order to apply LDF and QDF analyses, the source types of the seismic events need to be initially defined. KOERI-RETMC determines the source type without resorting to technical analyses, solely based on observation and field knowledge. Therefore, the initial categorization was done on a case-by-case basis. As a result, preliminary information about source types was obtained through observational analyses such as amplitude of P and S waves, first motion direction of P waves, observation of R_g phase, and decay rate of coda waves, based on the vertical component seismograms recorded at the station LFK (Figure 4).

Theoretically, the amplitudes of S -waves for quarry blast signals are significantly lower compared to P -wave amplitudes in vertical component seismograms, whereas for earthquakes, it is vice versa. The P -wave first motion direction generally tends to be positive for quarry blasts, while it varies for earthquakes. In quarry blasts signals with a close epicentral distance, the emergence of the R_g wave phase is generally observed. The attenuation of tectonic events is characterized by a logarithmic decay and extended duration, whereas for explosions, it is vice versa [9, 10, 35, 36].

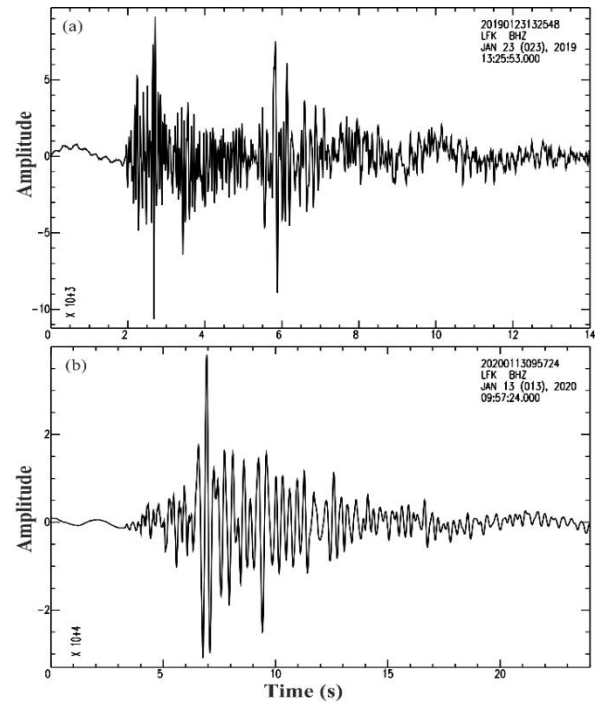


Figure 4. a) Vertical component seismograms of the earthquake on 23.01.2019 at 13:25:48.48 ($M_l=1.6$) and b) quarry blast on 13.01.2020 at 09:57:24.40 ($M_l=1.8$) recorded at the station LFK

In seismology, the complexity method, which is user-friendly and quick, is commonly employed to determine the source types of natural and anthropogenic vibrations. Within this method, two distinct parameters, namely complexity and spectral ratio, are computed and their relationships are compared graphically [5, 6]. In this approach, vertical component seismograms are divided into two separate time windows (t_0-t_1 , t_1-t_2), and their powers ($s^2(t)$) are calculated to determine the complexity (C) parameter (Equation 1). Subsequently, by considering the two windows holistically, a two-stage band-pass filter (h_1-h_2 , l_1-l_2 ; high and low corner frequencies) is applied to calculate the spectral ratio- $a(f)$ parameter, denoted as Sr (Equation 2).

$$C = \int_{t_1}^{t_2} s^2(t) dt / \int_{t_0}^{t_1} s^2(t) dt \quad (1)$$

$$Sr = \int_{h_1}^{h_2} a(f) df / \int_{l_1}^{l_2} a(f) df \quad (2)$$

The low and high-frequency values are directly related to the frequency content of the signals and have been optimally determined for this study as 5-10 Hz and 1-5 Hz, respectively.

It is known that earthquakes and quarry blasts exhibit differences in their spectra due to their source mechanisms. In explosions, signals dominated primarily by *P*-waves are obtained, as explosions are predominantly characterized by a single-point source. In contrast, even though earthquakes may have lower energy, they occur through a linear source mechanism, resulting in the generation of higher-amplitude *S*-waves [36]. Spectra of earthquakes recorded in close proximity show energy distributed over a broader frequency range and damping at higher corner frequencies. In contrast, this behavior is reversed in explosions [10, 17, 37, 38].

Theoretically, there is a direct relationship between the corner frequency and the magnitude of a seismic event [39, 40]. Thus, corner frequency values (f_c) for each event are calculated from vertical component seismograms due to the whole waveform (*P* to final), while local magnitudes (*M_L*) are directly obtained from KOERI-RETMC catalogs.

Both complexity and corner frequency method parameters are represented on a graph. To determine the source type, a third group alongside the parameters corresponding to the horizontal and vertical axes is introduced, and Linear and Quadratic Discriminant Functions (LDF and QDF) are employed. These statistical approaches are based on classification techniques using the principle of calculating the smallest error for data from different groups generated from different normal distributions [41-44].

For LDF, a single covariance matrix is determined for all groups, whereas for QDF, a separate covariance matrix is provided for each group [45]. The formulas for LDF and QDF are shown in Equation 3 and Equation 4.

$$F_{LDF} = K + L(1) * x + L(2) * y \quad (3)$$

$$F_{QDF} = K + L_1 * x + L_2 * y + \sum \{ (L_3 * x + L_4 * y) * Q_1 * (L_3 * x + L_4 * y) \} \quad (4)$$

Here, the parameter *K* represents the constant value of the boundary equation, while the parameters *L* and *Q* respectively denote the linear and quadratic coefficients of the same equation system.

5. Results

In this study, vertical component seismograms of 122 events recorded at the seismic station LFK, operated by KOERI-RETMC, and ranging in magnitude from $0.9 \leq M_L \leq 2.7$, were subjected to complexity and corner frequency methods for analysis. Considering the errors in determining source types in KOERI-RETMC catalogs, the event types were initially determined through visual analysis. Of the 122 events in the KOERI-RETMC catalogs, 87 were identified as artificial and 35 as natural. However, visual examination in this study revealed that these numbers were actually 109 and 13, respectively (Table 1, Appendix A). Accordingly, based on the aforementioned initial categorization, classification of seismic events using discriminant functions was performed.

In general, it is observed that artificial events are more successfully discriminated compared to natural ones (Table 1). The signal characteristics of quarry blasts are known to be more consistent depending on the distance to the epicenter, while earthquakes exhibit a more complex distribution due to their different mechanisms. Therefore, artificial events are more effectively distinguished. While earthquakes were classified with full success using the corner frequency method, a discrimination rate of approximately 95.41% for explosions in the complexity method and 85.21% for corner frequency method was observed. However, when examined based on the methods, the corner frequency method achieved a success rate of up to 87%, while the complexity analysis reached a success rate of up to 91% (Table 1). The QDF applied to the complexity method yielded a slightly higher success rate of 90.98% compared to the LDF result of 90.16% (Table 1, Figure 5). Both discriminant functions achieved a source type classification success rate of 86.89% in the corner frequency method (Table 1, Figure 6). Although similar results were obtained between the discriminant functions, it was observed that QDF provided slightly better results than LDF. Furthermore, as a second-degree function, QDF demonstrated more reliable discriminant analysis compared to LDF,

which is a first-degree function. The parameters of the functions are shown in Table 2.

Table 1. Analysis results based on method and statistical approach. LDF: Linear Discriminant Function, QDF: Quadratic Discriminant Function, E: Earthquake, B: Blast, M-E: Misclassified Earthquake, M-B: Misclassified Blast

Method	Statistical Approach	Numbers				Success Rate (%)		
		E	B	M-E	M-B	E	B	Overall
KOERI-RETMC		35	87	-	-	-	-	-
Initial Categorization		13	109	-	-	-	-	-
Complexity	LDF	6	104	7	5	46.15	95.41	90.16
	QDF	7	104	6	5	54.85	95.41	90.98
Corner Frequency	LDF	13	93	-	11	100.00	85.21	86.89
	QDF	13	93	-	11	100.00	85.21	86.89
Final Result		10	96	16				86.89

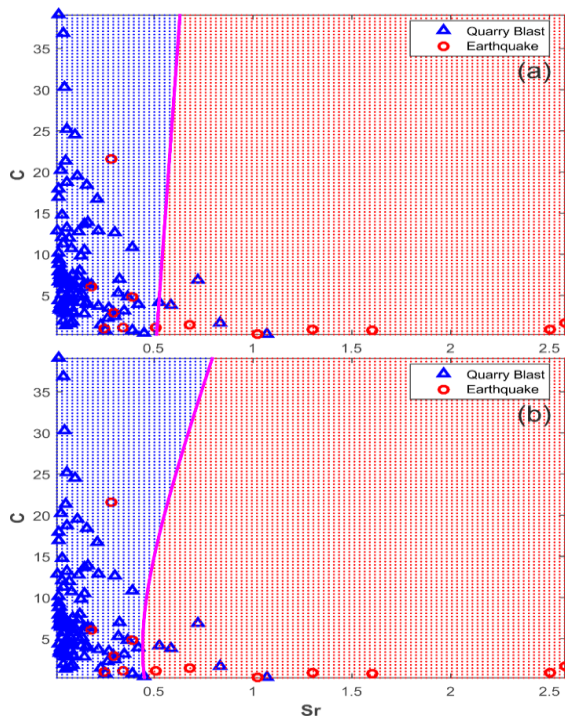


Figure 5. a) LDF b) QDF graphs for the Complexity method

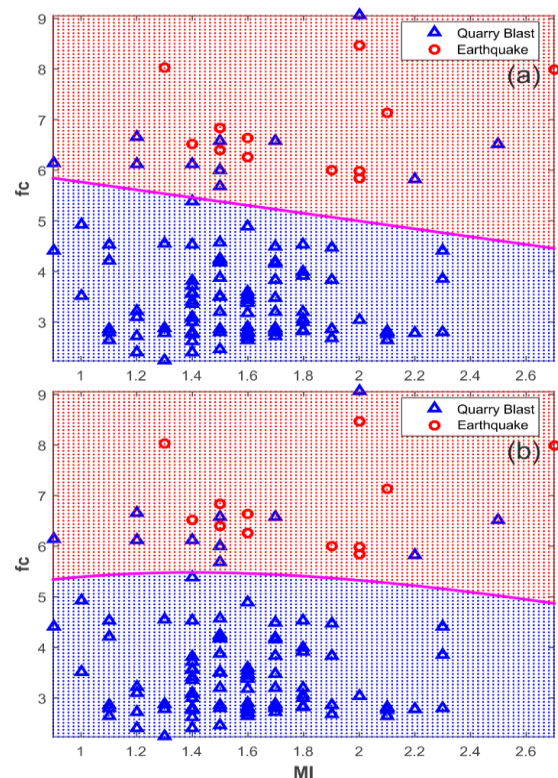


Figure 6. a) LDF b) QDF graphs for the Corner Frequency method

To determine the source types of seismic events, all methods and statistical analyses were jointly evaluated, resulting in the identification of 10 events as earthquakes and 96 events as quarry blasts out of the analyzed 122 ground shaking events. Additionally, 16 events exhibited different outcomes when the aforementioned methods and discriminant functions were employed, hence they were classified as unidentified events after this study. As a result, a general success rate of 86.89% was achieved for the classification of the source types of 122 events (Table 1, Figure 7, Appendix A).

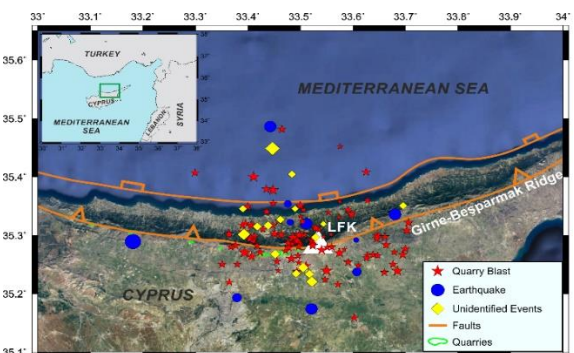


Figure 7. Distribution of source types obtained after the analyses. Faults from Seyitoğlu et al., 2022, and locations of quarries obtained from Google Earth Pro

Table 2. The discrimination functions of station LFK

Complexity	$F_{LDF}=4.0098+[-7.8357 \quad 0.0239]* \begin{bmatrix} Sr \\ C \end{bmatrix}$
	$F_{QDF}=(1.1363)+[5.1763 \quad 0.0203]* \begin{bmatrix} Sr \\ C \end{bmatrix}+[Sr \quad C]* \begin{bmatrix} -17.0587 & -0.0779 \\ -0.0779 & -0.0063 \end{bmatrix} * \begin{bmatrix} Sr \\ C \end{bmatrix}$
Corner Frequency	$F_{LDF}=15.5270+[-1.8324 \quad -2.3743]* \begin{bmatrix} Ml \\ fc \end{bmatrix}$
	$F_{QDF}=(19.3113)+[8.0652 \quad -6.0939]* \begin{bmatrix} Ml \\ fc \end{bmatrix}+[Sr \quad C]* \begin{bmatrix} -1.5012 & -0.3523 \\ -0.3523 & -0.3711 \end{bmatrix} * \begin{bmatrix} Ml \\ fc \end{bmatrix}$

5. Conclusion and Discussion

In this study, source type determination analysis of 122 seismic events recorded in Northern Cyprus and cataloged by KOERI-RETMC was conducted using complexity and corner frequency methods, through Linear and Quadratic Discriminant Functions. The results reveal that the complexity method yields more successful outcomes compared to the corner frequency analysis, and similarly, the Quadratic Discriminant Function outperforms the Linear Discriminant Function. According to the obtained results, the source types of 10 earthquakes and 96 quarry blasts were reliably identified, while the source types of 16 events could not be determined. As a result, the overall success rate was calculated as 86.89%.

Seismic centers employ various seismic stations, algorithms, and crustal structures, and in user-based studies, different phase picks are made. Therefore, differences in the determination of location, magnitude, depth, and particularly source type are observed for seismic events, especially at the micro-scale. KOERI-RETMC identifies the source type solely based on proximity to quarry blast areas and visual inspection, without resorting to technical analysis.

Erroneous source type identification in micro-seismic activity can be rectified by secondary analyses, resulting in more reliable catalog descriptions. Updating past catalogs and comprehensively examining future seismic events can minimize error margins, ensuring the presentation of the most reliable results. This approach can facilitate the creation of more reliable earthquake catalogs for studies such as seismology, seismotectonics, seismicity, and

earthquake hazard analysis, while eliminating the need for researchers to engage in time-consuming secondary analyses.

Due to the limited number of stations across the island and the considerable distance from stations in Türkiye, the error rates in location solutions of seismic events increase, leading to challenges in determining the source types. Therefore, increasing the number of stations throughout the island, and even deploying seafloor seismometers in the surrounding waters, is recommended not only for identifying artificial events but also for revealing the region's active tectonic activity more clearly

Article Information Form

Acknowledgments

The seismograms used in the study were obtained from the database of the Boğaziçi University Kandilli Observatory and Earthquake Research Institute Regional Earthquake-Tsunami Monitoring Center (KOERI-RETMC).

Funding

The author (s) has no received any financial support for the research, authorship or publication of this study.

The Declaration of Conflict of Interest/ Common Interest

No conflict of interest or common interest has been declared by the authors.

The Declaration of Ethics Committee Approval

This study does not require ethics committee permission or any special permission.

The Declaration of Research and Publication Ethics

The authors of the paper declare that they comply with the scientific, ethical and quotation rules of SAUJS in all processes of the paper and that they do not make any falsification on the data collected. In addition, they declare that Sakarya University Journal of Science and its editorial board have no responsibility for any ethical violations that may be encountered, and that this study has not been evaluated in any academic publication environment other than Sakarya University Journal of Science.

Copyright Statement

Authors own the copyright of their work published in the journal and their work is published under the CC BY-NC 4.0 license.

References

- [1] E. J. Kelly, "A Study of Two-short-period Discriminants," MIT Lincoln Laboratory, pp. 60, 1968.
- [2] R. Blandford, "Discrimination between earthquakes and underground explosions," *Annual Review of Earth and Planetary Science*, vol. 5, no. 1, pp. 111-122, 1977.
- [3] T. J. Bennett J. R. Murphy, "Analysis of seismic discrimination capabilities using regional data from western United States events," *Bulletin of the Seismological Society of America*, vol. 76, no. 4, pp. 1069-1086, 1986.
- [4] S. R. Taylor, N. W. Sherman, M. D. Denny, "Spectral discrimination between NTS explosions and western United States earthquakes at regional distances," *Bulletin of the Seismological Society of America*, vol. 78, no. 4, pp. 1563-1579, 1988.
- [5] Y. Gitterman, A. Shapira, "Spectral discrimination of underwater explosions," *Israel Journal of Earth Sciences*, vol. 42, pp. 37-44, 1993.
- [6] N. Arai, Y. Yosida, "Discrimination by short-period seismograms," *International Institute of Seismology and Earthquake Engineering, Building Research Institute (IISEE). Lecture Note, Global Course, Tsukuba, Japan*, p. 10, 2004.
- [7] G. Horasan, A. B. Güney, A. Küsmezer, F. Bekler, Z. Ögütçü, N. Musaoğlu, "Contamination of seismicity catalogs by quarry blasts: An example from Istanbul and its vicinity, northwestern Turkey," *Journal of Asian Earth Sciences*, vol. 34, pp. 90-99, 2009.
- [8] Ş. Yılmaz, Y. Bayrak, H. Çınar, "Discrimination of earthquakes and quarry blasts in the eastern Black Sea region of Turkey," *Journal of Seismology*, vol. 17, pp. 721-734, 2013.
- [9] E. Budakoğlu, G. Horasan, "Classification of seismic events using linear discriminant function (LDF) in the Sakarya region, Turkey," *Acta Geophysica*, vol. 66, no. 1, pp. 895-906, 2018.
- [10] E. Yavuz, F. Sertçelik, H. Livaoğlu, H. Woith, B. G. Lühr, "Discrimination of quarry blasts from tectonic events in the Armutlu Peninsula, Turkey," *Journal of Seismology*, vol. 23, pp. 59-76, 2019.
- [11] E. Yavuz, H. Livaoğlu, T. S. Irmak, F. Sertçelik, "Gaziantep-Kahramanmaraş Bölgesinde Meydana Gelen Deprem ve Taş Ocağı Patlatmalarının Zaman ve Frekans Ortamı Yöntemleri ile Sınıflandırılması," *Bitlis Eren Üniversitesi Fen Bilimleri Dergisi*, vol. 8, no. 2, pp. 642-651, 2019.
- [12] A. Tan, G. Horasan, D. Kalafat, A. Gülbağ, "Discrimination of earthquakes and quarries in the Edirne district (Turkey) and its vicinity by using a linear discriminate function method and artificial neural networks," *Acta Geophysica*, vol. 69, no. 1, pp. 17-27, 2021.
- [13] W. Y. Kim, D. W. Simpson, P. G. Richards, "Discrimination of earthquakes and explosions in the eastern United States using regional high-frequency data"

- Geophysical Research Letters, vol. 20, no. 14, pp. 1507-1510, 1993.
- [14] M. Kiszely, B. Süle, P. Mónus, I. Bondár, "Discrimination between local earthquakes and quarry blasts in the Vértes Mountains, Hungary," *Acta Geodaetica et Geophysica*, vol. 56, no. 3, pp. 523-537, 2021.
- [15] A. Badawy, M. Gamal, W. Farid, M. S. Soliman, "Decontamination of earthquake catalog from quarry blast events in northern Egypt," *Journal of Seismology*, vol. 23, no. 6, pp. 1357-1372, 2019.
- [16] I. M. Korrat, A. Lethy, M. N. ElGabry, H. M. Hussein, A. S. Othman, "Discrimination Between Small Earthquakes and Quarry Blasts in Egypt Using Spectral Source Characteristics," *Pure and Applied Geophysics*, vol. 179, no. 2, pp. 599-618, 2022.
- [17] G. Ataeva, Y. Gitterma, A. Shapira, "The ratio between corner frequencies of source spectra of P-and S-waves—a new discriminant between earthquakes and quarry blasts," *Journal of Seismology*, vol. 21, pp. 209-220, 2017.
- [18] R. Wang, B. Schmandt, E. Kiser, "Seismic discrimination of controlled explosions and earthquakes near Mount St. Helens using P/S ratios" *Journal of Geophysical Research: Solid Earth*, vol. 125, no. 10, e2020JB020338, 2020.
- [19] R. Wang, B. Schmandt, M. Holt, K. Koper, "Advancing Local Distance Discrimination of Explosions and Earthquakes With Joint P/S and ML-MC Classification," *Geophysical Research Letters*, vol. 48, no. 23, e2021GL095721, 2021.
- [20] E. Yavuz, M. C. Iban, E. Arpaz, "Identifying the source types of the seismic events using discriminant functions and tree-based machine learning algorithms at Soma Region, Turkey," *Environmental Earth Sciences*, vol. 82, no. 11, pp. 1-15, 2023.
- [21] Q. Kong, R. Wang, W. R. Walter, M. Pyle, K. Koper, B. Schmandt, "Combining Deep Learning With Physics Based Features in Explosion-Earthquake Discrimination," *Geophysical Research Letters*, vol. 49, no. 13, e2022GL098645, 2022.
- [22] A. Lethy, A. Othman, M. ElGabry, H. Hussein, G. El-Qady, "Discrimination between Small Earthquakes and Local Quarry Blasts Using Committee Machine", *ResearchSquare*, 2021.
- [23] H. Saadalla, H. E. Abdelhafiez, T. Hayashida, "Discrimination between earthquakes and quarry blasts in the Aswan region, southern Egypt, using P-wave source spectra," *Journal of Seismology*, vol. 27, no. 2, pp. 279-289, 2023.
- [24] I. M. Korrat, M. N. Elgabry, A. Lethy, H. M. Hussein, E. Yavuz, A. S. Othman, "Discrimination of quarry blasts from earthquakes in Northern and Central Egypt using linear and quadratic discriminant functions," *Journal of Seismology*, vol. 27, no. 4, pp. 609-626, 2023.
- [25] CGSD (Cyprus Geological Survey Department), 1995. *Geological Map of Cyprus*, Scale 1/250.000, Nicosia, Cyprus.
- [26] F. R. S. Henson, R. V. Browne, J. McGinty, "A synopsis of the stratigraphy and geological history of Cyprus," *The Quarterly Journal of the Geological Society of London*, vol. 105, pp. 1-41, 1949.
- [27] C. Ducloz, "Notes on the geology of the Kyrenia Range," *Cyprus Geological survey Dept., Annual Report for 1963*, pp. 57-67, 1964.
- [28] İ. Ketin, "A comparison between the tectonic units of Cyprus and the Southern Taurus - Amanos Mountains" *METU Journal of Pure and Applied Sciences*, vol. 21/1-3, pp. 169-182, 1988.

- [29] H. Y. Hakyemez, "Kuzey Kıbrıs'ın Temel Jeolojik Özellikleri," TPJD Bülteni, vol. 26, no. 2, pp. 7-46, 2014.
- [30] S. McClusky, R. Reilinger, S. Mahmoud, D. Ben Sari, A. Tealeb, "GPS constraints on Africa (Nubia) and Arabia plate motions," *Geophysical Journal Int.*, vol. 155, no.1, pp. 126-138, 2003.
- [31] R. Reilinger, S. McClusky, P. Vernant, S. Lawrence, S. Ergintav, R. Cakmak, ... G. Karam, "GPS constraints on continental deformation in the Africa-Arabia-Eurasia continental collision zone and implications for the dynamics of plate interactions," *Journal of Geophysical Research: Solid Earth*, vol. 111(B5), 2006.
- [32] S. Yolsal, T. Taymaz, A. C. Yalçiner, "Understanding tsunamis, potential source regions and tsunami-prone mechanisms in the Eastern Mediterranean," *Geological Society, London, Special Publications*, vol. 29, no. 1, pp. 201-230, 2007.
- [33] S. Yolsal-Çevikbilen, T. Taymaz, "Earthquake source parameters along the Hellenic subduction zone and numerical simulations of historical tsunamis in the Eastern Mediterranean," *Tectonophysics*, vol. 536, pp. 61-100, 2012.
- [34] G. Seyitoğlu, E. Tunçel, B. Kaypak, E. Korhan, E. Gökkaya, "The Anatolian Diagonal: a broad left-lateral shear zone between the North Anatolian Fault Zone and the Aegean/Cyprus arcs," *Türkiye Jeoloji Bülteni*, vol. 65, no. 2, pp. 93-116, 2022.
- [35] M. A. Hedlin, J. B. Minster, J. A. Orcutt, "The time-frequency characteristics of quarry blasts and calibration explosions recorded in Kazakhstan, USSR," *Geophysical Journal International*, vol. 99, no. 1, 109-121, 1989.
- [36] P. Bormann, "New manual of seismological observatory practice," 2002.
- [37] P. M. Shearer, B. P. Allmann, "Spectral studies of shallow earthquakes and explosions in Southern California," *Proceedings of the 29th Monitoring Research Review: Ground-Based Nuclear Explosion Monitoring Technologies*, pp. 656-662, 2007.
- [38] B. P. Allmann, P. M. Shearer, E. Hauksson, "Spectral discrimination between quarry blasts and earthquakes in southern California," *Bulletin of the Seismological Society of America*, vol. 98, no. 4, pp. 2073-2079, 2008.
- [39] T. C. Hanks, D. M. Boore, "Moment-magnitude relations in theory and practice," *Journal of Geophysical Research: Solid Earth*, vol. 89(B7), pp. 6229-6235, 1984.
- [40] T. S. Irmak, E. Yavuz, H. Livaoğlu, E. Şentürk, E. Y. Sahin, "Source parameters for small-moderate earthquakes in Marmara Region (Turkey)," *Geosciences Journal*, vol. 24, pp. 541-555, 2020.
- [41] R. A. Fisher, "The use of multiple measurements in taxonomic problems" *Annals of Eugenics*, vol.7, no. 2, pp. 179-188, 1936.
- [42] G. A. F. Seber, "Multivariate Observations," Hoboken, John Wiley & Sons Inc., 1984.
- [43] W. J. Krzanowski, "Principles of multivariate analysis: a user's perspective," Clarendon, 1988.
- [44] V. Franc, V. Hlavác, "Statistical pattern recognition toolbox for Matlab," Prague, Czech: Center for Machine Perception, Czech Technical University, 2004.
- [45] H. S. Kuyuk, E. Yildirim, E. Dogan, G. Horasan, "Clustering seismic activities using linear and nonlinear discriminant analysis," *Journal of Earth Science*, vol. 25, pp. 140-145, 2014.

Appendix A. The information of 122 seismic events and the results of the analysis. NoS: number of stations, NoP, number of phases, ST: source type, KOERI: Bogazici University Kandilli Observatory and Earthquake Research Institute Regional Earthquake-Tsunami Monitoring Center, IC: initial categorization, fc/CF: corner frequency, C: complexity, SR: spectral ratio, LDF: Linear Discriminant Function, QDF: Quadratic Discriminant Function, EQ: earthquake, QB: quarry blast, UI: unidentified event.

Date	Origin Time (GMT)	Latitude (o)	Longitude (o)	NoS	NoP	GAP	ML	ST (KOERI)	ST (IC)	fc	C	SR	Complexity Method		CF Method		Final Result
													LDF	QDF	LDF	QDF	
03.01.2018	09:41:02.45	35.3228	33.4805	4	6	244	1.2	QB	QB	6.116	6.831	0.719	EQ	EQ	EQ	EQ	EQ
03.01.2018	10:42:48.37	35.3018	33.3923	5	8	190	2.2	QB	QB	5.829	1.435	0.229	QB	QB	EQ	EQ	UI
08.01.2018	09:53:34.29	35.3780	33.4477	6	8	177	2.1	QB	QB	2.761	24.481	0.099	QB	QB	QB	QB	QB
11.01.2018	09:26:06.74	35.2602	33.4828	7	8	122	1.9	QB	QB	2.866	4.106	0.132	QB	QB	QB	QB	QB
13.01.2018	13:43:12.65	35.3255	33.4597	6	10	113	1.6	QB	QB	2.782	2.747	0.095	QB	QB	QB	QB	QB
23.01.2018	09:56:10.96	35.2923	33.6063	4	6	301	0.9	EQ	QB	6.142	1.670	0.836	EQ	EQ	EQ	EQ	EQ
27.01.2018	10:14:39.81	35.2398	33.5498	5	6	214	2.2	QB	QB	2.785	18.695	0.060	QB	QB	QB	QB	QB
31.01.2018	10:26:38.11	35.2163	33.5715	6	9	146	1.4	EQ	QB	2.756	11.272	0.039	QB	QB	QB	QB	QB
06.02.2018	10:09:07.16	35.2210	33.5215	4	6	183	2.0	QB	QB	9.053	10.778	0.390	QB	QB	EQ	EQ	UI
09.02.2018	09:52:33.88	35.2763	33.5837	3	6	281	0.9	QB	QB	4.403	2.459	0.304	QB	QB	QB	QB	QB
16.02.2018	09:57:47.31	35.3443	33.5910	5	6	292	1.4	EQ	QB	3.407	7.945	0.123	QB	QB	QB	QB	QB
19.02.2018	14:23:22.51	35.2968	33.5287	5	9	254	1.5	QB	EQ	6.843	21.596	0.283	QB	QB	EQ	EQ	UI
20.02.2018	14:17:15.06	35.2713	33.6787	4	7	299	1.4	QB	QB	2.991	25.184	0.056	QB	QB	QB	QB	QB
26.02.2018	10:06:34.93	35.2908	33.4930	5	7	192	2.3	QB	QB	4.409	12.836	0.217	QB	QB	QB	QB	QB
08.03.2018	09:53:50.85	35.3015	33.5067	5	9	220	1.6	QB	QB	2.789	9.804	0.129	QB	QB	QB	QB	QB
10.03.2018	11:31:26.61	35.2797	33.5510	6	8	140	1.4	QB	QB	2.798	7.074	0.053	QB	QB	QB	QB	QB
15.03.2018	10:19:45.80	35.3513	33.4993	5	7	255	1.8	QB	QB	2.818	10.156	0.016	QB	QB	QB	QB	QB
20.03.2018	16:02:31.45	35.2803	33.5598	5	7	279	1.5	QB	QB	4.244	3.920	0.160	QB	QB	QB	QB	QB
27.03.2018	09:03:43.21	35.3542	33.4758	6	9	171	1.3	QB	EQ	8.037	1.395	0.682	EQ	EQ	EQ	EQ	EQ
28.03.2018	13:52:52.86	35.3603	33.6280	4	7	312	1.4	QB	QB	5.376	5.147	0.133	QB	QB	QB	QB	QB
29.03.2018	09:03:47.36	35.2967	33.4860	5	7	199	2.2	QB	QB	2.789	5.725	0.080	QB	QB	QB	QB	QB

06.04.2018	08:30:10.64	35.3458	33.3905	5	7	217	1.4	QB	QB	6.111	16.682	0.210	QB	QB	EQ	EQ	UI
06.04.2018	09:23:46.01	35.2678	33.4518	9	11	162	1.7	QB	QB	6.576	12.649	0.302	QB	QB	EQ	EQ	UI
13.04.2018	09:26:47.65	35.2508	33.3508	3	5	191	1.6	QB	QB	2.703	39.056	0.015	QB	QB	QB	QB	QB
19.04.2018	12:27:39.18	35.2348	33.4922	5	5	151	1.5	QB	EQ	6.406	6.026	0.184	QB	QB	EQ	EQ	UI
24.04.2018	09:55:51.55	35.3512	33.6955	3	6	326	1.4	QB	QB	3.071	0.336	1.071	EQ	EQ	QB	QB	UI
25.04.2018	07:41:55.16	35.3017	33.5583	3	6	327	1.0	QB	QB	4.926	2.248	0.266	QB	QB	QB	QB	QB
30.04.2018	09:04:09.75	35.3030	33.4507	8	10	96	1.9	QB	QB	2.865	3.615	0.079	QB	QB	QB	QB	QB
30.04.2018	09:33:29.39	35.2848	33.5230	6	7	154	1.6	QB	QB	3.186	30.331	0.044	QB	QB	QB	QB	QB
30.04.2018	14:25:01.26	35.3363	33.5972	5	9	293	1.8	EQ	QB	2.845	8.068	0.029	QB	QB	QB	QB	QB
08.05.2018	08:09:51.62	35.3108	33.4287	5	7	200	1.4	QB	QB	3.567	10.515	0.148	QB	QB	QB	QB	QB
11.05.2018	15:03:48.71	35.3550	33.4483	3	5	302	1.5	QB	QB	4.167	6.100	0.105	QB	QB	QB	QB	QB
14.05.2018	09:03:39.46	35.3437	33.5060	4	8	256	1.2	QB	QB	3.22	3.466	0.269	QB	QB	QB	QB	QB
28.05.2018	09:08:44.65	35.3155	33.4175	6	8	100	1.5	QB	QB	6.003	3.651	0.219	QB	QB	EQ	EQ	UI
28.05.2018	09:14:05.84	35.2858	33.4847	5	5	112	1.2	QB	QB	3.108	6.284	0.180	QB	QB	QB	QB	QB
28.05.2018	09:17:09.07	35.3095	33.5353	6	7	176	1.3	QB	QB	2.885	21.310	0.052	QB	QB	QB	QB	QB
30.05.2018	07:53:53.46	35.3457	33.4898	3	5	311	1.3	QB	QB	4.553	3.754	0.587	EQ	EQ	QB	QB	UI
30.05.2018	08:59:27.73	35.2712	33.3935	7	8	94	2.3	QB	QB	3.859	12.797	0.117	QB	QB	QB	QB	QB
30.05.2018	12:20:48.09	35.4818	33.4648	3	5	332	1.6	EQ	QB	3.434	13.666	0.146	QB	QB	QB	QB	QB
31.05.2018	12:57:38.67	35.4520	33.5753	3	6	349	1.1	EQ	QB	2.632	2.751	0.045	QB	QB	QB	QB	QB
10.12.2018	14:42:15.44	35.3178	33.4060	8	12	98	1.7	QB	QB	2.878	4.414	0.019	QB	QB	QB	QB	QB
13.12.2018	09:44:04.94	35.3220	33.7060	4	6	305	1.8	EQ	QB	3.991	2.751	0.149	QB	QB	QB	QB	QB
18.12.2018	10:01:10.25	35.2242	33.5470	9	13	191	1.4	QB	QB	3.094	2.781	0.048	QB	QB	QB	QB	QB
18.12.2018	12:02:22.44	35.2980	33.4115	9	14	85	1.7	QB	QB	2.81	7.105	0.042	QB	QB	QB	QB	QB
21.12.2018	10:00:29.64	35.2395	33.6848	4	7	225	2.1	EQ	QB	2.799	4.305	0.069	QB	QB	QB	QB	QB
24.12.2018	09:52:13.16	35.2917	33.5225	9	12	125	2.3	QB	QB	2.805	3.145	0.033	QB	QB	QB	QB	QB
26.12.2018	10:12:29.02	35.4487	33.4470	5	7	178	2.5	EQ	QB	6.526	4.800	0.367	QB	QB	EQ	EQ	UI
27.12.2018	11:23:41.12	35.2907	33.4102	4	6	183	1.4	QB	QB	2.799	1.512	0.076	QB	QB	QB	QB	QB

28.12.2018	09:47:27.72	35.2380	33.6078	5	8	234	1.5	EQ	QB	6.581	4.199	0.526	EQ	EQ	EQ	EQ	EQ
14.01.2019	10:40:10.76	35.2870	33.4993	3	6	206	1.3	QB	QB	2.774	36.845	0.042	QB	QB	QB	QB	QB
18.01.2019	09:48:35.06	35.2977	33.6610	7	9	207	1.6	EQ	QB	2.774	1.931	0.042	QB	QB	QB	QB	QB
21.01.2019	09:53:33.31	35.2982	33.5442	4	8	207	1.1	QB	QB	2.797	4.396	0.068	QB	QB	QB	QB	QB
23.01.2019	13:25:48.48	35.1935	33.3792	6	9	103	1.6	QB	EQ	6.642	0.890	2.504	EQ	EQ	EQ	EQ	EQ
24.01.2019	10:14:03.51	35.3012	33.4978	9	14	112	1.9	QB	QB	2.691	17.951	0.018	QB	QB	QB	QB	QB
25.01.2019	13:01:22.18	35.2507	33.3798	5	10	174	1.4	QB	QB	2.761	1.297	0.053	QB	QB	QB	QB	QB
31.01.2019	10:21:38.91	35.3410	33.4357	11	13	70	1.6	QB	QB	4.88	4.796	0.126	QB	QB	QB	QB	QB
04.02.2019	11:41:29.08	35.2895	33.1813	18	19	86	2.7	EQ	EQ	7.99	0.245	1.023	EQ	EQ	EQ	EQ	EQ
13.02.2019	10:43:59.88	35.3243	33.5037	5	8	243	1.4	QB	QB	2.625	7.036	0.033	QB	QB	QB	QB	QB
15.02.2019	08:45:41.67	35.2482	33.5108	5	6	161	1.7	QB	QB	2.808	3.232	0.022	QB	QB	QB	QB	QB
18.02.2019	09:56:13.77	35.3582	33.5747	5	7	291	1.1	QB	QB	4.528	3.101	0.350	QB	QB	QB	QB	QB
19.02.2019	10:10:42.48	35.3202	33.5438	3	6	346	1.2	QB	QB	6.667	7.031	0.326	QB	QB	EQ	EQ	UI
20.02.2019	08:51:46.79	35.2827	33.3763	4	8	97	1.7	QB	QB	4.16	4.202	0.158	QB	QB	QB	QB	QB
21.02.2019	08:14:46.47	35.3318	33.5740	5	7	162	1.2	QB	QB	2.406	5.820	0.039	QB	QB	QB	QB	QB
21.02.2019	11:52:25.42	35.2538	33.4973	7	8	123	1.3	QB	QB	2.234	6.436	0.027	QB	QB	QB	QB	QB
01.03.2019	10:41:37.98	35.2790	33.4780	8	9	97	1.6	QB	QB	2.792	12.838	0.008	QB	QB	QB	QB	QB
08.03.2019	08:56:47.97	35.3327	33.5000	4	8	245	1.1	QB	QB	2.857	7.450	0.024	QB	QB	QB	QB	QB
08.03.2019	12:53:31.77	35.3175	33.4383	4	7	227	1.5	QB	QB	5.691	6.422	0.146	QB	QB	EQ	EQ	UI
14.03.2019	09:54:59.35	35.2962	33.4055	7	8	104	1.5	QB	QB	4.578	18.383	0.162	QB	QB	QB	QB	QB
01.04.2019	09:00:56.14	35.2673	33.6948	6	9	216	1.8	QB	QB	3.053	3.481	0.021	QB	QB	QB	QB	QB
04.04.2019	08:50:51.65	35.3172	33.4480	6	9	155	1.4	QB	QB	3.812	7.573	0.091	QB	QB	QB	QB	QB
02.05.2019	08:49:00.89	35.2828	33.5233	5	6	118	1.8	QB	QB	3.2	6.761	0.054	QB	QB	QB	QB	QB
06.05.2019	09:29:38.13	35.2838	33.6630	5	8	209	1.7	EQ	QB	3.196	4.947	0.057	QB	QB	QB	QB	QB
07.05.2019	08:52:58.42	35.2540	33.5910	4	6	198	1.6	EQ	QB	3.473	7.933	0.034	QB	QB	QB	QB	QB
08.05.2019	12:16:15.58	35.2878	33.4763	4	6	169	1.6	QB	QB	2.825	8.890	0.022	QB	QB	QB	QB	QB
14.05.2019	09:38:19.31	35.2557	33.4552	7	10	132	1.5	QB	QB	4.189	7.314	0.117	QB	QB	QB	QB	QB

17.05.2019	08:30:36.83	35.2340	33.5170	7	8	194	1.6	QB	EQ	6.25	0.979	0.246	QB	QB	EQ	EQ	UI
23.05.2019	09:28:17.29	35.2807	33.4968	4	6	165	1.5	QB	QB	3.203	6.338	0.078	QB	QB	QB	QB	QB
24.05.2019	10:14:01.41	35.3272	33.4620	5	7	116	1.5	QB	EQ	6.834	4.859	0.390	QB	QB	EQ	EQ	UI
24.05.2019	10:19:07.71	35.2825	33.4173	5	7	122	1.5	QB	QB	2.855	5.205	0.035	QB	QB	QB	QB	QB
29.05.2019	11:34:58.92	35.3128	33.5293	7	10	106	1.7	QB	QB	2.846	9.309	0.019	QB	QB	QB	QB	QB
12.06.2019	09:34:05.95	35.2753	33.5405	11	12	129	1.9	QB	QB	3.835	13.907	0.168	QB	QB	QB	QB	QB
01.07.2019	09:09:56.39	35.3087	33.7025	4	7	305	1.8	QB	QB	3.91	3.462	0.079	QB	QB	QB	QB	QB
08.07.2019	09:21:29.38	35.2917	33.4937	6	9	138	1.6	QB	QB	2.641	6.476	0.041	QB	QB	QB	QB	QB
15.07.2019	09:38:38.47	35.2202	33.3647	9	10	97	1.5	QB	QB	4.236	0.390	0.449	QB	QB	QB	QB	QB
22.07.2019	08:54:11.49	35.3393	33.5537	4	5	287	1.2	QB	QB	2.714	10.747	0.081	QB	QB	QB	QB	QB
23.07.2019	09:14:57.84	35.3060	33.3922	7	11	87	2.1	QB	QB	2.649	5.680	0.042	QB	QB	QB	QB	QB
01.11.2019	09:57:24.80	35.2507	33.6763	5	7	223	1.6	EQ	QB	3.588	7.256	0.032	QB	QB	QB	QB	QB
10.12.2019	09:54:00.21	35.2940	33.4030	5	7	154	1.5	QB	QB	2.468	3.875	0.028	QB	QB	QB	QB	QB
18.12.2019	10:27:20.90	35.2653	33.4952	7	8	144	1.4	QB	QB	4.522	0.725	0.392	QB	QB	QB	QB	QB
23.12.2019	09:57:57.74	35.2400	33.4582	4	7	146	1.1	QB	QB	4.215	1.761	0.088	QB	QB	QB	QB	QB
13.01.2020	09:01:04.55	35.2738	33.4717	6	8	121	1.4	QB	QB	3.551	2.903	0.294	QB	QB	QB	QB	QB
13.01.2020	09:57:24.40	35.3005	33.6465	6	8	215	1.8	EQ	QB	3.007	7.831	0.019	QB	QB	QB	QB	QB
17.01.2020	09:37:22.01	35.2703	33.5745	4	7	208	2.0	EQ	QB	3.032	16.949	0.015	QB	QB	QB	QB	QB
03.02.2020	10:27:39.42	35.2367	33.6597	3	6	222	1.5	EQ	QB	3.502	6.837	0.042	QB	QB	QB	QB	QB
19.02.2020	10:07:34.54	35.2668	33.6382	4	5	217	1.5	QB	QB	3.514	6.729	0.075	QB	QB	QB	QB	QB
20.02.2020	10:28:00.09	35.1742	33.5213	3	4	236	2.0	EQ	EQ	5.836	1.100	0.511	QB	EQ	EQ	EQ	EQ
02.03.2020	09:57:26.78	35.2657	33.6472	4	7	218	1.5	EQ	QB	3.872	6.396	0.163	QB	QB	QB	QB	QB
06.03.2020	10:09:16.08	35.2955	33.6460	6	7	217	1.7	EQ	QB	3.477	6.949	0.044	QB	QB	QB	QB	QB
13.05.2020	09:01:21.64	35.3010	33.4637	6	8	152	1.8	QB	QB	4.537	5.320	0.320	QB	QB	QB	QB	QB
09.06.2020	09:24:17.34	35.3495	33.4000	6	9	155	1.7	QB	QB	2.715	13.195	0.059	QB	QB	QB	QB	QB
03.07.2020	09:18:43.83	35.2643	33.4067	6	8	270	1.9	QB	QB	4.48	3.900	0.422	QB	QB	QB	QB	QB
15.07.2020	09:09:06.12	35.3792	33.4353	3	5	180	1.7	EQ	QB	4.492	0.715	0.255	QB	QB	QB	QB	QB

16.07.2020	07:36:03.16	35.3180	33.3900	5	7	157	1.6	QB	QB	2.714	12.123	0.033	QB	QB	QB	QB	QB
24.07.2020	09:29:08.33	35.2447	33.5052	6	9	175	1.9	EQ	EQ	6.002	2.917	0.297	QB	QB	EQ	EQ	UI
12.08.2020	19:01:20.69	35.4863	33.4425	6	12	178	2.0	EQ	EQ	5.972	1.713	2.576	EQ	EQ	EQ	EQ	EQ
18.08.2020	08:59:38.13	35.2803	33.3675	5	9	133	1.4	QB	QB	2.408	20.246	0.028	QB	QB	QB	QB	QB
20.08.2020	01:38:24.70	35.3363	33.6803	11	13	153	2.1	EQ	EQ	7.136	0.786	1.600	EQ	EQ	EQ	EQ	EQ
04.09.2020	08:56:34.58	35.2488	33.6100	5	6	215	1.4	EQ	QB	3.571	2.992	0.059	QB	QB	QB	QB	QB
10.09.2020	09:14:00.90	35.4047	33.4838	3	6	266	1.4	EQ	EQ	6.525	1.076	0.342	QB	QB	EQ	EQ	UI
12.10.2020	08:07:49.53	35.1588	33.6025	3	6	177	1.6	EQ	QB	2.904	14.782	0.035	QB	QB	QB	QB	QB
14.10.2020	09:06:38.29	35.2378	33.4932	8	9	143	1.7	QB	QB	2.878	4.368	0.082	QB	QB	QB	QB	QB
01.12.2020	09:52:51.30	35.4087	33.6252	3	5	214	1.6	EQ	QB	3.539	5.159	0.074	QB	QB	QB	QB	QB
07.12.2020	10:17:01.83	35.2767	33.6998	4	7	223	1.7	EQ	QB	3.838	6.367	0.079	QB	QB	QB	QB	QB
26.01.2021	10:32:24.22	35.4007	33.4107	4	7	162	2.1	EQ	QB	2.821	19.583	0.109	QB	QB	QB	QB	QB
07.04.2021	09:35:24.63	35.3022	33.3643	6	10	162	1.8	QB	QB	2.813	8.842	0.017	QB	QB	QB	QB	QB
25.06.2021	09:32:57.48	35.3207	33.3958	3	6	243	1.4	QB	QB	3.352	4.278	0.051	QB	QB	QB	QB	QB
25.06.2021	09:39:55.31	35.2662	33.6273	5	8	159	1.4	EQ	QB	3.713	6.590	0.019	QB	QB	QB	QB	QB
09.07.2021	09:41:56.78	35.4075	33.2993	3	5	204	1.6	EQ	QB	3.374	2.999	0.086	QB	QB	QB	QB	QB
09.07.2021	09:49:58.75	35.2908	33.5200	3	5	163	1.0	QB	QB	3.519	3.258	0.036	QB	QB	QB	QB	QB
23.07.2021	23:39:17.44	35.3205	33.5113	7	11	136	2.0	EQ	EQ	8.474	0.819	1.300	EQ	EQ	EQ	EQ	EQ
20.09.2021	10:08:15.16	35.2710	33.4233	6	12	261	1.7	QB	QB	4.184	11.961	0.069	QB	QB	QB	QB	QB
02.11.2021	10:25:06.09	35.2613	33.6260	3	6	216	1.5	EQ	QB	2.804	5.904	0.148	QB	QB	QB	QB	QB

Fog Harvesting: An Effective Solution to the Water Scarcity Problem

Kadriye Oktor¹ , Makoi Gai Riak Dhuol² , Merve Ercan Kalkan^{2*} 

¹ Kocaeli University, Faculty of Engineering, Department of Environmental Engineering, Kocaeli, Türkiye, oktor@kocaeli.edu.tr

² Kocaeli University, Faculty of Engineering, Department of Chemical Engineering, Kocaeli, Türkiye makoighai@gmail.com, merve.ercan@kocaeli.edu.tr

*Corresponding Author

ARTICLE INFO

ABSTRACT

Keywords:

Fog harvesting
Water
Water source
Sustainability
Water scarcity

Fog harvesting, also known as fog collection, is a sustainable approach to addressing water scarcity which captures water droplets from fog, providing a renewable water source for water-scarce regions. The aim of this study is to give more background about fog harvesting by introducing fog harvesting systems, their advantages and disadvantages, real world and laboratory projects and efficiency. This study emphasizes fog harvesting's potential in arid regions with frequent fog occurrence, discusses working mechanisms, and explores nature-inspired and nanotechnology-based fog collectors. Local climate data's importance for feasibility assessment is highlighted, along with the vital role of community involvement for long-term success. Fog harvesting offers a promising and environmentally friendly solution to alleviate water scarcity challenges when combined with innovative strategies and community engagement. Real-world projects have shown that fog water collection can be an effective and sustainable solution, particularly in regions with persistent fog and limited water resources. However, more work is needed on innovative fog collectors and advanced materials to increase sustainability.

Article History:

Received: 08.05.2024

Accepted: 01.07.2024

Online Available: 06.08.2024

1. Introduction

In the modern world, there is an ever-increasing need for clean and sustainable water. Unfortunately, many regions struggle to meet the increasing demand for water, and in some areas, its inferior quality limits its usability [1]. There are several factors contributing to this global pressing issue, including rapid population growth, ineffective water management practices, and inadequate infrastructure. Moreover, the looming threat of climate change is expected to worsen the situation further [2, 3]. As a result, addressing the challenge of water scarcity and ensuring access to safe water for all is becoming increasingly critical. Sustainable water management practices and measures are urgently required to confront this growing crisis. Alternative water sources such as desalination, rainwater harvesting, groundwater collection,

and fog harvesting are being studied and implemented worldwide to combat this issue [4, 5].

Fog harvesting, also known as fog collection, provides a renewable and sustainable water source for regions with limited access to conventional water supplies [6]. This technique is particularly vital for communities in arid or semi-arid regions and mountainous terrains, where traditional water sources such as rivers, lakes, and underground aquifers may be scarce or unreliable and where fog is a frequent occurrence [7]. These systems are installed in coastal and mountainous areas where fog presence is naturally high.

This technique involves the use of specialized nets or meshes, known as fog collectors or fog catchers, placed strategically in areas where fog

formation is prevalent. These structures capture tiny water droplets suspended in the fog, which then accumulate and drip down into collection troughs. The collected water is then directed into storage tanks or reservoirs for immediate use or future distribution [8]. The effectiveness of fog harvesting systems largely depends on the design and efficiency of fog collectors [9]. However, the most commonly used for collectors, such as vertical mesh nets, have certain limitations. These collectors often experience reduced efficiency due to issues such as water droplet runoff, clogging, and low collection rates [10]. Consequently, there is a need for innovative techniques and materials that can overcome these limitations and improve the overall performance of fog collectors.

To address these challenges, researchers have explored various strategies to enhance fog collection efficiency [11–13]. Many researchers have focused on the optimization of the materials and coatings used in fog collection systems making it easy to harvest water under light fog conditions [14]. By developing hydrophilic-hydrophobic pattern coatings or modifying mesh surfaces, researchers have aimed to increase droplet capture rates and minimize water loss through runoff or evaporation [15, 16].

Additionally, advancements in fog characterization techniques have provided valuable insights into the properties of fog. Studying parameters such as fog droplet size distribution, fog density, and fog water content enables researchers to better understand fog behavior and optimize fog collection systems accordingly [17].

With the improvement of materials science, technology, and understanding of fog dynamics, fog harvesting has evolved significantly over the past few decades. Numerous experimental projects and real-world applications have been implemented in diverse geographical locations, from foggy coastal areas in Chile and Peru to mountainous regions in Morocco and Nepal. These projects vary in scale, ranging from small community-based initiatives to larger-scale installations supporting entire towns [18]. By examining these ongoing initiatives, we can gain valuable insights into the adaptability and

potential limitations of fog water collection in various settings.

This study is aimed at exploring the principles, applications, challenges, and benefits of fog water collection, shedding light on its significance in addressing the global water crisis and promoting environmental conservation. The originality of this work is to raise awareness of the potential of fog harvesting as a sustainable and scalable solution to water scarcity problems by critically examining existing research, case studies, and real-world applications as well as literature.

A Mini Database Based Review

In this section, the Web of Science (WOS) database was reviewed in terms of publication year, origin, highly cited papers and their motivation, and disciplinary categories for the “fog harvesting” keyword.

When the number of WOS publications is examined by year, it has been observed that interest in the subject has increased systematically in the last decade as seen in Figure 1.

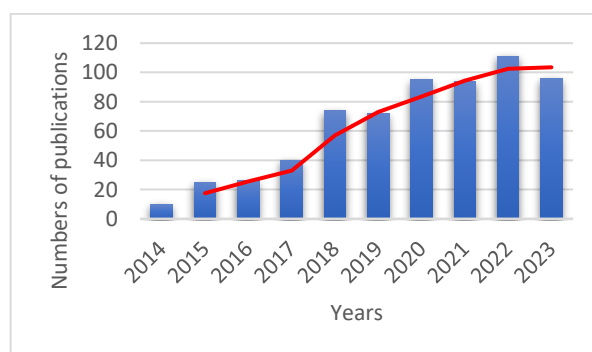


Figure 1. Numbers of publications by year

Considering the number of publications, the most published disciplinary categories (number of publications) according to WOS are as follows: Materials Science Multidisciplinary (206), Chemistry Physical (135), Chemistry Multidisciplinary (108), Nanoscience Nanotechnology (103), Physics Applied (85), Environmental Sciences (69), Water Resources (44), Engineering Chemical (42), Physics Condensed Matter (38), and Energy Fuels (37). As can be seen here, fog harvesting and

technologies are a versatile and multidisciplinary subject.

The origins of the publications in the WOS database are listed as follow in the form of Country (publication number) as China (288), USA (122), England (42), South Korea (35), India (33), Germany (31), Australia (26), Saudi Arabia (23), France (22), and Canada (21). It can be concluded that significant parts of the studies are carried out by China and USA.

Yu et al. (2022) have provided in-depth information about design basics and production technologies of fog harvesting devices [19]. Tu et al. (2018) comprehensively reviewed current developments in atmospheric water harvesting technologies [20]. Song et al. (2023) conducted a comprehensive study on the controlled wettability of surfaces [21]. Wu et al. (2021) reviewed the recent advances in special membranes, which include both hydrophobic and hydrophilic structures, to control surface wettability [22]. Shi et al. (2021) focused on the membrane technologies for water harvesting [23]. A (PVA)/polypyrrole (PPy) based hydrogel membrane, which is effective in both fog collection and purification stages, has been developed. Yin et al. (2017) obtained a hybrid superhydrophobic-hydrophilic surface by coating the copper network with polytetrafluoroethylene nanoparticles [24].

Fathieh et al. (2018) designed a system to produce water from desert air [25]. LaPotin et al. (2019) and Zhou et al (2020) drew attention to absorbent materials that can be used in atmospheric water harvesting systems [26, 27]. Additionally, LaPotin et al. (2019) focused on modeling of a solar thermal water harvesting system in presence of adsorbent [26]. Kim et al. (2017) designed a metal-organic based porous framework that take up water from the atmosphere at ambient conditions [28].

The most cited fog harvesting papers in the WOS database were also examined. These studies can be summarized as reviewing current knowledge, focusing on wettability and surface properties, designing a system/device and modelling operating conditions as in seen in Table 1.

Table 1. The most cited papers and their motivations

Author (Year)	Reference	Working area
Yin et al. (2017)	[24]	Material
Fathieh et al. (2018)	[25]	Design
Tu et al. (2018)	[20]	Review
LaPotin et al. (2019)	[26]	Modelling
Kim et al. (2019)	[28]	Design
Zhou et al (2020)	[27]	Material
Wu et al. (2021)	[22]	Material
Shi et al. (2021)	[23]	Material
Yu et al. (2022)	[19]	Review
Song et al. (2023)	[21]	Material

2. The Principles of Fog Harvesting

2.1. Fog harvesting system

The principles of fog collection focus on capturing tiny water droplets from fog using specialized materials and surfaces. A basic fog harvesting system comprises fog collectors, collecting channels or troughs, storage tanks, and a distribution network. Depending on the intended use of the collected water, a treatment component may be included. The primary components of the system are the fog collectors, typically constructed from meshes made of materials like nylon, polyethylene, polypropylene, or high-density polyethylene. The material choice depends on factors such as cost, durability, and local availability [29].

The most common type of fog collector in fog water harvesting is the vertical, rectangular panel, offering dimensions of approximately 4 meters in height and 10-12 meters in length, providing an extensive surface area for capturing fog droplets. For different applications, fog harvesting systems may use either standard fog collectors (SFC) or large fog collectors (LFC).

The SFC, with a fog-collecting area of 1.0 square meter, is primarily utilized for research purposes. Conversely, the LFC, boasting a panel surface area of 40 to 48 square meters, is extensively employed in various fog harvesting projects [30]. Fog collectors exhibit flexibility in terms of installation options, as they can be affixed to various support structures such as wooden or metal poles, concrete pillars, or existing buildings as shown in fog harvesting system in

Figure 2 [18]. The choice of support structure depends on factors such as terrain conditions, material availability, and local considerations [31]. Additionally, certain fog collectors are designed to be collapsible or portable, facilitating easy transport and installation. This portability allows for their disassembly and reassembly at different locations, making them well-suited for temporary deployments or research ventures [32].

2.2. Fog collection mechanism

The mechanism of fog collection involves two main stages: fog-capturing and liquid transport as shown in Figure 3 (a) and (b) respectively [33]. During the first stage, fog droplets are captured either during a fog event or through condensation on the solid mesh surface of the fog collector. This occurs through two mechanisms: capturing droplets from fog during a fogging event and collecting dew condensed on surfaces with temperatures below the atmospheric dew point [34].

As wind-driven fog passes through the strategically positioned mesh, the water droplets present in the fog deposit on the mesh surface [35]. Over time, these deposited droplets accumulate and combine to form larger ones, which then fall under gravity into the trough

below the panel. Alternatively, when the surface temperature drops below the dew point of the surrounding air, water vapor in the atmosphere condenses into droplets on the surface. Fog collectors designed to promote condensation effectively capture this dew, which eventually accumulates and flows into collection points [9, 34].

In the second stage, the captured water droplets need to be efficiently transported from the mesh surface to a central collection point, such as a trough or gutter, from where they can be directed to storage tanks or reservoirs. This liquid transport is primarily achieved through gravity-driven flow. As water droplets accumulate and coalesce on the mesh surface, they gain sufficient mass to overcome the surface tension and flow down the mesh under the force of gravity [9, 36]. The mesh is strategically designed to allow water to flow towards the collection channels, ensuring a steady and controlled movement of the captured water [37].

The collecting channels or troughs are positioned below the fog collector panel to catch the falling water droplets. These channels are designed to efficiently channel the water towards a centralized point, where it can be collected and further directed for storage or distribution.

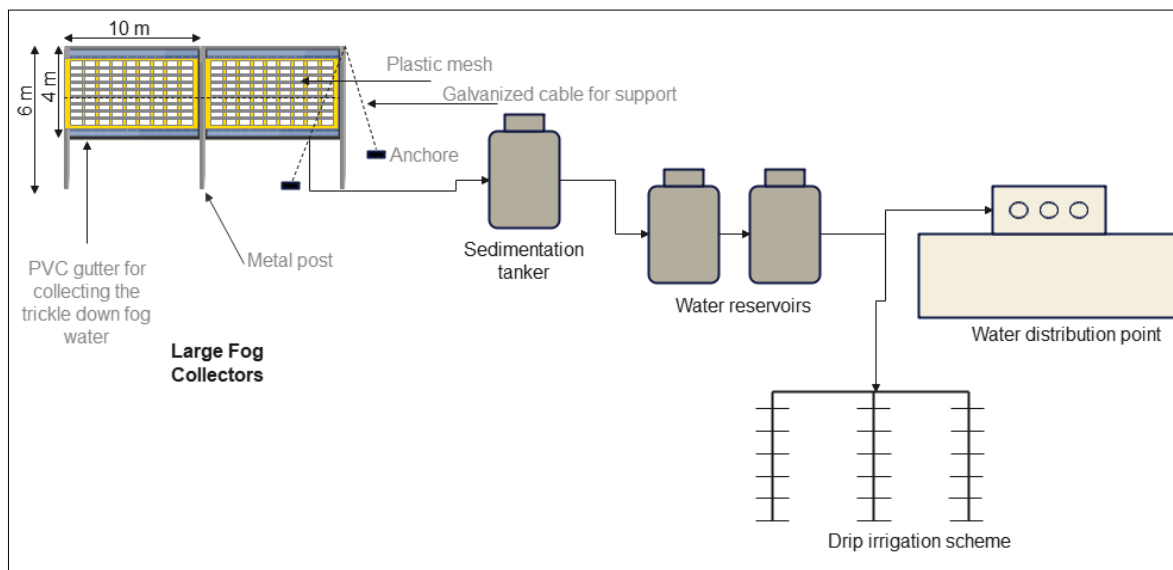


Figure 2. Fog harvesting system [18]

The efficiency of fog collection depends on various factors, including the wettability and topography of the surface, the air-liquid fraction,

and the drop mobility derived from the optimization of superhydrophobic properties [37]. Properly designing and managing these

aspects contribute to maximizing water yield and optimizing the overall performance of the fog harvesting system.

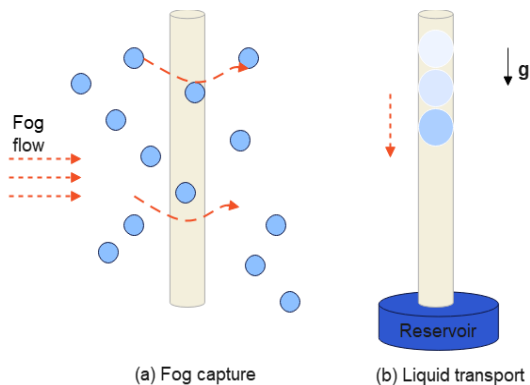


Figure 3. Schematics of the two key steps of fog collection. (a) Fog capture process. (b) Captured liquid transport process [33].

3. Advantages of Fog Water Collection

Fog water collection offers several compelling advantages as a viable and sustainable water resource, making it an increasingly popular solution in regions facing water scarcity challenges. One of its primary benefits is the provision of an alternative water source, reducing reliance on traditional sources such as groundwater. As climate change and increasing demand put pressure on conventional water supplies, fog water collection offers a complementary and reliable source, particularly in areas where fog is a frequent occurrence.

The simplicity and low operating costs associated with fog water collection technology make it an attractive option for communities with limited financial resources. The infrastructure required is minimal, and the systems are easy to maintain, enabling cost-effective implementation and operation. This affordability enhances accessibility, making fog water collection a feasible option for marginalized communities and remote areas where establishing extensive water infrastructure may not be practical or economically viable [19].

Moreover, fog water's inherent cleanliness and freedom from pollutants make it a valuable resource for various applications, including domestic use, irrigation, and livestock watering. In comparison to other water sources that may require extensive treatment, fog water often

meets high-quality standards directly after collection, saving costs and effort in purification processes.

Fog water collection's suitability in arid and semi-arid regions is particularly advantageous, where rainfall is scarce, and traditional water sources may be unreliable. By harnessing fog, communities in these regions can enhance their water security, ensuring a steady supply even during prolonged dry periods [38].

The versatility of fog water collection is reflected in its diverse design options. From traditional mesh-based fog collectors to cutting-edge systems featuring advanced materials and technologies, fog water collection can be tailored to suit specific environmental conditions and water demands. The adaptability of these designs ensures efficiency and effectiveness across various geographical locations [39].

As a sustainable and environmentally friendly solution, fog water collection operates on natural processes without the need for energy-intensive infrastructure or chemical treatments [40]. This aspect aligns with global efforts towards sustainable water management and conservation, contributing to environmental preservation and reduced carbon footprints [29].

Fog water collection's capacity to supplement existing water supplies, such as rainwater harvesting or groundwater pumping, adds an additional layer of resilience to water management strategies. By diversifying water sources, communities can better withstand fluctuations in rainfall patterns and other climate-related uncertainties.

Moreover, fog water collection supports reforestation efforts, providing water to ridge lines and mountainous regions where importing water from conventional sources may be impractical. This promotes forest growth and ecological restoration, contributing to ecosystem health and biodiversity conservation [35].

Properly designed fog water collection systems can produce water that meets drinking water standards set by organizations like the World Health Organization (WHO) [41]. This ensures

that the collected water is safe for consumption, further enhancing its value as a reliable and potable water source for communities.

4. Real-World Fog Harvesting Projects

Real-world fog harvesting projects have demonstrated the practicality and potential of this technology in providing a sustainable water source in regions facing water scarcity. Governments, NGOs, and researchers collaborate to implement fog harvesting systems and study their effectiveness in different climatic conditions [34].

Table 2. Number of foggy days for some countries [18, 42]

Countries	Foggy days per year
Cape Verde, Serra Malgagueta	365
Peru, Mejia	210
Canary Islands, Tenerife	354
Chile, Alto Patache	365
Eritrea, Arborobu	166
Guatemala, Tojquian	210
S. Africa, Lepelfontain	184
Yemen, Hajja	121
Ecuador, P. Grande	210
Nepal, Pathivara	122
Spain, Valencia	142
Eritrea, Nefasit	90
S Africa, Soutpansbergn	200
Chile, El Tofo	365
Chile, Padre Hurtado	365
Colombia, Andres Mountain	210
Chile, Falda Verde	365

One notable project is the Fog Quest organization's initiatives, which have been successfully implemented in countries like Chile, Nepal, and Eritrea. Table 2 and Figure 4 show some of the countries that successfully established fog collection projects together with amount of fog collected per area per day. These projects have used from 10 to 100 fog collectors and have shown success even in areas with minimal annual precipitation, as low as 1 mm per year [18, 42].

In Chile, fog water collection has been instrumental in providing water for irrigation and

reforestation projects in one of the world's driest regions, Cerro Talinay [43]. Similarly, in Morocco, the village of Boutmezguida has witnessed increased crop yields and improved livelihoods through fog water collection for irrigation and livestock watering [40]. Peru's village of Huancavelica has benefited from improved access to safe drinking water through fog water collection, enhancing the community's well-being [44].

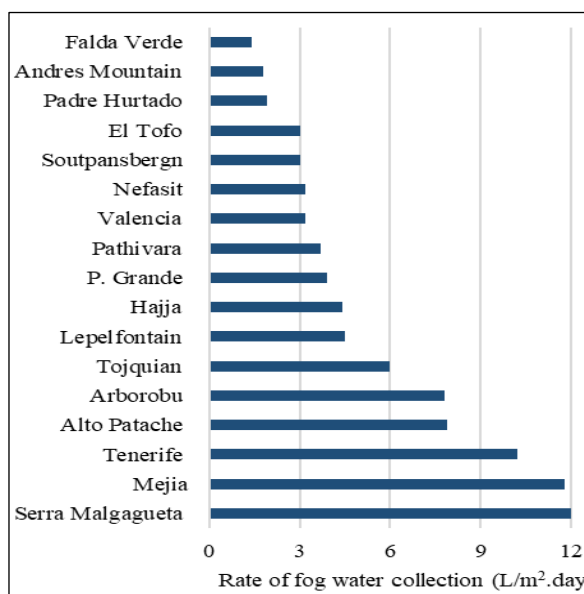


Figure 4. Rate of fog collected (L/(m².day)) for the countries that utilized the technology of fog collection. [18,42]

Other real-world projects have showcased innovative approaches to fog water collection. For instance, the Warka Tower project in Ethiopia utilizes a unique fog collector design inspired by local flora, providing drinking water to rural communities and earning recognition for its ingenuity [32].

In addition to Fog Quest's efforts, various experiments and research projects in Chile, Spain, and Oman have explored different fog water collector designs and their feasibility in supplementing existing water sources [44].

These studies have further demonstrated the potential of fog water collection as a sustainable and affordable solution, particularly in arid and semi-arid regions where fog is abundant. Figure 5 shows a map of potential areas for fog harvesting in the world [45].



Figure 5. The map illustrates areas where fog collection has been successful, currently successful, and potential for future success [45].

Croatia, in Southern Europe, has also successfully implemented fog water collection on Mount Velebit, highlighting the potential of fog as a significant water source, especially during dry summer seasons. Spain has maintained a fog collection network since 2003, covering a vast area along the eastern fringe of the Iberian Peninsula, further establishing fog water as a valuable resource in the western Mediterranean basin [44].

In summary, real-world fog harvesting projects have shown that fog water collection can be an effective and sustainable solution, particularly in regions with persistent fog and limited water resources. While challenges such as proper design, maintenance, and local climate conditions exist, the success of these initiatives underscores the importance of fog water collection in addressing water scarcity and improving the quality of life for communities worldwide.

As technology and understanding continue to advance, fog water harvesting will likely play an increasingly vital role in water resource management and environmental conservation efforts.

5. Challenges and Limitations

Fog water collection, while holding significant promise as a solution to water scarcity, presents several challenges and limitations that must be

carefully considered for successful implementation. One of the primary constraints of fog harvesting is its dependence on the availability of suitable fog. This technique thrives in regions with frequent and dense fog occurrences, limiting its applicability to areas with such favorable meteorological conditions. Consequently, fog water collection may not be viable in regions with low fog frequency, making it essential to carefully assess the feasibility of fog harvesting projects based on local climate data.

Maintenance emerges as a critical challenge in sustaining efficient fog collectors. The delicate nature of fog-catching infrastructure exposes it to damage caused by strong winds, intense sunlight, and other environmental factors. Regular maintenance becomes imperative to ensure the longevity and effectiveness of fog collectors. However, the logistical difficulty and associated costs of maintaining fog collection systems can pose significant barriers, particularly for remote or economically challenged regions [40].

Moreover, the collection efficiency of fog harvesting systems can be influenced by multiple variables. The size and design of the mesh, wind speed and direction, and the presence of airborne pollutants and dust can all impact the rate at which water droplets are captured from the fog [6]. Consequently, achieving consistent and optimal collection rates may prove challenging,

necessitating careful design and monitoring of fog collectors.

Water quality is another crucial aspect to consider in fog water collection. Fog water can be susceptible to contamination by airborne pollutants, including industrial emissions and particulate matter. The presence of pollutants can affect the suitability of the collected water for direct human consumption, requiring proper treatment before use. Ensuring water quality compliance becomes essential to safeguarding the health of the communities relying on fog harvesting as a freshwater source [41].

The cost of implementing and maintaining fog water collection systems poses a significant limitation to its widespread adoption. The initial investment and ongoing expenses associated with fog collectors may not be financially feasible for all regions, particularly in areas with limited resources or competing priorities. Addressing cost concerns may require innovative financing models and exploring partnerships with governmental, non-governmental, or private entities.

Additionally, fog harvesting heavily relies on specific atmospheric conditions, necessitating high humidity and wind speeds for effective water droplet capture. This inherent reliance on environmental factors may limit the applicability of fog water collection in regions with comparatively lower humidity or calmer winds. Community involvement and education play a pivotal role in the success of fog harvesting projects. The motivation, training, and active participation of local populations are key factors in ensuring the long-term sustainability of fog collection initiatives. Inadequate engagement with the local community can undermine the effectiveness and acceptance of fog water collection systems [46].

Despite these challenges, successful fog harvesting projects have demonstrated their feasibility in regions with favorable climatic conditions, particularly in arid and semi-arid areas with persistent fog. Ongoing research and technological advancements aim to optimize fog collector designs and overcome limitations, making fog water collection a viable and

sustainable option for addressing water scarcity challenges in select geographical locations. Careful planning, innovative approaches, and collaboration between stakeholders are essential to unlocking the full potential of fog harvesting as an environmentally friendly and locally appropriate water supply solution.

6. Enhancing Fog Collection Efficiency

Enhancing the efficiency of fog collection is a critical aspect of making fog water harvesting a reliable and sustainable source of fresh water. Researchers and engineers have explored various innovative approaches to optimize fog collectors and maximize water yield [47]. Some of these methods are inspired by nature, while others involve improved design configurations and material selection [48].

Bioinspired surfaces have been a focal point of research in enhancing fog collection efficiency. By emulating the fog-collecting characteristics of creatures like beetles, cacti, and trees, researchers have developed novel fog collector designs. Nanocones decorated with a 3D fiber network, beetle-inspired and cactus-inspired surfaces, and tree-shaped hierarchical cones on superhydrophobic films are some examples of bioinspired fog-collecting surfaces. These bioinspired structures promote water droplet condensation and facilitate more efficient water collection [49].

Moreover, nanotechnology has contributed to advancements in fog collection efficiency. The introduction of nanowire structures on cone tips and wettable gradient microchannels has shown promising results in improving water harvesting efficiency [7, 49]. By incorporating superhydrophobic nanowires, Sarracenia-inspired microchannels, and spider-inspired wetting gradients, researchers have achieved a confined effect and ultrafast water transport, further enhancing the fog collection process.

Integration of multiple bioinspired surfaces has also been explored to achieve high fog harvest efficiency. Combining the fog-collecting characteristics of various creatures in an integrated fog collector system maximizes water

droplet capture and enhances overall water yield [50].

In addition to surface design, fog collector placement plays a crucial role in optimizing water capture rates. Installing fog collectors perpendicular to the prevailing wind direction allows for the maximum interception of fog, ensuring efficient water collection [43, 51].

Mesh material optimization is another key strategy. Selecting mesh material with a pore size of 0.2 to 0.4 mm strikes a balance between capturing fog droplets effectively and allowing sufficient air passage, reducing clogging and improving overall collection efficiency [52]. Furthermore, it has also been reported that fog harps demonstrate a significantly higher number of droplets sliding down the harvester compared to meshes [53]. This observation reveals a key advantage of fine-scale harps in avoiding the clogging problem frequently encountered with fine meshes. The increased number of droplets sliding down the harp's surface ensures a continuous and efficient fog water collection process.

To mitigate the impact of wind on fog collectors, the installation of windbreaks has been proposed [30]. These barriers reduce wind speed and turbulence around the fog collector, creating a calmer environment that enhances water droplet capture rates during windy conditions.

Furthermore, proper water storage and protection are essential to maintain water quality and quantity [46]. Storing the collected fog water in clean, covered containers shielded from sunlight prevents contamination and evaporation, ensuring the water remains suitable for various uses.

Additionally, advancements in 3D printing technology have led to the development of new fog collectors with innovative designs as in seen in Figure 6. For instance, 3D-printed fog collectors with cactus-inspired spine structures and peristome-like arc-pitted grooves have shown impressive efficiency in capturing fog water [54].

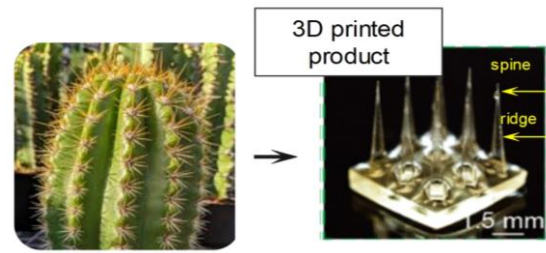


Figure 6. Bioinspired 3D product design of the fog-collection structure [54]

By integrating these approaches and continually exploring advancements in materials, design, and fog characterization techniques, fog water collection can be significantly enhanced. Such improvements have the potential to make fog harvesting a more reliable and scalable solution for addressing water scarcity in foggy environments.

7. Conclusion

In conclusion, fog harvesting presents a promising solution to the pressing issue of water scarcity and the need for sustainable water sources. By capturing water droplets from fog, this renewable and eco-friendly technique offers a reliable water supply, especially in arid regions with frequent fog occurrences.

Despite challenges such as fog availability, maintenance costs, and water quality concerns, ongoing research and technological advancements continue to enhance fog collection efficiency. Innovations inspired by nature, nanotechnology, optimized materials, and improved designs contribute to maximizing water yield and economic viability.

Real-world fog harvesting projects and laboratory researches have demonstrated the effectiveness of this approach in providing sustainable water access to communities facing water scarcity. Collaboration between stakeholders and local community involvement are vital for successful implementation.

Fog harvesting's potential to shape a more water-secure world is undeniable. By embracing this eco-friendly solution and fostering innovation, we can move towards a sustainable future where clean water access is a fundamental human right for all.

Article Information Form

Funding

The authors has no received any financial support for the research, authorship or publication of this study.

Authors' Contribution

The authors contributed equally to the study.

The Declaration of Conflict of Interest/ Common Interest

No conflict of interest or common interest has been declared by the authors.

The Declaration of Ethics Committee Approval

This study does not require ethics committee permission or any special permission.

The Declaration of Research and Publication Ethics

The authors of the paper declare that they comply with the scientific, ethical and quotation rules of SAUJS in all processes of the paper and that they do not make any falsification on the data collected. In addition, they declare that Sakarya University Journal of Science and its editorial board have no responsibility for any ethical violations that may be encountered, and that this study has not been evaluated in any academic publication environment other than Sakarya University Journal of Science.

Copyright Statement

Authors own the copyright of their work published in the journal and their work is published under the CC BY-NC 4.0 license.

References

- [1] E. Summary, "Partnerships and cooperation for water," December 12, 2023.[Online].Available:<https://www.unesco.org/reports/wwdr/2023/en>
- [2] M. M. Mekonnen, A. Y. Hoekstra, "Sustainability: Four billion people facing severe water scarcity," *Science Advances*, vol. 2, no. 2, pp. 1-7, 2016.
- [3] K. Oktor, "Decolorization of Real Slaughterhouse Wastewater with a Freshwater Microalga," *Water, Air, & Soil Pollution*, vol. 234, no. 1, 2023.
- [4] H. Shemer, S. Wald, R. Semiat, "Challenges and Solutions for Global Water Scarcity," *Membranes*, vol. 13, no. 6, pp. 612, 2023.
- [5] H. Jarimi, R. Powell, S. Riffat, "Review of sustainable methods for atmospheric water harvesting," *International Journal of Low-Carbon Technologies*, vol. 15, no. 2, pp. 253-276, 2020.
- [6] J. K. Domen, W. T. Stringfellow, M. K. Camarillo, S. Gulati, "Fog water as an alternative and sustainable water resource," *Clean Technologies and Environmental Policy*, vol. 16, no. 2, pp. 235-249, 2014.
- [7] A. Feng, N. Akther, X. Duan, S. Peng, C. Onggowarsito, S. Mao, Q. Fu, S. D. Kolev, "Recent Development of Atmospheric Water Harvesting Materials: A Review," *American Chemical Society Materials Au*, vol. 2, no. 5, pp. 576-595, 2022.
- [8] Z. Ismail, Y. I. Go, "Fog-to-Water for Water Scarcity in Climate-Change Hazards Hotspots: Pilot Study in Southeast Asia," *Global Challenges*, vol. 5, no. 5, 2000036, 2021.
- [9] D. M. Fernandez, A. Torregrosa, P. S. Weiss-Penzias, B. J. Zhang, D. Sorensen, R. E. Cohen, G. H. McKinley, J. Kleingartner, A. Oliphant, M. Bowman, "Fog water collection effectiveness: Mesh intercomparisons," *Aerosol and Air Quality Research*, vol. 18, no. 1, pp. 270-283, 2018.
- [10] S. Sharifvaghefi, H. Kazerooni, "Fog harvesting: combination and comparison of different methods to maximize the collection efficiency," *Discover Applied Sciences*, vol. 3, no. 4, pp. 1-11, 2021.
- [11] R. Sun, J. Zhao, C. Liu, N. Yu, J. Mo, Y. Pan, D. Luo, "Design and optimization of hybrid superhydrophobic-hydrophilic

- pattern surfaces for improving fog harvesting efficiency,” *Progress in Organic Coatings*, vol. 171, no. 107016, 2022.
- [12] J. Li, W. Li, X. Han, L. Wang, “Sandwiched nets for efficient direction-independent fog collection,” *Journal of Colloid and Interface Science*, vol. 581, pp. 545-551, 2021.
- [13] Y. Guo, Y. Li, G. Zhao, Y. Zhang, G. Pan, H. Yu, M. Zhao, G. Tang, Y. Liu, “Patterned Hybrid Wettability Surfaces for Fog Harvesting,” *Langmuir*, vol. 39, no. 13, pp. 4642-4650, 2023.
- [14] W. Shi, T. W. van der Sloot, B. J. Hart, B. S. Kennedy, J. B. Boreyko, “Harps Enable Water Harvesting under Light Fog Conditions,” *Advanced Sustainable Systems*, vol. 4, no. 6, pp. 1-10, 2020.
- [15] M. Gürsoy, “All-dry patterning method to fabricate hydrophilic/hydrophobic surface for fog harvesting,” *Colloid and Polymer Science*, vol. 298, no. 8, pp. 969-976, 2020.
- [16] X. Gou, Z. Guo, “Hybrid Hydrophilic-Hydrophobic CuO@TiO₂-Coated Copper Mesh for Efficient Water Harvesting,” *Langmuir*, vol. 36, no. 1, pp. 64-73, 2020.
- [17] R. Spirig, R. Vogt, C. Feigenwinter, “Droplet size distribution, liquid watercontent and water input of the seasonally variable, nocturnal fog in the Central Namib Desert,” *Atmospheric Research*, vol. 262, no. July, p. 105765, 2021.
- [18] M. Fessehaye, S. A. Abdul-Wahab, M. J. Savage, T. Kohler, T. Gherezghiher, H. Hurni, “Fog-water collection for community use,” *Renewable and Sustainable Energy Reviews*, vol. 29, pp. 52-62, 2014.
- [19] Z. Yu, T. Zhu, J. Zhang, M. Ge, S. Fu, Y. Lai, “Fog Harvesting Devices Inspired from Single to Multiple Creatures: Current Progress and Future Perspective,” *Advanced Functional Materials*, vol. 32, no. 26, pp. 1-20, 2022.
- [20] Y. Tu, R. Wang, Y. Zhang, J. Wang, “Progress and Expectation of Atmospheric Water Harvesting,” *Joule*, vol. 2, no. 8, pp. 1452-1475, 2018.
- [21] J. Song, R. Shi, X. Bai, H. Algadi, D. Sridhar, “An overview of surface with controllable wettability for microfluidic system, intelligent cleaning, water harvesting, and surface protection,” *Advanced Composites and Hybrid Materials*, vol. 6, no. 22, 2023.
- [22] Z. Wu, K. Yin, J. Wu, Z. Zhu, J. An Duan, J. He, “Recent advances in femtosecond laser-structured Janus membranes with asymmetric surface wettability,” *Nanoscale*, vol. 13, pp. 2209-2226, 2021.
- [23] Y. Shi, O. Ilic, H. A. Atwater, J. R. Greer, “All-day fresh water harvesting by microstructured hydrogel membranes,” *Nature Communications*, vol. 12, no. 1, pp. 1-10, 2021.
- [24] K. Yin, H. Du, X. Dong, C. Wang, J. Duan, J. He, “Wettability surface with micro/nanopatterns for efficient fog collection,” *Nanoscale*, vol. 9, no 38, pp. 14620-14626, 2017.
- [25] F. Fathieh, M. J. Kalmutzki, E. A. Kapustin, P. J. Waller, J. Yang, O. M. Yaghi, “Practical water production from desert air,” *Science Advances*, vol. 4, no. 6, pp. 1-10, 2018.
- [26] A. LaPotin, H. Kim, S. R. Rao, E. N. Wang, “Adsorption-Based Atmospheric Water Harvesting: Impact of Material and Component Properties on System-Level Performance,” *Accounts of Chemical Research*, vol. 52, no. 6, pp. 1588-1597, 2019.
- [27] X. Zhou, H. Lu, F. Zhao, G. Yu, “Atmospheric Water Harvesting: A Review of Material and Structural Designs,” *ACS Materials Letters*, vol. 2, no. 7, pp. 671-684, 2020.
- [28] H. Kim, S. Yang, S. R. Rao, S. Narayanan,

- E. A. Kapustin, H. Furukawa, A. S. Umans, O. M. Yaghi, E. N. Wang, "Water harvesting from air with metal-organic frameworks powered by natural sunlight," *Science*, vol. 356, no. 6336, pp. 430-434, 2017.
- [29] Climate Technology Centre and Network (CTCN), "Climate Change Adaptation Technologies for Water", March 12, 2024. [Online]. Available: <https://www.ctcn.org/resources/climate-change-adaptation-technologies-water-practitioner-s-guide-adaptation-technologies>
- [30] R. Holmes, J. de D. Rivera, E. de la Jara, "Large fog collectors: New strategies for collection efficiency and structural response to wind pressure," *Atmospheric Research*, vol. 151, pp. 236-249, 2015.
- [31] M. Qadir, G. C. Jiménez, R. L. Farnum, L. L. Dodson, V. Smakhtin, "Fog water collection: Challenges beyond technology," *Water*, vol. 10, no. 4, pp. 1-10, 2018.
- [32] B. Bhushan, "Commercial Applications, Projections of Water Collection, and Design of Water Harvesting Towers," *Springer Series in Materials Science*, vol. 299, pp. 155-160, 2020.
- [33] Y. Jiang, C. Machado, K. C. K. Park, "From capture to transport: A review of engineered surfaces for fog collection," *Droplet*, vol.2, no. e55, 2023.
- [34] D. Nioras, K. Ellinas, V. Constantoudis, E. Gogolides, "How Different Are Fog Collection and Dew Water Harvesting on Surfaces with Different Wetting Behaviors?," *ACS Applied Materials & Interfaces*, vol. 13, no. 40, pp. 48322-48332, 2021.
- [35] G. Morichi, L. B. Calixto, A. Zanelli, "Novel Applications for Fog Water Harvesting," *Journal of Geoscience and Environment Protection*, vol. 06, no. 03, pp. 26-36, 2018.
- [36] K. Wan, X. Gou, Z. Guo, "Bio-inspired Fog Harvesting Materials: Basic Research and Bionic Potential Applications," *Journal of Bionic Engineering*, vol. 18, no. 3, pp. 501-533, 2021.
- [37] O. Klemm, R. S. Schemenauer, A. Lummerich, P. Cereceda, V. Marzol, D. Corell, J. van Heerden, D. Reinhard, T. Gherezghiher, J. Olivier, P. Osses, J. Sarsour, E. Frost, M. J. Estrela, J. A. Valiente, G. M. Fessehaye, "Fog as a fresh-water resource: Overview and perspectives," *Ambio*, vol. 41, no. 3, pp. 221-234, 2012.
- [38] N. Zamani, M. Maleki, F. Eslamian, "Fog water harvesting investigation as a water supply resource in arid and semi-arid areas," *Water Productivity Journal*, vol. 1, no. 4, pp. 43-52, 2021.
- [39] K. C. Park, S. S. Chhatre, S. Srinivasan, R. E. Cohen, G. H. McKinley, "Optimal design of permeable fiber network structures for fog harvesting," *Langmuir*, vol. 29, no. 43, pp. 13269-13277, 2013.
- [40] M. Qadir, G. C. Jiménez, R. L. Farnum, P. Trautwein, "Research History and Functional Systems of Fog Water Harvesting," *Frontiers in Water*, vol. 3, no. 37, pp. 1-11, 2021.
- [41] R. S. Schemenauer, P. Cereceda, P. Osses, "Fog Water Collection Manual", 3rd ed., Toronto, Canada: FogQuest, 2022, pp. 166.
- [42] R. S. Schemenauer, P. Cereceda, P. Osses, "Fog Water Collection Manual", 1st ed., Toronto, Canada: FogQuest, 2005, pp. 1-92.
- [43] D. Carvajal, M. Mora-Carreño, C. Sandoval, S. Espinoza, "Assessing fog water collection in the coastal mountain range of Antofagasta, Chile," *Journal of Arid Environments*, vol. 198, no. 104679, 2022.
- [44] S. A. Abdul-Wahab, V. Lea, "Reviewing fog water collection worldwide and in

- Oman,” *International Journal of Environmental Studies*, vol. 65, no. 3, pp. 487-500, 2008.
- [45] Munich Re Foundation, “Fog Net Technology,” March 12, 2024. [Online]. Available: https://www.munichre-foundation.org/en/climate-adaptation/fognets/fognet_technology.html
- [46] A. F. Batisha, “Feasibility and sustainability of fog harvesting,” *Sustainability of Water Quality and Ecology*, vol. 6, pp. 1-10, 2015.
- [47] M. Zhang, M. Xiao, C. Li, D. Li, J. Li, K. Yu, Y. Pan, “Enhancing fog collection by optimizing wettability combination and fork-row collector arrangement: light and heavy fog,” *Journal of Physics D: Applied Physics*, vol. 56, no. 49, 2023.
- [48] M. Azeem, M. Tayyab, J. Wiener, M. Petru, P. Louda, “Environmental Technology & Innovation Structural design of efficient fog collectors: A review,” *Environmental Technology & Innovation*, vol. 20, no. 101169, 2020.
- [49] H. Sun, Y. Song, B. Zhang, Y. Huan, C. Jiang, H. Liu, T. Bao, S. Yu, H. Wang, “Bioinspired micro- and nanostructures used for fog harvesting,” *Applied Physics A Material and Science Processing*, vol. 127, no. 6, pp. 1-12, 2021.
- [50] H. Yue, Q. Zeng, J. Huang, Z. Guo, W. Liu, “Fog collection behavior of bionic surface and large fog collector: A review,” *Advances in Colloid and Interface Science*, vol. 300, no. 102583, 2022.
- [51] H. Dong, Y. Zheng, N. Wang, H. Bai, L. Wang, J. Wu, Y. Zhao, L. Jiang, “Highly Efficient Fog Collection Unit by Integrating Artificial Spider Silks,” *Advanced Materials Interfaces*, vol. 3, no. 11, pp. 1-5, 2016.
- [52] I. Höhler, C. Suau, “Fog collectors and collection techniques,” in *5th International Conference on Fog, Fog Collection and Dew*, Münster, Germany, 2010, pp. 135.
- [53] Q. Wang, Y. He, X. Geng, Y. Hou, Y. Zheng, “Enhanced Fog Harvesting through Capillary-Assisted Rapid Transport of Droplet Confined in the Given Microchannel,” *ACS Applied Materials & Interfaces*, vol. 13, no. 40, pp. 48292-48300, 2021.
- [54] L. Liu, S. Liu, M. Schelp, X. Chen, “Rapid 3D Printing of Bioinspired Hybrid Structures for High-Efficiency Fog Collection and Water Transportation,” *ACS Applied Materials & Interfaces*, vol. 13, no. 24, pp. 29122-29129, 2021.